THE REGULATION OF SYNAPTIC EFFICACY AT REGENERATED AND CULTURED NEUROMUSCULAR JUNCTIONS

by

Peter H. Chipman

Submitted in partial fulfilment of the requirements
for the degree of Doctor of Philosophy

at

Dalhousie University
Halifax, Nova Scotia
August 2012

DALHOUSIE UNIVERSITY

DEPARTMENT OF ANATOMY AND NEUROBIOLOGY

The undersigned hereby certify that they have read and recommend to the Faculty of Graduate Studies for acceptance a thesis entitled "THE REGULATION OF SYNAPTIC EFFICACY AT REGENERATED AND CULTURED NEUROMUSCULAR JUNCTIONS" by Peter H. Chipman in partial fulfilment of the requirements for the degree of Doctor of Philosophy.

Dated: August 2, 2012

External Examiner: _____

Research Supervisor: _____

Examining Committee: _____

_____

_____

Departmental Representative: _____

DALHOUSIE UNIVERSITY

DATE: August 2, 2012

AUTHOR: Peter H. Chipman

TITLE: THE REGULATION OF SYNAPTIC EFFICACY AT REGENERATED AND CULTURED NEUROMUSCULAR JUNCTIONS

DEPARTMENT OR SCHOOL: Department of Anatomy and Neurobiology

DEGREE: PhD CONVOCATION: October YEAR: 2012

_____

Signature of Author

To Mom and Dad,

Thank you for encouraging me to discover the things I enjoy most of all and for teaching me to investigate their significance.

TABLE OF CONTENTS

LIST OF TABLES

LIST OF FIGURES

ABSTRACT

The neuromuscular junction (NMJ) is a synapse formed between a motoneuron and a muscle fiber which transmits the signals required to initiate muscle contraction. The functional state of the NMJ is intimately tied to the structure and function of the motoneuron, such that reductions in postsynaptic activity retrogradely stimulate sustained reorganization of presynaptic motor terminals in an attempt to maintain normal contractile output. In the adult, these plastic changes occur most notably as regenerative responses following traumatic injury and during the progression of motoneuron diseases (MNDs), and can contribute to a considerable amount of functional repair. However, limitations to the regeneration capacity of motoneurons place an upper limit on the effectiveness of endogenous repair mechanisms and can restrict the extent of functional recovery. Using a combination of immunofluorescence, sharp electrode electrophysiology and live labeling of synaptic vesicle recycling during various forms of synaptic growth and regeneration *in vivo* and *in vitro*, I have identified that the neural cell adhesion molecule (NCAM) is a key regulator of the regenerative capacity of motoneurons. *In vivo* experiments revealed that NCAM influences the maturation and stabilization of regenerated synapses via the recruitment and recycling of synaptic vesicles necessary for effective synaptic transmission. The presence of both pre- and post-synaptic NCAM were necessary to maintain the abundance of recycling synaptic vesicles at regenerated synapses, demonstrating a coordinated influence of these molecules in regenerative synaptic plasticity *in vivo*. To accurately assess the regenerative potential of motoneurons *in vitro*, it was necessary to develop a system which could reliably and consistently generate mature NMJs amenable to experimental investigation. Motoneurons differentiated from embryonic stem cells were grown for 3-5 weeks in co-culture with muscle fibers and generated mature NMJs which possessed morphological and functional criteria consistent with NMJs formed *in vivo*. NMJs formed by *NCAM*$^{-/-}$ motoneurons did not mature and were found to exhibit deficits consistent with their *in vivo* counterparts. These studies have revealed that NCAM is a key mediator of regenerative plasticity at the NMJ and may be a target for efforts to enhance endogenous repair following traumatic injury or during the progression of neurodegenerative disease.

LIST OF ABBREVIATIONS USED

ACh	Acetylcholine
AChR	Acetylcholine receptor
ALS	Amyotrophic lateral sclerosis
ANOVA	Analysis of variance
AP	Adaptor protein
ARIA	Acetylcholine receptor inducing activity (aka Neuregulin)
ATX/Aga	Agatoxin
BDNF	Brain derived neurotrophic factor
BFA	Brefeldin A
CAM	Cell adhesion molecule
CaMKII	Calcium/calmodulin-dependent protein kinase II
CGRP	Calcitonin gene related peptide
CNTF	Ciliary neurotrophic factor
cT	Contacted terminal
CTB	Cholera toxin-β
CSA	Cross sectional area
Cre	'Causes recombination'
CV	Coefficient of variation
DHPR	Dihydropyridine receptor
DMSO	Dimethyl sulfoxide
dTC	D-Tubocurare
E	Embryonic day
E-C	Excitation- contraction
ECM	Extracellular matrix
EMG	Electromyograph
Endo-N	Endoneuraminidase –N
EPP	Endplate potential
ER	Endoplasmic reticulum
ESC	Embryonic stem cell
ESCMN	Embryonic stem cell derived motoneuron
FasII	Fasciclin II
FGF	Fibroblast growth factor
FGFR	Fibroblast growth factor receptor
Flx	Flanked by lox P (lox P - 'locus of crossing (x) over P1')
FN	Fibronectin
GDNF	Glial derived neurotrophic factor
GFP	Green fluorescent protein
GPI	Glycophosphatidylinositol
Hb9	Homeobox gene 9
HSA	Human α-skeletal actin
ICM	Inner cell mass
Ig	Immunoglobulin
iMN	Induced motoneuron
IR	Innervation ratio

iPS	Induced pluripotent stem cell
L-VDCC	L (long lasting) -type voltage dependent calcium channel; aka $Ca_v1.1$-1.4
m	Quantal content
mEPP	Miniature endplate potential
MN	Motoneuron
MND	Motoneuron disease
mRNA	Messenger ribonucleic acid
MSD	Muscle specific domain
MU	Motor unit
MuSK	Muscle-specific kinase
n	Number of synaptic release sites
NCAM	Neural Cell Adhesion Molecule
Nif	Nifedipine
NF	Neurofilament
NMJ	Neuromuscular junction
N-VDCC	N (neural)-type voltage dependent calcium channel; aka $Ca_v2.2$
ns	Not statistically significant
OCT	Optimal cutting temperature
p	Probability of release at individual active zones
PD	Partial denervation
pPD	Post partial denervation
PFA	Paraformaldehyde
PKC	Protein kinase C
PLC	Phospholipase C
PMEF	Primary mouse embryonic fibroblasts
pT	Parent terminal
p_r	Average probability of release across entire presynaptic terminal
PSA	Polysialic acid
P/Q-VDCC	P/Q (Purkinje) -type voltage dependent calcium channel; aka $Ca_v2.1$
RA	Retinoic acid
Regen	Regenerated
RP	Recycling pool
RRP	Readily releasable pool
rT	Reinnervated terminal
S100	calcium binding protein; 100% soluble in ammonium sulphate
SEM	Standard error of mean
Shh	Sonic hedgehog
SOD1	Superoxide dismutase 1
SMA	Spinal muscular atrophy
Stim	Stimulation
SV2	Synaptic vesicle protein 2
Syp/synap	Synaptophysin
tB	Terminal bridge
TEM	Transmission electron microscopy
TFE	Terminal field expansion
TGN	Trans-golgi network

TMR α-BTX	Tetramethylrhodamine conjugated α-bungarotoxin
tSC	Terminal Schwann cell
tSp	Terminal axon sprout
TTX	Tetrodotoxin
Unop	Unoperated
VAMP	Vesicle associated membrane protein
VAChT	Vesicular acetylcholine transporter
VASE	Variable alternatively spliced exon
VDCC	Voltage-dependent calcium channel
Wld^s	Wallerian degeneration slow

CHAPTER 1: Introduction

1.1 The motor unit

Structural plasticity of the motor circuit

Locomotor behaviour is generated by patterns of skeletal muscle contraction derived from the circuit activity of interneurons and motoneurons in the spinal cord. Cortical information relating the intentional state of the organism integrates with information delivered via propriosensory afferents, Renshaw cells and a variety of interneurons to influence the output of central pattern generators (CPGs) which function to inform target muscles of desired behavioural patterns. Motoneurons are the ultimate output cells of spinal CPGs and relay neural information to skeletal muscle via synaptic transmission at the neuromuscular junction (NMJ). A single unit of this assembly (i.e. one motoneuron and all the muscle fibers it innervates) is referred to as a motor unit (MU), and the relative number of muscle fibers contained in a MU is known as its innervation ratio (IR). Together, these interacting units function to produce graded muscle contraction and to generate patterned flexor and extensor alternation for the performance of a variety of smooth and robust locomotor behaviours.

The integrity of the locomotor system is incredibly resilient and homeostatically maintained over the course of an animal's lifetime with little net structural change in the healthy animal (Courtney and Steinbach, 1981; Lichtman et al 1987). However, injury, disease, and advanced ageing can influence a variety of circuit functions and lead to the reorganization of synaptic inputs in the spinal cord (Himes and Tessler, 1989; Marques et al 2006) and extensive remodeling of the neuromuscular junction (Brown and Ironton, 1978; Caccia et al 1979; Banker at al 1983; Smith, 1984; Rochel and Robbins, 1988; Rafuse et al 1992; Kadhiresan et al 1996; Schefer et al 2005). In particular, alterations to the rate and strength of presynaptic and postsynaptic activity are accompanied by signs of extensive compensatory sprouting by terminal motor axons and perisynaptic terminal Schwann cells (tSCs). Such changes are most striking following full or partial axotomy (Brown and Ironton, 1978; Son and Thompson, 1995a, b) and occur early during the progression of motoneuron diseases (MND) (Maselli et al. 1993; Frey et al. 2000; Rich et

al. 2002; Gould et al. 2006; Schefer et al 2005; Kong et al. 2009). The NMJ is therefore a primary and potent locus at which the motor circuit can affect structural plasticity to homeostatically maintain appropriate locomotor function in response to a variety of presynaptic pathologies.

The remainder of this introduction will focus on the general organizational and functional principles of neuromuscular innervation with the ultimate goal of introducing the mechanisms used by regenerating and sprouting motor axons to maintain motor output in response to presynaptic pathology.

Synaptic innervation and prepatterning

Motor axons exit the spinal cord and project toward target muscle groups in response to a number of attractive and repulsive intermediate cues before ultimately stopping to form motor terminals at preformed synaptic sites along the midbelly of muscle fibers. Some of the earliest reports examining the regulation of peripheral targeting and synaptic patterning come from the work of Dr. Lynn Landmesser. Using the chick embryo as a model system, Landmesser and colleagues were among the first to describe that specific motor pools in the developing spinal cord project to specific muscle populations (Landmesser and Morris, 1975; Landmesser, 1978a, b) and that neuromuscular innervation patterns and motoneuron survival were closely regulated by activity (Dahm and Landmesser, 1988, 1991) and adhesion molecules (Landmesser and Szente, 1986; Landmesser et al 1990; Rafuse et al 1996; Rafuse and Landmesser, 2000). Based on these early investigations, other studies have demonstrated that the instructions required for appropriate peripheral targeting and patterning are derived from a combination of intrinsic programs initiated by the transcriptional identities of spatially grouped populations of motoneuron in the spinal cord (Landmesser, 1978a,b; Kania et al 2000; Jessell, 2000; Bonanomi and Pfaff, 2010), along with extrinsic programs intiated by central activity (Myers et al 2005; Hanson and Landmesser, 2006; Kastanenka and Landmesser, 2010), and from peripheral targets themselves (Haase et al 2002; Livet et al 2002; Li et al 2008). These same guidance programs are implicated in the regulation of muscle-specific intramuscular branching patterns (Rafuse et al 1996; Rafuse and Landmesser, 2000; Haase et al 2002; Livet et al 2002) which are in turn closely regulated

by the prepatterning of postsynaptic acetylcholine receptors (AChRs) clustered along the midbelly of the target muscle (Lin et al 2001; Yang et al 2001; Misgeld et al 2002; Chen F. et al 2011).

Muscle fibers possess the ability to express and cluster AChRs to form endplates along the central muscle regions in the complete absence of innervating motor axons and/or cholinergic neurotransmission (Lin et al 2001; Misgeld et al 2002), although the number of postsynaptic clusters is significantly decreased in chick muscles in the absence of a neural tube (Dahm and Landmesser, 1991). The central positioning of AChR clusters along the muscle fiber midbelly require postsynaptic activity mediated by L-type voltage-dependent Ca^{2+} channels (L-VDCCs), traditionally involved in excitation contraction (E-C) coupling (Chen et al 2011). On the other side of the synapse, presynaptic differentiation is highly dependent upon the identification of retrograde, muscle-derived signals (Nguyen et al 200l; Chakkalakal et al 2010) which can aggregate in the extracellular matrix (ECM) to induce Ca^{2+} channel and synaptic vesicle clustering at active zone sites (Nishimune et al 2004; Fox et al 2007). The refinement of pre and postsynaptic matching at single synapses is largely determined by activity-dependent secretion of proteases, proteoglycans and neurotransmitters from growing nerve terminals (Lin et al 2001, 2005; Misgeld et al 2002, 2005; Buffelli et al 2003; Heeroma et al 2003; de Castro et al 2009; Bollinger et al 2010). Together, these signals lead to the generation of highly specific patterns of motor innervation required for appropriate locomotor output.

Synaptic specificity

In mammals, developing MUs are initially very large with axon terminals contacting the majority of the fibers in a muscle region (Tapia et al 2012). All but one innervating terminal is eventually pruned away in a competition-based refinement of axonal arborization (Redfern, 1970; Bagust et al 1973; Brown et al 1976; Buffelli et al 2003; Tapia et al 2012). This stereotyped organization is a product of both activity-dependent and independent competitive innervation, where the physical withdrawal of the 'losing' terminal is correlated with a relative weakening in its synaptic efficacy (O'Brian et al 1978; Colman et al 1997; Kopp et al 2000). This competitive-based refinement of

synaptic innervation has been applied to the development of other neural circuits in the nervous system (Lichtman and Purves 1980; Chen and Regehr, 2000; Lorenzetto et al 2009; Ben Fredj et al 2010), suggesting a conserved process for the patterning of specific neuronal connections.

The pruning of motor terminal arbors innervated skeletal muscles ultimately contributes to the grouping of MUs into functional sub-units which effectively allow a graded and progressive recruitment of force during a motor task (Henneman and Olson, 1965; Sypert and Munson, 1981). Slow (type I) muscle fibers contract slowly and are stimulated first because they are innervated by small motoneurons with high input resistances in the spinal circuit. Slow muscle fibers utilize oxidative catabolism to derive energy and are resistant to fatigue during periods of prolonged activation. Slow MUs are generally small, but have a high density of mitochondria in order to allow for continuous activation of muscle fibers needed for sustained contraction. Fast (type II) fibers are recruited later because they have relatively large soma sizes with lower input resistances. Fast fibers contract quickly, utilize anaerobic catabolism and possess unique myosin heavy chain isoforms which allow them be further subdivided into type IIA, X and B. Fast MUs typically have larger IRs than slow MUs and are progressively recruited A>X>B during a motor task.

Fast and slow motor terminals exhibit presynaptic release kinetics and firing properties which closely match those of the postsynaptic muscle fiber they innervate (Reid et al 1999; Rowley et al 2007), suggesting an intimate pre and postsynaptic relationship (Chakkalakal et al 2010). Interestingly, the distribution of fiber types in a muscle are malleable and can be manipulated by a variety of factors including exercise, hormones, denervation and ageing (Chakkalakal et al 2012). Recent studies have highlighted that motoneurons innervating fast fibers are preferentially vulnerable to motoneuron disease (Frey et al 2000; Pun et al 2006) and have led to the design of novel therapies designed to activate specific MUs and/or manipulate fiber type expression in vulnerable muscles (Deforges et al 2009).

1.2 The Neuromuscular Junction

Principle and players

The neuromuscular junction is a tripartite synapse composed of the motor terminal, the muscle fiber and several tSCs. Figure 1.1 illustrates the general cellular organization of the mammalian neuromuscular junction with some of the principle components identified. The following section will detail developmental and stabilization mechanisms responsible for effective functional organization of the NMJ throughout the lifetime of the organism.

Postsynaptic differentiation and stabilization

The postsynaptic apparatus is composed of AChRs and related signaling machinery including muscle-specific kinase (MuSK), the low density lipoprotein receptor 4 (Lrp4), rapsyn, and others (Gautam et al 1996; Okada et al 2006; Kim et al 2008; Linnoila et al 2008; Zhang et al 2008), which together participate in the progressive clustering, refinement and homeostatic maintenance of AChR abundance at specific synaptic sites. The maturation of the postsynaptic complex involves the selective expression of these synapse-specific genes, including MuSK, acetylcholinesterase and AChR mRNA by subsynaptic nuclei in the myofiber (Hippenmeyer et al 2007; Jevsek et al 2006) and the appearance of postsynaptic perforations in endplate plaques, the development of postsynaptic junctional folds, the concentration of AChRs at the tips of these folds, and the emergence of appropriate neurotransmission phenotypes (Sanes and Lichtman, 2001; Jevsek et al 2006).

Expression of postsynaptic AChR mRNA by subsynaptic nuclei is directed, in part, by the presynaptic release of ARIA (acetylcholine receptor inducing activity) from the innervating nerve terminal (Falls et al 1993; Sandrock et al 1997). ARIA is a member of the neuregulin family and activates ErbB transmembrane tyrosine kinase receptors expressed on postsynaptic muscle and perisynaptic Schwann cells to mediate its effects at the NMJ (Altiok et al 1995; Sanes and Lichtman, 2001). Likewise, neuronal agrin is released from motoneurons and aggregates in the synaptic ECM where proteolytic cleavage by synapse-specific proteases regulates its postsynaptic activity (Nitkin et al

1987; Reist et al 1992; Denzer et al 1995; Bolliger et al 2010). Agrin binds to, and activates a postsynaptic complex composed of Lrp4, Tid1 and MuSK to induce downstream signaling and AChR aggregation via rapsyn and Dox-7 (Gautam et al 1996; Okada et al 2006; Kim et al 2008; Linnoila et al 2008; Zhang et al 2008). Interestingly, neurally-derived agrin and cholinergic transmission provide opposing influences on the stability of AChR clusters (Lin et al 2005; Misgeld et al 2005), suggesting a dynamic activity-dependent interplay between pre and postsynaptically derived organizational elements at individual synapses.

The kinetics of receptor subunit turnover, stabilization and maturation can be profoundly influenced by pre and postsynaptic activity (Avila et al 1989; Tsay and Schmidt, 1989; Martinou and Merlie, 1991; Caroni et al 1993; Missias et al 1996; Bezakova et al 2001; Bruneau et al 2005). For instance, the AChR is initially composed of four distinct subunits, α, β, γ, δ in a 2:1:1:1 ratio, but developmental changes initiate the gradual replacement of the γ subunit with an ε subunit, which alters the kinetics of ion flux through the channel (Mishina et al 1986) and increases the half life of receptor complexes in the postsynaptic membrane from~3-5 days to~10-11 days (Sala et al 1997). Denervation results in the re-expression of the γ subunit and destabilization of the ε subunit, reverting back to the immature channel kinetics (Berg and Hall, 1974; Tsay and Schmidt, 1989). Furthermore, the transcriptional regulation of subunit replacement during development differs between fast and slow MUs (Missias et al 1996) and is accelerated by denervation and paralysis (Tsay and Schmidt, 1989; Sanes and Lichtman, 2001; Bruneau and Akaaboune, 2010), suggesting a tight activity-dependent control over postsynaptic receptor dynamics at the NMJ.

Indeed, components of the postsynaptic apparatus turn over continuously and function to dynamically maintain the integrity of the postsynaptic structure. For instance, the AChR scaffolding molecule, rapsyn was recently shown to turnover faster than AChRs (Bruneau and Akaaboune, 2010), suggesting rapid and ongoing recycling of multiple components of the postsynaptic apparatus at mature NMJs. Neural agrin can influence this homeostatic remodeling by binding to dystroglycans (Gee et al 1994) which are capable of regulating AChR recycling and subunit composition through an interaction with dystrobrevin (Akaaboune et al 2002). Dystrogylcans and associated

proteins are essential for normal muscle function, as mutations in their genes cause muscular dystrophy in humans (for review see Blake et al 2002). Together these findings suggest a dynamic and ongoing regulation of postsynaptic receptor abundance and subunit composition which can be actively controlled by synaptic activity and which are essential for normal motor function.

Presynaptic differentiation and stabilization

Presynaptic differentiation can generally be characterized by the arrest of presynaptic outgrowth, the accumulation of presynaptic vesicles to terminal synapses and the alignment of presynaptic active zones with postsynaptic sites. These processes are intimately controlled by retrograde muscle activity and ultimately allow for the emergence of functional and stable neurotransmission properties required for normal muscle function.

For appropriate synaptogenesis, motoneuron growth cones must first transit from a cellular organelle specific for growth and guidance into a highly differentiated nerve terminal specialized for the transmission of electrochemical information. Recently, *in vivo* imaging experiments have revealed that the arrest of terminal arbor growth highly depends on the formation and stabilization of synapses along axon branches (Ruthazer and Cline, 2006; Meyer and Smith, 2006; Sann et al 2008; Ben Fredj et al 2010). The most highly stable synapses are generally those exhibiting a robust accumulation of presynaptic vesicles (Ruthazer and Cline, 2006; Meyer and Smith, 2006), suggesting that stable synaptogenesis is correlated with enhanced vesicle abundance and that the distribution of synaptic vesicles ultimately guides the development of axon aborizations in the CNS and PNS.

Recent evidence demonstrates that the differential mobilization of presynaptic resources, including synaptic vesicles and related fusion machinery, throughout the arborization may influence the selection of stable synaptic partners (Krueger et al 2003; Frischknecht et al 2008; Staras et al 2010; Ratnayaka et al 2011). Indeed, growing motor axons mobilize active axonal synaptic puncta to sites of myotube contact *in vitro* (Young and Poo, 1983; Zakharenko et al 1999; Hata et al 2007) and developing motor terminal arbors actively redistribute the axonal resources of pruned terminal branches *in vivo*

(Tapia et al 2012). The direct redistribution of presynaptic resources may be governed by local calcium signaling which influences the mobility of synaptic vesicles and active zones at developing *Drosophila* NMJs (Reiff et al 2002; Shakiryanova et al 2007). Refined activity of this developmental program could lead to the differential distribution of distinct populations of synaptic vesicles which could differentially contribute to the formation and stabilization of new synapses (Zakharenko et al 1999; Hata et al 2007; Andreae et al 2012).

Extracellular matrix (ECM) -related molecules play a fundamental role in presynaptic differentiation and contribute to stabilization and maturation of the NMJ through a number of sequential signaling pathways (Porter et al 1995; Nishimune et al 2004; Fox et al 2007). Fibroblast growth factors (FGFs) are required for appropriate clustering of synaptic vesicles to synaptic sites and act through the presynaptic 2b receptor isoform (FGFR2b) early in the development of mouse NMJs (Fox et al 2007). Collagen IV chains are highly enriched in the synaptic ECM (Sanes et al 1990), are also required for appropriate clustering of presynaptic vesicles early in the development of mouse NMJs, and function throughout adulthood to maintain the integrity of postsynaptic apparatus (Fox et al 2007). Likewise, ECM-bound laminin β2 chains are synthesized by developing muscles and are localized specifically to ECM synaptic sites (Patton et al 1997). Consistent with a growth inhibitory influence (Porter et al 1995), laminin β2 chains bind to N ($Ca_v2.2$) and P/Q-VDCC ($Ca_v2.1$) to organize the differentiation of presynaptic motor terminals and to regulate their stability *in vivo* (Nishimune et al 2004). The β1 and β4 subunits of these Ca^{2+} channels in turn form complexes with presynaptic scaffolding molecules such as bassoon and CAST/Erc2 to precisely align synaptic vesicle fusion machinery and VDCCs to promote the appropriate development of neurotransmission and muscle function (Chen J. et al 2011).

Synaptic transmission

Stable motor terminals are characterized by their very large size and their abundance of presynaptic vesicles and active zones which together determine the strength and reliability of neuromuscular synaptic transmission. Pioneering studies on the frog NMJ, performed in the laboratory of Dr. Bernhard Katz at University College, London were

instrumental in determining the basic biophysical and statistical mechanisms of quantal neurotransmission at mature synapses (Del Castillo and Katz, 1954a, b, c). In short, these studies have demonstrated that presynaptic terminals package neurotransmitter in discrete quantal units which are released into the synaptic cleft in a probabilistic fashion by action-potential initiated presynaptic Ca^{2+} currents (Del Castillo and Katz, 1954a, b; Katz and Miledi, 1968). Later studies examining the ultrastructure of presynaptic nerve terminals immediately following a presynaptic stimulus identified synaptic vesicles as the carriers of quantal units and demonstrated that these vesicles undergo exo-endocytic recycling in response to presynaptic excitation (Miller and Heuser, 1980). The statistical regulation of synaptic vesicle fusion and recycling controls the strength of transmission at individual synapses and hence, the reliability of information transfer in neural circuits, and continues to be a topic of great interest in neuroscience (Branco and Staras, 2009).

Synaptic vesicle pools

Synaptic vesicles effect neurotransmission through regulated, synchronous fusion in response to action potential-mediated increases in intracellular Ca^{2+} (Katz and Miledi, 1967) or by spontaneous, asynchronous fusion which occurs in the absence of action potential excitation but can likewise be modulated by extracellular Ca^{2+} (Elmqvist and Feldman, 1965; Silinsky et al 1977; Groffen et al 2010). The likelihood of synaptic transmission at a given synapse (its probability of release; p_r) depends a multitude of presynaptic variables, including the abundance of vesicles in the presynaptic terminal, the likelihood that a single synaptic vesicle will dock and fuse with the presynaptic membrane upon the presentation of a given stimulus (vesicular probability of release or p) and the number of active zone sites which are available to support vesicle fusion (n).

Optical assessments of synaptic transmission with the styryl dyes FM1-43 and its derivatives have clearly demonstrated that specific subclasses of synaptic vesicles can be differentially mobilized at the NMJ and fuse with the presynaptic membrane under varying stimulation conditions (Betz et al, 1992; Betz and Bewick, 1993; Richards et al 2000, 2003). Vesicles from the readily releasable pool (RRP) fuse immediately following a presynaptic stimulus and possess the highest values of p; while vesicles from the recycling pool (RP) are recruited under more intense and prolonged stimulation and

therefore possess a relatively lower value of *p* (Hua et al 2011). Vesicles from the reserve pool are only reluctantly released during periods of intense or very high frequency stimulation and function to supplement transmission mediated by RP vesicles and have a very low *p* value.

This differential recruitment of synaptic vesicles during various forms of presynaptic stimulation may be due to the anatomical localization of vesicle pools in the presynaptic terminal or the association of different *p* values to vesicles belonging to specific pools. Ultrastructural evidence suggests that different synaptic vesicle pools are distributed homogenously throughout a terminal, arguing against a spatial regulation of fusion efficiency (Richards et al 2003; Rizzoli and Betz, 2004; Denker and Rizzoli 2010; Hua et al 2011). Rather, individual synaptic vesicle pools can be molecularly distinguished based on their complement of vesicular proteins and calcium sensors (Ramirez et al 2012; Cao et al 2011; Hua et al 2011), which together influence the vesicle population`s unique *p* value (Stein et al 2007; Xu et al 2007; Holt et al 2008; Lee et al 2010; Groffen et al 2010). Further, these molecularly defined synaptic vesicle populations are known to be generated via the sorting of recycled synaptic membrane through specified endocytic routes (Richards et al 2000; Voglmaier et al 2006, 2007; Cheung et al 2010; Chung et al 2010; Hua et al 2011), suggesting a rapid and modifiable mechanism for the regulation of p_r (Ratyanaka et al 2012).

While both high and low *p* vesicles fuse spontaneously (Hua et al 2011), some evidence suggests that low *p* vesicles preferentially recycle at rest (Sara et al 2005; Ramirez et al 2012) and may therefore be in a position to regulate specific aspects of circuit development (Saito et al 2001; Sutton et al 2006; Andreae et al 2012). Recent investigation into the mechanisms of presynaptic plasticity at CNS synapses in hippocampal slice preparations or dissociated hippocampal culture have revealed a dynamic mobilization and exchange of functional synaptic vesicles within and between existing synapses and to novel synaptic sites during long term potentiation (LTP) and synaptogenesis (Krueger et al 2003; Staras et al 2010; Ratnayaka et al 2012), demonstrating that distinct synaptic vesicle pools are differentially implicated in the formation and strengthening of new synapses. These findings are especially relevant for the understanding of the preferential distribution of synaptic resources across terminal

arbors, where p_r can vary profoundly from one synaptic terminal to the next on the same axon (Bennett et al, 1986; Robitaille and Tremblay, 1991; Cooper et al 1996; Branco et al 2008).

Synaptic homeostasis at the motor terminal

Presynaptic motor nerve terminals are established and maintained throughout the life of the animal and depend highly on the functional state of the postsynaptic muscle for their structural and functional integrity. Early investigations into the molecular factors which contribute to the maintenance of motor nerve terminals of *Drosophila* larva have identified the cell adhesion molecule (CAM) Fasciclin II (*FasII*) as an important regulator of terminal growth and stability (Schuster et al 1996; Stewart et al 1996). *FasII* is a member of the Ig superfamily (IgSF) of CAMs and is the *Drosophila* homologue to the neural cell adhesion molecule (NCAM) in vertebrates. Loss of function mutations in the *fasII* gene leads to presynaptic withdrawal of motor terminals in *Drosophila* larva, although initial neuromuscular innervation was found to proceed normally (Schuster et al 1996). Interestingly, both pre and postsynaptic expression of *FasII* is required to rescue this phenotype, suggesting a requirement for trans-synaptic CAM signaling in the regulation of presynaptic stability. Furthermore, although transmission strength was found to be unaffected at developing *FasII*-deficient NMJs, presynaptic terminals were observed to be significantly smaller and individual boutons were found to exhibit enhanced quantal amplitudes, suggesting a dynamic regulation of presynaptic density and strength by altered *FasII* levels (Stewart et al 1996). These findings can be at least partially attributed to a retrograde signal derived from the postsynaptic muscle fiber (Davis and Goodman, 1998) as similar phenotypes are observed in larva with altered glutamate receptor subunit composition (*DGluRIIA* mutants) (Petersen et al 1997; Reiff et al 2002) or in experiments where postsynaptic receptor activity is acutely blocked (Frank et al 2006). The nature of this retrograde regulation may be attributed to mechanisms of postsynaptic differentiation and protein translation which are known to influence the efficacy of presynaptic transmission at *Drosophila* terminals (Sigrist et al 2000) and the structural integrity of the presynaptic terminal at mouse NMJs (Nguyen et al 2000; McCann et al 2007). These findings

demonstrate that not only the functional state of the postsynaptic cell, but the metabolic activity in the postsynaptic cell may contribute to the structure and function of the innervating motor terminal.

Mechanisms of presynaptic degeneration

In comparison to widespread postsynaptic blockade which is known to induce presynaptic strengthening at mature rodent NMJs (Plomp et al 1992), focal blockade of postsynaptic receptors induces motor terminal withdraw from the silenced subregion of the synapse (Balice-Gordon and Lichtman, 1993). This finding suggests that presynaptic homeostasis is not solely governed by the absolute amounts of postsynaptic activity, but rather is determined by the relative degree of activity generated across a single synapse. In addition, the findings demonstrate that motor terminal withdrawal is not simply a passive process, but the product of active signaling cascades derived through competitive signaling (Colman et al 1997; Buffelli et al 2003; Kasthuri and Lichtman, 2003).

Retrograde degeneration of motor terminals is observed in early stages of mouse models of motoneuron disease (MND) and exhibit striking similarities to that observed during developmental pruning and following axotomy (Miledi and Slater, 1970; Bishop et al, 2004; Schefer et al 2005: Song et al 2008), suggesting some conserved mechanisms of axonal and synaptic degeneration and withdrawal. However, the specific degenerative programs initiated following axotomy differ from those evoked during development (Gillingwater and Ribchester, 2003; Gillingwater et al 2003; Bishop et al 2004) primarily in the mechanism of induction, the extent of axon branch removal and in the involvement of protein ubiquitination pathways (Mack et al 2001; Watts et al 2003). For instance, Wallerian degeneration slow (Wld^s) mice exhibit delayed axonal degeneration following axotomy due to gain of function mutations in a gene coding for ubiquitination factor E4B (*Ube4b*) (Mack et al 2001). Although this mutation does not delay developmental axon pruning (Hoopfer et al 2006), it significantly delays disease progression in a mouse model of MND (Ferri et al 2003). These results suggest that degenerative mechanisms are tightly and differentially controlled in the developing and adult organism.

Principles of regeneration

Following denervation, peripheral motor nerves possess a robust ability to regenerate along appropriate motor pathways (Brushart, 1993; Franz et al 2005, 2008) and to reinnervate original endplate regions (Sanes et al 1978; Nguyen et al 2002). Although the mechanisms of denervation may vary, some principles of regeneration follow similar general guidelines, such as the contribution of glial cells (Son and Thompson, 1995a, b) and the requirement for the induction to regenerative growth programs in motor axons (Mehta et al 1993; Allodi et al 2012). However, motor axon regeneration can be generally subclassified into at least two distinct categories which differ in the identity and the extent of the contributing motoneurons. Figure 1.2 illustrates the organization of MUs in adulthood (Figure 1.2*A*), following regeneration after complete denervation by nerve crush injury (Figure 1.2*B*; see Chapter 2) and following partial muscle denervation by spinal root transection and ligation (Figure 1.2*C*; see Chapter 3). Complete muscle denervation leads to whole nerve regeneration which involves the regrowth and reinnervation of the entire motor pool of the denervated muscle. In comparison, partial denervation of skeletal muscle leads to local sprouting of the remaining motor axons and therefore only involves the 'regeneration' of a subpopulation of the motor pool which hasn't itself been directly afflicted by pathology. These mechanisms lead to substantial differences in the ultimate size of established motor units and have implications for functional outcomes.

Whole nerve regeneration

Motor axons initiate a regeneration program in response to whole muscle denervation which largely depends on the loss of retrograde support from the affected muscle (Shin et al 2012). Axons distal to the injury site degenerate following the initial insult while proximal collateral axons begin to sprout at the lesion site. These collateral axons function to sample the extracellular environment for guidance cues which will target them to appropriate Schwann cell-derived conduits and eventually lead to their appropriate end organ (Sanes et al 1978; Brushart, 1993; Franz et al 2005, 2008). At the muscle itself, terminal Schwann cells proliferate and sprout extensively in response to

denervation to guide the reinnervation of regenerating motor axons (Son and Thompson, 1995a; Love and Thompson, 1998). This response can be mimicked through the selective initiation of neuregulin (aka ARIA) signaling in Schwann cells which also induces the extension of axon sprouts along Schwann cells processes in the absence of denervation (Hayworth et al 2006). Neuregulin is known to be highly expressed by Schwann cells in axotomized nerve (Carroll et al 1997), suggesting an autocrine regulation of glial reactivity in response to muscle denervation.

Once having attained a target muscle, regenerating motor axons initially reform MU with larger IRs, as many reinnervated postsynaptic sites are initially innervated by several regenerating axons (Ribchester and Taxt, 1983). Supernumerary terminals are later retracted through a process of competition similar to that observed during developmental reorganization (Ribchester and Taxt, 1983) and IRs of MUs are reduced to levels observed during development (Gordon and Stein, 1982). These data suggest a conserved MU size across a motor pool following regeneration.

Motor unit / Terminal field expansion

Motor terminal sprouting in response to partial muscle denervation is fundamentally distinct from whole nerve regeneration, as it involves a local regenerative response from motor axons which had not been directly affected by axotomy or degeneration (Brown and Ironton, 1978; Rochel and Robbins, 1988; Chang and Keshishian, 1996). Upon partial muscle denervation, nearby motor terminals sprout to reinnervate denervated endplates; forming axon bridges between synapses and effectively increasing the IR of the remaining MUs (Brown and Ironton, 1978). Importantly, sprouting MU enlarge in direct proportion to their original size (Rafuse et al 1992). Induction of this compensatory response is primarily due to the sprouting of tSCs which sprout extensively at denervated junctions and stimulate the extension of terminal axon sprouts from NMJs with intact innervation (Son and Thompson, 1995b; Love and Thompson, 1999). This process is tightly regulated by the level of neuromuscular activity, as enhancing or decreasing activity of muscle fibers or of the remaining innervation reduces motor axon reinnervation by inhibiting the formation of axon sprouts and/or Schwann cell bridges (Tam et al 2001; Love et al 2003; Tam and Gordon, 2003).

Motor units do not have the capacity to expand indefinitely, as severely partially denervated muscles do not fully recover complete reinnervation or maximal contractile force of the afflicted muscle (Brown and Ironton, 1978; Rafuse et al 1992). In addition, a subset of sprouted innervation can be replaced by other regenerating motor terminals under severely denervated conditions (Brown and Ironton, 1978; Rafuse et al 1992), suggesting that presynaptic resources supplying a spouted MU are limited and that extensively sprouted MUs contain a subset of innervation which can be easily displaced by competing axons (Laskowski et al 1998). The factors which limit extensive MU expansion are therefore limited by the supply of some resource which is involved in competitive neuromuscular transmission.

1.3 Cell adhesion molecules

Cell adhesion molecules (CAMs) are a very broad class of cell surface molecules which function to regulate the physical interaction and adhesion of cellular membranes to generate the grouping of cells into functional units (Rutishauser and Landmesser, 1996; Clegg et al 2003; Maness and Schachner, 2007; Takeichi, 2007; Demireva et al 2011). Many different kinds of CAMs are known to participate in the initial organization and maintenance of synaptic function and the immunoglobulins (Ig) in particular are known to influence the patterned organization of neural tissue (Buskirk et al 1980; Rafuse and Landmesser, 2000). Ig molecules such as NCAM and L1 can bind in cis along the membrane, or in trans across cell membranes locally via direct adhesion (Rutishauser et al 1982) or systemically via secretion of solubilized forms (Bock et al 1987). Extracellular binding affinities can be manipulated by the addition or removal of chains of polysialic acid (PSA) to the extracellular domains of NCAM (Rutishauser and Landmesser, 1996), by the exocytic addition or endocytic removal of CAMs at the cell surface (Thelen et al 2008; Yap et al 2010; Chernyshova et al 2011), and/or by the manipulation of ECM integrity (Probstmeier, 1989, 1992; Reist et al 1992; Edvardsen et al, 1993). This manipulation of CAM binding and signaling functions to tightly control homeostatic cell growth and plasticity.

Here I will review the organizational properties of the NCAM, a member of the IgSF and one of the first adhesion molecules described to be implicated in the development of the nervous system (Rutishauser et al 1982).

NCAM – The neural cell adhesion molecule

Function

NCAM was originally isolated from purified chick retina where it was found to promote cell-to-cell adhesion and the appropriate organization of retinal tissues (Thiery et al 1977; Buskirk et al 1980). These studies, performed in the laboratory of Dr. Gerald Edelman, were among the first to directly investigate the molecular mechanisms responsible for the patterning of the nervous system and paved the way for a field of study investigating the organizational role of CAMs in development and regeneration of complex tissues. Interestingly, the very early studies on CAMs were derived from Dr. Edelman's work on the immune system in which he and his collaborators provided evidence for the molecular anatomy of a cell membrane as the effectors of cellular recognition (Edelman et al 1961). Indeed, members of IgSF function widely in the immune system (Husmann et al 1989), demonstrating that they convey a highly developed mechanism of cellular self identification.

Form

NCAM is widely distributed throughout the nervous system and exists in a wide variety of isoforms which are generated via the alternative splicing of a single gene product (Cunningham et al 1987). A generic NCAM protein can be functionally divided into two subunits; an extracellular domain composed of five Ig domains and two fibronectin domains (FN); and a transmembrane domain of variable length or a glycophosphatidylinositol (GPI)-linked membrane domain (Figure 1.3*A*-*B*).

The extracellular domains are relatively conserved throughout all NCAM isoforms and can bind the Ig domains of other IgSF molecules (Frei et al 1992; Zhou et al 1993; Horstkorte et al 1993; Milev et al 1994; Anderson et al 2005). Chains of PSA molecules bind to the Ig5 domain of NCAM (Crossin et al 1984) and promotes cellular de-adhesion required for synaptic plasticity (Muller et al 1996; Eckhardt et al 2000;

Dityatev et al 2004), peripheral pathfinding (Tang et al 1992; Franz et al 2005) and terminal arborization (Landmesser et al 1990; Rafuse and Landmesser, 2000). Unpolysialyated extracellular NCAM domains are free to bind in cis to FGFRs via the FN domains or to GDNF molecules at the Ig3 domain to influence the kinetics of outgrowth (Paratcha et al 2003; Anderson et al 2005; Kiselyov et al 2005; Nielsen et al 2009; Chernyshova et al 2011). In addition, the extracellular domains of NCAM are susceptible to alternative splicing which can regulate the molecule's adhesive and signaling properties. For instance, the VASE domain (variable domain spliced exon) in Ig4 is highly expressed in the CNS and negatively influences NCAM's outgrowth promoting properties (Doherty et al 1992), while the muscle-specific domain (MSD) is highly expressed by muscle cells and may be involved in myotube fusion (Thompson et al 1989; Peck and Walsh, 1993).

In general, three major NCAM isoforms exist in the nervous system and are named according to their molecular weights; NCAM180, 140 and 120kD. NCAM-180kD contains the longest intracellular domain which includes an alternatively spliced insert at exon 18 to provide binding sites on the NCAM protein for cytoskeletal elements such as spectrin (Cunningham et al 1987; Leshchyns'ka et al 2003). Both NCAM-180kD and NCAM-140kD contain a conserved C-terminal domain which includes a PDZ-like binding motif, referred to as the KENESKA domain which participates in synaptic vesicle recruitment during repetitive stimulation at the mouse NMJ (Figure 1.3*B, C*) (Polo-Parada et al 2005). NCAM-120 lacks an intracellular domain and is linked to the cell membrane via a GPI linker (Figure 1.3*B*). Due to the variability in structure, distinct NCAM isoforms differentially contribute to a variety of NCAM-mediated signaling mechanisms (Edvardsen et al 1993; Leshchyns'ka et al 2003; Polo-Parada et al 2004; Hata et al 2007).

Localization and regulation of NCAM expression at the NMJ

NCAM is broadly expressed by growing motor axons and developing muscle fibers before cell-to-cell contact, after which it becomes concentrated at synaptic regions (Covault and Sanes, 1986). Ultrastructural analysis of NCAM distribution at adult NMJs have demonstrated the localization of NCAM to synaptic regions of ECM, to

extracellular contacts between tSCs and motor terminals, to synaptic vesicles in nerve terminals, at the base of postsynaptic junctional folds, in subsynaptic T-tubules, and along the surface of muscle satellite cells (Covault and Sanes, 1986). All NCAM isoforms are distributed throughout these cell types and subcellular compartments at the mouse NMJ (Reiger et al 1985; Hamshere et al 1991; Rafuse and Landmesser, 1996), although nerve terminals mostly contain NCAM-140kD and 180kD (Reiger et al 1985; Polo-Parada et al 2005), while the 120 is mainly expressed by glial cells (Noble et al 1985; Bhat and Silberberg, 1986). The addition of the MSD sequence to the *NCAM* gene expressed by skeletal muscle generates heavier isoforms of 130, 145 and 155kD which are differentially regulated by contractile activity via Ca^{2+} influx through L-VDCCs and activation of PKC (Hamshere et al 1991; Rafuse and Landmesser, 1996).

NCAM in the development and stability of the synapse

NCAM expression is high in muscle and nerve during development, reduced throughout adulthood, and strongly re-expressed following muscle denervation or paralysis (Reiger et al 1985, 1988; Covault and Sanes, 1985), suggesting a control of NCAM expression by neural activity. NCAM maintains a presence at synaptic sites throughout the lifetime of the animal (Covault and Sanes, 1986) and actually becomes more highly expressed during later stages of ageing (Kobayashi et al 1992; Andersson et al 1993). Together these findings suggest an activity-dependent regulation of NCAM function at the mammalian NMJ throughout the lifespan of the animal which may influence the normal functioning of the synapse.

NCAM in synaptogenesis

Studies performed at the *Drosophila* NMJ were the first to examine a dynamic regulation of IgSF adhesion molecules in synaptic stability (Schuster et al 1996, Stewart et al 1996; Landmesser, 1997, 1998; Davis and Goodman, 1998). Later studies examining the function of NCAM at peripheral and central synapses in mice have identified a specific role for this CAM in presynaptic vesicle mobilization, neurotransmission strength and postsynaptic remodeling (Dityatev et al 2000; Rafuse et al 2000; Sytnyk et al 2002, 2006; Polo-Parada et al 2001, 2004, 2005). I will now conclude this introduction with a focus

on recent work performed in the laboratory of Dr. Lynn Landmesser which has highlighted a fundamental requirement for NCAM in the functional and structural maturation of the mammalian NMJ.

NCAM as a regulator of synaptic vesicle cycling and neurotransmission

During motoneurite outgrowth and early motoneuron/myotube contact *in vitro*, NCAM-180kD and 140kD are localized to cycling synaptic puncta along the length of the axon and are shuttled to sites of early cell to cell contact (Hata et al 2007). Synaptic vesicle recycling at axonally distributed synaptic puncta requires the activity of L-VDCCs and is inhibited by application of brefeldin A (BFA) (Zakharenko et al 1999, Hata et al 2007); a specific inhibitor of AP-3 mediated synaptic vesicle biogenesis (Faúndez et al 1997). Interestingly, these 'immature' axonally-localized synaptic puncta are down-regulated upon putative synaptic contact *in vitro* (Hata et al 2007) and require the presence of NCAM for down-regulation *in vivo* (Polo-Parada et al 2001). The emergence of mature mechanisms of synaptic transmission which rely on the activity of the P/Q-VDCC and which are insensitive to BFA, are coincident with the silencing of the immature transmission phenotype, suggesting these processes may be mechanistically linked. Remarkably, postsynaptic expression of NCAM is required for the specific shuttling of the presynaptic NCAM-140 isoform (Hata et al 2007), demonstrating a specific postsynaptic influence over presynaptic isoform mobilization and vesicle recycling phenotype. Indeed, other studies examining the strength and plasticity of hippocampal synapses have identified a fundamental role for postsynaptic NCAM in the regulation of synaptic strength (Dityatev et al 2000; Kochlamazashvili et al 2012).

NCAM signaling is specifically important in the regulation of different forms of synaptic vesicle cycling (Rafuse et al 2000; Polo-Parada et al 2001, 2004, 2005). *NCAM*$^{-/-}$ motor terminals exhibit a higher synaptic p_r at basal transmission rates, reduced paired-pulse facilitation, and heightened depression during high frequency stimulation which coincides with periodic failures in presynaptic transmission (Rafuse et al 2000; Polo-Parada 2001, 2004, 2005). Some of these deficits may be due to improper Ca^{2+} handling in presynaptic terminals (Polo-Parada et al 2001, 2004). These findings suggest parallel increases in the p_r under low stimulation conditions and reduced p_r during high frequency

stimulation. These functional alterations correspond to significant changes in gross synaptic morphology, characterized by reduced endplate areas and altered distribution of presynaptic vesicles (Rafuse et al 2000; Polo-Parada et al 2001). These results suggest the presence of homeostatic mechanisms which compensate for deficits in gross synaptic organization with increases in synaptic efficacy - remarkably similar to the effects observed at FasII-deficient fly NMJs (Stewart et al 1996).

Further studies have implicated distinct NCAM isoforms in mediating these influences on synaptic release. Neuromuscular junctions in NCAM180kD specific knock-out mice (*NCAM180*$^{-/-}$) appropriately down-regulate BFA and L-VDCC sensitive cycling machinery and have normal transmission strengths, suggesting the 140kD and/or 120kD isoform is specifically involved in the regulation of growth-specific vesicle cycling mechanisms and the regulation of basal synaptic strength (Polo-Parada et al 2004). In comparison, *NCAM180*$^{-/-}$ motor terminals exhibit aggravated transmission failures during repetitive stimulation and altered Ca^{2+} sensitivities, implicating the 180kD isoform in Ca^{2+}-mediated, high frequency transmission. Using a novel peptide introduction technique, the KENESKA domain of NCAM-180 isoform was found to be responsible for myosin light chain kinase (MLCK) activation to enable effective mobilization of synaptic vesicles during high frequency stimulation at mouse NMJs (Polo-Parada et al 2005; Maeno-Hikichi et al 2011). However, although *in vitro* assessments have revealed fundamental and distinct organization of pre and postsynaptically derived NCAM in NMJ organization (Hata et al 2007), the cell-type specific functional roles of these proteins have yet to be determined *in vivo*.

1.4 Summary of objectives

The overall objective of this thesis is to describe the functional implications of synaptic regeneration and stabilization of the NMJ in the mouse. We decided to focus on the organizational properties of NCAM because of its presence during neuromuscular regeneration (Covault and Sanes, 1985, 1986; Franz et al 2005), its role in presynaptic resource distribution (Rafuse et al 2000; Sytnyk et al 2002; Hata et al 2007), and its dynamic control over neurotransmission strength at mammalian NMJs (Rafuse et al 2001; Polo-Parada et al 2001, 2004, 2005). Furthermore, through the use of conditional

knock-out technology and stem cell biology, we aimed to determine a cell-type specific role for NCAM in the organization of the NMJ.

The specific objectives of this thesis are:

Chapter 2:

1. To determine the contribution of NCAM to the time course of functional muscle recovery following complete muscle denervation via nerve crush injury.
2. To determine the functional properties of reinnervated synapses following a complete muscle denervation and the role of NCAM in re-establishing appropriate neurotransmission.
3. To determine the role of pre and postsynaptic NCAM in the maintenance of neurotransmission and the structural integrity of regenerated synapses following a complete nerve crush injury.

Chapter 3:

4. To investigate the functional relationship between synaptic resource redistribution and the functional properties of neurotransmission at sprouting and reinnervated NMJs during MU expansion.
5. To investigate the role of pre and postsynaptic NCAM in the functional recovery of muscle function following partial muscle denervation.
6. To investigate the mechanisms limiting extensive MU expansion in the mouse.

Chapter 4:

7. To generate a reproducible and sensitive model of mature neuromuscular synaptic function *in vitro*.
8. To describe the developmental characteristics of neuromuscular synaptogenesis in this model system.
9. To use this *in vitro* system of mature NMJs to investigate presynaptic NCAM-mediated mechanisms in the regulation of neurotransmission required for synaptic stability.

CHAPTER 1 FIGURES

Figure 1.1: The cellular anatomy of the tripartite neuromuscular junction (NMJ). **(A)** An adult mouse NMJ immunolabeled with antibodies against neurofilament and SV2 to identify presynaptic motor nerve terminals (green), tetramethylrhodamine-conjugated α-bungarotoxin (α-BTX) to identify postsynaptic AChRs on the surface of the muscle fiber (red), and with S100 to identify Schwann cells (blue). **(B)** A cut-away illustration by Frank Netter, Medical Illustrator of a NMJ with several important structures identified.

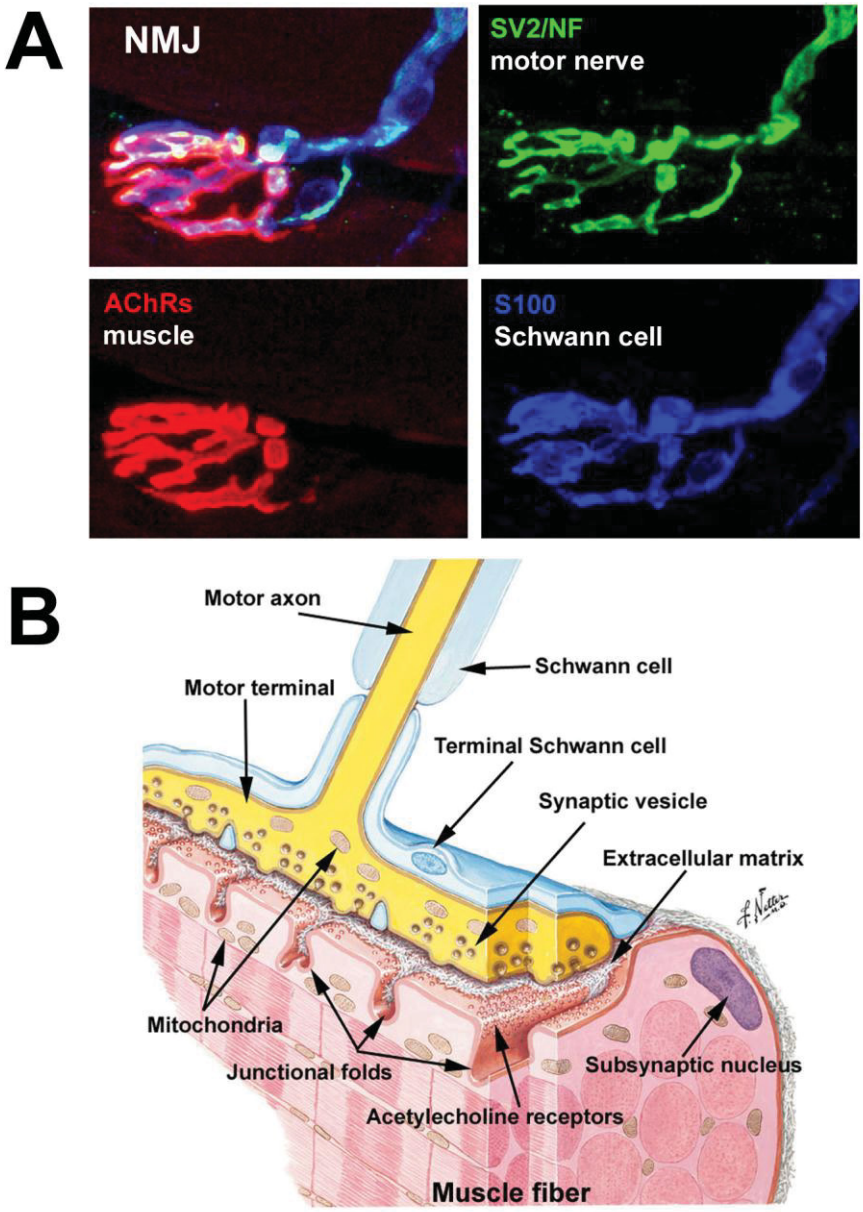
A
NMJ
SV2/NF
motor nerve
AChRs
muscle
S100
Schwann cell
B
Motor axon
Schwann cell
Motor terminal
Terminal Schwann cell
Synaptic vesicle
Extracellular matrix
Mitochondria
Junctional folds
Subsynaptic nucleus
Acetylecholine receptors
Muscle fiber

Figure 1.2: Differences between MU reorganization following nerve crush and partial denervation. **(A)** Unoperated motor units (MUs) are established and refined during development to provide complete innervation (yellow/blue filled circles) to the target muscle. Different MUs are distributed throughout the muscle and are intermingled with one another. **(B)** Nerve crush injuries result in the regeneration of the entire motor pool of the afflicted muscle and ultimately lead to the re-establishment of original MU sizes. **(C)** Partial denervation leads to the expansion of intact MUs by local terminal and nodal axon sprouting. Large MUs are maintained, but often muscles remain incompletely reinnervated and some endplates remain denervated (red circles).

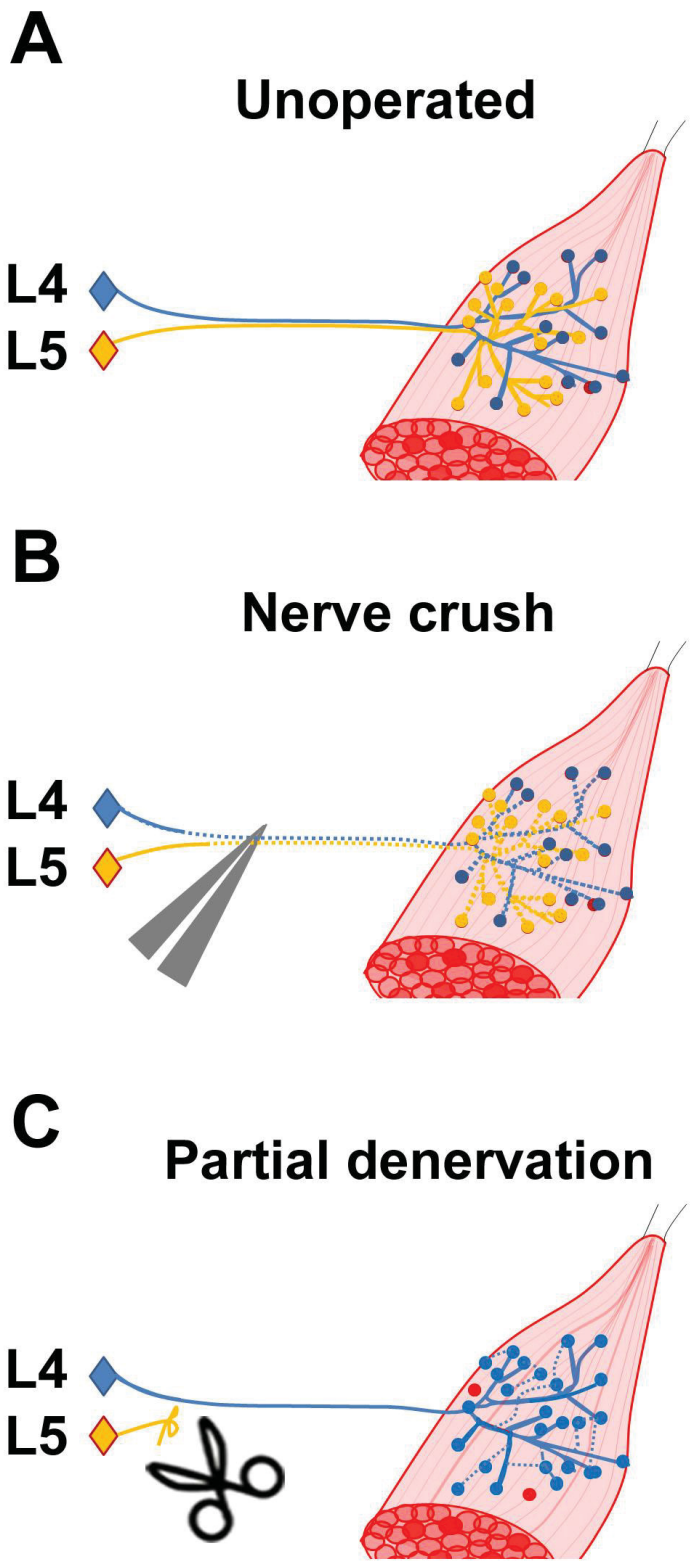
A
Unoperated
L4
L5
B
Nerve crush
L4
L5
C
Partial denervation
L4
L5

Figure 1.3: The molecular anatomy of NCAM and its role in synaptic transmission. **(A)** Illustration of the molecular composition and orientation of three NCAM isoforms in the cell membrane. Five immunoglobulin domains (Ig1-5) and two fibronectin III domains (FN1,2) characterize the extracellular components of NCAM120kD, 140kD and 180kD and participate in homeophilic binding with other Ig molecules and heterophilic binding to growth factors and growth factor receptors. **(B)** The membrane linkages and intracellular domains differ between NCAM isoforms and participate in distinct intracellular signaling events. The C-terminal domains of NCAM140kD and 180kD contain a PDZ-like binding domain, referred to as the KENESKA domain. **(C)** KENESKA domains participate in synaptic vesicle recycling at mouse motor terminals during Ca^{2+}-mediated high frequency stimulation by activating intracellular kinases such as the myosin light chain kinase (MLCK). *(A)* Adapted with permission from Sandi, 2004, *(B)* and *(C)* adapted with permission from Polo-Parada et al 2005.

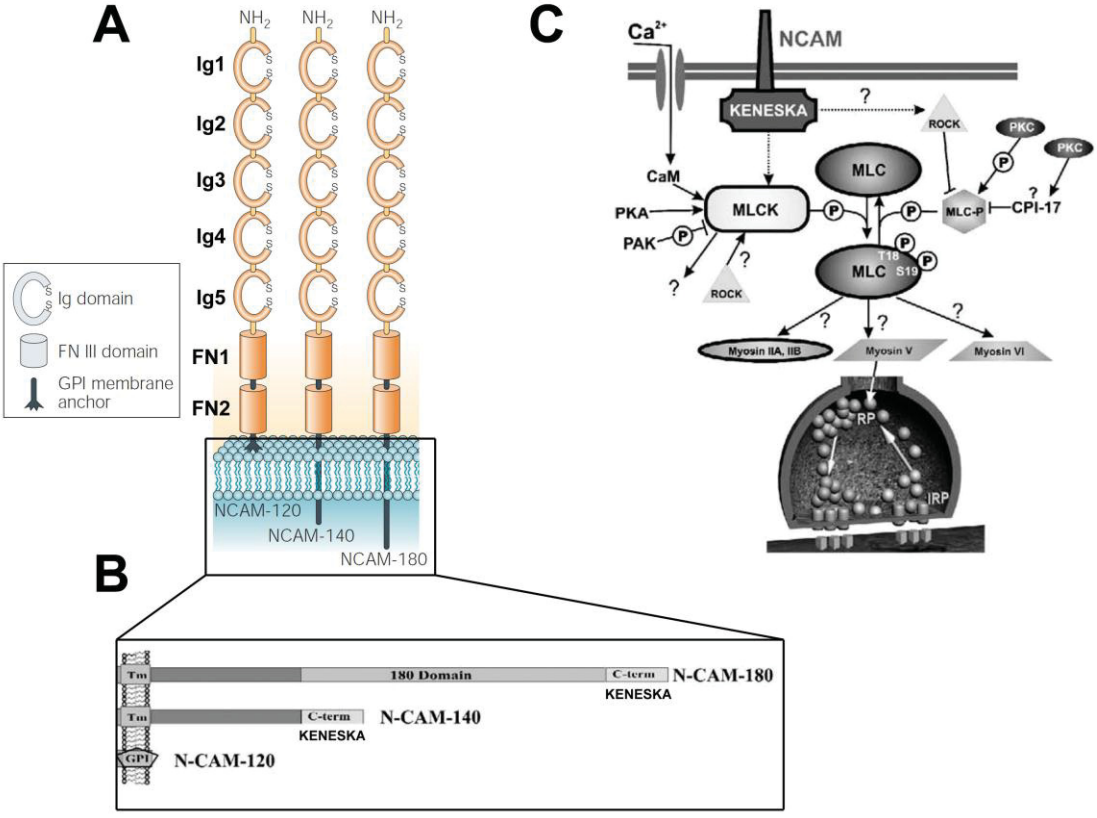
A
NH2
NH2
NH2
Ig1
Ig2
Ig3
Ig4
Ig5
FN1
FN2
Ig domain
FN III domain
GPI membrane anchor
NCAM-120
NCAM-140
NCAM-180
B
Tm
180 Domain
C-term
N-CAM-180
KENESKA
Tm
C-term
N-CAM-140
KENESKA
GPI
N-CAM-120
C
Ca2+
NCAM
KENESKA
?
ROCK
PKC
PKC
P
CaM
MLC
PKA
MLCK
P
P
MLC-P
CPI-17
?
PAK
P
?
P
T18
MLC
S19
P
?
ROCK
?
?
?
Myosin IIA, IIB
Myosin V
Myosin VI
RP
IRP

CHAPTER 2: The neural cell adhesion molecule (NCAM) is required for stability of regenerated neuromuscular junctions

Abstract

Studies examining the etiology of motoneuron diseases usually focus on motoneuron death as the defining pathophysiology of the disease. However, impaired neuromuscular transmission and synapse withdrawal often precede cell death, raising the possibility that abnormalities in synaptic function contribute to disease onset. While little is known about the mechanisms maintaining synaptic integrity of neuromuscular junctions (NMJs), *Drosophila* studies suggest that Fasciclin II (FasII) plays an important role. Inspired by these studies we used a reinnervation model of synaptogenesis to analyze neuromuscular function in mice lacking the neural cell adhesion molecule (NCAM), the FasII vertebrate homolog. Our results showed that recovery of contractile force was the same in wild-type and *NCAM-/-* mice 1 month after nerve injury indicating that endplates were appropriately reformed. This normality was only transient because contractile force and myofiber number decreased 3 months after injury in *NCAM-/-* mice. Both declined further 3 months later. Myofibers degenerated, not because motoneurons died, but because synapses were withdrawn. Although neurotransmission was initially normal at reinnervated *NCAM-/-* NMJs, it was significantly compromised 3 months later. Interestingly, selective ablation of NCAM from motoneurons, or muscle fibers, did not mimic the deficits observed in reinnervated *NCAM-/-* mice. Taken together, these results indicate that NCAM is required to maintain normal synaptic function at reinnervated NMJs, although its loss pre- or post-synaptically is not sufficient to induce synaptic destabilization. Consideration is given to the role of NCAM on terminal Schwann cells for maintaining synaptic integrity and how NCAM dysfunction may contribute to motoneuron disorders.

Introduction

Progressive muscle weakness and wasting are defining symptoms associated with motoneuron diseases including amyotrophic lateral sclerosis (ALS) and spinal muscular atrophy (SMA). While these symptoms are usually attributed to motoneuron death, it remains to be determined whether this accurately reflects the pathophysiology of the disease process. For example, abnormalities in synaptic function appear in patients with ALS prior to electrophysiological signs of motoneuron degeneration (Maselli et al. 1993). Impaired neuromuscular transmission and synaptic withdrawal precedes motoneuron death in animal models of motoneuron disease (Frey et al., 2000; Kong et al., 2009). Finally, a transgenic mouse model of familial ALS dies due to synapse withdrawal at the neuromuscular junction (NMJ) even when cell death is prevented by genetic deletion of Bax (Gould et al, 2006). Together, these studies indicate that loss of synaptic integrity proceeds, and may even precipitate, muscle weakness and motoneuron death in various motoneuron diseases (Conforti et al., 2007). Unfortunately, the molecular mechanisms underlying destabilization of NMJs in motoneuron disease are not known. This is due, in part, because the cellular components responsible for synaptic stability are poorly understood.

Neural cell adhesion molecule (NCAM) is a candidate synaptic stability molecule because it is expressed on axons, terminal Schwann cells (tSCs) and myofibers during development (Nieke and Schachner, 1985; Covault and Sanes, 1986; Martini and Schachner, 1986; Rafuse and Landmesser, 2000). After nerve-muscle contact, NCAM is down-regulated along motor axons and muscle fibers in an activity-dependent manner (Rieger et al., 1985; Covault and Sanes, 1986). However, even into adulthood, NCAM remains highly expressed in pre-synaptic terminals, at the base of junctional folds, in subsynaptic T-tubules, and tSCs (Covault and Sanes, 1986). This continued expression suggests that NCAM regulates neuromuscular function after synaptic contact. Indeed, this is the case in *Drosophila* where its homolog, Fasciclin II (FasII; Harrelson and Goodman, 1988), is essential for maintaining NMJs during larval development (Schuster et al., 1996). In its absence, *Drosophila* larvae die because motor axons withdraw from newly formed synapses. While motor axons do not withdraw in *NCAM-/-* mice, they do form

smaller NMJs and exhibit neurotransmission deficits when stimulated at high frequencies (i.e. 200Hz; Rafuse et al., 2000; Polo-Parada et al., 2001).

Absence of axonal withdrawal in *NCAM-/-* mice indicates that it is either not required for synaptic stability or other gene products compensate for its loss during development (Moscoso et al., 1998; Gu et al., 2003). The present study was designed to address this issue using a reinnervation model of synaptogenesis. The rationale for this approach was based on the fact that many genes expressed during peripheral nerve development are not re-expressed after injury (Bosse et al., 2006). Our results show that recovery of contractile force was the same in wild-type and *NCAM-/-* mice 1 month after nerve injury. This similarity was only transient, however, because many newly formed synapses were later eliminated in *NCAM-/-* mice. This elimination was concurrent with deficits in neurotransmitter release, withdrawal of motor axons, and the presence of degenerating muscle fibers.

Materials and Methods

Mice

Four different strains of male and female mice were used. Wild-type C57BL/6 mice (Charles River, Wilmington, MA, USA) and *NCAM-/-* mice, generated on a C57BL/6 background (Cremer et al., 1994), were bred and housed locally. $NCAM^{flx/flx}$::$Hb9^{cre/+}$, which lack NCAM in motoneurons, were generated by breeding NCAM-floxed ($NCAM^{flx/flx}$) mice (Bukalo et al., 2004) with mice expressing cre-recombinase under control of the Hb9 promoter (Yang et al., 2001) while $NCAM^{flx/flx}$::$HSA^{cre/+}$ mice, which lack NCAM on muscle fibers, were generated by crossing $NCAM^{flx/flx}$ mice with mice expressing cre-recombinase under control of the HSA promoter (Miniou et al., 1999; Cifuentes-Diaz et al., 2001). Hb9 and HSA promoters are activated at E12.5 and P10, respectively (Yang et al., 2001; Cifuentes-Diaz et al., 2001). All procedures were conducted in accordance to the guidelines of the Canadian Council on Animal Care and the policies of Dalhousie University.

Surgery

All surgeries were performed on 12-week-old adult mice unless otherwise noted. Animals were anesthetized with isoflurane (Baxter, Toronto, ON, Canada) and 1 of 2 surgeries was performed under aseptic conditions. (1) A small incision was made in the skin above the knee in order to expose the tibial nerve. Using fine forceps, the tibial nerve was crushed 2 times consecutively 10 mm distal to its divergence from the sciatic. Denervation was visually confirmed by noting muscle contraction and subsequent transparency of the nerve at the crush site. (2) A small incision was made in the skin overlaying the dorsal shank muscles. The soleus muscle was exposed and 0.5 µl of 1% cholera toxin subunit b (CTB) conjugated to Alexa Fluor 594 (C22842; Invitrogen, Burlington, ON, Canada) was injected into the soleus muscle near the nerve entry point. To minimize pain and discomfort, all animals were provided with a 5 mg/kg subcutaneous injection of Anafen (Merial, Morgan Baie d`Urle, Quebec, Canada) immediately following each surgery as a postoperative analgesic.

In vitro isometric tension and EMG recordings

Mice were killed and their right hindlimb quickly dissected and placed into ice cold, oxygenated Tyrode's (125 mM NaCl, 24 mM NaHCO3, 5.37 mM KCl, 1 mM MgCl2, 1.8 mM CaCl2, and 5% dextrose). The soleus muscle and nerve supply was isolated and cut free at its insertion points on the femur and calcaneous bones. The proximal muscle tendon was securely pinned down on a Sylgard (Dow Corning, Midland, MI, USA) coated recording chamber that was perfused with oxygenated Tyrode's solution maintained at 20-22ºC. A suture (2-0) was tied to the distal tendon and connected to a force transducer (FT 03; Grass Technologies, West Warwick, RI, USA). A fine-tipped polyethylene stimulating suction electrode (PE-190; Clay Adams, Sparks, MD, USA) was used to deliver electrical current to the soleus nerve via a S88 stimulator (Grass Technologies) that was isolated from ground using a stimulus isolation unit (PSIU6; Grass Technologies). EMG was always recorded from the midbelly of the soleus muscle with a second polyethylene suction electrode and amplified with a bandwidth between 3 Hz and 10 kHz (EX4-400; Dagan Corporation, Minneapolis, MN, USA) as described by Rafuse et al. (2000). Monophasic electrical stimuli (0.01 ms) were used to elicit maximal isometric contractions and EMG responses which were acquired at 10 kHz using a Digidata 1322A A/D board and Axoscope 9.2 software (Axon Instruments, Union City, CA, USA).

Intracellular muscle fiber electrophysiology

Intracellular muscle fiber recordings were performed from unoperated and reinnervated soleus muscle fibers in well-oxygenated Tyrodes (95% O_2 and 5% CO_2). To reduce the number of quanta released upon nerve stimulation and thus prevent action potential responses in muscle fibers we used a low calcium Tyrode's solution containing 125mM NaCl, 5.37mM KCl, 24mM $NaHCO_3$, 5mM $MgCl_2$, 0.6mM $CaCl_2$ and 5% dextrose. Evoked responses were recorded by stimulating the soleus nerve at a rate of 0.5Hz via a tight-fitting suction electrode connected to a Grass S88 stimulator with SIU5 stimulus isolation unit. Responses were recorded with a Duo 773 intracellular amplifier (WPI, New Haven, Connecticut, USA) connected to a Dagan amplifier and digitized as described above. Micropipettes used for recording were filled with 3M KCl and had

resistances from 20-25MΩ. Electrophysiological measurements were not recorded if the initial resting potential (-70 to -85 mV) decreased by 10% of its original value (Rafuse et al., 2000). A failure was scored as a stimulus without a subsequent change in resting membrane potential (0 mV amplitude). Quantal content was calculated by the ratio of the mean EPP/mean mEPP amplitude per fiber sampled.

Immunofluorescence and histology

Immediately following cessation of the physiological recordings the muscles were pinned at their physiological length and immersed in a 1:2 mixture of 20% sucrose/PBS and O.C.T. compound mixture and then rapidly frozen in isopentane cooled with dry ice. In some instances, the pinned muscles were fixed overnight in 4% paraformaldehyde/PBS for later endplate analysis (see below). Frozen muscles were sectioned at 30 μm on a cryostat, dried overnight, incubated with anti-slow myosin IgA primary antibody (1:10; S58; Developmental Studies Hybridoma Bank, Iowa City, IA, USA) overnight at 4ºC and washed several times in PBS. Slides were postfixed for 15 minutes in 4% paraformaldehyde/PBS, washed several times in PBS, incubated with anti-fast myosin IgG primary antibody (1:500; M4276; Sigma Aldrich, Oakville, ON, Canada) at room temperature for 1 hour, washed several times in PBS, incubated with Alexa Fluor 546 goat anti-mouse IgG (1:500; A11003; Invitrogen) and Fluorescein-conjugated goat anti-mouse IgA (1:500; 55492; Cappel, Aurora, OH, USA) secondary antibodies for 1 hour at room temperature, washed several times in PBS, and finally mounted in 50% glycerol/PBS mixture containing 0.03 mg/ml ρ-phenylenediamine to prevent fading. Sections were photographed with a digital camera (C4742; Hamamatsu Photonics, Hamamatsu, Japan) using IPLab acquisition software (Version 4.0; BD Biosciences, Rockville, MD).

For endplate morphology, fixed soleus muscles were teased into small bundles of muscle fibers, incubated in 0.1M glycine for 1 hour, washed in PBS, and placed in rhodamine conjugated α-bungarotoxin (α-btx) (1:100 Invitrogen) for 1-2 hours at room temperature. After several washes in PBS, the fibers were incubated overnight at room temperature in rabbit anti-synaptophysin IgG (1:500 Invitrogen) or in mouse anti-Pan-Axonal Neurofilament IgG (1:500; SMI-312; Covance, Hornby, ON, Canada) primary

antibody. Muscle fibers were then washed in PBS, incubated for 1 hour in either goat anti-rabbit or goat anti-mouse IgG secondary antibody conjugated to Alexa Fluoro 488 (1:500 Invitrogen). Fibers were finally washed in PBS and mounted in 50% glycerol/PBS mixture containing 0.03 mg/ml ρ-phenylenediamine. Representative projection images of motor endplates were acquired using a Zeiss LSM510 laser scanning confocal microscope (Zeiss Microimaging, Thornwood, NY, USA) and managed using LSM Image Browser (Zeiss Microimaging). All measurements were performed on images captured with a Leica DMLFS wide field fluorescence microscope (Leica Microsystems, Bannockburn, IL, USA) mounted with a digital camera (C4742; Hamamatsu Photonics, Hamamatsu, Japan) using IPLab acquisition software (Version 4.0; BD Biosciences, Rockville, MD, USA). α-btx binding areas were highlighted from background as regions of high rhodamine fluorescence intensity using IPLab software. These highlighted regions were analyzed for areas using the Analysis function in the IPLab software. α –btx binding areas and the number of discrete AChR clusters (regions of α-btx binding within individual endplates separated by an identifiable non-stained region) were measured by a volunteer who was blinded to the experimental conditions.

Quantification of motoneuron and myofiber numbers

Spinal cords from CTB injected mice were sectioned longitudinally at 40 μm as previously described (Franz et al., 2005). Raw cell counts were corrected by the Abercrombie method (Abercrombie, 1946). Whole muscle and individual muscle fiber cross sectional areas (CSAs) were measured on slides stained for fast and slow myosin using IPLab software (Version 4.0; BD Biosciences, Rockville, MD). The number of fast and slow fibers was enumerated by counting all of the fast and slow myosin-positive ($myosin^{+}$) myofibers in a single section at the soleus midbelly. The sums of these counts closely agreed with an indirect assessment of the total number of fibers quantified by ratio of whole muscle CSA/average muscle fiber CSA (30-60 fibers/muscle; 50% fast, 50% slow). All quantification was performed by a volunteer who was blind to the experimental conditions.

Statistical analyses

A one-way ANOVA was performed to examine differences between groups over time. Tukey's honestly significant difference post-hoc test was used to determine where the significant differences occurred if the F-value exceeded F-critical. Two tailed-Student's t-tests were then used to make comparisons between genotypes at a given time-point. Statistical significance was considered to be achieved if $P < 0.05$.

Results

The stability of reinnervated NMJs is compromised in mice lacking NCAM

Synapse formation, function and stability were initially characterized by comparing soleus muscle contractile force 1-9 months after crushing the tibial nerve 20 mm proximal to the soleus nerve/muscle entry point. At this distance, crushed sciatic motoneurons reinnervate all endplates in denervated shank muscles 1 month after nerve injury (Magill et al., 2007). For comparison, the same isometric tetanic contractions, elicited by a 50 Hz train of pulses (0.5 s train duration), were recorded from unoperated, contralateral soleus muscles of wild-type and *NCAM -/-* mice (Figure 2.1*A*). As observed for medial gastrocnemius muscles (Rafuse et al., 2000), unoperated soleus muscles in *NCAM -/-* mice generated the same amount of force as soleus muscles in wild-mice (Figure 2.1*B*). These results indicate that neurotransmission, excitation-contraction (E-C) coupling, and muscle fiber contractile properties are not noticeably compromised during development when NCAM is absent. Tetanic forces of reinnervated soleus muscles in wild-type and *NCAM -/-* mice were also not significantly different from each other 1 month after nerve crush injury (Figure 2.1*A*, *B*) indicating that motor axon regeneration and synapse reformation were not markedly affected in mice lacking NCAM (see also Moscoso et al., 1998).

Interestingly, however, reinnervated *NCAM -/-* soleus muscles did not maintain comparable force values as time passed. In fact, tetanic force decreased to about one third wild-type values 3-6 months after nerve injury (Figure 2.1*A*, *B*; 3 mo, $P<0.01$). While tetanic forces in both experimental groups increased 7-9 months after injury (Figure 2.1*B*; 7 mo), the forces generated by reinnervated *NCAM-/-* muscles remained significantly less than reinnervated wild-type muscles ($P<0.05$).

Several factors can account for a loss of contractile strength over time. Force output would decrease if neurotransmission or E-C coupling were progressively compromised. Contractile force would also decline if reinnervated muscle fibers later atrophied or became denervated due to the withdrawal of axons. To address these possibilities we first analyzed electromyograms (EMGs) recorded from unoperated and reinnervated wild-type and *NCAM -/-* soleus muscles during a train of stimuli (50 Hz, 0.5

s duration). Surface EMGs are the sum of all recorded motor unit action potentials. Its peak to peak amplitude is proportional to the number and size of contracting muscle fibers (Henneman and Olson, 1965; Kosarov, 1974; Milner-Brown and Stein, 1975) in normal and reinnervated muscles (Totosy de Zepetnek et al., 1991). A simultaneous decrease in force and EMG over time indicates that muscle fibers atrophied or degenerated (Kernell, 2006). A progressive decrease in force, in the absence of smaller EMGs, suggests that muscle fibers weakened due to metabolic or E-C coupling deficiencies.

EMG peak to peak amplitudes did not differ between unoperated wild-type and *NCAM -/-* soleus muscles (Figure 2.2*C*). Similarly, the amplitudes of the EMGs recorded from reinnervated soleus muscles in wild-type and *NCAM -/-* mice were not significantly different from each other 1 month after nerve crush injury (Figure 2.2*C*). However, as observed in the force recordings, EMGs from reinnervated *NCAM -/-* soleus muscles (Figure 2.2*B, C*) were significantly smaller than those recorded from wild-type muscles 3 months after nerve injury (Figure 2.2*A*,*C; P*<0.01). EMGs remained significantly smaller in *NCAM -/-* mice 3-9 months after injury (data not shown). These results indicate that the loss of contractile force in *NCAM -/-* mice was due to muscle fiber atrophy and/or degeneration and not due to deficient E-C coupling or a progressive metabolic myopathy.

Reinnervated muscle fiber numbers decrease in mice lacking NCAM

To determine whether reinnervated soleus muscles in *NCAM -/-* mice contained smaller, or fewer muscle fibers, we quantified whole muscle cross-sectional area, mean myofiber cross-sectional area and the number of fibers spanning the midbelly of unoperated and reinnervated muscles 1, 3-6, and 7-9 months after nerve injury. Muscle cross-sections from wild-type and *NCAM -/-* mice were immunolabeled for fast (Figure 2.3*A, B*) and slow (not shown) myosin heavy chains for better visualization. Gross morphological analysis (Figure 2.3*A, B*) and cross-sectional area measurements (Figure 2.3*C*) showed that soleus muscles in unoperated wild-type and *NCAM -/-* mice were the same size and had a similar fiber type distribution. As expected from the force recordings, reinnervated wild-type and *NCAM -/-* muscles were slightly smaller than unoperated muscles 1 month after nerve injury (Figure 2.3*A-C*). The smaller muscle size was due to atrophy (Figure

2.3*D*) rather than a loss of muscle fibers (Figure 2.3*E*). Muscle fiber atrophy is commonly observed in newly reinnervated muscles if they are denervated for at least 2 weeks (Magill et al., 2007). As predicted from the force and EMG measurements, reinnervated *NCAM -/-* muscles were significantly smaller ($P<0.01$) than reinnervated wild-type muscles 3-6 months after nerve injury (Figure 2.3*A*-*C*; 3 mo). Unexpectedly, this decrease in size was due to a loss of muscle fibers (Figure 2.3*E*) rather than continued atrophy (Figure 2.3*D*). Interestingly, the decrease in fiber number was almost entirely due to the selective loss of fast muscle fibers as evident by the change in fast fiber morphology (Figure 2.3*B*; 3&6 mo) and number (Figure 2.3*F*; 3 mo). On average, reinnervated soleus muscles in *NCAM -/-* mice contained two thirds of their normal complement of myofibers 3-6 months after injury (Figure 2.3*E*; 3 mo). Muscles enlarged in both experimental groups 7-9 months after injury (Figure 2.3*C*; 7 mo) because of muscle fiber hypertrophy (Figure 2.3*D*). This enlargement likely explains the increase in contractile force observed in both experimental groups 7-9 months after injury (Figures 2.1*A*, *B*). Surprisingly, the number of fast fibers increased to near normal values 7-9 months after injury in the *NCAM -/-* mice (Figure 2.3*F*; 7 mo). However, because there was a simultaneous decrease in slow fibers (not shown) the reinnervated *NCAM -/-* soleus muscles remained significantly smaller ($P<0.05$) than their wild-type counterparts because a third of their fibers remained absent (Figure 2.3*E*; 7 mo, $P<0.05$).

Motor axons withdraw from endplates and muscle fiber degenerate in reinnervated NCAM -/- mice

Both denervation atrophy and muscular dystrophy (i.e. loss of muscle fibers without nervous system involvement) can result in muscle fiber degeneration. To assess which process was responsible for the loss of fibers in the reinnervated *NCAM -/-* mice we examined endplates for signs of axon withdrawal using rhodamine conjugated α-bungarotoxin (α-btx; to visualize acetylcholine receptors; AChRs) and neurofilament immunohistochemistry. As expected, AChR rich synaptic endplates in unoperated wild-type and *NCAM -/-* soleus muscles were innervated by a single motor axon which extended neurofilament^{+} branches into the junction (Figure 2.4*A, B*). The same endplate morphology was also observed in reinnervated wild-type mice 3 months after injury

(Figure 2.4*C*). While the majority of the reinnervated endplates in the *NCAM -/-* mice were normally innervated (data not shown), many endplates were contacted by fragmented neurofilament+ axons (Figure 2.4*D;* small arrow) and thinned axons (Figure 2.4*D*; arrow) terminating in bulbous neuronal protrusions (Figure 2.4*D*; arrowheads). Such abnormal morphologies are reminiscent of axonal remnant formation and axosome shedding exhibited by withdrawing axons during the elimination of polyneuronal innervation during postnatal development (Bishop et al., 2004). While not conclusive, these observations support that notion that axon withdrawal caused the loss of muscle fibers in the *NCAM -/-* mice.

Following denervation, myofibers atrophy, necrotize and then regenerate via resident satellite cells. This process recycles until newly formed muscle fibers are reinnervated (Schmalbruch et al., 1991). To ascertain whether degenerating and/or regenerating muscle fibers were present in reinnervated soleus muscles we first performed H & E staining on muscle cross-sections from wild-type and *NCAM -/-* mice. Soleus muscle fibers in unoperated wild-type and *NCAM -/-* mice were uniformly shaped with peripherally located nuclei (Figure 2.5*A*, *B*). Although reinnervated wild-type and *NCAM -/-* muscles fibers were smaller than normal 1 month after injury, they appeared healthy with nuclei located next to the cell membrane (Figure 2.5*A*, *B*, 1 mo). Unlike wild-type muscles 3 months after nerve injury (Figure 2.5*A*; 3 mo), reinnervated *NCAM -/-* muscles showed several signs of fiber degeneration including swollen myofibers (Figure 2.5*B*, 3 mo; asterisk) and prevalent regions containing many small nuclei (Figure 2.5*B*; 3 mo arrows); a sign indicative of macrophage infiltration (Swash and Schwartz, 1984). Macrophage infiltration diminished 9 months after nerve injury in reinnervated *NCAM -/-* soleus muscles. However, the muscles remained abnormal because they contained many small muscle fibers with centrally located nuclei (Figure 2.5*B*, 9 mo; arrows); a morphological characteristic of newly formed myofibers (Chargé and Rudnicki, 2004).

The prevalence of muscle fibers with centrally located nuclei suggests that myofiber regeneration was ongoing 9 months after nerve injury in *NCAM -/-* mice. To investigate this possibility we combined nuclear Hoechst staining with MyoD immunohistochemistry to determine whether activated $MyoD^{+}$ satellite cells (Cornelison

et al., 2000) were present in long-term reinnervated muscles. As expected, MyoD$^+$ cells were absent in longitudinal muscle sections from unoperated wild-type and *NCAM -/-* mice (Figure 2.6*A, C*). Similarly, reinnervated wild-type muscles were devoid of MyoD$^+$ satellite cells 9 months after injury (Figure 2.6*B*). In contrast, activated MyoD$^+$ satellite cells were interspersed throughout reinnervated *NCAM -/-* muscles 9 months after injury (Figure 2.6*D*; arrows) indicating that muscle fiber regeneration was ongoing at this late time point (Chargé and Rudnicki, 2004). Taken together with the fact that the number of muscle fibers did not change between 3 and 9 months after nerve injury, these results suggest that reinnervated muscles in *NCAM -/-* mice continuously regenerated myofibers in a failed attempt to recover complete muscle function.

Decreased muscle force and myofiber number is not due to motor neuron death

Muscle fiber denervation occurs if motoneurons die or if intact neurons withdraw some synapses. To distinguish between these two possibilities we quantified the number of motoneurons innervating unoperated and reinnervated soleus muscles in wild-type and *NCAM-/-* mice using standard CTB back labeling techniques. Consistent with previous studies (Franz et al., 2005), unoperated wild-type and *NCAM -/-* mice contained the same number of soleus motoneurons (38.5 ± 2.0 and 39.3 ± 3.4, respectively; n=3 in both groups). Interestingly, the numbers of motoneurons reinnervating soleus muscles in wild-type and *NCAM -/-* mice were not significantly different from each other 3 months after nerve injury (36.7 ± 2.5 and 42.1 ± 1.6, respectively; n=3 in both groups) when force differences were clearly evident. These results indicate that the decrease in myofiber number was due to a reduction in motor unit size (i.e. the number of muscle fibers innervated by each motoneuron) rather than motoneuron death.

Neuromuscular transmitter release is compromised in reinnervated muscles in NCAM -/- mice

To determine whether withdrawal of axons in the *NCAM -/-* mice correlated with defects in neuromuscular synaptic transmission, we performed intracellular recordings from individual soleus muscle fibers in unoperated and reinnervated wild-type and *NCAM -/-* mice. Low extracellular calcium and high magnesium was used to reduce the number of

quanta released upon nerve stimulation to prevent action potentials in the muscle fibers. Figure 2.7 (*A* and *B*) shows typical miniature endplate potentials (MEPPs) and seven evoked endplate potentials (EPPs) recorded from unoperated wild-type and *NCAM -/-* muscles. Consistent with other studies investigating synaptic transmission at *NCAM-/-* NMJs under these conditions (Rafuse et al 2000; Polo Parada et al 2001), none of the parameters measured were significantly different between unoperated wild-type and *NCAM -/-* mice including: EPP amplitude, quantal content, percent failures (i.e. percentage of stimuli that failed to evoke an EPP), MEPP amplitude and MEPP frequency (Figure 2.7*F-J*). The amplitudes of the EPPs were significantly smaller (Figure 2.7*F*), and the percentage of failures was higher (Figure 2.7*H*), in both experimental groups 2 months after nerve injury. However, quantal content (Figure 2.7*G*) in both groups remained similar to unoperated values because there was a corresponding decrease in mean MEPP amplitude (Figure 2.7*I*). Interestingly, two abnormal patterns of evoked responses emerged in *NCAM -/-* muscles (Figure 2.7*D*, *E*), but not wild-type muscles (Figure 2.7*C*), 3 months after nerve injury. Some reinnervated *NCAM -/-* fibers exhibited an unusually large number of failed responses and had small EPPs (Figure 2.7*D*), suggesting a decreased probability of release at these synapses. In another group of myofibers, the number of failures was normal, but the distribution of EPPs was skewed to smaller values (Figure 2.7*E*) compared to those recorded from wild-type fibers at the same time point (Figure 2.7*C*). On average, EPP amplitude (Figure 2.7*F*; 3 mo), quantal content (Figure 2.7*G*; 3 mo), number of failures (Figure 2.7H; 3 mo), and MEPP frequency (Figure 2.7J; 3 mo) were all significantly less in *NCAM -/-* mice, compared to wild-type mice, 3-6 months after nerve injury. The same parameters, as well as MEPP amplitude (Figure 2.7*I*), remained significantly less in *NCAM -/-* muscles 7-9 months after nerve injury (Figure 2.7 *F-J*; 7 mo). Thus, the emergence of neurotransmission abnormalities correlated well with the appearance of withdrawing axons and the onset of muscle fiber degeneration. Whether abnormal neurotransmission led to the withdrawal of axons is not known (see Discussion). However, the persistence of neurotransmission deficits and the presence of regenerating muscle fibers 7-9 months after injury suggest that the two anomalies are likely interrelated.

Endplate morphology is abnormal in reinnervated NCAM -/- muscles

To determine whether a lack of NCAM leads to changes in NMJ morphology we assayed AChR clusters at endplates using rhodamine conjugated α-btx. Presynaptic morphology and alignment of synaptic structures were assessed using synaptophysin immunohistochemistry. Figure 2.8 shows examples of α-btx$^+$ AChR clusters and presynaptic morphology in endplates from unoperated wild-type and *NCAM -/-* mice (Figure 2.8*A, B*). As expected, AChRs were distributed in 1-2 clusters/NMJ (Figure 2.8*A, F*) in wild-type mice and occupied a surface area ~300 μm^2 (Figure 2.8*E*). Compared to wild-type, AChRs in unoperated *NCAM -/-* mice were distributed in more fragments/NMJ (Figure 2.8*F*). However, despite the larger number fragments, AChRs occupied significantly less area (Figure 2.8*E*) (see also Rafuse et al., 2000).

The α-btx$^+$ AChR binding area (Figure 2.8*C, E*) and number of AChR fragments (Figure 2.8*C, F*) gradually increased over time in reinnervated wild-type muscles and was a direct consequence of reinnervation, as aged matched controls did not demonstrate this increase (data not shown). Interestingly, the morphology of the endplates in *NCAM -/-* mice did not change very much over time. The α-btx-binding area (Figure 2.8*E*) and number of discrete fragments (Figure 2.8*F*) were essentially the same before (Figure 2.8*E, F*; 2 mo) and after (Figure 2.8*E, F*; 6 mo) the withdrawal of axons and subsequent decrease in muscle force. Consequently, while endplates in *NCAM -/-* mice are different from wild-type, progressive changes in their morphology do not appear to precipitate the observed decrease in muscle function 3 months after nerve injury.

Lack of NCAM in motoneurons or muscle fibers alone does not lead to synaptic dysfunction

The NMJ is a tripartite synapse consisting of a presynaptic motoneuron, postsynaptic muscle fiber, and perisynaptic tSC. Each cell type expresses NCAM at the adult NMJ (Rieger et al., 1985; Covault and Sanes, 1986). As a result, the disorders observed in reinnervated *NCAM -/-* mice could be due to a loss of NCAM pre-, post- and/or perisynaptically. To help distinguish between these possibilities, we generated mutant mice in which the floxed NCAM gene (Bukalo et al., 2004) was inactivated by cre-recombinase under the control of the Hb9 (Yang et al., 2001), or HSA promoter (Miniou

et al., 1999; Cifuentes-Diaz et al., 2001). This breeding strategy selectively abolishes NCAM expression in motoneurons (mice termed NCAM$^{flx/flx}$/Hb9$^{cre/+}$; see Franz et al., 2008) and NCAM expression in muscle fibers (mice termed NCAM$^{flx/flx}$/HSA$^{cre/+}$) (see Appendix Figure A2), respectively. Surprisingly, neither the NCAM$^{flx/flx}$/Hb9$^{cre/+}$ nor NCAM$^{flx/flx}$/HSA$^{cre/+}$ mutant mice exhibited deficits in whole muscle tension (Figure 2.9*A*) or evoked neurotransmission (i.e. mean EPP amplitude, mean quantal content and mean % failures; Figure 2.9*B*) before, or 3 months after, nerve injury. The mutant mice, however, had some irregularities. Functionally, MEPPs were significantly larger than normal in both conditional mutants 3 months after injury (Figure 2.9*B*) while the frequency of MEPPs at reinnervated NMJs in NCAM$^{flx/flx}$/Hb9$^{cre/+}$ was less than that observed in wild-type mice (data not shown).

NMJs were significantly larger than normal in unoperated NCAM$^{flx/flx}$/Hb9$^{cre/+}$ and NCAM$^{flx/flx}$/HSA$^{cre/+}$ mice (Figure 2.9C). Furthermore, both conditional mutants contained significantly more AChR fragments than unoperated wild-type mice (Figure 2.9*C*), with endplates in NCAM$^{flx/flx}$/HSA$^{cre/+}$ mice being the most fragmented (Figure 2.9*C*). Interestingly, endplates in unoperated NCAM$^{flx/flx}$/HSA$^{cre/+}$ mice contained the same number of AChR fragments as those in *NCAM -/-* mice (Figure 2.8*F*). These results suggest that muscle-, and to a lesser extent, neural-derived NCAM plays a role in maintaining the interegrity of the postsynaptic structure during adulthood (Fox et al 2007). AChRs in all three experimental groups were more fragmented than their unoperated counterparts 3 months after injury (Figure 2.9*C*). Taken together, while pre- and post-synaptic NCAM is important for normal endplate development, the loss of either one alone is not sufficient to recapitulate the functional deficits observed in reinnervated *NCAM -/-* mice.

Long term deficit in terminal Schwann cell capping at reinnervated NCAM-/- NMJs

Perisynaptic tSCs actively modulate the formation, function and maintenance of vertebrate NMJs (Koirala et al., 2003). For example, tSCs modulate neurotransmission (Colomar and Robitaille, 2004) and participate in the functional recovery of partially denervated muscles by promoting and directing the growth of sprouts from intact motoneurons to denervated endplates (Son and Thompson, 1995b). Based on these

known functions it seemed reasonable to speculate that synaptic function may be compromised in mice with tSCs lacking NCAM. Unfortunately, selective ablation of NCAM in tSCs is currently problematic using a cre-lox approach. However, because many tSC functions have been elucidated using standard immunohistochemistry (e.g. Love and Thompson, 1999) we decided to examine tSC morphology in the various NCAM mutant mice before and 3 months after injury. Figure 2.10*A* shows the morphology of a wild-type α-btx labeled endplate innervated by a motor axon myelinated with a $S100^{+}$ Schwann cell (Figure 2.10*A*; arrowhead) and completely capped with a $S100^{+}$ tSCs (Figure 2.10*A*, arrow). Although the morphology of the AChR clusters differed somewhat between *NCAM -/-*, $NCAM^{flx/flx}/Hb9^{cre/+}$ and $NCAM^{flx/flx}/HSA^{cre/+}$ endplates, each were capped with a tSC and innervated by a single myelinated axon (Figure2.10*B-D*). Quantification showed that ~90% of the endplates were entirely capped by tSCs in all 4 groups of unoperated mice (Figure 2.10*I*).

The vast majority (~90%) of reinnervated endplates in wild-type, $NCAM^{flx/flx}/Hb9^{cre/+}$ and $NCAM^{flx/flx}/HSA^{cre/+}$ mice were entirely capped by a $S100^{+}$ tSC 3 months after injury (Figure 2.10*E-I*). In contrast, more than 30% of the reinnervated *NCAM-/-* endplates either lacked $S100^{+}$ tSCs altogether (data not shown), or contained faintly labeled tSCs that failed to extend processes over the AChRs (Figure 2.10*F* arrow). Consequently, neuromuscular transmission irregularities and muscle dysfunction correlated well with the presence of reinnervated endplates lacking tSCs.

The lack of capping by tSCs may suggest the possibility of an early deficit in the cellular response to denervation. To examine the sprouting response of tSCs to muscle denervation, wild-type and *NCAM-/-* denervated soleus muscles were examined for tSC morphology 4 days following a nerve crush injury when tSC are known to extensively extend processes (Son and Thompson, 1995a) (Figure 2.11*A-B*). *NCAM-/-* tSCs appropriately extended processes from endplate regions and no deficits in outgrowth were observed at this time. Quantification of sprout lengths demonstrated a similar extent of outgrowth by wild-type and *NCAM-/-* tSC processes 4 days (Figure 2.11*C* $P>0.05$) and 14 days after nerve crush (Figure 2.11*C* $P=0.735$).

Overall, these results suggest that tSCs lacking NCAM extend sprouts appropriately in response to muscle denervation, but degenerate over the long term

following reinnervation. In addition, the data presented here support previous results in frog showing that the loss of tSC integrity at the NMJ leads to neurotransmission dysfunction, synapse retraction and reduced force tension over time (Reddy et al., 2003).

Discussion

Although NCAM is not essential for motor axon regeneration per se (Moscoso et al., 1998; Franz et al., 2005), our results indicate that it is required for maintaining normal muscle function after a peripheral nerve injury. The most striking neuromuscular irregularities detected ≥3 months after nerve injury included a significant decrease in contractile force, inappropriate withdrawal of synapses, degeneration of myofibers, impaired synaptic neurotransmission, signs of continual muscle regeneration and abnormal tSC morphology. Selective ablation of NCAM from motoneurons, or muscle fibers, did not mimic the deficiencies observed in the *NCAM -/-* mice. These latter results, combined with the abnormal capping morphology of tSCs in *NCAM -/-* mice, suggest that perisynaptic expression of NCAM is required for synaptic stability of reinnervated NMJs.

NCAM, neurotransmission, synaptic stabilization and sprouting

Three unusual, and potentially related, events occurred in *NCAM -/-* mice ≥3 months after injury. First, fast motoneurons withdrew axons and formed smaller motor units (i.e. motoneurons innervated fewer muscle fibers). Second, slow motoneurons did not sprout collaterals to reinnervate myofibers left denervated by the withdrawing axons. Third, tSCs failed to cap many reinnervated endplates. Motor axon withdrawal, and the formation of smaller motor units, is a natural phenomenon occurring during the elimination of polyneuronal innervation in developing muscles (Redfern, 1970; Brown et al., 1976). Although the precise mechanisms underlying this phenomenon are not understood, it is well established that quantal content of the remaining axons become increasingly greater than those destined to withdraw (Colman et al., 1997; Kopp et al., 2000). This disparity ultimately contributes to the withdrawal of the weaker synapse (Colman et al., 1997). In the present study, quantal content became significantly less in reinnervated *NCAM -/-* mice when axon withdrawal was first detected anatomically and physiologically. Based on the developmental studies, it is tempting to speculate that synaptic instability at reinnervated *NCAM -/-* mice was due, in part, because quantal content was insufficient to signal continued maintenance of the terminal.

It is currently not known why quantal content became less at reinnervated endplates in *NCAM -/-* mice three months after injury. However, the normality of neurotransmission in mice with NCAM deficient motoneurons, or muscle fibers (Figure 2.8), suggests that it was not due to the sole loss of NCAM pre- or post-synaptically. While selective ablation of NCAM from tSCs was not performed in the present study, it is interesting to note that, unlike the conditional NCAM knock-out mice, ~30% of the reinnervated NMJs in *NCAM -/-* mice were not capped by tSCs (Figure 2.10). Neurotransmitter released during high frequency stimulation, as occurs when fast motoneurons are depolarized (Grimby et al., 1979), activates G-protein-coupled receptors on tSCs and causes the release of intracellular Ca^{2+} from internal stores (Robitaille, 1998). In return, increased Ca^{2+} in tSCs potentiates neurotransmitter release at the NMJ (Castonguay and Robitaille, 2001; Colomar and Robitaille, 2004; Todd et al 2010). Based on these studies it seems reasonable to hypothesize that synaptic transmission is compromise at *NCAM -/-* endplates not capped by tSCs, particularly those innervated by fast motoneurons. This notion is supported by studies in adult frogs where selective ablation of tSCs leads to a decrease in quantal content, axon withdrawal and decline in contractile force one week later (Reddy et al., 2003). Like the present study, these deficits were not accompanied by changes in the amplitude of MEPPs (Reddy et al., 2003; Feng and Ko, 2008). Taken together, these results are consistent with the hypothesis that tSCs must express NCAM in order to maintain structure and function of adult NMJs.

Motoneurons have a tremendous capacity to sprout and functionally innervate up to 5 times as many muscle fibers as normal in partially denervated (Brown and Ironton 1978; Fisher et al. 1989; Gordon et al. 1993; Gorio et al. 1983; Rafuse et al. 1992; Thompson and Jansen 1977; Yang et al. 1990) and reinnervated muscles (Rafuse and Gordon, 1996). Thus, it was somewhat surprising to find that slow motoneurons did not sprout collaterals to functionally innervate myofibers denervated by the withdrawing fast motor axons. Reinnervation of denervated myofibers in partially denervated muscles normally occurs because tSCs at denervated endplates extend processes towards innervated synapses. These tSC bridges direct, and promote, the growth of terminal sprouts to denervated myofibers (Son and Thompson, 1995b). If tSC bridges do not

form, sprouting cannot occur (Lubischer and Thompson, 1999; Tam and Gordon, 2003). Consequently, slow motoneurons may not have sprouted in *NCAM -/-* mice because their tSCs did not form bridges or the bridges were less conducive for growth (Schäfer and Wernig, 1998; see below). Alternatively, motoneurons in *NCAM -/-* mice may be incapable of forming enlarged motor units because quantal content at sprouted terminals is simply too low to signal continued maintenance of the NMJ (Rochel and Robbins, 1988).

Presynaptic NCAM signaling

NCAM interacts with a number of intracellular molecules important for synapse stabilization. For example, spectrin co-purifies with the 180 kD isoform of NCAM in adult mouse brain protein fractions (Pollerberg et al., 1987). NCAM-180 is selectively targeted from the axonal shaft to the presynaptic terminals of motoneurons after myotube contact *in vitro* (Hata et al., 2007). In cultured hippocampal neurons, contacts between axons and dendrites transform into functional synapses, in part, because synaptic proteins within Trans-Golgi network-organelles are linked to clusters of NCAM-180 in the plasma membrane via spectrin (Sytnyk et al., 2004). Heterotetramers of α- and ß-spectrin subunits also form spectrin-actin filamentous scaffoldings that are important in maintaining plasma membrane integrity and cytoskeletal structure (Bennet and Baines, 2001). Selective loss of pre-synaptic spectrin at mature NMJs in *Drosophila* leads to a decrease in quantal content and synapse elimination (Featherstone et al., 2001; Pielage et al., 2005). Interestingly, FasII is removed at sites of retraction prior to the synapse withdrawal when presynaptic spectrin is experimentally reduced (Pielage et al., 2005). Taken together, it is tempting to speculate that spectrin helps stabilize newly formed NMJs through its interaction with NCAM-180. However, unlike *Drosophila*, results from $NCAM^{flx/flx}/Hb9^{cre/+}$ mice indicate that loss of presynaptic NCAM alone is not sufficient to precipitate neurotransmission dysfunction or axon withdrawal in mice.

Postsynaptic NCAM signaling

NCAM initiates signaling by activating intracellular signaling molecules such as Fyn (reviewed by Ditlevsen et al., 2008). Fyn and Src, members of the Src-family of

nonreceptor tyrosine kinases (SFKs), functionally interact with AChRs in myofibers *in vitro* (Fuhrer and Hall, 1996) and *in vivo* (Smith et al., 2001). Interestingly, muscle development, motor axon pathfinding, and AChR clustering are normal in Fyn/Src double mutant mice (Smith et al., 2001) indicating that they are not essential for neuromuscular development. However, disruption of their function post-natally results in AChR fragmentation (Sadasivam et al., 2005) in a manner that is very similar to that observed in *NCAM* -/- and $NCAM^{flx/flx}$/ $HSA^{cre/+}$ mice (Figures 2.8&2.10). In addition, ECM-associated collagen is known to bind NCAM (Probstmeier et al 1989, 1992) and the loss of collagen IV induces postsynaptic degeneration at mouse NMJs (Fox et al 2007). It is therefore possible that increased fragmentation of AChRs in *NCAM* -/- muscle fibers is due to a lack of NCAM-mediated Fyn/Src signaling and/or a loss of NCAM-collagen interaction.

Perisynaptic NCAM signaling

Non-injured motoneurons in partially denervated muscles grow axonal sprouts along tSC bridges that form between innervated and denervated endplates (Son and Thompson, 1995b). This expansion in motor unit size can functionally compensate for an 80% loss in motoneuron number before a decline in contractile force is observed (Rafuse et al., 1992). The absence of sprouting in the *NCAM* -/- mice suggests that tSC bridges did not form or that they were less conducive for growth. Several growth pathways are stimulated through NCAM activation. For example, NCAM-mediated growth requires activation of fibroblast growth factor receptor (FGFR) and recruitment of $PKC\beta_2$ to detergent insoluble lipid rafts (Neithammer et al 2002; Leshchyns'ka, 2003). This FGFR/PKC pathway can then associate with growth-associated molecules such as GAP-43, CAP23 and MARCKS (Laux et al 2000). GAP-43 has been implicated in NCAM-mediated neurite outgrowth (Meiri et al 1998; Korshunova et al 2007) and is significantly up-regulated by tSCs after injury (Woolf et al 1992). It is therefore temping to speculate that NCAM-mediated growth mechanisms may be responsible for the extension of sprouts along tSC bridges in partially denervated muscles (Reynolds and Woolf, 1992; Son and Thompson, 1995b). However, we found that tSCs sprout extensively following nerve crush, suggesting that NCAM is dispensable for tSCs outgrowth. Instead,

expression of NCAM on the surface of tSCs may influence NCAM-mediated neurite outgrowth of motor axons in response to partial denervation.

NCAM and neuromuscular disorders

Although it is commonly believed that motoneuron death causes the loss of motor unit function in motoneuron disease, it is not clear whether this reflects the actual sequence of pathological events. For example, abnormalities in synaptic function (including decreased quantal content) occur while motoneurons are still capable of producing action potentials in patients with ALS (Maselli et al. 1993). Mice expressing mutant SOD1 die due to muscle denervation even when motoneuron death is prevented (Gould et al., 2006). Decreased release of transmitter from motor terminals underlies motor unit dysfunction, and likely death, in hereditary canine spinal muscular atrophy (Rich et al., 2002). Interestingly, like the preferential withdrawal of fast motoneurons in the present study, the largest motoneurons are usually the first to succumb to motoneuron disease (Kernell, 2006). Polysialylated NCAM is induced in surviving motoneurons in SOD1 mutant mice (Warita et al., 2001). While NCAM is routinely used to identify putative denervated fibers in animal models of ALS (e.g. Hegedus et al., 2008), recent studies have challenged the notion that NCAM is only up-regulated on myofibers after denervation (Grumbles et al., 2008). Consequently, motoneurons and muscle fibers may actively up-regulate NCAM in response to disease related challenges in an attempt to stabilize the synapse. Whether changes in NCAM function participate in motoneuron disease is not known, but results from the present study suggest that this notion is worth pursuing.

CHAPTER 2 FIGURES

Figure 2.1: Contractile force of reinnervated muscles in *NCAM -/-* mice decreases with time after injury. **(A)** Overlay of individual isometric tetanic force tracings shows that reinnervated wild-type (+/+) and *NCAM -/-* soleus muscles (light gray trace) generate the same amount of force as unoperated muscles (black trace) 1 month after injury. In contrast to reinnervated wild-type muscles, *NCAM -/-* muscles did not maintain their force generating capacity 3 months after nerve crush injury (gray trace). **(B)** Mean (± SEM) tetanic muscle force generated by unoperated and reinnervated wild-type and NCAM -/- soleus muscles 1, 3-6 (3 mo), and 7-9 (7 mo) months after tibial nerve crush injury. **P*<0.05; ***P*< 0.01 wild-type compared with corresponding *NCAM -/-*.

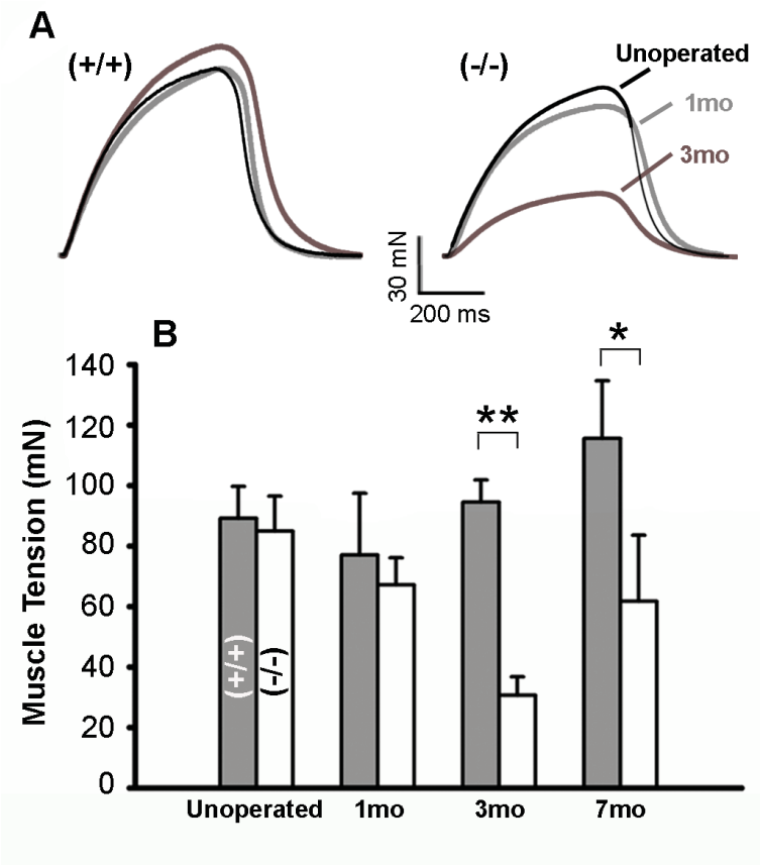
A
(+/+)
(-/-)
Unoperated
1mo
3mo
30 mN
200 ms
B
Muscle Tension (mN)
140
120
100
80
60
40
20
0
(+/+)
(-/-)
**
*
Unoperated
1mo
3mo
7mo

Figure 2.2: EMGs recorded from reinnervated *NCAM -/-* soleus muscles are smaller than those recorded from wild-type muscles 3 months after nerve injury. **(A-B)** The amplitudes of EMGs recorded from a reinnervated *NCAM -/- (B)* soleus muscle are noticeably smaller than those recorded from reinnervated wild-type muscles *(A)* 3 months after nerve injury (50 Hz stimulus train, 0.5 s duration). **(C)** Mean (± SEM) EMG peak to peak amplitude recorded from unoperated and reinnervated wild-type and *NCAM -/-* soleus muscles 1 and 3 mo after nerve injury. $^{**}P < 0.01$; wild-type compared with corresponding *NCAM -/-*.

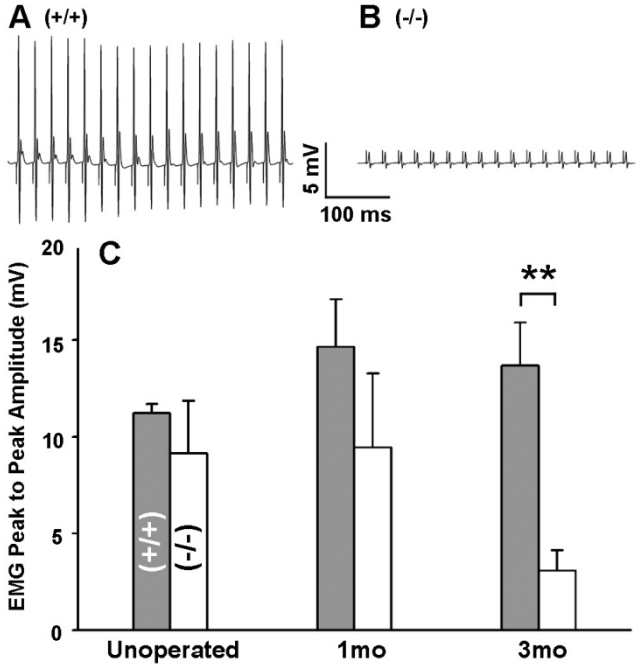
A (+/+)
B (-/-)
5 mV
100 ms
C
EMG Peak to Peak Amplitude (mV)
20
15
10
5
0
(+/+)
(-/-)
**
Unoperated
1mo
3mo

Figure 2.3: Reinnervated soleus muscles in *NCAM -/-* mice decrease in size because they lose muscle fibers. **(A-B)** Fast myosin immunolabeled cross-sections from the midbelly of unoperated and reinnervated wild-type *(A)* and *NCAM -/- (B)* soleus muscles 1, 3, 6 and 9 months after nerve injury. **(C-F)** Mean (± SEM) muscle cross-sectional area *(C)*, myofiber cross-sectional area *(D)*, myofiber number *(E)*, and number of fast muscle fibers *(F)* in unoperated and reinnervated wild-type and *NCAM -/-* soleus muscles 1, 3-6 (3 mo) and 7-9 (7 mo) months after nerve crush injury. $^{**}P < 0.01$ and $^{*}P < 0.05$; wild-type compared with corresponding *NCAM -/-*. CSA, cross-sectional area. Scale bar: 500μm

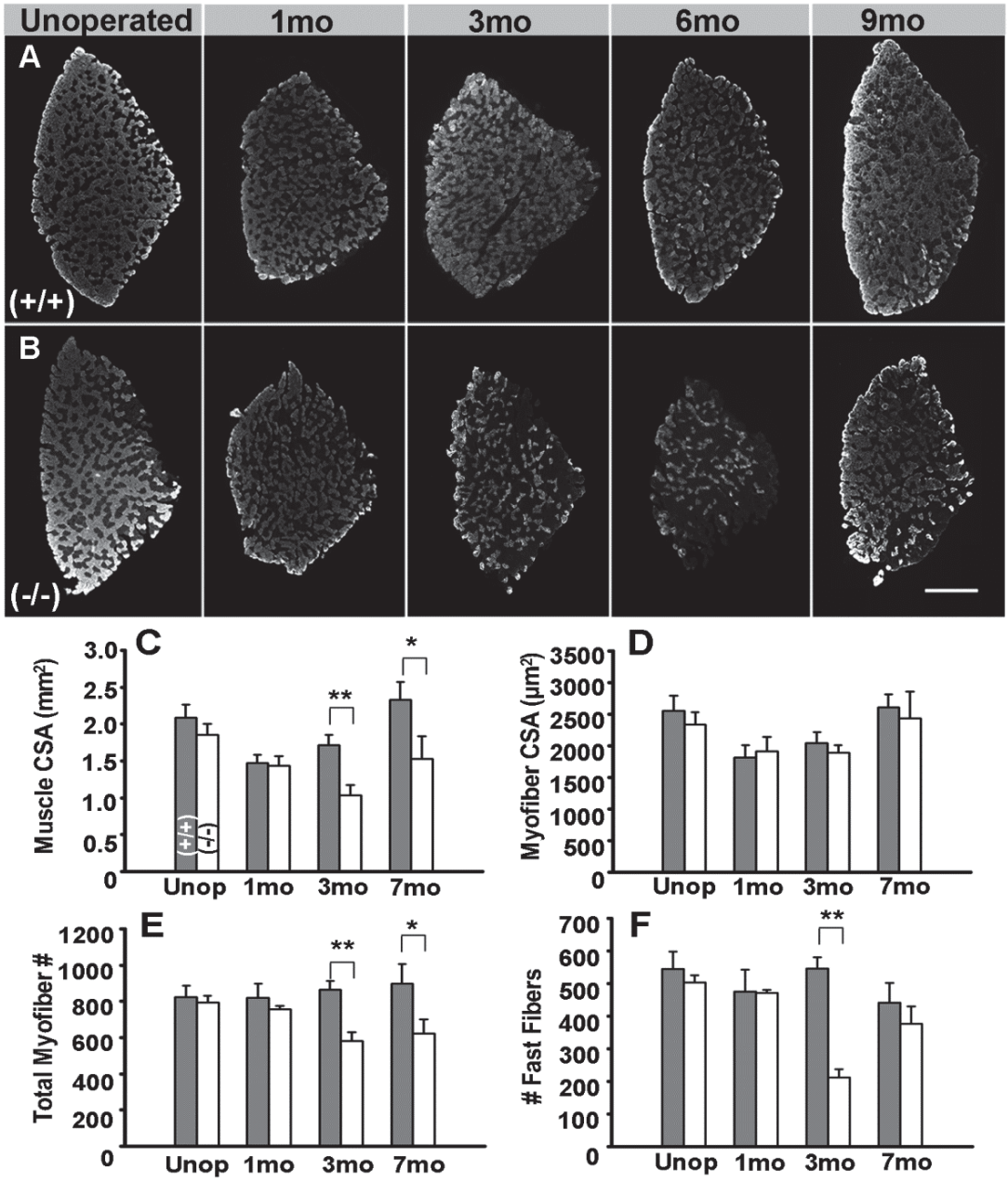
Unoperated
1mo
3mo
6mo
9mo
A
(+/+)
B
(-/-)
C
Muscle CSA (mm²)
3.0
2.5
2.0
1.5
1.0
0.5
0
(+/+)
(-/-)
**
*
Unop
1mo
3mo
7mo
D
Myofiber CSA (µm²)
3500
3000
2500
2000
1500
1000
500
0
Unop
1mo
3mo
7mo
E
Total Myofiber #
1200
1000
800
600
400
200
0
**
*
Unop
1mo
3mo
7mo
F
Fast Fibers
700
600
500
400
300
200
100
0
**
Unop
1mo
3mo
7mo

Figure 2.4: Axonal remnant formation and axosome shedding are associated with some reinnervated endplates in *NCAM -/-* mice 3 months after injury. **(A)** Neurofilament (NF) immunohistochemistry shows a single motor axon contact rhodamine-conjugated α-btx labeled AChRs at unoperated wild-type (+/+) and **(B)** *NCAM-/-*NMJs. **(C)** Similar morphology is observed at a reinnervated endplates in a wild-type soleus muscle 3 months after nerve injury. NF staining is continuous along the axon shaft. **(D)** While the majority of reinnervated endplates in *NCAM -/-* mice were similar to those in wild-type mice 3 months after injury, some endplates were contacted by discontinuous axons (*B*; arrow) connected by small neuronal remnants (*B*, small arrows) and neuronal protrusions (*B*, arrowhead). Scale bar: 10μm.

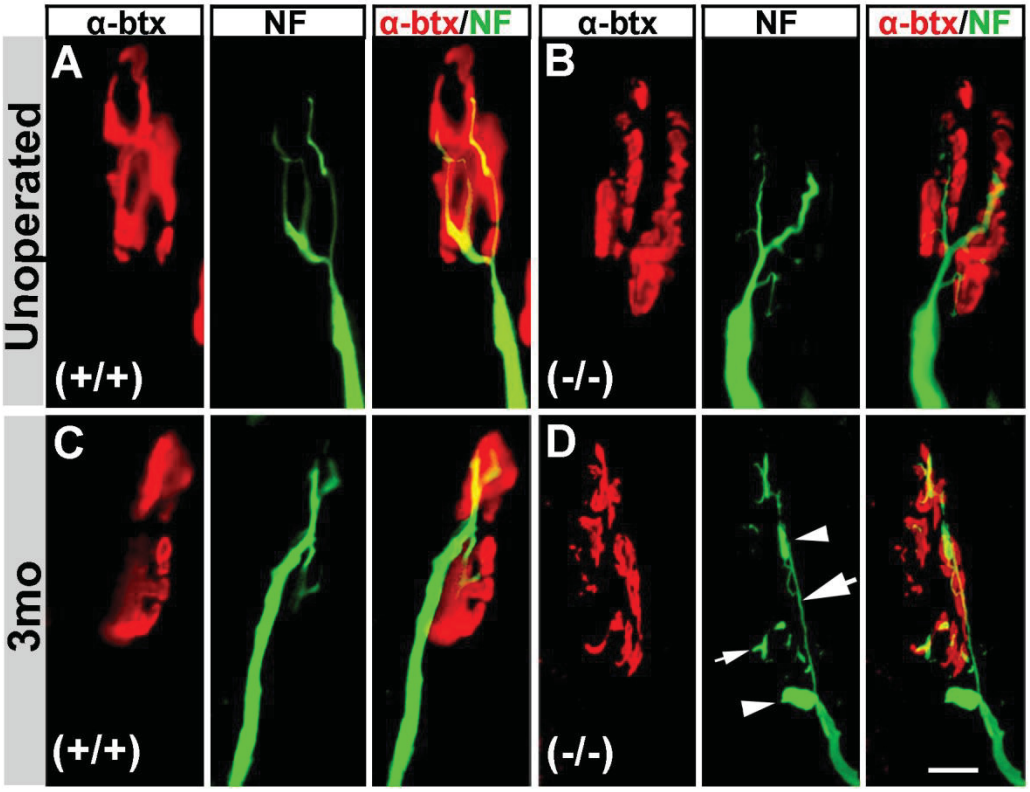
α-btx
NF
α-btx/NF
α-btx
NF
α-btx/NF
Unoperated
A
(+/+)
B
(-/-)
3mo
C
(+/+)
D
(-/-)

Figure 2.5: Morphological analysis indicated that a subset of soleus muscle fibers degenerated in *NCAM -/-* mice 3 months after injury. **(A-B)** H & E staining of unoperated and reinnervated soleus muscles in wild-type *(A)* and *NCAM -/-* mice *(B)* 1, 3 and 9 months after nerve injury. Three months after injury reinnervated *NCAM -/-* soleus muscles showed signs of degeneration including swollen fibers (*B*; asterisks, 3 mo) and macrophage infiltration (*B*; multiple nuclei indicated by arrows; 3 mo). Reinnervated *NCAM -/-* contained many small fibers with centrally located nuclei 9 months after injury (*B*, 9 mo; arrows) suggesting that myofiber regeneration was ongoing at this late time point. Scale bar: 100µm

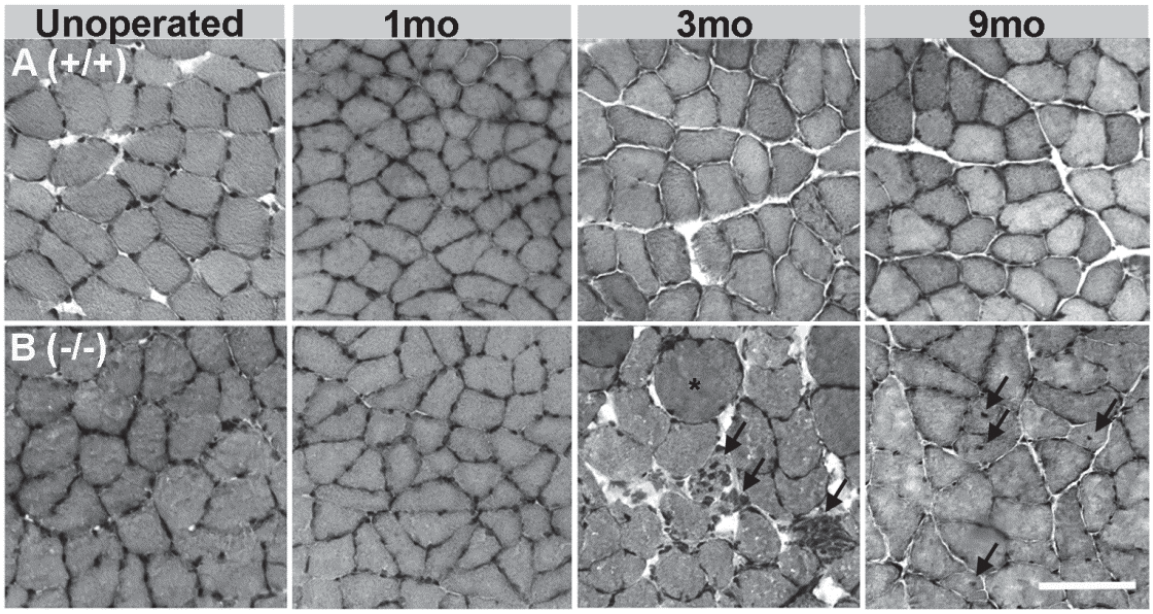
Unoperated
1mo
3mo
9mo
A (+/+)
B (-/-)
*

Figure 2.6: Reinnervated NCAM -/- muscles show signs of myofiber regeneration 9 months after injury. **(A-D)** Longitudinal sections of muscles stained with Hoechst and immunolabeled for MyoD shows that soleus muscles in unoperated wild-type *(A)* and *NCAM -/-* mice *(C)* are devoid of activated $MyoD^+$ satellite cells. In contrast to reinnervated wild-type muscles *(B)*, activated $MyoD^+$ satellite cells were interspersed throughout reinnervated NCAM -/- muscles 9 months after injury (*D*, arrows), although not all Hoechst+ cells were labeled with MyoD (*D*, arrowheads). Scale bar: 25µm

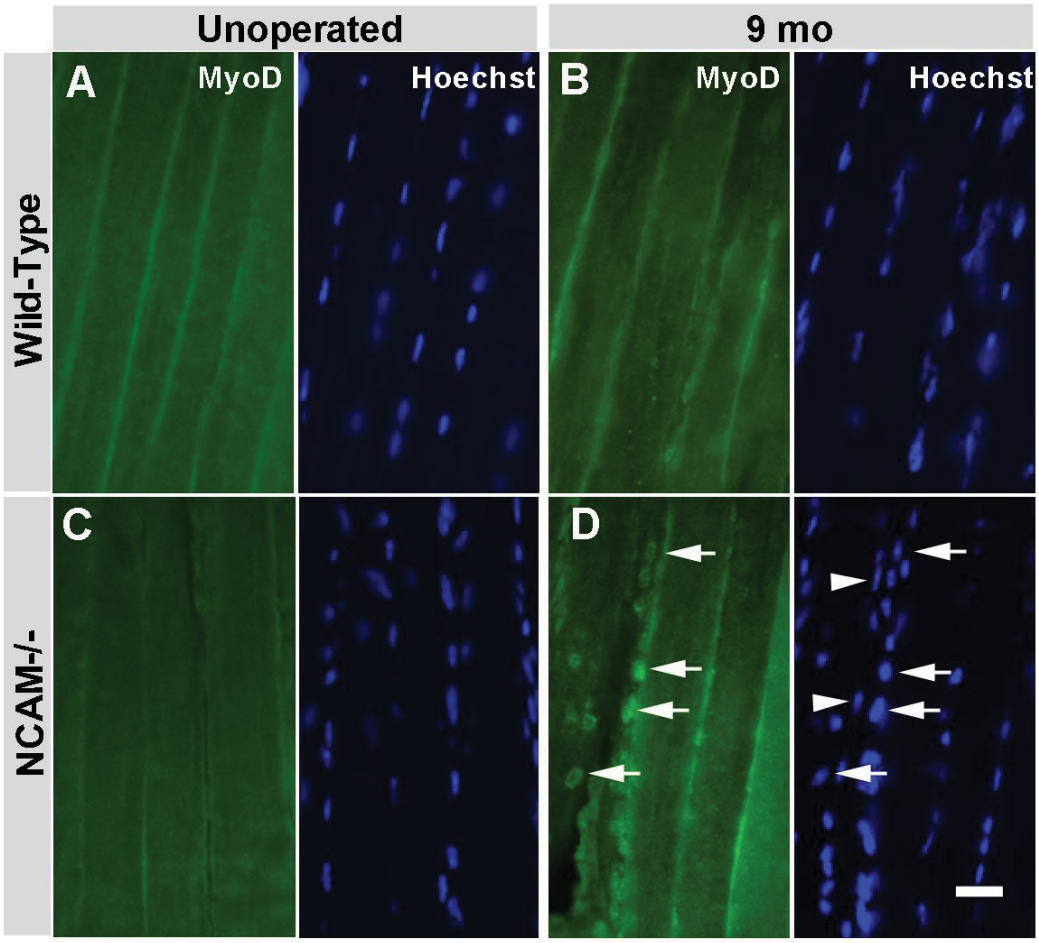
Unoperated
9 mo
Wild-Type
NCAM-/-
A
MyoD
Hoechst
B
MyoD
Hoechst
C
D

Figure 2.7: Reinnervated NCAM -/- mice exhibit alterations in transmitter release properties ≥3 mo after nerve injury. **(A-B)** Representative MEPPS and EPPs recorded from unoperated soleus muscles in wild-type *(A)* and NCAM -/- *(B)* mice. **(C-E)** Representative MEPPs and EPPs recorded from reinnervated wild-type *(C)* and NCAM -/- (*D* and *E*) muscles 3 months after injury. Some reinnervated NCAM -/- myofibers exhibited a large number of failed responses and small EPPs *(D)* while others had evoked EPPs that were skewed to smaller values *(E)*. Frequency histograms are for all EPPs recorded from the myofiber shown above. Failures are scored at 0 mV. **(F-J)** Mean (±SEM) EPP amplitude *(F)*, quantal content *(G)*, % failures *(H)*, MEPP amplitude *(I)* and MEPP frequency *(J)*. **P*<0.05, ***P*< 0.01, wild-type compared with corresponding *NCAM -/-*.

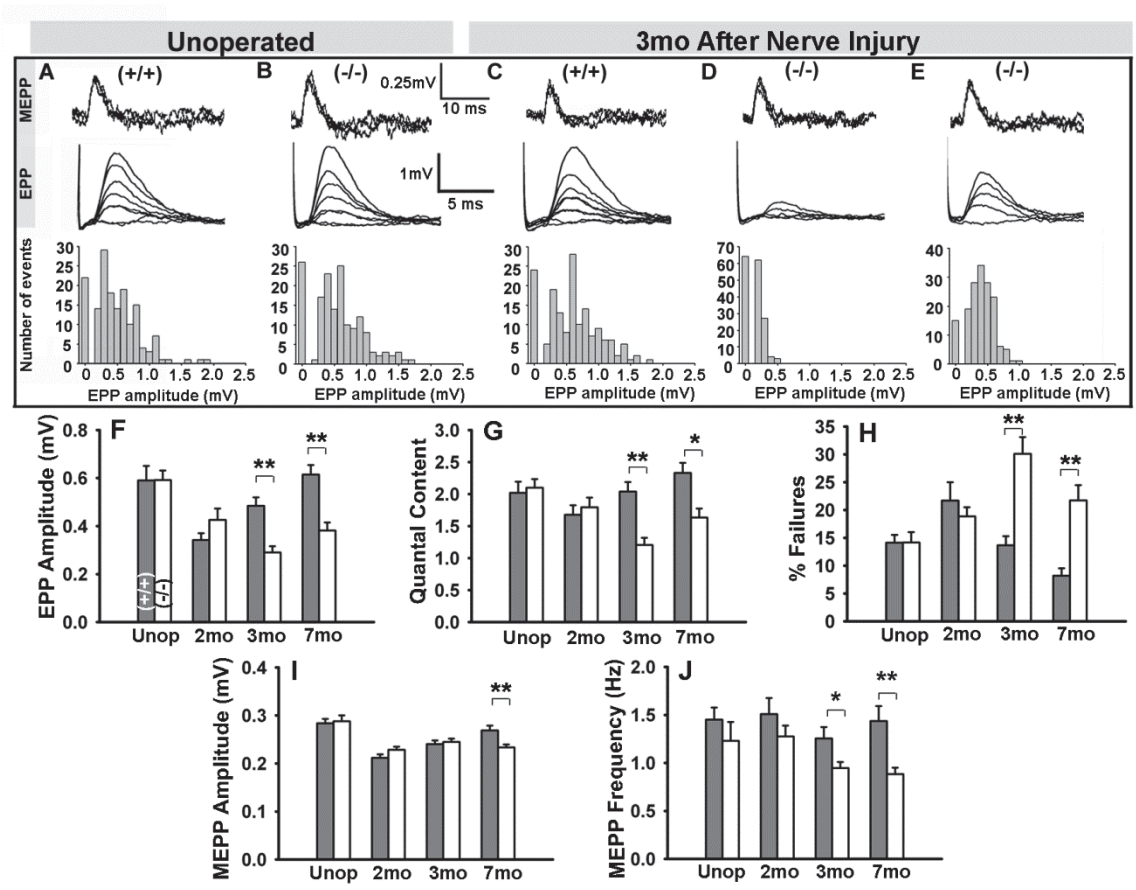
Unoperated
3mo After Nerve Injury
A
(+/+)
B
(-/-)
C
(+/+)
D
(-/-)
E
(-/-)
MEPP
EPP
0.25mV
10 ms
1mV
5 ms
Number of events
EPP amplitude (mV)
F
EPP Amplitude (mV)
G
Quantal Content
H
% Failures
I
MEPP Amplitude (mV)
J
MEPP Frequency (Hz)
Unop
2mo
3mo
7mo

Figure 2.8: Morphology of endplates in unoperated and reinnervated wild-type and *NCAM -/-* soleus muscles differ. **(A-D)** α-btx^{+} AChR clusters in unoperated wild-type *(A)* and *NCAM -/- (B)* mice align with presynaptic structures as revealed by antibodies to synaptophysin. However, some *NCAM -/-* endplates contained terminal sprouts that were not associated with α-btx^{+} AChRs *(B)*. Misalignments between pre- and post-synaptic structures were observed in both reinnervated wild-type *(C)* and *NCAM -/- (D)* muscles 6 months after injury. α-btx^{+} AChRs were distributed in more discrete fragments in reinnervated wild-type muscles *(D)* compared to unoperated controls *(A)*. **(E-F)** Mean (±SEM) α-btx binding area/NMJ *(E)* and number of fragments/NMJ *(F)*. **P*<0.05, ***P*< 0.01, wild-type compared with corresponding *NCAM -/-*. Scale bar: 10μm.

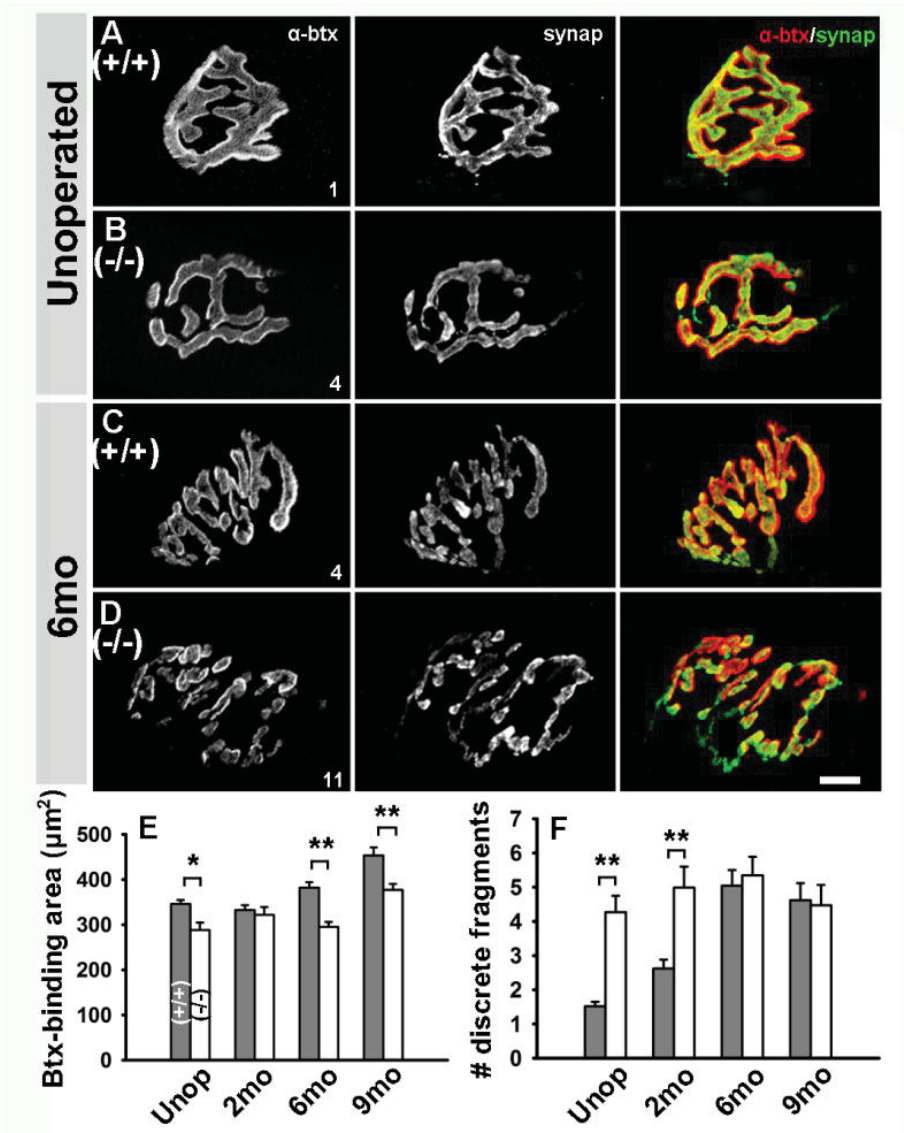
Unoperated
6mo
A
(+/+)
α-btx
synap
α-btx/synap
1
B
(-/-)
4
C
(+/+)
4
D
(-/-)
11
E
Btx-binding area (μm²)
500
400
300
200
100
0
*
**
**
(+/+)
(-/-)
Unop
2mo
6mo
9mo
F
discrete fragments
7
6
5
4
3
2
1
0
**
**
Unop
2mo
6mo
9mo

Figure 2.9: Conditional ablation of NCAM from motoneurons or muscle fibers does not disrupt neuromuscular function ≥3 months after nerve injury. **(A)** Overlay of individual isometric tetanic force tracings and quantification (% mean unoperated ± SEM) indicates that reinnervated wild-type, $NCAM^{flx/flx}/Hb9^{cre/+}$ and $NCAM^{flx/flx}/HSA^{cre/+}$ soleus muscles generate the same amount of force as unoperated muscles ≥3 month after injury. **(B)** NMJs in reinnervated $NCAM^{flx/flx}/Hb9^{cre/+}$ and $NCAM^{flx/flx}/HSA^{cre/+}$ mice have normal evoked neurotransmitter release properties (mean EPP amplitude, mean quantal content and % failures). However, the amplitudes of MEPPs were significantly larger than normal in both transgenic mice ≥3 months after injury. **(C)** Morphology of AChR clusters is abnormal in unoperated $NCAM^{flx/flx}/Hb9^{cre/+}$ and $NCAM^{flx/flx}/HSA^{cre}$ soleus muscles. Interestingly, morphological differences between endplates in the three strains of mice dissipated after injury. $P^{*}<0.05$, $^{**}P< 0.01$, as compared to corresponding wild-type. Hb9 cre, $NCAM^{flx/flx}/Hb9^{cre/+}$; HSA cre, $NCAM^{flx/flx}/HSA^{cre/+}$.

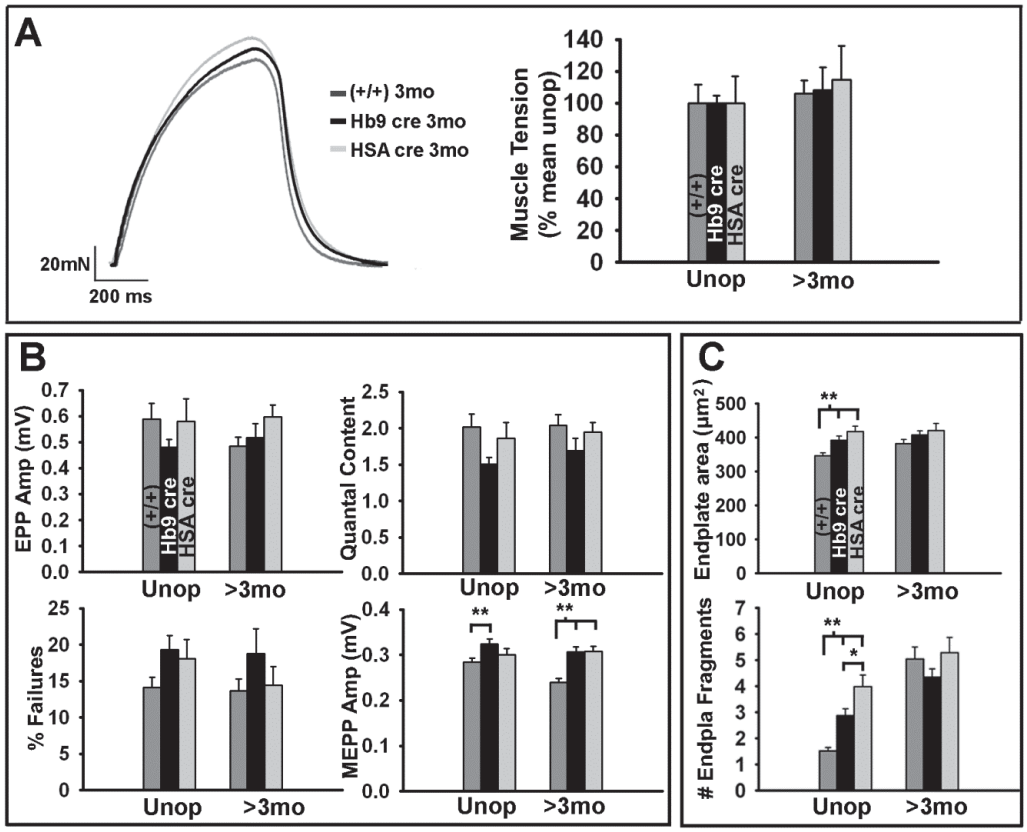
A
(+/+) 3mo
Hb9 cre 3mo
HSA cre 3mo
20mN
200 ms
Muscle Tension (% mean unop)
140
120
100
80
60
40
20
0
(+/+)
Hb9 cre
HSA cre
Unop
>3mo
B
EPP Amp (mV)
0.7
0.6
0.5
0.4
0.3
0.2
0.1
0.0
Quantal Content
2.5
2.0
1.5
1.0
0.5
0.0
% Failures
25
20
15
10
5
0
MEPP Amp (mV)
0.4
0.3
0.2
0.1
0.0
**
C
Endplate area (µm²)
500
400
300
200
100
0
Endpla Fragments
7
6
5
4
3
2
1
0
*

Figure 2.10: Many reinnervated NCAM-/- endplates are not capped by S100+ tSCs. **(A)** Unoperated wild-type **(B)**, NCAM-/- **(C)**, $NCAM^{flx/flx}/Hb9^{cre/+}$ and **(D)** $NCAM^{flx/flx}/HSA^{cre/+}$ btx^{+} endplates are innervated by an $S100^{+}$ myelinated axon (e.g. arrowhead in *A*) and completely capped with $S100^{+}$ tSC processes (e.g. arrow in *A*). **(E-H)** The vast majority of reinnervated wild-type *(E)*, $NCAM^{flx/flx}/Hb9^{cre/+}$ *(G)*, and $NCAM^{flx/flx}/Hb9^{cre/+}$ *(H)* endplates were capped by $S100^{+}$ tSCs. In contrast, ~30% of reinnervated NCAM-/- endplates lacked $S100^{+}$ tSCs altogether, or contained faintly labeled TCs that failed to extend processes over the AChRs (*F*, arrow; arrowhead indicates S100+ myelinating Schwann cell). Scale bar 10µm. **(I)** Mean (±SEM) percentage of motor endplates which were not capped by $S100^{+}$ tSC processes. ANOVA $^{**}P< 0.01$.

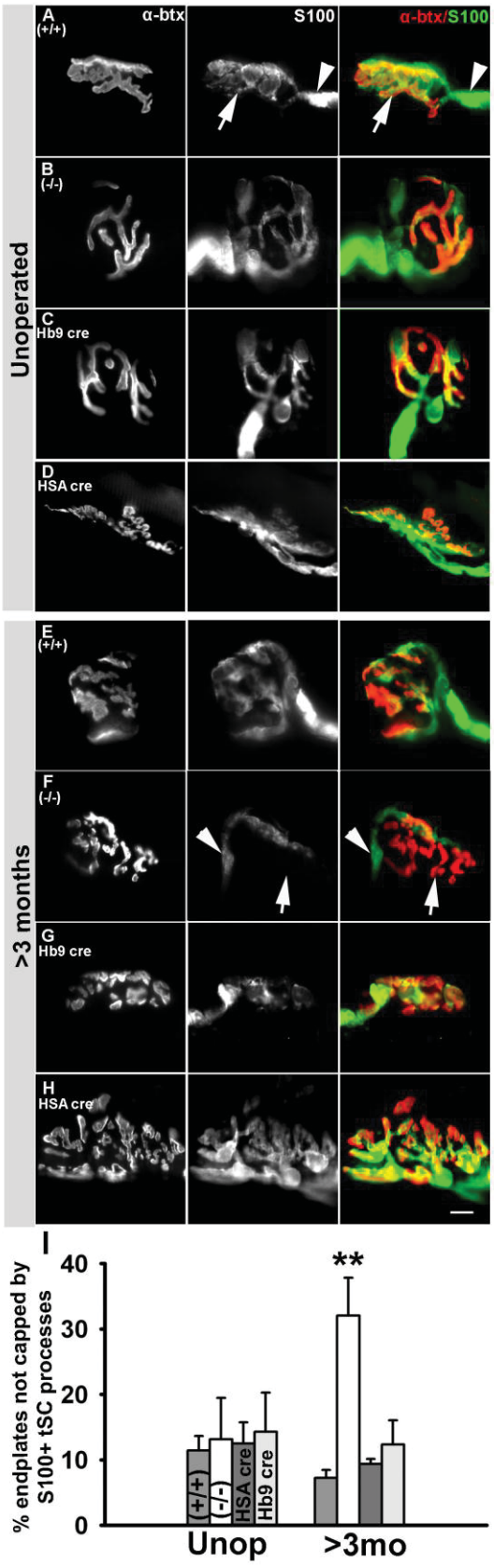
A
(+/+)
α-btx
S100
α-btx/S100
B
(-/-)
C
Hb9 cre
D
HSA cre
Unoperated
E
(+/+)
F
(-/-)
G
Hb9 cre
H
HSA cre
>3 months
I
% endplates not capped by S100+ tSC processes
40
30
20
10
0
**
(+/+)
(-/-)
HSA cre
Hb9 cre
Unop
>3mo

Figure 2.11: Terminal Schwann cells sprout extensively in denervated *NCAM-/-* muscles 4 days after nerve crush injury. **(A)** Four days following tibial nerve crush, WT and **(B)** *NCAM-/-* soleus muscles were stained for AChRs with α-btx and tSCs with anti s100. WT and *NCAM*$^{-/-}$ tSCs maintain contact with endplates and sprout extensively throughout the muscle following complete muscle denervation. Scale bars 40μm.

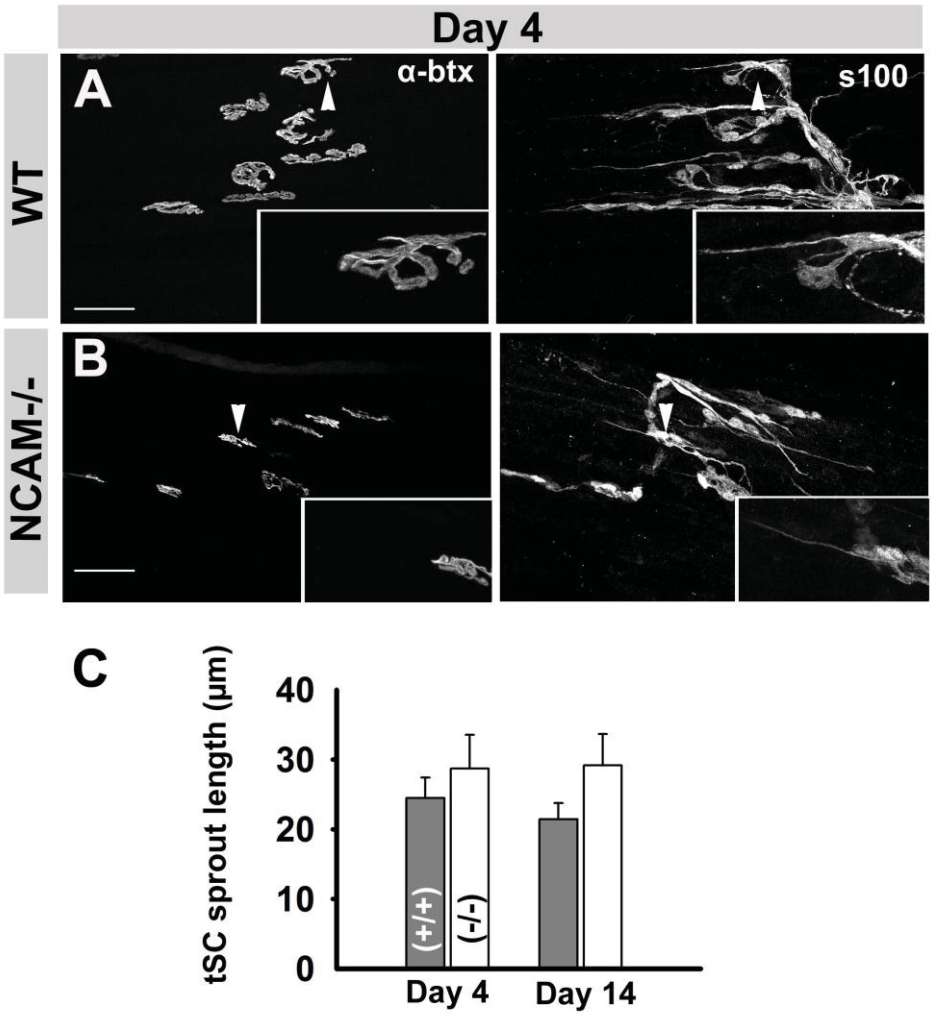
Day 4
WT
NCAM-/-
A
B
α-btx
s100
C
tSC sprout length (μm)
40
30
20
10
0
(+/+)
(-/-)
Day 4
Day 14

Chapter 3: The abundance of recycling synaptic vesicles limits the extent of terminal field expansion

Abstract

Terminal fields reorganize extensively throughout development and again in adulthood following periods of synaptic pathology brought on by trauma, disease or age-related challenges. In the neuromuscular system, the process of motor unit (MU) expansion is a well established model of terminal field reorganization, although the mechanisms which drive the remodeling process remain unknown. Surgically-induced partial muscle denervation allows the standardization of MU expansion in the adult animal and many studies have documented fixed limitations to the degree by which intact MUs can expand in response to severe denervation. The factors which limit extensive MU expansion in response to severe denervation remain elusive, although several studies have suggested that the strength of neurotransmission at sprouted synapses plays a crucial role. Here we describe that the extent of MU expansion is tightly correlated with the abundance of recycling synaptic vesicles which become available for redistribution within an axon arbor. Our findings demonstrate that sprouted synapses progressively strengthen because of a presynaptic, NCAM-dependent accumulation of synaptic resources delivered from NMJs extending terminal sprouts. We further demonstrate that postsynaptic NCAM provides a retrograde signal which determines the abundance of vesicles available for redistribution at sprouting synapses. Our data therefore provide insight into the coordinated regulation of synaptic strengths across a number of synapses on a terminal arbor undergoing reorganization by trans-synaptic adhesion molecule signaling.

Introduction

Activity-dependent synaptic remodeling is a primary feature of the neonatal and adult nervous systems and can range from small changes in local synaptic strengths (Branco et al 2008; Béïque et al 2011; Ratyanaka et al 2012) to large scale organization of entire terminal fields (Brown and Ironton, 1978; Dahm and Landmesser, 1988, 1991; Tapia et al 2012). Large scale reorganizations are most pronounced in the adult animal following injury or disease, where favourable functional outcomes depend on the effective redistribution of synaptic resources and the formation of new presynaptic terminals (Rochel and Robbins, 1988; Schaefer et al 2005). The local release of neurotransmitter and other secreted molecules is essential for functional synaptogenesis along growing axon branches and to contribute to the ultimate synaptic architecture of axonal arborizations (Dahm and Landmesser, 1988, 1991; Brandon et al 2003; Meyer et al 2006; Ruthazer et al 2006; Ben Fredj et al 2010; Bolliger et al 2010). Recent observations have revealed that actively cycling presynaptic vesicle puncta are constitutively mobile within mature axons and are shared between stable and putative presynaptic terminals in an activity-dependent manner (Kruegar et al 2003; Shakiryanova et al 2006; Staras et al 2010; Ratyanaka et al 2011). These studies, therefore, raise the possibility that activity-dependent redistribution of presynaptic resources may guide structural and functional remodeling of terminal arbors in adulthood.

Cell adhesion molecules are trans-synaptic regulators of synaptogenesis and NCAM in particular has received attention for its role in managing presynaptic resources at developing and adult synapses (Rafuse et al 2000; Polo-Parada et al 2001; Sytnyk et al 2002; Hata et al 2007; Galimberti et al 2010). Notably, the aggregation of presynaptic vesicles and cycling synaptic puncta to synaptic sites is disrupted at *NCAM*$^{-/-}$ neuromuscular junctions (NMJs) and these puncta fail to adopt mature Ca^{2+}-mediated cycling characteristics (Polo-Parada 2001, 2004). As a consequence, NCAM-deficient motor terminals demonstrate potentiated release probabilities under basal release conditions and impaired vesicle mobilization during high frequency repetitive stimulation (Rafuse et al 2000; Polo-Parada et al 2001, 2004, 2005). *NCAM*$^{-/-}$ NMJs are unstable and ultimately retract when reinnervated following nerve injury (Chipman et al 2010),

suggesting that NMJs lacking NCAM are functionally compromised, particularly after periods of pronounced structural plasticity.

Partial denervation of skeletal muscle induces remodeling of terminal arbors of motoneurons and has long been used as a model system to study structural synaptic plasticity in the adult animal (Brown and Ironton, 1978). Motor units (MUs) can expand to innervate up to 2-4 times their original complement of muscle fibers in partially denervated muscles (Brown and Ironton, 1978; Rochel and Robbins 1988; Rafuse et al 1992). As a result of MU expansion, contractile force in partially denervated muscles is usually restored even when ≤75% of the innervating motor neurons are lost, although the factors limiting more extensive MU expansion remain unknown. Interestingly, MUs in highly partially denervated muscles (i.e. >75%) contain a population of unstable synapses, presumably due to the exhaustion of the presynaptic release capabilities of the sprouting motoneuron (Rochel and Robbins, 1988; Rafuse et al 1992). If so, these results indicate that the adequate mobilization of synaptic resources may be an important factor regulating functional synaptic remodeling.

Here we demonstrate that pre- and postsynaptic NCAM is essential for compensatory functional reorganization of sprouting MUs under standardized partial denervation conditions. In the absence of presynaptic NCAM, MUs undergo structural expansion, but sprouted synapses fail to fully differentiate into functional NMJs because of an inability to redistribute and/or replenish the recycling pool of synaptic vesicles across populations of remodeling synapses. These findings suggest that homeostatic changes in the size of presynaptic vesicle pools are controlled by synaptic adhesion molecules and ultimately function to coordinately regulate the reorganization of synapses on a terminal axon arbor.

Materials and Methods

Mice

Four different strains of mice were used in this study. *NCAM* $^{-/-}$ mice, generated on a C57BL/6 background, were bred and housed locally. Hb9$^{cre/+}$::NCAM$^{flx/flx}$ mice (designated throughout as *Hb9*^{cre}*NCAM*^{flx}), which lack NCAM in motoneurons, were generated by breeding NCAM-floxed (NCAM$^{flx/flx}$) mice (Bukalo et al., 2004) with mice expressing cre-recombinase under control of the Hb9 promoter (Yang et al., 2001). HSA$^{cre/+}$::NCAM$^{flx/flx}$ mice (designated throughout as *HSA*^{cre}*NCAM*^{flx}), which lack NCAM on muscle fibers, were generated by crossing NCAM$^{flx/flx}$ mice with mice expressing cre-recombinase under control of the HSA promoter (Miniou et al., 1999; Cifuentes-Diaz et al., 2001). Wild-type control mice (designated *NCAM*$^{+/+}$ throughout) were cre negative littermates of *Hb9*^{cre}*NCAM*^{flx} and *HSA*^{cre}*NCAM*^{flx} mice. All procedures were conducted in accordance to the guidelines of the Canadian Council on Animal Care and the policies of Dalhousie University.

Partial denervation surgery and motoneuron back-labeling procedures

All surgeries were performed on 12 week old adult mice unless otherwise noted. Animals were anesthetized with isoflurane (Baxter, Toronto, ON, Canada) and a small incision was made in the skin in the dorso-medial aspect of the thorax. An incision was made in the fascia overlying the superior iliac crest and spinal muscles were separated to visualize the L4-S1 transverse spinous processes. The L5 spinous process was removed and the L5 root was carefully separated from surrounding tissue and ligated with a suture (10-0) to prevent regeneration. In some animals, a second procedure was performed to backlabel motoneurons immediately following the L5 root transection. A small incision was made in the skin overlaying the dorsal shank muscles. The soleus muscle was exposed and 0.5 µl of 1% Cholera toxin subunit b (CTB) conjugated to Alexa Fluor 594 or 488 (C22842; Invitrogen, Burlington, ON, Canada) was injected into either the ipsilateral or contralateral soleus muscle near the nerve entry point. A second surgery was performed in a subset of animals and has been described previously (Chipman et al 2010). Briefly, a small incision was made in the skin above the dorsal aspect of the knee in order to expose the tibial nerve which was crushed 2 times consecutively 10 mm distal to its divergence

from the sciatic. Denervation was visually confirmed by noting muscle contraction and subsequent transparency of the nerve at the crush site.

In vitro isometric tension recordings

Mice were killed and their right hindlimb quickly dissected and placed into ice cold, oxygenated Tyrode's (125 mM NaCl, 24 mM NaHCO3, 5.37 mM KCl, 1 mM $MgCl_2$, 1.8 mM $CaCl_2$, and 5% dextrose). The soleus muscle and nerve supply was isolated and cut free at its insertion points on the femur and calcaneous bones. The proximal muscle tendon was securely pinned down on a Sylgard (Dow Corning, Midland, MI) coated recording chamber that was perfused with oxygenated Tyrode's solution at room temperature. A suture (2-0) was tied to the distal tendon and connected to a force transducer (FT 03; Grass Technologies, West Warwick, RI). A fine-tipped polyethylene stimulating suction electrode (PE-190; Clay Adams, Sparks, MD) was used to deliver electrical current to the soleus nerve via a S88 stimulator (Grass Technologies) that was isolated from ground using a stimulus isolation unit (PSIU6; Grass Technologies). Monophasic electrical stimuli (0.05 ms) were used to elicit maximal isometric contractions that were acquired at 10 kHz using a Digidata 1322A A/D board and Axoscope 9.2 software (Axon Instruments, Union City, CA).

Intracellular muscle fiber electrophysiology and the estimation of binomial statistics

Intracellular muscle fiber recordings were performed on unoperated, partially denervated or completely reinnervated soleus muscles in well-oxygenated (95% O_2 and 5% CO_2) Tyrode's solution containing 125mM NaCl, 5.37mM KCl, 24mM $NaHCO_3$, 1 mM $MgCl_2$, 1.8 mM $CaCl_2$ and 5% dextrose according to previously published procedures (Rafuse et al., 2000; Chipman et al. 2010). 5μM μ-contoxin GIIIB (Alomone Labs, Jerusalem, Israel) was added to the bath to block postsynaptic muscle contraction via inhibition of muscle Na^+channels. In some indicated experiments, the calcium channel blockers nifedipine (Sigma; 50μM; used to block L-VDCCs) and ω-agatoxin IVA (Alomone Labs, Jerusalem, Israel; 100nM; used to block P/Q type VDCCs) diluted in 0.001% ethanol were sequentially applied to the recording chamber. 0.001% ethanol was used as a control vehicle treatment in these studies.

Estimation of binomial statistics was peformed as described by Del Castillo and Katz (1954a,b), Martin (1955) and Searl and Silinsky (2003). Briefly, recorded EPPs were corrected for non-linear summation as described by McLachlan and Martin (1981) and quantal contents (*m*) were calculated by the ratio of the mean endplate potentials generated at 1Hz to the mean miniature endplate potential amplitude:

$$(1)\ m = \frac{EPP}{mEPP}$$

Where *m* is the quantal content, EPP is the mean corrected EPP and mEPP is the mean mEPP. The probability of release (*p*) was estimated based on the following equation, derived in Searl and Silinsky (2003):

$$(2)\ p = 1 - \frac{\mathrm{Var_{EPP}}}{\mathrm{EPP\ X\ mEPP}} + \frac{\mathrm{Var_{mEPP}}}{\mathrm{mEPP^2}}$$

where *p* is the probability of release at individual release sites, Var_{EPP} is the variance of corrected EPPs, Var_{mEPP} is the variance of mEPPs.

Finally, the number of available sites for release (*n*) was estimated based on the relationship of *m* to *p*:

$$(3)\ n = \frac{m}{p}$$

Immunofluorescence and imaging

Immediately following cessation of physiological recordings, soleus muscles were pinned at physiological length, fixed for 20 minutes in 4% paraformaldehyde/PBS and then teased into bundles of approximately 20-40 muscle fibers. For diaphragm immunofluorescence, E15 and E18.5 embryos were removed and placed in ice-cold Tryrode's solution as described above to maintain the integrity of the tissue during dissection. Whole diaphragm muscles were excised and fixed for 20 minutes in 4% paraformaldehyde with attachments to the rib cage preserved. All muscles were incubated in 0.1M glycine for 1 hour, washed in PBS and placed in a PBS solution containing α-bungarotoxin (α-BTX, 1:500 Invitrogen) for 1 hour at room temperature. After several washes in PBS, the fibers were incubated overnight at room temperature in primary antibodies which included; rabbit anti-synaptophysin IgG (1:500 Invitrogen), mouse anti-SV2 IgG (1:50: Developmental Studies Hybridoma Bank, Iowa City, Iowa), mouse anti-

Pan-Axonal Neurofilament IgG (1:500; SMI-312; Covance, Hornby, ON, Canada), rabbit anti-S100 IgG (1:500; Z0311; DakoCytomation, Glostrup, Denmark) and rabbit anti-p75 (1:200; ab8874; Abcam, Cambridge MA, USA). Muscle fibers were then washed in PBS and incubated for 1 hour in a cocktail of secondary antibodies which included; goat anti rabbit IgG conjugated to Alexa Fluor 488 or 647 (1:500 Invitrogen), goat anti-mouse IgG secondary antibody conjugated to Alexa Fluor 488 or 647 (1:500; Invitrogen). All antibodies were applied in the presence of 10% blocking solution and 0.3% TritonX-100/PBS (except FM4-64FX experiments, see below). Fibers were finally washed in PBS and mounted in 50% glycerol/PBS mixture containing 0.03 mg/ml ρ-phenylenediamine.

For quantification of endplate morphology and synaptic vesicle immunofluorescence, muscle fibers were digitally photographed using a wide-field fluorescence microscope equipped with a broad focal plane lens (Leica Microsystems, Bannockburn, IL, USA attached to a digital camera; C4742; Hamamatsu, Japan). Endplates were only quantified if the captured imaged accurately reflected the entire three-dimensional structure. Captured images were analyzed for pre and postsynaptic areas and synaptic vesicle fluorescence (corrected for background) using IPLab software (Version 4.0; BD Biosciences) as previously described (Chipman et al 2010). Representative images are shown as collapsed z-stacks acquired using an LSM510 laser scanning confocal microscope (Zeiss Microimaging, Thornwood, NY, USA) and managed using Zen 2009 software (Zeiss Microimaging).

FM4-64FX loading and imaging

5μM FM4-64FX (Invitrogen) was added to the recording chamber 5 minutes prior to stimulating the soleus nerve at 50Hz for 10 minutes (1 second train of pulses every 2 seconds). The stimulated muscles were left unstimulated for 5 minutes to allow for residual endocytosis (Gaffield and Betz, 2006). Loaded muscles were then washed for 40 minutes with low calcium Tyrode's solution (125mM NaCl, 5.37mM KCl, 24mM $NaHCO_3$, 5mM $MgCl_2$, 0.6mM $CaCl_2$ and 5% dextrose) to prevent vesicle cycling during the wash (Maeno-Hikichi et al 2011), fixed for 20 minutes with 4% paraformaldehyde/PBS, teased into bundles of approximately 20-40 muscle fibers, incubated in 0.1M glycine for 1 hour, washed in PBS and placed in a PBS solution

containing α-BTX (1:500) for 1 hour at room temperature. After several washes in PBS, fibers were incubated overnight at room temperature in rabbit anti-synaptophysin IgG (1:500) primary antibodies in the presence of 10% blocking serum and 0.15% Triton X-100/PBS, washed in PBS, incubated for 1 hour in goat anti rabbit IgG secondary antibody conjugated to Alexa Fluor 488 (1:500) in 10% blocking serum and 0.1% Triton X-100/PBS. Muscles were then washed with PBS and mounted in 50% glycerol/PBS mixture containing 0.03 mg/ml ρ-phenylenediamine to prevent fading. Z stacks of identified NMJs were captured with an LSM510 laser scanning confocal microscope (Zeiss Microimaging, Thornwood, NY, USA). Synaptophysin fluorescence was excited with a 488nm excitation laser and emission was captured with a 500-530nm bandpass filter. α-BTX fluorescence was excited with a 543nm laser excitation and emission was captured with a 565-615nm bandpass filter. FM4-64FX was excited with a 488nm laser and emission was captured with a 685 longpass filter. Fluorescence intensity measurements were corrected for background and was performed on collapsed z-stacks using Zen 2009 software (Zeiss Microimaging).

Quantification of motoneuron number

Spinal cords from CTB injected mice were sectioned longitudinally at 40 μm as previously described (Franz et al., 2005; Chipman et al., 2010). Raw cell counts were corrected by the Abercrombie method (Abercrombie, 1946).

Estimation of total recycling pool (RP) size of unoperated and sprouting motoneurons

The total complement of RP vesicles of partially denervated $NCAM^{+/+}$, $Hb9^{cre}NCAM^{flx}$ and $HSA^{cre}NCAM^{flx}$ motoneurons was estimated based on the mean number of parent and regenerated synapses per partially denervated muscle (as determined by syp/NF immunohistochemistry; Figure 3.2*E*), the mean number of RP vesicles per parent and regenerated synapse (Figure 3.9*K*), and the number of soleus motoneurons remaining following L5 partial denervation (Figure 3.1*C*). Corrections were made where appropriate to control for the relative abundance of cycling synaptic vesicles mislocalized to non-synaptic regions (Figure 3.3*G, I*). Similar analysis was performed for unoperated soleus

motoneurons, using data obtained from contralateral soleus muscles. Ratios of expanded MUs as compared to unoperated MUs are shown in Figure 3.14.

Statistical Analysis

One-way ANOVAs were performed to examine the differences between groups over time. Holm-Sidak or Dunn's pairwise multiple comparisons test were then used to determine where significant differences occurred if the F-value exceeded F-critical. Two tailed-Student's t-tests were used when comparing between two groups if normality was achieved. If normality was not achieved, Mann-Whitney tests or ANOVA on ranks were used to compare between groups. Statistical significance was considered to be achieved when $P < 0.05$.

Results

Partial denervation of the mouse soleus

A remarkable form of synaptic plasticity occurs in partially denervated skeletal muscles as uninjured motor axons sprout new processes that quickly form additional synapses with neighboring denervated muscle fibers (Brown and Ironton, 1978; Rochel and Robbins, 1988; Son and Thompson, 1995b). In so doing, motor axons can increase their peripheral field of innervation by 3-4 times their original size (Rafuse et al., 1992). This expansive synaptic reorganization requires rapid mobilization, and defined redistribution, of presynaptic resources to the newly formed synapses at the NMJ. However, the cellular mechanisms regulating this targeted mobilization of presynaptic resources are not well understood. NCAM is required for proper management of presynaptic resources at the NMJ (Rafuse et al 2000; Polo-Parada et al 2001, 2004, 2005; Hata et al 2007) and in the structural and functional plasticity of central synapses (Muller et al 1996; Dityatev et al 2004; Kochlamazashvili et al 2012). It therefore seemed reasonable to examine whether NCAM is necessary for functional recovery of muscle function in partially denervated muscles and, if so, does it do so by regulating the mobilization of presynaptic resources. Because NCAM is expressed in adult motor neurons, terminal Schwann cells and muscle fibers at the NMJ (Covault and Sanes, 1986), we chose to examine these issues using a cre/lox breeding strategy to generate transgenic mice that only lack NCAM in motor neurons ($Hb9^{cre}NCAM^{flx}$ mice; see Appendix Figure A1). The soleus muscles in $Hb9^{cre}NCAM^{flx}$ mice were partially denervated and their physiology/anatomy was compared to partially denervated soleus muscles in their wild-type littermates ($NCAM^{+/+}$). However, before doing so we first needed to determine if the soleus muscle in $Hb9^{cre}NCAM^{flx}$ mice is partially denervated to the same extent as wild-type mice when the motor innervation is reduced by cutting one of its two contributing spinal roots. This issue is pertinent because changing NCAM expression during development alters motor axon pathfinding (Landmesser et al., 1988).

In rodents, the soleus muscle receives 30-35% of its innervation via the L4 spinal root with the remaining 65-70% coming from the L5 root (Brown and Ironton, 1978; Rochel and Robbins, 1988; Tam et al 2001). To compare the spinal root contribution to

the innervation of the soleus in wild-type mice ($NCAM^{+/+}$), $NCAM^{-/-}$ mice and $Hb9^{cre}NCAM^{flx}$ mice, the L5 spinal root was cut and ligated. The contralateral and ipsilateral muscles were then injected with CTB conjugated to different fluorphores to unambiguously identify soleus motor pools with and without L5 innervation (Figure 3.1*A, B*). We found that the L5 spinal root contributed approximately 65% of soleus innervation in all three genotypes (Figure 3.1*C*; unop P=0.94; L5 PD P=0.39, one way ANOVA), suggesting that the rostral/caudal distribution of spinal motor neurons innervating the soleus is not noticeably altered in $Hb9^{cre}NCAM^{flx}$ mice. In addition, we did not observe differences in intramuscular branching patterns between the three genotypes suggesting that the compartmentalization of motor units was also similar (Appendix Figure A2). Taken together, these results indicate that the neuromuscular anatomy of $Hb9^{cre}NCAM^{flx}$ mice is not dramatically different from normal and that L5 spinal root transection consistently denervates the soleus to the same extent.

Compensatory recovery of motor output by collateral sprouting requires presynaptic NCAM

The functional consequence of motor unit loss in $Hb9^{cre}NCAM^{flx}$ mice was assessed by measuring tetanic forces generated from partially denervated soleus muscles in response to a one second train of stimuli delivered at 50Hz (Figure 3.2*A-B*). This assessment permitted functional analysis of sprouting capacity because only synapses strong enough to induce postsynaptic depolarization would contribute to force generation. Figure 3.2*A-B* shows that the soleus in unoperated $NCAM^{+/+}$ and $Hb9^{cre}NCAM^{flx}$ mice generated comparable force values (Figure 3.2*A,B*; P=0.136, Student's t-test; see also Chipman et al 2010). As expected by the degree of denervation (Figure 3.1*C*), the tetanic forces of the partially denervated soleus muscles in $NCAM^{+/+}$ and $Hb9^{cre}NCAM^{flx}$ mice decreased by ~ 80% seven days post surgery (Figure 3.2*A,B P*=0.94 Student's t-test). The contractile force of the soleus muscles in the $NCAM^{+/+}$ mice increased significantly 14 days post partial denervation (pPD) and maintained this output throughout the remainder of the recovery period studied (Figure 3.2*A,B*). Interestingly, the tetanic forces of the partially denervated soleus muscles in the $Hb9^{cre}NCAM^{flx}$ mice did not increase significantly over time (Figure 3.2*A, B P*<0.05, one way ANOVA), and remained weaker than those

recorded from the *NCAM*$^{+/+}$ mice (Figure 3.2*B*; $P<0.05$ Student's t-test). Thus, functional recovery from partial denervation requires NCAM expression in motor neurons.

To determine whether reduced tetanic forces in the partially denervated muscles was due to muscle fiber denervation, we used a combination of pre and postsynaptic markers to anatomically assess innervation of the NMJs in a subset of muscles used in the force recordings (Figure 3.2*C, D*). Four types of endplates were classified in the partially denervated muscles based on synaptophysin (syp) and neurofilament (NF) immunohistochemistry and rhodamine conjugated α-bungarotoxin (α-BTX) staining (see Schaefer et al 2005). First, 'parent' terminals were identified as uniform, intensely labeled syp$^+$ puncta that overlapped the majority of the postsynaptic α-BTX$^+$ acetylcholine receptors (AChRs; Figure 3.2*D* arrows) and were innervated by a large caliber, variegated axon as identified by NF immunolabeling (Figure 3.2*D;* arrow). This morphology is comparable to NMJs in unoperated mice (data not shown; see Schaefer et al 2005). Second, completely denervated endplates were classified as characteristic clusters of α-BTX$^+$ AChRs that were not adjacent to syp$^+$ and NF$^+$ staining (Figure 3.2*D*, asterisks). Third, 'reinnervated' endplates were identified as punctate syp immunolabeling that overlapped with α-BTX$^+$ AChRs (Figure 3.2*D*, filled arrowheads) and were innervated by smooth, thin axonal sprouts emanating from a 'parent' terminal (Figure 3.2*D*; Day 30) or node of Ranvier (not shown). Finally, NMJs were classified as 'contacted' endplates if syp$^+$ puncta covered <5% of the α-BTX$^+$ endplates (Figure 3.2*D*, open arrowhead).

Consistent with our force recordings, the percentage of innervated endplates (parent + reinnervated) in the soleus was reduced to ~25% that of control values in both genotypes 7 days pPD (Figure 3.2*C, D*; P=0.95, Student's t-test). This percentage increased to ~80% in the *NCAM*$^{+/+}$ mice 14 days pPD and remained at this value 30 days pPD (Figure 3.2*C*; $P<0.05$ one way ANOVA). Interestingly, wild-type soleus muscles never recovered 100% innervation, suggesting some limitation to the reinnervation capacity of sprouting MUs (Rafuse et al 1992). As expected from the force recordings, the percentage of innervated endplates (parent + reinnervated) in the *Hb9*^{cre}*NCAM*^{flx} mice was significantly lower than that observed in the *NCAM*$^{+/+}$ mice at pPD day 14 and 30 (Figure 3.2*C*; $P<0.05$ Student's t-test). These deficits agree with the reduced force values

recorded at these time points (Figure 3.2*B*) and suggest that axonal sprouting and/or synaptogenesis is hampered in *Hb9^{cre}NCAM^{flx}* mice.

Presynaptic NCAM mediates regenerative presynaptic differentiation

Because NCAM mediates axonal growth (Doherty et al 1990) we measured the number and length of NF+ terminal sprouts emanating from a parent terminal or node of Ranvier in *NCAM$^{+/+}$* and *Hb9^{cre}NCAM^{flx}* soleus muscles 7 days pPD. Surprisingly, we found no difference in length (*NCAM$^{+/+}$* 26.76±2.57μm; *Hb9^{cre}NCAM^{flx}* 26.55±2.31μm; P=0.846 Mann-Whitney rank sum test) or number (*NCAM$^{+/+}$* 1.70±0.12 sprouts/endplate; *Hb9^{cre}NCAM^{flx}* 2.06±0.17 sprouts/endplate; P=0.055 Mann-Whitney rank sum test) of axonal sprouts between *NCAM$^{+/+}$* and *Hb9^{cre}NCAM^{flx}* muscles one week after partial denervation. In addition, terminal Schwann cells, which participate directly in the recovery from partial denervation (Son and Thompson, 1995b; Tam and Gordon, 2003; Love et al 2003), were found to sprout appropriately and formed bridges between endplates in *Hb9^{cre}NCAM^{flx}* which guided the growth of motor axons (Appendix Figure A3). Together, these results suggest that the sprouting process, at least with respect to growth, is not hindered when NCAM is absent from the innervating motor neuron.

To quantify the distribution of synaptic vesicles during terminal field expansion, we measured the percent overlap between syp+ and AChR+ puncta (Figure 3.2*E*; % occupation) at contacted, reinnervated, and parent motor terminals and compared those to control values in unoperated mice (Figure 3.2*E*). Consistent with previous studies (Fox et al 2007; Williams et al 2009), we found that synaptic vesicles occupied~80% of the postsynaptic endplate in unoperated *NCAM$^{+/+}$* mice (ranged from 60 – 100%). Although the distribution of synaptic vesicles was not readily different, the percent occupancy at *Hb9^{cre}NCAM^{flx}* NMJs in unoperated mice was significantly smaller than *NCAM$^{+/+}$* NMJs (Figure 3.2*E*, unoperated; P=0.007 Student's t-test). The range in percent occupancy increased dramatically at NMJs in partially denervated soleus muscles in the *NCAM$^{+/+}$* and *Hb9^{cre}NCAM^{flx}* mice 14 and 30 days pPD (Figure 3.2*E*). This was due to the appearance of reinnervated endplates with very low percent occupancy (Figure 3.2*E*; red histograms) as well as a broadening of the range in the parent terminals (Figure 3.2*E*; blue histograms). Despite having similar trends in synaptic vesicle distribution, there

were several significant differences between the two genotypes. First, the percent occupancy at regenerated *Hb9^{cre}NCAM^{flx}* terminals was significantly smaller than *NCAM$^{+/+}$* terminals at 14 and 30 days pPD (Figure 3.2*E*; $P<0.001$ Mann-Whitney rank sum test). Second, percent occupancy at the parent terminal decreased significantly between 14 and 30 days pPD in *Hb9^{cre}NCAM^{flx}* (Figure 3.2*E, P*<0.001 Mann Whitney rank sum test), but not *NCAM$^{+/+}$* mice (Figure 3.2*E*, P>0.05 Mann Whitney rank sum test). Third, the percent occupancy at reinnervated terminals increased between 14 and 30 days in *NCAM$^{+/+}$* muscles (Figure 3.2*E*, *P*>0.001), while it progressively decreased at *Hb9^{cre}NCAM^{flx}* endplates (Figure 3.2*E*, *P*=0.041) during the same time period. Finally, partially denervated soleus muscles in *Hb9^{cre}NCAM^{flx}* mice contained many 'contacted' endplates while *NCAM$^{+/+}$* muscles did not (Figure 3.2*E*; yellow histograms). Taken together, these observations indicate that the distribution of synaptic vesicles at NMJs is abnormal in motor axons lacking NCAM after partial denervation and that this difference correlates well with the poor recovery in force observed in these mice.

Synaptic vesicle redistribution is altered in the absence of presynaptic NCAM

Synaptic plasticity associated with the formation of *de novo* synapses involves the mobilization of vesicles from established terminals to newly formed synapses (DePaiva et al 1999; Krueger et al 2003). To determine whether synaptic vesicles mobilize in a similar manner in partially denervated muscles, we quantified syp immunofluorescence intensity at the parent and reinnervated α-BTX+ endplates as well as along NF+ axons bridging the parent and reinnervated terminals in *NCAM$^{+/+}$* and *Hb9^{cre}NCAM^{flx}* mice. Double labeling with antibodies against syp and NF demonstrated that synaptic vesicles were abundant in both *NCAM$^{+/+}$* and *Hb9^{cre}NCAM^{flx}* terminal bridges 7 days after partial denervation, indicating that vesicles were being shuttled between established and developing endplates (Figure 3.3*A*; arrowheads). To quantify whether there were differences between the two genotypes we examined the intensity and distribution of syp+ immunofluorescent puncta at parent (pT) and reinnervated (rT) terminals as well as in sprouts that bridged terminals (tB) or simply grew away from a parent terminal (tSp) (Figure 3.3*B-E*; insets). Fluorescence was quantified by generating a syp/SV2/α-BTX intensity line plots through the parent terminal (pT), along the terminal bridge (tB) and

through the reinnervated terminal (rT). Using this approach we found that the immunofluorescence intensity at the parent terminals in both genotypes was only one third that observed in unoperated terminals (Figure 3.3*F, H*; compare dark blue with light blue bars), which is consistent with active mobilization of vesicles away from parent terminals during MU reorganization. Several other changes in vesicle distribution occurred in the partially denervated muscles between 7 and 30 days pPD. First, syp fluorescence increased and reached a plateau at reinnervated $NCAM^{+/+}$ terminals (Figure 3.3*G*, light red bars, $P<0.001$ one way ANOVA), while the fluorescence intensity throughout the terminal bridges gradually decreased over the same time period (Figure 3.3*G,* dark red bars; $P<0.001$ one way ANOVA). In contrast, the fluorescence intensity of syp in $Hb9^{cre}NCAM^{flx}$ reinnervated terminals did not increase over time (Figure 3.3*I*, light red bars; $P=0.108$ one way ANOVA), nor did syp fluorescence in terminal bridges decrease (Figure 3.3*I*, dark red bars; $P=0.971$ one way ANOVA). These data suggest that synaptic vesicles are shuttled along the terminal bridge from established to newly formed terminals and that this process is hindered when NCAM is absent from the innervating motor neuron.

NCAM is present along terminal sprouts and co-distributes with cycling synaptic puncta

Mobilized synaptic vesicles actively cycle with the plasma membrane and participate in the formation of new synapses during synaptic plasticity (DePaiva et al 1999; Tarsa and Goda, 2002; Ruthazer et al 2006; Meyer and Smith, 2006). To assess whether vesicle cycling occurs in intramuscular axonal sprouts after partial denervation, we loaded motor axons with FM4-64FX 7 days pPD using a 50Hz stimulation paradigm (Figure 3.4*A*). The muscles were then washed, fixed and co-labeled with antibodies against syp and with α-BTX for AChRs (Figure 3.4*B, C*). Figure 3.3*B* shows that a subset of syp+ puncta extending from both $NCAM^{+/+}$ and $Hb9^{cre}NCAM^{flx}$ NMJs exhibited FM dye loading at synaptic (Figure 3.4*B, C* black arrowheads) and non-synaptic (Figure 3.4*B, C* white arrows), indicating that the vesicles were not only shuttling along the axon but they were also actively cycling with the plasma membrane en route. To examine whether cycling synaptic vesicles in axonal sprouts express NCAM, we immunolabeled FM4-64FX loaded $NCAM^{+/+}$ muscles with anti-syp and anti-NCAM antibodies 7 days pPD. Figure

3.4*D* shows a confocal image of a FM4-64 loaded puncta, co-labeled with NCAM and syp in an axonal sprout (puncta indicated by arrow shown on orthogonal view). Because NCAM is expressed on denervated muscles fibers it was difficult to conclusively identify presynaptic expression of NCAM in terminal sprouts, even when confocal microscopy was used. To address this concern, we partially denervated $HSA^{cre}NCAM^{flx}$ mice, which lack NCAM expression in skeletal muscle fibers (Appendix Figure A1*F*), and immunolabeled α-BTX+ endplates in the soleus with syp and NCAM antibodies (Figure 3.4*E*). Using this approach, we found that NCAM was co-distributed with syp+ puncta at (Figure 3.4*E* black arrowheads) and extending away from (Figure 3.4*E* white arrowheads) axonal sprouts emanating from parent terminals. These results indicate NCAM is present at cycling synaptic puncta in growing terminal sprouts of wild-type mice during the recovery from partial denervation.

Mislocalized synaptic puncta are associated with postsynaptic pathology

The size and distribution of AChRs in partially denervated soleus muscles were quantified in $NCAM^{+/+}$ and $Hb9^{cre}NCAM^{flx}$ mice to determine if the cycling synaptic vesicles remaining in axonal bridges spanning endplates induced a postsynaptic response. Figure 3.5 shows that, unlike $NCAM^{+/+}$ muscles (Figure 3.5*A*), clusters of AChRs in partially denervated $Hb9^{cre}NCAM^{flx}$ muscles were elongated and closely associated with syn+/SV2+ immunofluorescence (Figure 3.5B,C,F) 30 days pPD. The ectopic AChR clusters were also often found to localize to regions occupied by cycling synaptic puncta, identified by co-labeling with syp immunohistochemistry and FM4-64FX signal, loaded by 50Hz stimulation (Figure 3.5*C* arrowheads). The presence of synaptic and non-synaptic puncta could reflect the fact that different synaptic cargos (i.e. agrin and ACh) differentially influence postsynaptic receptor aggregation (Misgeld et al 2005; Lin et al 2005). Indeed, the presence of ectopic AChR clusters was found to be the direct result of disorganized presynaptic activity, as complete denervation of both $NCAM^{+/+}$ and $Hb9^{cre}NCAM^{flx}$ muscles soleus muscles did not recapitulate the postsynaptic phenotype (Figure 3.5*D, E, G;* P=0.325 Student's t-test). Further, measurements of endplate lengths in unoperated and partially denervated muscles reveal a quantifiable effect of genotype on postsynaptic organization (Figure 3.5*G*). Analysis of unoperated endplates revealed

that AChR clusters were longer in unoperated *Hb9^{cre}NCAM^{flx}* and *Hb9^{cre}NCAM^{flx}* muscles than *NCAM$^{+/+}$* and *NCAM$^{-/-}$* muscles (P<0.05 one way ANOVA), consistent with slightly larger postsynaptic areas in these genotypes (Chipman et al 2010). Partially denervated *Hb9^{cre}NCAM^{flx}* endplates were on average longer than all other genotypes 30 days after partial denervation (Figure 3.5*G*, P>0.001 one way ANOVA), demonstrating a specific effect of presynaptic NCAM in the regulation of synaptic organization during terminal field remodeling.

Previous studies examining *NCAM$^{-/-}$* motor terminals have identified a population of cycling puncta mislocalized to non-synaptic regions which could be inhibited by blocking L-type voltage dependent calcium channels (L-VDCCs) (Polo-Parada et al 2001). To determine if this same population is mislocalized during terminal field expansion, we examined FM4-64FX loading fluorescence of partially denervated NMJs in the presence or absence of 50μm nifedipine, a potent inhibitor of the L-VDCC (Figure 3.5*I-L*). We found that nifedipine inhibited the cycling of non-synaptic presynaptic puncta to wild-type levels (Figure 3.5*K* P<0.05 one way ANOVA) and actually enhanced cycling at synaptic puncta in *NCAM$^{+/+}$* muscles (Figure 3.5*L* P <0.05 one way ANOVA). These data demonstrate that a population of synaptic vesicles, sensitive to the activity of L-VDCC are mislocalized in the absence of NCAM and may differentially contribute to postsynaptic organization.

Presynaptic NCAM is required for functional maturation of motor terminals

Motor neurons lacking NCAM have a reduced capacity sprout and form enlarged, functional MUs. Anatomical analysis indicated that partially denervated soleus in *Hb9^{cre}NCAM^{flx}* mice contain a large number of completely denervated endplates, endplates with poor innervation, and axonal sprouts with mislocalized vesicles. We performed sharp electrode intracellular recordings in μ-conotoxin GIIIB to evaluate the functional synaptic properties of motor terminals on unoperated or partially denervated terminal fields in NCAM$^{+/+}$ and *Hb9^{cre}NCAM^{flx}* mice. All data were corrected for non-linear summation (McLachlan and Martin, 1981) and plotted as quantal contents (m) in order to directly assess presynaptic efficacy. Because NMJs in adult mice lacking pre- and post-synaptic NCAM exhibit periodic neurotransmission failure and synaptic vesicle

cycling defects we decided to first compare synaptic function at soleus NMJs in unoperated $NCAM^{+/+}$ and $Hb9^{cre}NCAM^{flx}$ mice. We found that $Hb9^{cre}NCAM^{flx}$ motor terminals exhibited higher quantal release as compared to $NCAM^{+/+}$ under low frequency (i.e. 1Hz) stimulation conditions (Figure 6*B-C*, unop; $P<0.05$ Mann-Whitney test 50th pulse). Interestingly, this increase in basal quantal output was due to the availability of presynaptic active zone sites, as the binomial parameter *n* was specifically increased compared to $NCAM^{+/+}$ (Figure 3.7*H*, unop; P<0.05, Mann-Whitney rank sum test), while *p* was unchanged (Figure 3.7*I*, unop; P=0.647, Mann Whitney rank sum test). This is also consistent with measurements of spontaneous activity, which was significantly elevated at unoperated NCAM-deficient terminals (Figure 3.7J, K, M, N; $P<0.001$ Mann Whitney rank sum test). Surprisingly, when we challenged terminals with more intense stimulation (i.e. 50Hz), we found no difference in summed quantal content ($\sum m$) between genotypes (Figure 3.6*B, C*, $P=0.627$ Mann-Whitney test 50th pulse), although NMJs were found to exhibit significantly enhanced depression (data not shown). When we directly quantified the size of readily releasable pool (RRP) at low and high stimulation frequency (Ruiz et al 2011) we found a significant and selective increase in the size of the RRP NCAM-deficient terminals in response to low, but not high stimulation frequencies (Figure 3.6*D, E,* $P<0.001$). These data suggest that presynaptic NCAM functions to regulate the probability of release (p_r) at mature, unoperated NMJs by restricting the number and/or availability of presynaptic active zones.

Previous studies of partially denervated soleus muscles revealed at least two functionally distinct populations of motor terminals with high and low quantal contents which likely corresponded to parent and reinnervated terminals respectively (Rochel and Robbins, 1988). We did not have the capacity to visually identify parent and reinnervated synapses in *ex vivo* partially denervated muscle preparations during the recording session, so it was necessary to functionally distinguish transmission qualities exhibited by immature/reinnervated synapses versus those exhibited by mature/parent terminals. To accurately distinguish these populations, the transmission properties and quantal transmission parameters of freshly regenerated synapses were recorded seven days following a complete nerve crush injury and were compared to those exhibited by unoperated, contralateral motor terminals (Figures 3.7). Consistent with previous studies

of reinnervated mouse soleus NMJs (Tonge, 1974); reinnervated motor terminals could be characterized by significantly reduced *m* (Figure 3.7*A*-*G*) and a reduced rate, but not amplitude, of spontaneous mEPPs as compared to unoperated terminals (Figure 3.7*J*-*O*). Regenerated terminals of both genotypes were found to exhibit a reduction in both *n* and *p* parameters as compared to unoperated terminals (Figure 3.7*H*-*I*), consistent with a global reduction in p_r at regenerated synapses.

The criteria determined above were then used to identify and differentiate functionally *immature* terminals (those with an $m \leq 25$; red) from *mature* terminals (those with an $m > 25$; blue) in partially denervated muscles (Figure 3.8*A*-*E*). We chose to use the terms *immature* and *mature*, instead of *reinnervated* and *parent*, because reinnervated synapses most likely matured and acquired stronger transmission qualities, at least in $NCAM^{+/+}$ muscles, as the recovery process progressed but would still fundamentally maintain a reinnervated identity. We also encountered a number of completely denervated terminals which, by definition did not elicit a postsynaptic response when the motor nerve was stimulated (Figure 3*A*). Predictably, many fibers did not elicit a response at early time points in both genotypes or at later time points in $Hb9^{cre}NCAM^{flx}$ mice, although these endplates were not directly quantified.

As observed in our anatomical assessments of presynaptic occupancy, a population of immature synapses ($m \leq 25$; red) emerged in both genotypes at day 10 pPD (Figure 3.8B, C). This population of synapses had a low p_r as compared to mature synapses (m>25; blue), because they also exhibited reduced spontaneous transmission (detailed in Appendix Figure A4) and had high paired pulse ratios (Figure 3.8*I, J*) and therefore likely correspond to reinnervated synapses (Rochel and Robbins, 1988). Overall, the distribution of synaptic strengths at this time point was comparable between genotypes (Figure 3.8 *B, C* inset; $P=0.861$ Mann Whitney rank sum test). However, when assessed at later time points (i.e. 30 days pPD), the distribution of synaptic strengths clearly diverged between genotypes (Figure 3.8*D*-*E*, insert $P<0.001$ Mann Whitney rank sum test). While *m* values recorded from $NCAM^{+/+}$ muscles were found to renormalize towards stronger and more mature transmission strengths, *m* values recorded from $Hb9^{cre}NCAM^{flx}$ were significantly skewed toward weaker values (Figure 3.8*D,E,* insert

P<0.001 Mann Whitney rank sum test), suggesting that regenerated terminals do not functionally mature in the absence of presynaptic NCAM.

Immature synapses of both genotypes were found to exhibit normal Gaussian distributions of *m* in response to 30-50 sweeps of 1Hz stimulation (Figure 3.8*B-E* single synapses), allowing for the application of binomial statistics to this population and subsequent comparison of *p* and *n* parameters (Figure 3.8*F-H*). As expected based on the histogram distributions, the collective strength of synapses in sprouting arbors decreased immediately following partial denervation and gradually returned to unoperated levels by day 30 pPD in $NCAM^{+/+}$ muscles (Figure 3.8*F, P*<0.05 one way ANOVA). In comparison, the combined strength of sprouting synapses on $Hb9^{cre}NCAM^{flx}$ arbors also dropped immediately following partial denervation but never recovered, and remained significantly less than unoperated values (Figure 3.8*F, P*<0.05, one way ANOVA on ranks) and wild-type values at 30 days pPD (Figure 3.8*F P*<0.05 Student's t-test). This initial drop in *m* was due to a reduction to *p* (Figure 8*G,* P<0.05 one way ANOVA) as opposed to *n* (Figure 8*H*). Values of *p* were specifically reduced at $Hb9^{cre}NCAM^{flx}$ synapses as compared to $NCAM^{+/+}$ by day 10 pPD (Figure 3.8*G, P*=0.035 Mann-Whitney rank sum test), a time when the two genotypes are otherwise fairly similar (Figure 3.8*B,C*). This difference was maintained by day 30 pPD (Figure 3.8G *P*=0.002 Mann Whitney rank sum test), although $NCAM^{+/+}$ terminals never fully recovered to unoperated values (Figure 3.8*G P*<0.05 one way ANOVA on ranks), consistent with a limitation in regenerative potential even in wild-type mice. Together the above findings suggest that p_r is reduced at reorganizing motor terminals on MUs undergoing expansion.

The abundance of synaptic vesicles mobilized during high frequency transmission is reduced at mature terminals following partial denervation

The p_r of a synapse can be influenced by a number of presynaptic factors, including the abundance and fusion probability of populations of synaptic vesicles (Hua et al 2011; Ratyanaka et al 2012). We therefore focused on two vesicle populations which are mobilized in response to differing amount of presynaptic activity (i.e.1Hz vs. 50Hz) (see Ruiz et al 2011) (Figure 3.9). Because we observed a difference between the relative sizes of these pools between genotypes and stimulation frequencies, we classified 1Hz

stimulation as mobilizing vesicles from the readily releasable pool (RRP) and 50Hz as mobilizing vesicles from recycling pool (RP). Mature $NCAM^{+/+}$ and $Hb9^{cre}NCAM^{flx}$ terminals were found to exhibit remarkably similar profiles of $\sum m$ in response to 50Hz stimulation at 10 and 30 days pPD, as did immature terminals (Figure 3.9*A-B,D-E*) although the contribution of immature terminals to the total synaptic population was significantly more in 30 day partially denervated $Hb9^{cre}NCAM^{flx}$ muscles as compared to wild-type (Figure 3.9*F;* $P<0.001$, Student's t-test) than at 10 days pPD (Figure 3.9*C;* $P>0.05$, Student's t-test). This significance arose because the number of immature synapse in the $NCAM^{+/+}$ muscles decreased over time (compare Figures 3.9*C* and *F*). Overall, the continued presence of immature synapses in the $Hb9^{cre}NCAM^{flx}$ mice likely influenced the mean strength of all synapses in expanded MUs (Figure 3.9*G, J*).

Estimations of RRP sizes across synapses revealed a very similar pattern as did values of *m* generated by 1Hz stimulation (compare Figure 3.9*G* to Figure 3.8*F*), validating the estimation of vesicle pool sizes. The average size of the RRP dropped across terminal fields of both genotypes, but only recovered in $NCAM^{+/+}$ muscles (Figure 3.9*G*, $P<0.001$, one way ANOVA on ranks). This drop was specifically due to a reduction in the RRP of immature synapses, as the RRP of mature synapses was not significantly influenced by sprout extension in $NCAM^{+/+}$ muscles (Figure 3.9*H,* $P=0.188$, one way ANOVA). $Hb9^{cre}NCAM^{flx}$ synapses on the other hand, demonstrated a significant reduction in mature RRP size at 10 and 30 days (Figure 3.9*H*, $P<0.05$, one way ANOVA on ranks) which, combined with a higher proportion of immature synapses at day 30 (Figure 3.9*F*), resulted in significantly fewer vesicles participating in low frequency release by this time point (Figure 3.9*G*, *I*; $P<0.001$ Mann-Whitney rank sum test).

The finding that RRP vesicle populations were not reduced at mature synapses in $NCAM^{+/+}$ muscles by 5 and 10 days suggest that this population is not directly mobilized from parent synapses during MU remodeling, or that they are sufficiently compensated for by synapse-specific mechanisms. We therefore assessed the number of RP vesicles at mature and immature synapses with 50Hz stimulation in order to determine if these vesicles belong to the population which is actively mobilized from sprouting wild-type synapses (Staras et al 2010; Orenbuch et al 2012). Indeed, the mean RP size of all

synapses on expanding $NCAM^{+/+}$ and $Hb9^{cre}NCAM^{flx}$ arbor was significantly reduced as compared to unoperated values as early as 5 days pPD (Figure 3.9*J*, $P<0.001$, one way ANOVA). Recycling pools of mature terminals were consistently reduced by~50% as compared to those of unoperated terminals in both genotypes (Figure 3.9*J, K*), whereas reinnervated terminals maintained less than~25% the number of RP vesicles as unoperated terminals. These findings are consistent with our previous assessments of vesicle abundance at parent and early-stage reinnervated terminals using syp+ fluorescence (see Figure 3.3*F-I*). Although the abundance of RP vesicles at individual $NCAM^{+/+}$ and $Hb9^{cre}NCAM^{flx}$ mature and immature synapses demonstrated very similar profiles, the higher proportion of immature synapses in $Hb9^{cre}NCAM^{flx}$ muscles led to a significant difference in the number of overall RP vesicles possessed by expanding $Hb9^{cre}NCAM^{flx}$ arbors 30 days pPD (Figure 3.9*J, L;* $P<0.001$ Mann Whitney rank sum test).

In summary, 1) extensively expanded wild-type MUs contain mature synapses with a normal complement of RRP vesicles, but a reduced complement of RP vesicles. 2) $Hb9^{cre}NCAM^{flx}$ MUs demonstrate impaired functional sprouting and possess mature terminals with fewer RRP and RP vesicles than wild-type. 3) Although $Hb9^{cre}NCAM^{flx}$ MUs contain proportionally more immature synapses and fewer synapses overall, they possess a similar complement of RRP and RP vesicles as wild-type. These data suggest that the number of recycling synaptic vesicles is tightly correlated with the expansion capabilities of the sprouting MU.

Variability in vesicle fusion during repetitive stimulation coincides with vesicle redistribution

Recycling synaptic vesicles are replenished through endocytic pathways induced during periods of repetitive stimulation and function to maintain stable patterns of postsynaptic output (Ruiz et al 2011; Maeno-Hikichi et al 2011; Rozas et al 2012). Vesicle replenishment was therefore assessed during the plateau phase of trains of 1Hz or 50Hz stimulation by estimating the coefficient of variation (CV) in presynaptic quantal output (m) during the plateau phase (i.e. the last 30 stimuli of a 50 stimulus train; see Figure 3.10A-D dotted line) (see Rozas et al 2012). Fifty stimuli delivered to unoperated motor

terminals at 1Hz or 50Hz generated plateaus of relatively constant quantal output with a low CV (i.e.~0.05) in both genotypes (Figure 3.10*E, H;* also see Figure 3.6*A*). In comparison, while mature terminals of both genotypes generated consistent repetitive output in response to 1Hz stimulation comparable to unoperated values (Figure 3.10*F;* $NCAM^{+/+}$ P=0.569; $Hb9^{cre}NCAM^{flx}$ P=0.076, one way ANOVA), 50Hz stimulation resulted in a small, but significant increase in variability throughout the recovery period in both genotypes as compared to unoperated terminals (Figure 3.10*A-D* blue; *I* P<0.001, one way ANOVA). These data support the above hypothesis that RP synaptic vesicles and/or the endocytic mechanisms which generate them are preferentially influenced by terminal field expansion.

Immature synapses were always found to exhibit more highly variable *m* during the plateau phase than unoperated and mature terminals (Figure 3.10*A-D, F, I;* red P<0.05 one way ANOVA). The variability of quantal transmission at immature $Hb9^{cre}NCAM^{flx}$ terminals began to diverge from $NCAM^{+/+}$ terminals as early as 5 days and reached significance by 10 days after partial denervation (Figure 3.10*F, I*). This divergence, coupled with a higher relative abundance of immature synapses (Figure 3.9*F*) led to a significant increase in mean CV across all synapses in sprouting $Hb9^{cre}NCAM^{flx}$ MUs at 30 days pPD as shown in cumulative frequency distributions (Figure 3.10 *G, J,* P<0.001 Mann-Whitney rank sum test). These data further support the hypothesis that immature NCAM-deficient synapses fail to develop mature synaptic vesicle recycling phenotypes.

Immature synapses exhibit differential sensitivities to L-VDCCs blockade

Several studies have identified fast, stimulus-driven Ca^{2+}-mediated endocytosis, initiated during repetitive stimulation (Miller and Heuser, 1984; Beutner et al 2001; Neves et al 2001; Gaffield et al 2009a) as being driven by L-VDCCs at mouse NMJs (Perrissinotti et al 2008). L-VDCCs also contribute to post-stimulus bulk endocytosis by regulating the formation of synaptic vesicles (Cheung et al 2010, 2012; Maeno-Hikichi et al 2011) and differentially contribute to exocytosis and endocytosis during developmental and regenerative synapse formation (Sugiura and Ko, 1997; Perrissinotti et al 2008; Maeno-Hikichi et al, 2011). Because NCAM is known to influence the localization and activity

of L-VDCCs at developing NMJs (Polo-Parada et al 2001, 2004; Hata et al 2007), we sought to determine the influence of Ca^{2+} channels on synaptic transmission during the course of terminal field expansion in $NCAM^{+/+}$ and $Hb9^{cre}NCAM^{flx}$ mice. We used 50μM nifedipine (nif) to block L-VDCCs and 0.1μM ω agatoxin IVA (ATX) to block P/Q-VDCCs at unoperated and reinnervated NMJs during 1Hz presynaptic stimulation (Polo-Parada et al 2001) (Figure 3.11*A-H*). Although nifedipine had no effect at mature NMJs (*m*>25; Figure 11*A, D, E, H*), subsequently blocking P/Q-VDCCs completely inhibited transmission at these synapses of both genotypes (Figure 3.11*D, H*), confirming that exocytosis is driven primarily by P/Q-VDCCs at mature mouse NMJs (Hong and Chang, 1995; Katz et al 1996). In comparison, nifedipine significantly, but transiently potentiated *m* at immature $NCAM^{+/+}$ terminals (Figure 3.11*A-D*, $P<0.01$ one way ANOVA) and has been previously observed at reinnervated synapses following nerve crush (Sugiura and Ko, 1997). Neurotransmission at immature synapses could then be completely abolished by blocking P/Q-VDCCs with ATX (Figure 3.11*D*). Miniature EPP amplitude was not influenced by nif or ATX (see Appendix Figure A5 for further details), highlighting the presynaptic influence of these channels on neurotransmission. Nifedipine similarly potentiated *m* at immature $Hb9^{cre}NCAM^{flx}$ synapses at 7 days pPD (Figure 3.11*F*, *H*, $P<0.05$ one way ANOVA). However, in contrast to $NCAM^{+/+}$ synapses, this potentiation was not transient and remained at day 14 pPD (Figure 11*G*, *H,* $P<0.05$, one way ANOVA). These data suggest that presynaptic NCAM regulates, in part, the maturational switch in Ca^{2+}-sensitive vesicle cycling during the transition from immature to mature synaptic transmission at sprouted synapses (see Hata et al 2007).

Motor units lacking postsynaptic NCAM do not expand following partial denervation because they lack synaptic vesicles

Recent studies have shown that Ca^{2+}-mediated presynaptic recycling mechanisms are influenced, at least in part, by postsynaptic activity and adhesion molecules in a developmentally regulated manner (Futai et al 2007; Branco et al 2008; Yamashita et al 2010; Vitureira et al 2012; Eguchi et al 2012). NCAM is highly expressed by muscle fibers during development and following denervation (Covault and Sanes, 1985, 1986). Overexpression of the NCAM 120kD isoform in healthy muscle fibers induces axonal

sprouting and increases the size of the NMJ in transgenic mice (Walsh et al., 2000). Although changes in neurotransmission were not observed, the altered size and complexity of the endplate in these animals suggest that that postsynaptic expression of NCAM regulates, at least in part, structural synaptic reorganization of the NMJ. Consequently, we sought to investigate the role of retrograde postsynaptic NCAM signaling in regenerative synaptogenesis during terminal field expansion using transgenic mice that specifically lack muscle-derived NCAM ($HSA^{cre}NCAM^{flx}$ mice; Appendix Figure A1*E-F*). The soleus muscle was partially denervated by cutting the L5 spinal root and motor neurons were back labeled with fluorescently labeled CTB and whole muscle contractile force was recorded 7, 14 and 30 days pPD as described above. The back labeling experiments confirmed a normal complement of L5 innervation to the soleus in $HSA^{cre}NCAM^{flx}$ mice (Figure 3.12*A*) while whole muscle force and presynaptic innervation were similarly reduced seven days after L5 partial denervation (Figure 3.12*B, C*) suggesting that postsynaptic NCAM does not participate in the developmental innervation of the mouse soleus muscle (Appendix Figure A6; see also Chipman et al 2010). However, similar to partially denervated $Hb9^{cre}NCAM^{flx}$ (Figure 3.2*A, B*) and $NCAM^{-/-}$ muscles (data not shown), the contractile force of $HSA^{cre}NCAM^{flx}$ soleus muscles did not increase in contractile strength 14 and 30 days pPD (Figure 3.12*B*, $P<0.05$ one way ANOVA). Likewise, presynaptic innervation was significantly reduced at 7 and 14 days pPD as measured by the number of endplates containing syp+ puncta (Figure 3.12*C*, $P<0.05$ one way ANOVA). Interestingly, while the number of innervated endplates in the partially denervated $HSA^{cre}NCAM^{flx}$ muscles was not significantly different from unoperated muscles 30 days pPD (Figure 3.12*C* $P>0.05$ one way ANOVA), the contractile force remained low. This discrepancy between contractile force and the degree of reinnervation suggests that many reformed presynaptic terminals did not elicit postsynaptic excitation or were functionally too immature to cause excitation-contraction coupling in the innervated fibers.

To further assess the qualities of reinnervated motor terminals, partial denervated $HSA^{cre}NCAM^{flx}$ muscles were immunolabeled with antibodies against NF and syp and AChRs were labeled with α-BTX 14 days pPD (Figure 3.12*D*). Parent terminals (pT) extended terminal sprouts that reinnervated (rT) and/or contacted (cT) terminal endplates

14 days pPD (Figure 3.12*D*). However, unlike the axonal sprouts bridging terminals in partially denervated *Hb9*^{cre}*NCAM*^{flx} muscles, the terminal bridges in the *HSA*^{cre}*NCAM*^{flx} mice did not contain more vesicles than comparable bridges in wild-type mice (Figure 3.12*E* $P>0.05$ one way ANOVA). The number of vesicles at reinnervated endplates was significantly less than those in partially denervated *NCAM*$^{+/+}$ soleus muscles 14 days pPD as measured by the degree of overlap between syp+ immunolabeling and α-BTX (% occupation; Figure 3.12*F,G*, $P=0.012$ Mann-Whitney test). Taken together, these results suggest that postsynaptic NCAM partially regulates the number of vesicles that are mobilized to new synapses during MU expansion in partially denervated muscles.

To determine if specific vesicle pools were being mobilized in *HSA*^{cre}*NCAM*^{flx} terminals and to more closely assess the functionality of reinnervated motor terminals, we estimated the sizes of the RRP and RP at 14 days pPD at mature ($m>25$; blue) and immature ($m\leq25$; red) synapses (Figure 3.13). Unoperated *HSA*^{cre}*NCAM*^{flx} motor terminals had RRP and RP sizes were comparable in size to *NCAM*$^{+/+}$ terminals (Appendix Figure A6*C-E*). In contrast, mature *HSA*^{cre}*NCAM*^{flx} terminals examined 14 days pPD revealed a specific reduction in the number of RP vesicles (Figure 13*A-B* $P<0.05$ one way ANOVA) but not RRP vesicles available for redistribution (Figure 13*C*). Likewise, *HSA*^{cre}*NCAM*^{flx} mature terminals, but not immature terminals (not shown), demonstrated significantly more variability in quantal output than wild-type during 50Hz, but not 1Hz stimulation (Figure 13*D*, $P<0.05$, Mann-Whitney rank sum test), suggesting frequency-dependent presynaptic vesicle recycling deficits at sprouting *HSA*^{cre}*NCAM*^{flx} NMJs. Motor endplates of *HSA*^{cre}*NCAM*^{flx} parent terminals appeared to degenerate in ways similar to *Hb9*^{cre}*NCAM*^{flx} (Figure 3.13*F*), except that AChRs were not as widely dispersed throughout the muscle membrane (see Figure 3.5) most likely because presynaptic resources were not mislocalized to extra synaptic regions as they were in *Hb9*^{cre}*NCAM*^{flx} muscles (Figure 3.12*D-E*). Overall, these data suggest the presence of a trans-synaptic signal mediated by muscle-specific NCAM to influence the local abundance of presynaptic vesicles required for effective reorganization of synaptic resources on expanding terminal arbors. In addition, this signal seems to operate in parallel to that of presynaptic NCAM which primarily acts influence the maturational differentiation of reinnervated motor terminals.

Discussion

We have systematically assessed the properties of functional MU expansion in the mouse and have identified two mechanisms which are required for appropriate remodeling. 1) The shuttling of recycling synaptic vesicles and associated fusion machinery away from sprouting parent synapses to nearby denervated endplates; and 2) The homeostatic upregulation of recycling synaptic vesicles at parent and regenerated synapses. Our studies have identified that these mechanisms together enable effective expansion of terminal synaptic fields during compensatory regeneration in the mouse and that dysfunction in either mechanism can severely restrict the extent of terminal field expansion.

The mobilization and targeting of recycling pool vesicles: Influences on neurotransmission

Recent evidence has demonstrated the constitutive sharing of synaptic vesicles between established synapses of central neurons (Krueger et al 2003; Darcy et al 2006; Frischknecht et al 2008; Staras et al 2010; Ratnayaka et al 2011) and much focus has been placed on understanding the mechanisms which regulate their dispersion from, and attraction to specific presynaptic sites (Bamji et al 2006; Sun and Bamji, 2011; Orenbuch et al 2012). The mobilization of synaptic vesicles away from sprouting parent synapses was normal in NCAM mutants, suggesting that NCAM is dispensable for the initial mobilization of synaptic vesicles away from synaptic sites. In cultured hippocampal networks, the initial mobilization of synaptic vesicles away from clustered presynaptic puncta is known to involve BDNF signaling through the TrkB receptor to induce the dissociation of cadherin/β-catenin adhesion complexes (Bamji et al 2006). Denervated muscle fibers upregulate the expression of BDNF which can act on TrkB receptors expressed by regenerating motor axons to influence the survival of motoneurons following axotomy (Koliastos et al 1993) and promote functional recovery of reinnervated muscles (Eberhardt et al 2006). It is possible that BDNF expression by denervated muscle fibers also induces the dispersion of synaptic vesicles away from

parent synapses in partially denervated muscles, although this hypothesis has yet to be directly tested.

Once synaptic vesicles are mobilized away from a synapse, what factors regulate their capture and retention at appropriate synaptic sites? A series of studies have recently demonstrated that dense core vesicles are stochastically distributed to developing *Drosophila* NMJs in an activity-dependent manner, leading to a progressive and even distribution of synaptic resources across all synaptic sites (Shakiryanova et al 2006, 2007; Wong et al 2012). Adhesion molecules are well known to regulate synaptic vesicle clustering at the mammalian NMJ (Rafuse et al 2000; Fox et al 2007) and likely play a key role in the activity-dependent tethering and retention of transiting vesicles to synaptic sites. Likewise, synaptic vesicle-specific proteins such as synapsin bind vesicles to the cytoskeleton in an activity-dependent manner (Chi et al 2001, 2003; Gitler et al 2008). In particular, the synapsin IIa isoform was recently shown to restrict the mobility of resting pool vesicles to synaptic puncta in hippocampal cultures (Orenbuch et al 2012) and its absence leads to enhanced synaptic depression during repetitive presynaptic stimulation (Gitler et al 2008). These findings suggest a possible link between vesicle stability at synaptic sites and vesicle recruitment during synaptic transmission which could be mediated by membrane-bound adhesion molecule to synaptic vesicle signaling events.

Indeed, our data demonstrate both a loss of vesicular shuttling and a reduction in repetitive quantal release during repetitive, high frequency stimulation. Many synaptic puncta were closely associated with NF+ sprouts in the absence of presynaptic NCAM (see Figure 3.3*A*) and an abnormally strong association with the cytoskeleton may impair their trafficking at the synapse. The abundance of phosphorylated CaMKII is reduced in brain homogenates isolated from *NCAM*$^{-/-}$ mice and is required for synapsin phosphorylation (Goold et al 1995), which is in turn, is required for the liberation of synaptic vesicles from their interaction with the cytoskeleton (Chi et al 2001). Presynaptic NCAM may therefore participate in this pathway by activating CaMKII in motor terminals to mobilize synaptic vesicles. Alterations in structure and function at *Drosophila* NMJs in the absence of CaMKII have been reported and closely parallel the functional alterations observed at mature NCAM-deficient motor terminals (Wang et al 1994). Indeed, preliminary experiments have revealed that acute application of KN-62, a

specific inhibitor of CaMKII to wild-type mouse NMJs was found to reproduce a number of key phenotypes of *Hb9^{cre}NCAM^{flx}* mouse motor terminals, including enhanced spontaneous activity, enhanced quantal output at low frequency stimulation, enhanced depression during repetitive stimulation and reduced paired pulse facilitation (P.H.C and V.F.R unpublished data). Together, these findings present the intriguing hypothesis that NCAM-CaMKII signaling pathway could influence the regulation of synaptic vesicle mobility and neurotransmission during terminal field reorganization.

Alternatively, NCAM is known to activate the presynaptic myosin light chain kinase (MLCK) to mobilize synaptic vesicles in order to maintain effective repetitive transmission at the mature mouse NMJs (Polo-Parada et al 2005; Maeno-Hikichi et al 2011). While the NCAM180kD was determined to be the isoform responsible for this activation via its intracellular KENESKA domain (Polo-Parada et al 2004, 2005), the 140kD and/or 120kD isoform were found to specifically regulate basal synaptic strength, possibly through a regulation of the AP3-dependent recycling pathway of bulk endosomes (Polo-Parada et al 2004; Cheung and Cousin, 2012). We did not observe a the periodic transmission failures which are characteristic of NCAM-deficient semitendinosus fast fiber synapses (Polo-Parada et al 2005) in this study, although we did observe several other features of fast *NCAM$^{-/-}$* motor terminals in the slow soleus *Hb9^{cre}NCAM^{flx}* motor terminals studied here. These included an increase in the release probability during low frequency stimulation, enhanced depression during high frequency stimulation, a reduction in paired-pulse facilitation and altered synaptic vesicle cycling at non-synaptic regions which were sensitive to L-VDCC blockade (Polo-Parada et al 2001, 2004). These findings raise the intriguing possibility of a muscle-type specific effect of NCAM on neuromuscular transmission and further suggest that different motor terminals with different functional requirements (Reid et al 1999; Rowley et al 2007) may require the activity of specific NCAM isoforms. Further investigation is required to determine the relative contribution of NCAM isoforms to the function of fiber-type specific motor terminals, and recent observations which suggest fast terminals are selectively vulnerable to degeneration in *NCAM$^{-/-}$* mice (Chipman et al 2010) and during the course of MND (Frey et al 2000; Pun et al 2006) make these investigations worthwhile.

Limitations to terminal field remodeling: Pre and postsynaptic mechanisms

During MU expansion, sprouting motor axons are confronted with a significant challenge – to expand in synaptic territory to functionally reinnervate as many postsynaptic sites as possible. Based on a combination of quantitative immunofluorescence, FM dye imaging and intracellular electrophysiology, we found evidence that the redistribution of parent terminal resources can support only a very limited number of sprouted synapses even in wild-type muscles (Figure 3.14). For instance, partially denervated $NCAM^{+/+}$ soleus muscles never regained 100% innervation and maintained a small population of morphologically immature (i.e. low % occupancy) and functionally weak synapses (i.e. $m \leq 25$) even at 30 days pPD. These data are consistent with others which demonstrate limitations in the expansion capabilities of motoneurons (Rochel and Robbins, 1988; Rafuse et al 1992) and highlight the delicate balance between compensatory sprouting and synaptic stability.

On average, wild-type MUs were estimated to undergo an approximate 3-fold increase in the total number muscle fibers they could stably innervate (Figure 3.14*A, B*). In comparison, the average number of RP vesicles possessed by these motoneurons was found only to double (Figure 3.14*C*). Pre or postsynaptic deletion of NCAM completely inhibited the potential for functional expansion and the abundance of recycling synaptic vesicles, although each mutant influenced complementary mechanisms of regeneration. For instance, $Hb9^{cre}NCAM^{flx}$ mice could not stably redistribute synaptic resources to newly formed NMJs and consequently demonstrated severely impaired presynaptic differentiation, including altered Ca^{2+}-mediated vesicle recycling. In contrast, $HSA^{cre}NCAM^{flx}$ mice were found to appropriately localize presynaptic resources to reinnervated motor terminals, although the availability of synaptic vesicles for redistribution was significantly impaired. Some of these vesicles are most likely derived from the cell soma (Calderó et al 1992; Jung et al 1997; Wong et al 2012) and delivered across expanding terminal arbors, while some are likely generated locally, via synapse specific endocytic mechanisms (Rozas et al 2012). Both scenarios would require a retrograde signal for their induction. Our data support a model for compensatory vesicle generation whereby both sprouted (reinnervated) and sprouting (parent) synapses

contribute to the homoeostatic upregulation of RP abundance and are controlled by pre and postsynaptic NCAM respectively.

Postsynaptic NCAM expression is highly regulated by the functional state of the innervating motoneuron (Covault and Sanes, 1985) and by the muscle itself (Rafuse and Landmesser, 1996) and is therefore a strong candidate to provide retrograde activity-dependent cues. The large size of the synaptic cleft and the presence of the extracellular matrix (ECM) surrounding muscle fibers, however, argue strongly against a direct cell-to-cell trans interaction between muscle-derived and neural-derived NCAM. Alternatively, NCAM can be released from the muscle surface through cleavage of the glycophosphatidylinositol (GPI) linker of the 120kD isoform by phosopholipase C (PLC) (He et al 1986; Sadoul et al 1986) in response to muscle denervation (Davis et al 1993). Solubilized NCAM can bind to the ECM-bound agrin (Storms et al 1996; Storms and Rutishauser, 1998) and collagen (Probstmeier et al 1989, 1992) to influence the structure and composition of the synaptic ECM. The ECM itself and the molecules sequestered within it are indispensible for the stability and regeneration of functional motor terminals (Sanes et al 1978; Fox et al 2007; Williams et al 2009; Bolliger et al 2010) and likely to play a key organizational role during MU expansion.

Presynaptic NCAM is in a position to receive retrograde cues sequestered in the ECM and transmit them to effect local or distant cellular influences. For instance, presynaptic endocytic mechanisms are known to be driven by postsynaptic activity and can influence the homeostatic adjustment of presynaptic vesicle abundance and p_r (Plomp et al 1992; Futai et al 2007; Weyhersmüller et al 2011; Lou et al 2012; Vitureira et al 2012; Ratnayaka et al 2012). In addition, trans-golgi derived synaptic vesicle packets are shuttled along developing axons and localized to sites of putative synaptic contact via presynaptic NCAM to participate in synaptogenesis (Zakharenko et al 1999; Ahmari et al 2000; Sytnyk et al 2002; Hata et al 2007). Functional shuttling and effective synaptogenesis requires NCAM expression by the postsynaptic cell (Dityatev et al 2000; Hata et al 2007), suggesting a trans-synaptic interaction. Finally, recent evidence has demonstrated signaling effects mediated by the nuclear transport of activated NCAM which requires extracellular activation by other NCAM molecules (Kleene et al 2010). It is likely that a combination of a number of these possible mechanisms coordinately

supply the required amount of vesicles and fusion machinery to expanding terminal fields.

Calcium channels, vesicle cycling and motor unit expansion

Here we demonstrated two possibly related roles of L-VDCCs during terminal field expansion. First, we found that blocking L-VDCCs with nifedipine significantly reduced vesicle recycling at non-synaptic regions in $Hb9^{cre}NCAM^{flx}$ muscles, but not in $NCAM^{+/+}$ muscles. Secondly, we found that blocking the L-VDCC potentiated quantal release by increasing the number of recycling synaptic vesicles only at very immature, regenerated synapses. This finding is supported by other studies which have documented potentiated presynaptic release nifedipine at newly formed mouse NMJs (Sugiura and Ko, 1997). While the study performed by Sugiura and Ko (1997) suggested a L-VDCC mediated release or inhibitory G-proteins from the motor terminal, other studies have demonstrated similar effects of potentiated vesicle fusion in response to inhibition of Ca^{2+}-mediated endocytic pathways (Douthitt et al 2011; Rosa et al 2011a, b). L-VDCCs contribute to bulk endocytosis at mouse NMJs (Perrissinotti et al 2008; Maeno-Hikichi et al 2011), and another study has recently linked altered endosomal recycling to potential presynaptic release at *Drosophila* NMJs (Uytterhoeven et al 2011). In addition, the effects of L-VDCCs may not be strictly presynaptic, as these channels are highly expressed in muscles and have recently been implicated in the organization of presynaptic innervation (Chen F. et al 2011). Finally, terminal Schwann cells NMJs are known to express L-VDCCs in frog muscles (Robitaille et al 1996) and this cell type can also strongly influence functional plasticity of mouse motor terminals (Todd et al 2011). Together, these studies suggest that the modulation of presynaptic release strength is complex and can be altered through a variety of synaptic mechanisms.

Regenerated $Hb9^{cre}NCAM^{flx}$ synapses did not undergo a developmental shift in Ca^{2+}-mediated vesicle recycling, which is associated with presynaptic maturation of a variety of synapses (Sugiura and Ko, 1997; Yamashita et al 2010; Eguchi et al 2012), nor did they exhibit a progressive strengthening in quantal output which may be required for the stability of motor terminals (Colman et al 1997; Buffelli et al 2003). Together these data suggests a fundamental role of presynaptic NCAM in the maturation of individual

synapses (Hata et al 2007) through its regulation of presynaptic strength and Ca^{2+}-mediated vesicle recycling. NCAM can bind L-VDCCs (Bodrikov et al 2008) and is highly expressed on synaptic vesicle membranes (Takamori et al 2006), putting it in a strategic position to couple the recycling of specific synaptic vesicle populations to L-VDCC-mediated Ca^{2+} currents.

The synaptic organization of terminal arbors

Parent terminals were found to contain on average one half the abundance of recycling vesicles as their unoperated counterparts, and were found to be relatively stable following partial denervation, at least in wild-type mice. These findings suggest that mature motor terminals contain at least twice the number of synaptic vesicles than the minimum needed to stably maintain a functionally effective neuromuscular synapse. Indeed, mature rodent NMJs contain on the order of a few hundred thousand synaptic vesicles available for fusion (Elmqvist and Quastel, 1965), although only a few thousand are used even during periods of high frequency stimulation (Ruiz et al 2011; Maeno-Hikichi et al 2011). In addition, the reserve pool composes a majority of the total pool of synaptic vesicles although it only rarely directly contributes to neurotransmission (Rizzoli and Betz, 2005). These findings raise two fundamental questions. 1. Why are these extra vesicles present? 2. What are they good for?

Synaptic vesicles belonging to the RP or the reserve pool contribute directly to synaptic plasticity because their pool-specific identity is malleable (Ratnayaka et al 2012) and because they can be mobilized between functional synapses (Staras et al 2010; Ratyanaka et al 2011; Orenbuch et al 2012). Here we have demonstrated that these vesicle populations are used specifically for the homeostatic maintenance of circuit output in response to presynaptic pathologies. Although the occurrence of traumatic partial denervation is too sporadic to have any meaningful effect on the emergence of such a compensatory trait throughout evolutionary processes, the maintenance of motor function during progressive partial muscle denervation in response to age-related motoneuron death and degeneration may provide a sufficiently strong selective pressure. Alternatively, the abundance of vesicles at individual NMJs may simply be a byproduct of a developmental redistribution of synaptic resources, where the removal of some

terminal branches supplying superfluous synapses is correlated with the growth and stabilization of others (Tapia et al 2012).

Some studies have highlighted highly conserved pattern of axonal arborization across a variety of cell types in the CNS (Snider et al 2010; Teeter and Stevens, 2011) and although the particular arborization patterns of motoneurons was not included in this analysis; there is reason to believe that ideal branching patterns for the arbors of these cells exist as well (Tapia et al 2012). The implications of resource redistribution during developmental refinement of arborization patterns suggest that this ideal pattern may be generated via the availability of presynaptic resources and the mechanisms of their distribution, and that these influences may determine the scope of arbor reorganization in the adult. Evidence consistent with this hypothesis comes from observations of MU sprouting in cats where the extent of expansion is directly proportional to the original size of the MU (Rafuse et al 1992) and from the identification of distinct populations of cells in the CNS and PNS which exhibit specific propensity for structural and functional plasticity in the adult (Frey et al 2000; De Paola et al 2006; Galimberti et al 2010). Therefore the initial functional and structural state of a terminal field may guide its future potential for plasticity or regeneration. These findings have particular implications for the capacity of endogenous regenerative mechanisms during the progression of MND, where subsets of arbors selectively degenerate while others expand (Schaefer et al 2005; Pun et al 2006).

Synaptic vesicle recycling and neurodegenerative disease

Many studies have described early deficits in synaptic organization which precede other indices of dysfunction in mouse models of MNDs (Frey et al., 2000; Gould et al 2006; Kong et al., 2009); suggesting developmental disruptions to neuromuscular organization may highlight a susceptibility to degeneration and/or a deficiency in regenerative potential in the adult (Hegedus et al 2008). Such developmental deficits are observed in MUs NCAM mutants, including a delay in the withdrawal of polyneuronal innervation, altered vesicle resource distribution and disruptions to synaptic transmission (Rafuse et al 2000). These deficits correspond to significant disruptions to neuromuscular function in

the adult (Polo-Parada et al 2001, 2004, 2005) and may also contribute to the emergence of age-related neuromuscular degeneration (see Appendix Figure A8).

This study demonstrates a relationship between the maximal extent of terminal field expansion in the adult mouse and the kinetics of recycling, replenishment and reuse of synaptic vesicles along axon arbors. Genetic mutation of pre and/or postsynaptic NCAM lead to significant impairment of these processes and also completely abolished functional MU expansion, strongly arguing for a fundamental role of synaptic vesicle recycling in compensatory synaptic sprouting. Synaptic vesicle proteins are sorted and old or dysfunctional proteins are replaced at endosomal intermediates (Fernández-Alfonso et al 2006; Uytterhoeven et al 2011; Cheung and Cousin, 2012). New proteins and fresh membrane are generated in the ER and recent studies have linked altered protein recycling and ER stress to neurodegeneration and to MND in particular (Rubinsztein, 2006; Kieran et al 2007; Saxena et al 2009; Douglas and Dillin, 2010; Esposito et al 2011). Furthermore, alterations in vesicle mobility and distribution are observed during early stage MND disease in mouse models of ALS (Pun et al 2006). Such deficits would severely restrict the ability of endogenous repair mechanisms to function appropriately in response to trauma or age and disease-related challenges, providing a critical junction in the control of compensatory regenerative mechanisms and the development of MND. Synaptic vesicle biogenesis and synaptic protein recycling are therefore fundamental for the preservation of presynaptic signaling required for synaptic stability and circuit homeostasis and could be the targets of future therapeutics.

CHAPTER 3 FIGURES

Figure 3.1: NCAM is dispensable for gross neuromuscular innervation. **(A)** Schematic representation of L5 partial denervation surgery and motoneuron back labeling experiment. **(B)** Representative images of spinal cords demonstrating the distribution of partial denervation (red) and unoperated/contralateral (green) soleus motoneuron pools back labeled with AlexaFluor-conjugated CTB injected into the soleus muscle directly following partial denervation surgery and sacrificed 3 days later. Scale bar 40μm. **(C)** Quantification of the number of CTB+ motoneurons from injections made into partially denervated (L5) and unoperated (unop) soleus muscles. The number of spinal cords examined is indicated in the bars. ns – not significantly different. L5 PD P=0.386; Unop P=0.942 one way ANOVA.

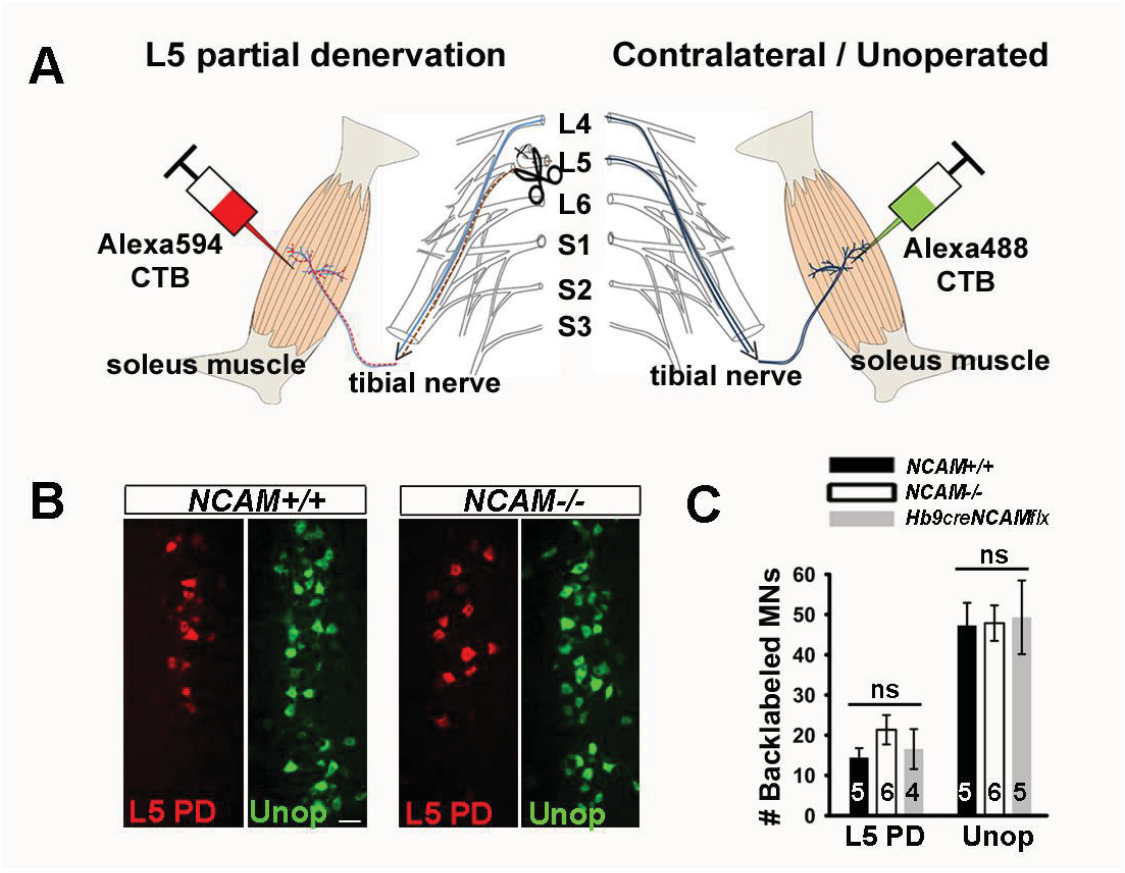
A
L5 partial denervation
Contralateral / Unoperated
L4
L5
L6
S1
S2
S3
Alexa594
CTB
Alexa488
CTB
soleus muscle
tibial nerve
tibial nerve
soleus muscle
B
NCAM+/+
NCAM-/-
L5 PD
Unop
L5 PD
Unop
C
NCAM+/+
NCAM-/-
Hb9creNCAMflx
Backlabeled MNs
60
50
40
30
20
10
0
ns
ns
5
6
4
5
6
5
L5 PD
Unop

Figure 3.2: Presynaptic NCAM is required for functional neuromuscular sprouting. **(A)** Representative tetanic force profiles generated by unoperated, contralateral (unop) and partially denervated soleus muscles 7 days and 14 days after surgery in $NCAM^{+/+}$ and $Hb9^{cre}NCAM^{flx}$ mice in response to a one second long train of stimuli delivered at 50Hz. **(B)** Quantification of whole muscle soleus tetanic forces generated in contralateral (unop) and partially denervated muscles 7 days, 14 days and 30 days after surgery. The number of muscles assessed at each time point is indicated in the bars. # $P<0.05$ effect of time, one way ANOVA and Holm-Sidak multiple comparisons test; * $P<0.05$ effect of genotype, Student's t-test. **(C)** Quantification of anatomical innervation of contralateral, unoperated muscles (unop, dark blue) and muscles harvested 7, 14 and 30 days following partial denervation. Four types of endplates were identified; *parent* endplates (blue; arrows in *D*); *reinnervated* endplates (red; white arrowheads in *D*); *contacted* endplates (black/yellow; black arrowheads in *D*); and completely *denervated* endplates (black; asterisk in *D*). See text for further description. The number of muscles assessed at each time point is indicated in the bars. * $P<0.05$ effect of genotype, Student's t-test. **(D)** Representative images of NMJs from muscles assessed at Day 14 and immunolabelled for the presynaptic vesicle protein, synaptophysin (syp, green) and with α-BTX for AChRs (red). Scale bars 20μm. (*Right*) Representative images of sprouted endplates at Day 30 immunlabeled for syp (green) and neurofilament (NF; blue) to identify axon sprouts along with α-BTX to identify AChRs (red). Scale bars 10 μm. Arrows identify parent endplates; white arrowheads identify regenerated endplates; black arrowheads identify contacted endplates; asterisks identify denervated NMJs. **(E)** Histograms and cumulative frequency plots (inserts) illustrating % occupancy of presynaptic motor terminals unoperated (dark blue; dashed line insert), reinnervated (red), and parent (blue) endplates in contralateral and partially denervated muscles. Unoperated: $NCAM^{+/+}$ n=60 NMJs from 3 muscles; $Hb9^{cre}NCAM^{flx}$ n=60 NMJs from 3 muscles. 14 days: $NCAM^{+/+}$ n=108 NMJs from 3 muscles; $Hb9^{cre}NCAM^{flx}$ n=111 NMJs from 3 muscles. 30 days: $NCAM^{+/+}$ n=167 NMJs from 3 muscles; $Hb9^{cre}NCAM^{flx}$ n=144 NMJs from 3 muscles.

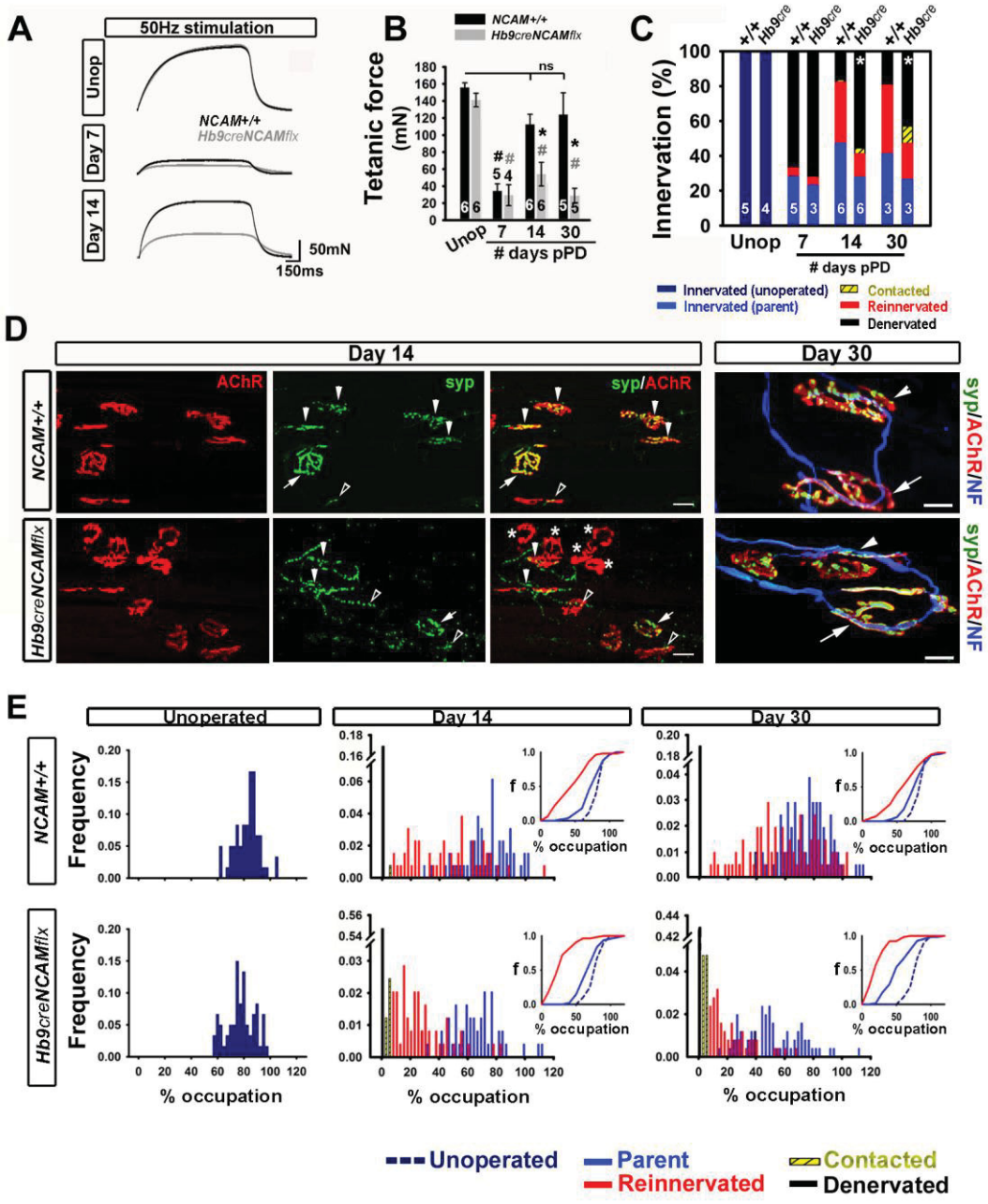
A
50Hz stimulation
Unop
Day 7
Day 14
NCAM+/+
Hb9creNCAMflx
50mN
150ms
B
NCAM+/+
Hb9creNCAMflx
Tetanic force (mN)
ns
Unop
days pPD
C
+/+
Hb9cre
Innervation (%)
Unop
days pPD
Innervated (unoperated)
Innervated (parent)
Contacted
Reinnervated
Denervated
D
Day 14
Day 30
NCAM+/+
Hb9creNCAMflx
AChR
syp
syp/AChR
syp/AChR/NF
E
Unoperated
Day 14
Day 30
Frequency
% occupation
f
Unoperated
Parent
Reinnervated
Contacted
Denervated

Figure 3.3: Mobilized synaptic vesicle puncta fail to populate regenerated *Hb9^{cre}NCAM^{flx}* terminals and remain ectopically localized to non-synaptic regions along terminal sprouts. **(A)** Representative images of *NCAM$^{+/+}$* and *Hb9^{cre}NCAM^{flx}* parent terminals immunolabeled with antibodies against syp (green) and NF (white, or blue in merge) and co-labeled with α-BTX for AChRs (red) 7 days post partial denervation. Some syp+ puncta are localized to the neurofilaments themselves (arrowheads) while others are not (arrows). Scale bar 10μm. **(B-E)** Representative images of synaptic vesicle puncta at parent and regenerated terminals 7 days *(B-C)* and 30 days *(D-E)* after partial denervation, immunolabeled with antibodies against syp (green) and SV2 (blue) and co-labeled with α-BTX for AChRs (red). Representative fluorescence intensity line plots *(bottom right)* were generated from images in *B-E* by drawing a line through the parent terminal (pT), along the terminal bridge (tB) and through the reinnervated terminal (rT). **(F)** Mean ±SEM peak fluorescence intensities of syp immunofluorescence at unoperated terminals (unop, dark blue), synaptic regions of sprouting parent terminals (pT, blue) and non-synaptic regions of terminal sprouts extending from parent terminals (tSP, blue hatched) in *NCAM$^{+/+}$*muscles. **(G)** Mean ±SEM peak fluorescence intensities of syp immunofluorescence measured at synaptic regions of reinnervated terminals (rTs, red) and non-synaptic regions of terminal bridges (tBs, dark red) in *NCAM$^{+/+}$*muscles. **(H-I)** Same analysis as described in *F-G* except performed on *Hb9^{cre}NCAM^{flx}* muscles. The number of endplates and their associated sprouts from the number of muscles assessed are indicated in the bars. Fluorescence of pTs and rTs were always measured with associated tSps and tBs respectively. $^{**}P<0.001$ one way ANOVA followed by Dunn's pairwise multiple comparisons test. ns- not statistically significant. All scale bars 10μm.

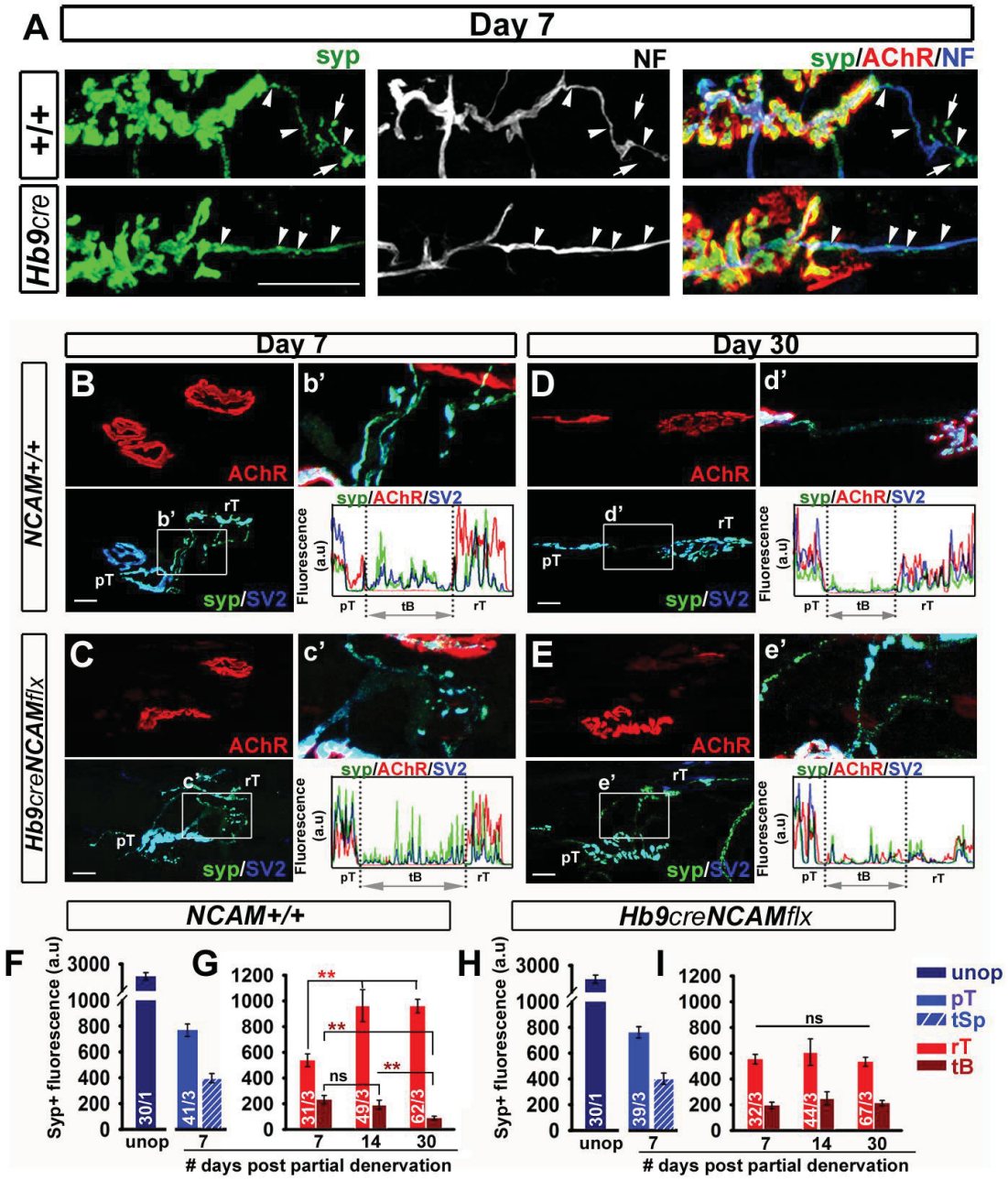
A
Day 7
syp
NF
syp/AChR/NF
+/+
Hb9cre
Day 7
Day 30
NCAM+/+
B
b'
D
d'
AChR
syp/AChR/SV2
syp/SV2
Fluorescence (a.u)
pT
tB
rT
Hb9creNCAMflx
C
c'
E
e'
NCAM+/+
Hb9creNCAMflx
F
G
H
I
Syp+ fluorescence (a.u)
unop
days post partial denervation
ns
**
30/1
41/3
31/3
49/3
62/3
39/3
32/3
44/3
67/3
unop
pT
tSp
rT
tB

Figure 3.4: Terminal sprouts contain functional synaptic puncta which are associated with NCAM immunolabeling. **(A)** Schematic representing FM6-64FX loading into regenerating motor terminals with 50Hz stimulation. **(B-C)** FM4-64FX (white or blue in merge) loading of presynaptic puncta as identified with syp immunohistochemistry (green) at synaptic (α-BTX+; black arrowheads) and non-synaptic (α-BTX-; white arrows) regions of $NCAM^{+/+}$ and $Hb9^{cre}NCAM^{flx}$ motor terminals 7 days after partial denervation. Scale bar 10 μm. **(D)** Partially denervated $NCAM^{+/+}$ motor terminals loaded with FM4-64FX (white or blue in merge) and counter-labeled with antibodies against NCAM (green) and syp (red) demonstrate that NCAM immunohistochemistry is associated with some synaptic puncta which actively cycle during 50Hz stimulation 7 days after partial denervation (arrowhead). (*ortho*) Orthogonal view of the region identified by the dotted line, demonstrating presynaptic expression of NCAM (green) and syp (red) and co-labeling with FM4-64FX signal (white). White arrowheads indicate presynaptic labeling while black arrowheads indicate labeling along the surface of the muscle fiber. Scale bar 5 μm. **(E)** Partially denervated soleus muscles lacking postsynaptic NCAM ($HSA^{cre}NCAM^{flx}$) and labeled with α-BTX and antibodies against syp and NCAM demonstrates presynaptic immunolabeling of NCAM in terminal sprouts. Black arrowheads identify co-distribution of NCAM+ and syp+ puncta at synaptic regions, while white arrowheads identify co-distribution of NCAM+ and syp+ puncta at non-synaptic regions.Scale bar 5 μm.

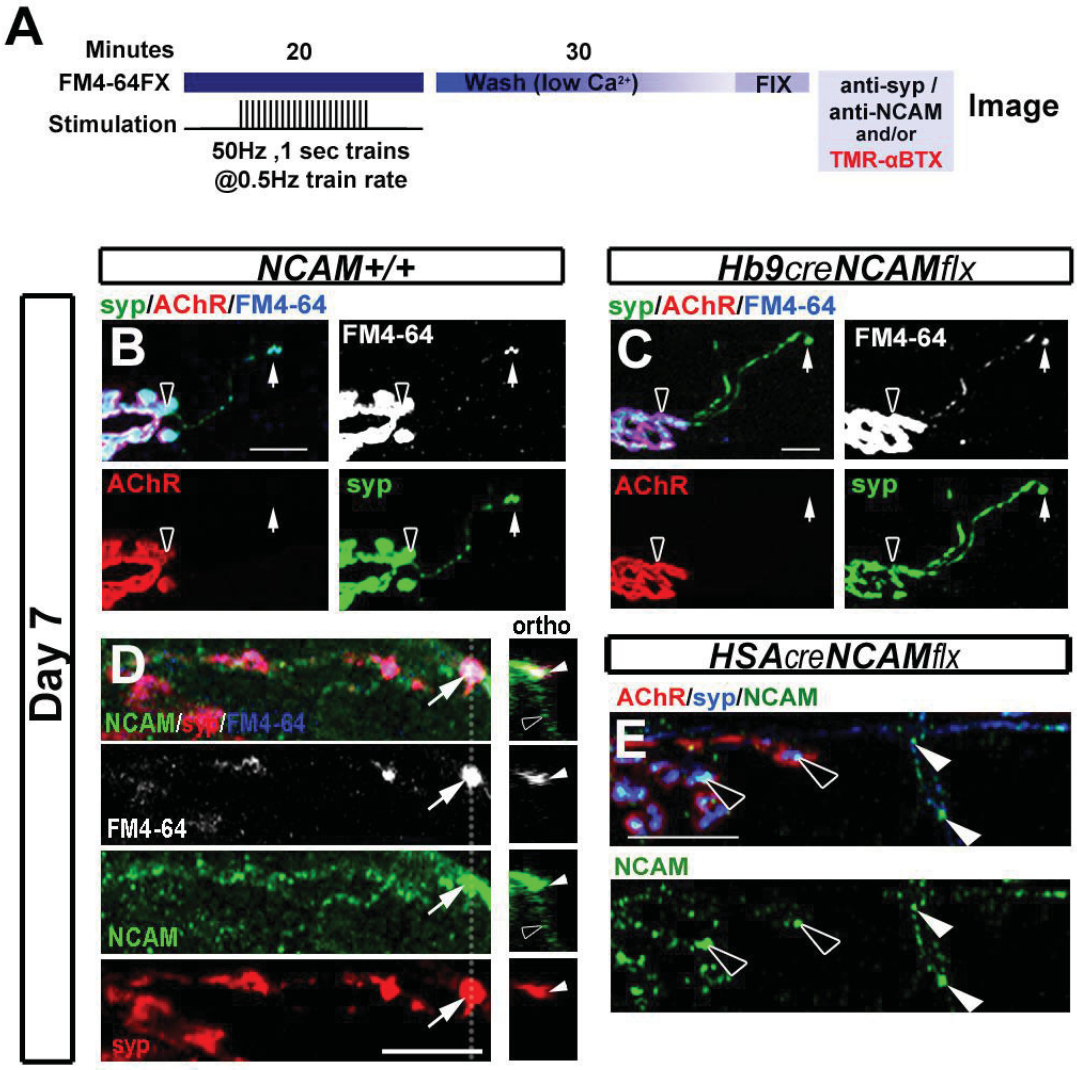
A
Minutes
20
30
FM4-64FX
Wash (low Ca2+)
FIX
anti-syp / anti-NCAM and/or TMR-αBTX
Image
Stimulation
50Hz ,1 sec trains @0.5Hz train rate
NCAM+/+
Hb9creNCAMflx
HSAcreNCAMflx
Day 7
syp/AChR/FM4-64
B
FM4-64
AChR
syp
C
D
ortho
NCAM/syp/FM4-64
NCAM
AChR/syp/NCAM
E

Figure 3.5: Extrasynaptic recycling synaptic vesicles are associated with ectopic clusters of AChRs and are sensitive to inhibition by nifedipine. **(A)** Synaptic vesicles (syp, green; SV2, blue) are tightly localized to $NCAM^{+/+}$ postsynaptic endplates 30 days after partial denervation and have very few vesicles at non synaptic regions in the innervating axon and terminal bridge (arrows). **(B)** Some mislocalized $HB9^{cre}NCAM^{flx}$ vesicular puncta are associated with ectopic clusters of AChRs (arrowheads) while others are not (arrows). **(C)** Many ectopic postsynaptic puncta correspond to of presynaptic FM4-64FX signal (white) induced by 10 minutes of 50Hz stimulation. Muscles were co-labeled with syp (green) and α-BTX (red) to identify presynaptic vesicles and postsynaptic AChRs respectively. **(D-E)** $NCAM^{+/+}$ and $Hb9^{cre}NCAM^{flx}$ NMJs maintain normal endplate morphology for 30 days after complete denervation. All scale bars 20μm. **(F)** Quantification of mean ±SEM postsynaptic endplate lengths as identified with α-BTX in contralateral (Unop) and 30 day partially denervated $NCAM^{+/+}$, $Hb9^{cre}NCAM^{flx}$, $HSA^{cre}NCAM^{flx}$ and $NCAM^{-/-}$ muscles. **(G)** Quantification of mean ±SEM postsynaptic endplate lengths as identified with α-BTX in 30 day completely denervated $NCAM^{+/+}$ and $Hb9^{cre}NCAM^{flx}$ muscles. The number of NMJs from the number of muscles in indicated in the bars. $*P<0.05$, $**P<0.001$ one way ANOVA and Dunn's pairwise multiple comparisons test. **(H-I)** Representative images of $NCAM^{+/+}$ and $Hb9^{cre}NCAM^{flx}$ NMJs 30 days after partial denervation loaded with FM4-64FX (blue/white) by 50Hz stimulation in the presence (+) or absence (-) of 50μM nifedipine and co-labeled with antibodies against syp (green). Arrowheads identify cycling non-synaptic vesicle puncta. **(J)** Mean ±SEM FM4-64FX fluorescence at non-synaptic puncta, as defined by a lack of α-BTX signal, before (red) and after (dark red hatched) application of nifedipine. **(K)** Mean ±SEM FM4-64FX fluorescence intensity at synaptic areas, defined by the presence of postsynaptic α-BTX signal, before (red) and after nifedipine (dark red hatched). $*P<0.05$ one way ANOVA followed by Dunn's pairwise multiple comparisons test. ns- not statistically significant. The numbers of NMJs from at least 3 different muscles are indicated in the bars. Scale bar 20 μm.

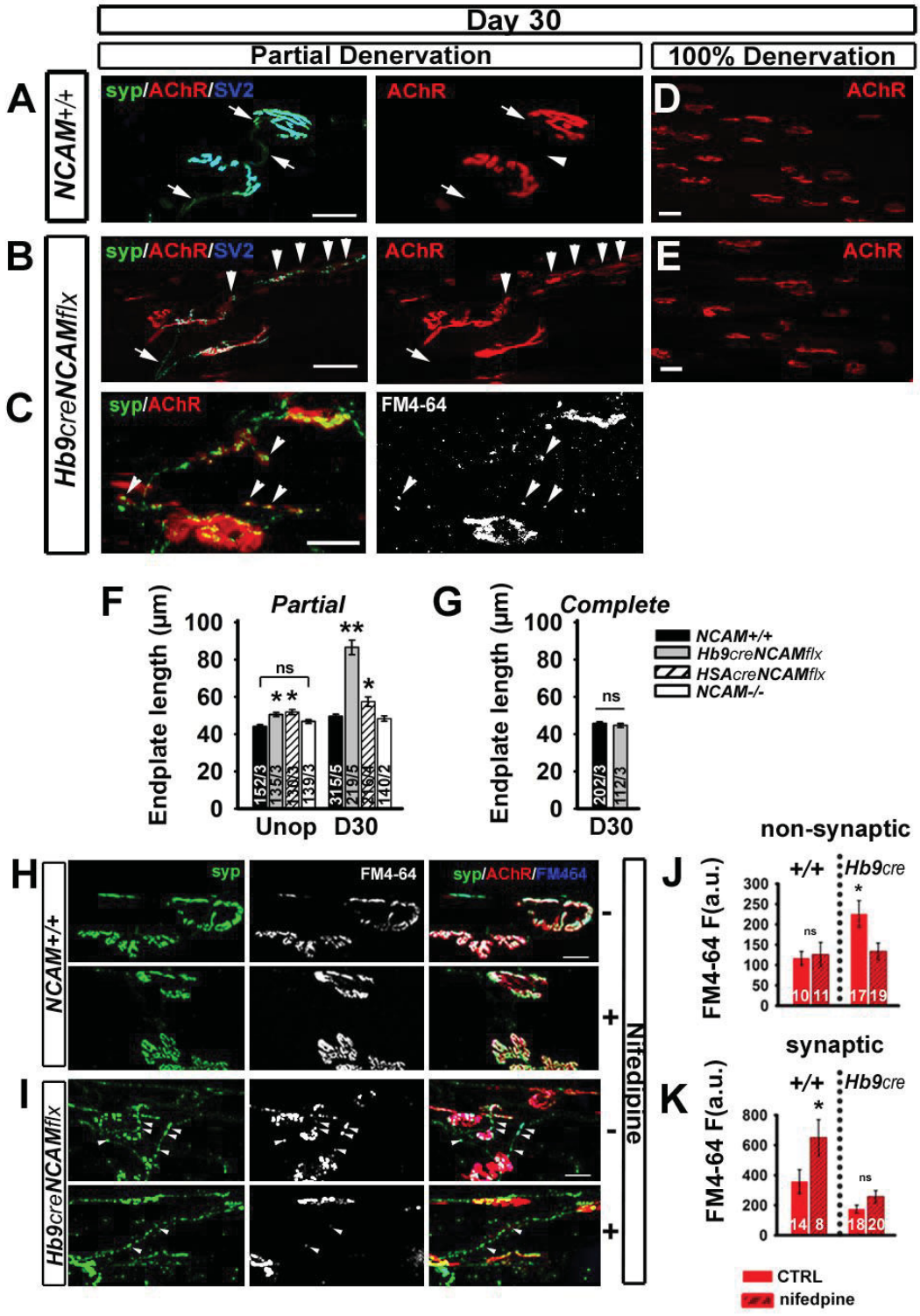
Day 30
Partial Denervation
100% Denervation
A
NCAM+/+
syp/AChR/SV2
AChR
D
AChR
B
Hb9creNCAMflx
syp/AChR/SV2
AChR
E
AChR
C
syp/AChR
FM4-64
F
Partial
Endplate length (µm)
100
80
60
40
20
0
**
ns
**
*
152/3
135/3
330/3
139/3
315/5
219/5
3X6/4
140/2
Unop
D30
G
Complete
Endplate length (µm)
ns
202/3
112/3
D30
NCAM+/+
Hb9creNCAMflx
HSAcreNCAMflx
NCAM-/-
H
NCAM+/+
syp
FM4-64
syp/AChR/FM464
I
Hb9creNCAMflx
Nifedipine
non-synaptic
J
FM4-64 F(a.u.)
+/+
Hb9cre
300
250
200
150
100
50
0
ns
*
10
11
17
19
synaptic
K
FM4-64 F(a.u.)
+/+
Hb9cre
800
600
400
200
0
*
ns
14
8
18
20
CTRL
nifedipine

Figure 3.6: Unoperated *Hb9^{cre}NCAM^{flx}* motor terminals release more vesicles than wild-type under low frequency stimulation conditions. **(A)** Representative traces of EPPs generated by *NCAM$^{+/+}$* (black) and *Hb9^{cre}NCAM^{flx}* (grey) during a 1 second train of 50Hz stimuli. **(B)** Mean ±SEM cumulative quantal contents ($\sum m$) of unoperated *NCAM$^{+/+}$* (black) and *Hb9^{cre}NCAM^{flx}* (grey) motor terminals during 50 stimuli delivered at 1Hz (triangles) and 50Hz (circles). **(C)** Mean ±SEM *m* at *NCAM$^{+/+}$* and *Hb9^{cre}NCAM^{flx}* NMJs over the course of 50 stimuli delivered at 1Hz or 50Hz. **(D)** Mean ±SEM *m* against mean ±SEM cumulative *m* ($\sum m$) during 50Hz stimulation. Extrapolation of the linear regression line, drawn through slope of the depression, to the Y axis provides an estimate of the number of recycling synaptic vesicles (Ruiz et al 2011). **(E)** Mean ±SEM number of vesicles as calculated in *D* under low (1Hz) or high (50Hz) stimulation conditions. $^{**}P<0.001$ Mann-Whitney rank sum test. $^{*}P<0.05$ Student's t-test of 50th pulse data. *NCAM$^{+/+}$* n=64 fibers from 4 muscles; *Hb9^{cre}NCAM^{flx}* n=63 fibers from 4 muscles.

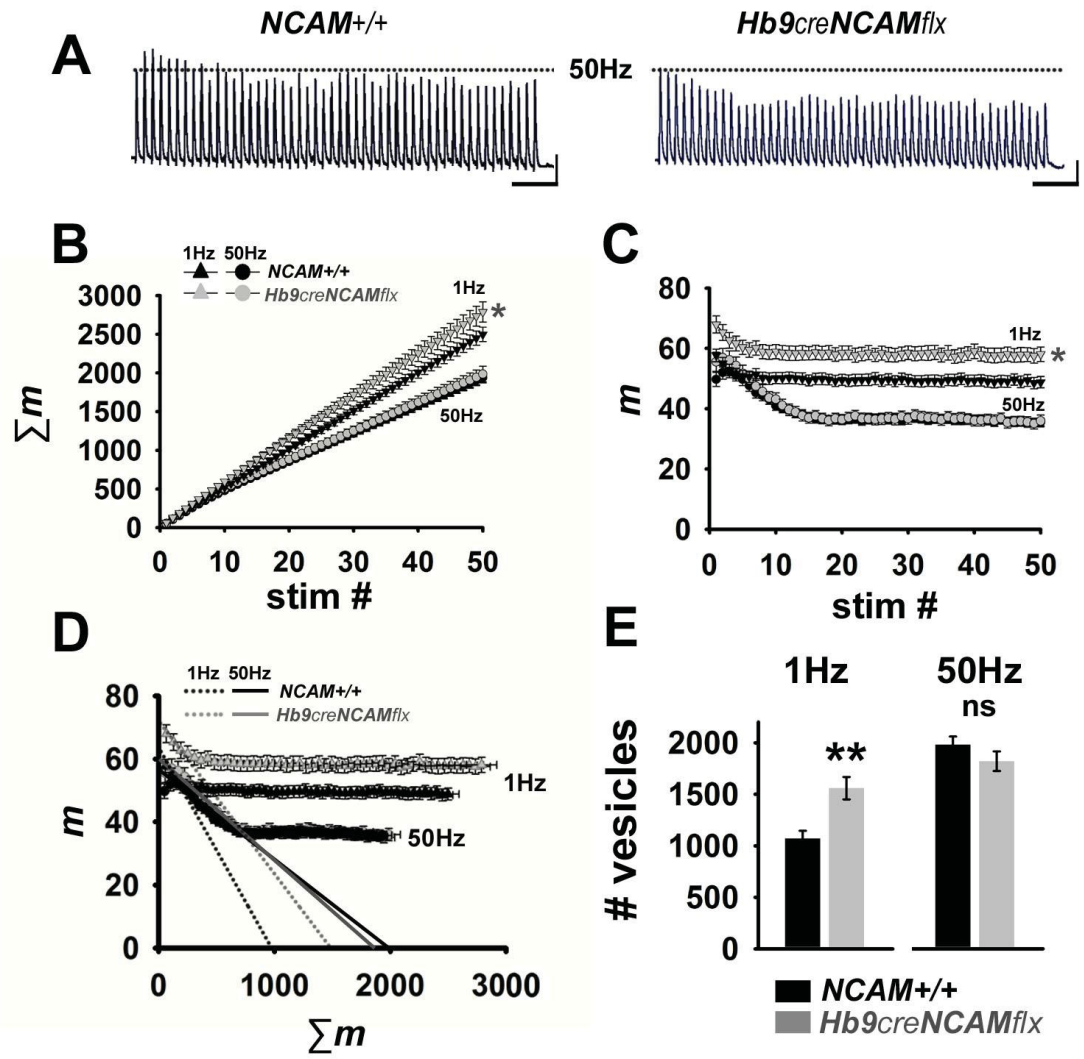
A
NCAM+/+
Hb9creNCAMflx
50Hz
B
1Hz 50Hz
NCAM+/+
Hb9creNCAMflx
1Hz
50Hz
*
∑m
stim #
C
1Hz
50Hz
*
m
stim #
D
1Hz 50Hz
NCAM+/+
Hb9creNCAMflx
1Hz
50Hz
m
∑m
E
1Hz
50Hz
ns
**
vesicles
NCAM+/+
Hb9creNCAMflx

Figure 3.7: Regenerating motor terminals have a reduced probability of release. **(A)** Representative EPP traces recorded from unoperated (dark blue) or regenerated (red) NMJs. **(B)** Histograms demonstrating the spread of quantal contents (*m*) recorded from single NMJs, or **(C)** from at all sampled NMJs in unoperated (dark blue) and reinnervated (red) $NCAM^{+/+}$ synapses. Populations were fit with a Gaussian-curve. **(D-F)** Same analysis as *A-C* except for $Hb9^{cre}NCAM^{flx}$ muscles. **(G)** Mean ±SEM and plots of quantal parameters *m,* **(H)** *n,* and **(I)** *p* assessed at unoperated (blue) and regenerated (red) $NCAM^{+/+}$ (black) and $Hb9^{cre}NCAM^{flx}$ (grey) NMJs (see methods for details on estimations of binomial parameters). **(J)** Scatter plots and regression lines demonstrating the relationship between spontaneous activity (mEPP frequency) and *m* in unoperated (dark blue) and regenerated (red) $NCAM^{+/+}$ motor terminals. **(K)** Representative traces (*top*) and cumulative frequency plot of spontaneous transmission demonstrating the distribution of mEPP frequency recorded from unoperated and regenerated $NCAM^{+/+}$ terminals. **(L)** Magnified mEPPs (*top*) and cumulative frequency plot of mEPP amplitudes recorded from unoperated and regenerated $NCAM^{+/+}$ terminals. **(M-O)** Same analysis as *J-L* except for $Hb9^{cre}NCAM^{flx}$ muscles. $^{**}P<0.001$, $^{*}P<0.01$, effect of genotype, Mann-Whitney test; $\#P<0.05$ effect of regeneration, one way ANOVA and Dunn's multiple comparisons test. ns- not statistically significant. Unoperated; $NCAM^{+/+}$ n=65 NMJs from 4 muscles; $Hb9^{cre}NCAM^{flx}$ n= 63 from 4 muscles. Reinnervated $NCAM^{+/+}$ n=30 NMJs from 3 muscles; $Hb9^{cre}NCAM^{flx}$ n =30 from 3 muscles.

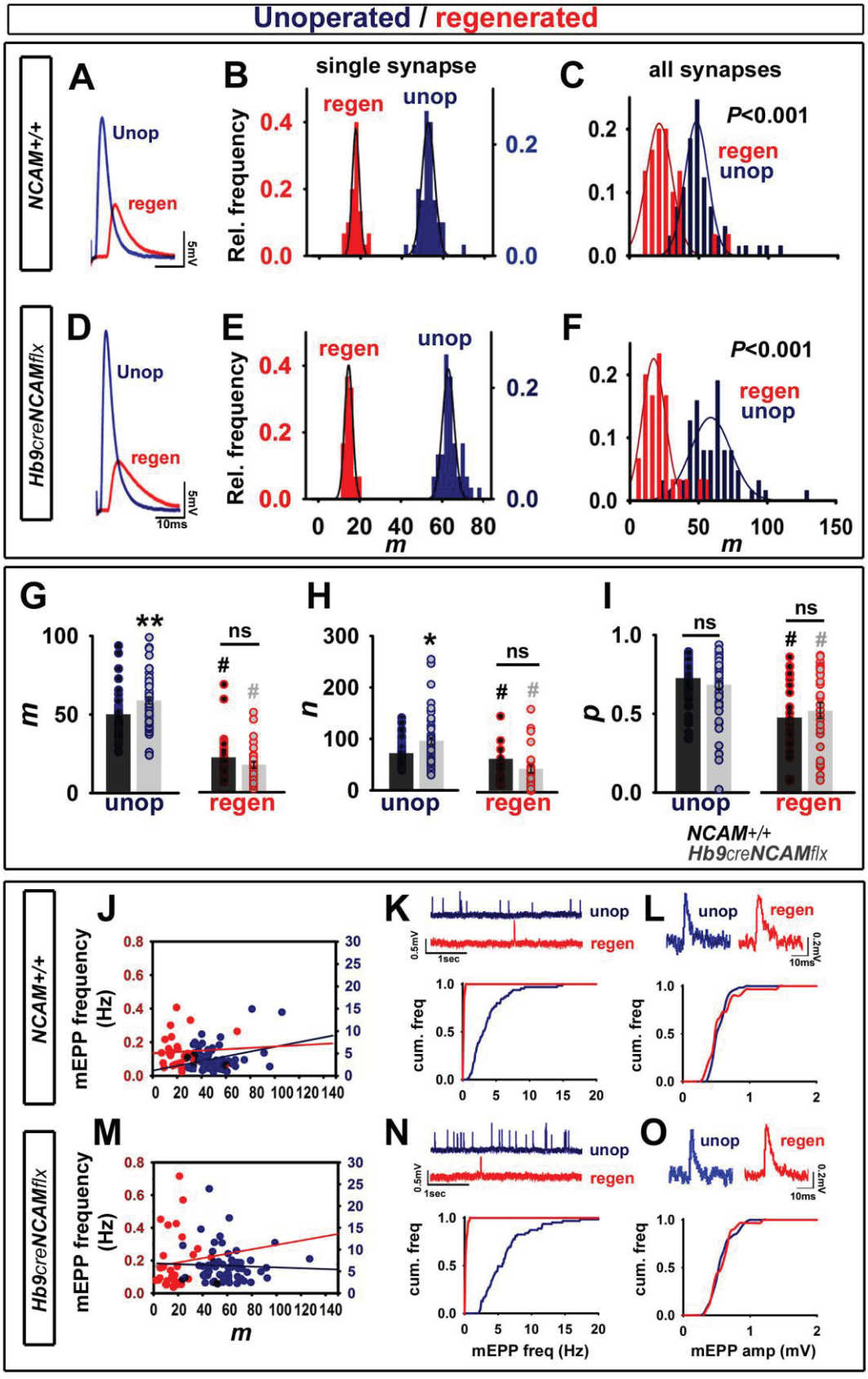
Unoperated / regenerated
NCAM+/+
Hb9creNCAMflx
A
B
single synapse
C
all synapses
Unop
regen
5mV
10ms
Rel. frequency
P<0.001
D
E
F
m
G
H
I
n
p
unop
regen
ns
NCAM+/+
Hb9creNCAMflx
J
K
L
M
N
O
mEPP frequency (Hz)
cum. freq
0.5mV
1sec
0.2mV
mEPP freq (Hz)
mEPP amp (mV)

Figure 3.8: The loss of presynaptic NCAM disrupts that maturation in transmission strength. **(A)** Cartoon summarizing the experimental rationale. Three populations of synapses were encountered when synapses were sampled in partially denervated muscles; *mature* synapses (blue) were classified as those which had an $m>25$; *immature* (red) synapses were classified as those which had an $m\leq25$; and *denervated* (black) synapses did not exhibit a response to presynaptic stimulation. Denervated synapses could not be reliably differentiated from recordings made from extrasynaptic regions of muscle fibers and were not further quantified. **(B-C)** Representative traces of EPPs (left) and histograms of quantal strengths (*m*) at single synapses (middle) and all synapses combined (right) determined by the average of 30 pulses delivered at 1Hz and recorded from $NCAM^{+/+}$ or $Hb9^{cre}NCAM^{flx}$ muscles. *Insert*; cumulative frequency plots of synaptic strengths recorded from $NCAM^{+/+}$ (black) and $Hb9^{cre}NCAM^{flx}$ (grey). **(D-E)** Distribution of mature and immature synapses recorded from 30 day partially denervated $NCAM^{+/+}$ and $Hb9^{cre}NCAM^{flx}$ soleus muscles. *Insert*; cumulative frequency plots of synaptic strengths recorded from $NCAM^{+/+}$ (black) and $Hb9^{cre}NCAM^{flx}$ (grey). *P* values were determined using Mann-Whitney rank sum test. **(F)** Quantification of *m* **(G)** *p* and **(H)** *n* as determined by 1Hz stimulation across sampled all synapses during the course of terminal field expansion. $*P<0.01$, **P<0.001, effect of genotype Mann-Whitney test, $\#P<0.05$, effect of time, one way ANOVA and Dunn's multiple comparisons test ($NCAM^{+/+}$ black; $Hb9^{cre}NCAM^{flx}$ grey). **(I-J)** Representative EPPs *(left)* and paired pulse ratios *(right)*, generated immature (red) and mature (blue) synapses in partially denervated $NCAM^{+/+}$ and $Hb9^{cre}NCAM^{flx}$ muscles. $*P<0.01$ Student's t-test $m\leq25$ vs. $m>25$ $**P<0.001$ Student's t-test $m\leq25$ vs. $m>25$. Unoperated, $NCAM^{+/+}$ n=65 NMJs from 4 muscles; $Hb9^{cre}NCAM^{flx}$ n= 63 from 4 muscles. Day 5, $NCAM^{+/+}$ n=28 NMJs from 3 muscles; $Hb9^{cre}NCAM^{flx}$ n= 31 from 3 muscles. Day 10, $NCAM^{+/+}$ n=42 NMJs from 5 muscles; $Hb9^{cre}NCAM^{flx}$ n= 45 from 4 muscles. Day 30, $NCAM^{+/+}$ n=51 NMJs from 4 muscles; $Hb9^{cre}NCAM^{flx}$ n= 59 from 5 muscles.

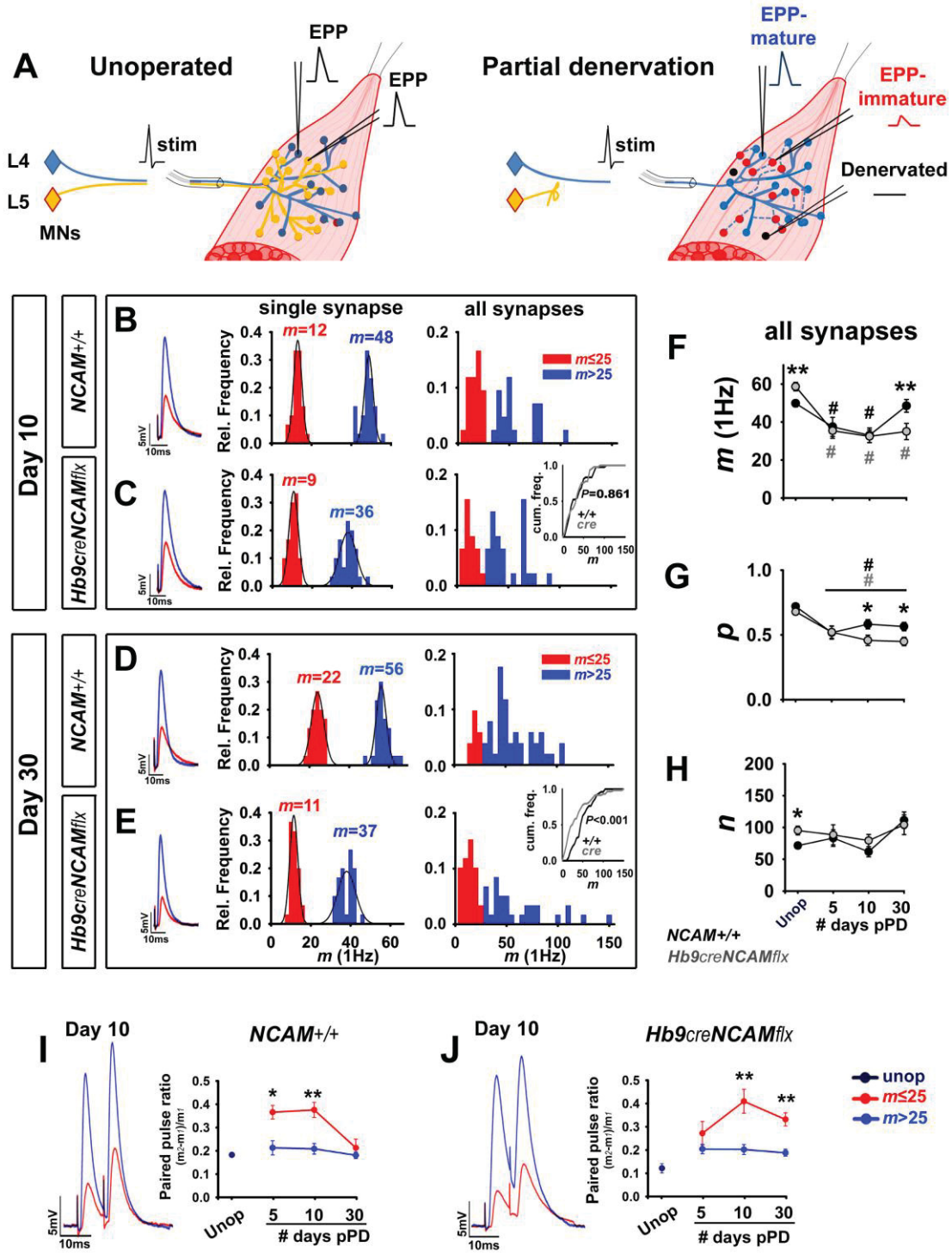
A
Unoperated
EPP
EPP
stim
L4
L5
MNs
Partial denervation
EPP-mature
EPP-immature
stim
Denervated
Day 10
NCAM+/+
Hb9creNCAMflx
B
C
single synapse
all synapses
m=12
m=48
m=9
m=36
m≤25
m>25
Rel. Frequency
cum. freq.
P=0.861
+/+
cre
m
5mV
10ms
Day 30
D
E
m=22
m=56
m=11
m=37
P<0.001
m (1Hz)
F
all synapses
m (1Hz)
G
p
H
n
Unop
days pPD
NCAM+/+
Hb9creNCAMflx
I
Day 10
NCAM+/+
Paired pulse ratio
J
Day 10
Hb9creNCAMflx
unop
m≤25
m>25

Figure 3.9: The number of synaptic vesicles mobilized during high frequency stimulation is reduced at mature synapses immediately following partial denervation. **(A)** Summed quantal contents ($\sum m$) of immature (red) and mature (blue) $NCAM^{+/+}$ (black) and $Hb9^{cre}NCAM^{flx}$ (grey) synapses plotted against stimulation number during a 1 second train of stimuli delivered at 50Hz 10 days after partial denervation. **(B)** Quantal contents (m) of immature (red) and mature (blue) $NCAM^{+/+}$ (black) and $Hb9^{cre}NCAM^{flx}$ (grey) synapses plotted against $\sum m$ during a 1 second train of stimuli delivered at 50Hz 10 days after partial denervation. **(C)** Frequency of synapses encountered which exhibited immature ($m \leq 25$; red) or mature ($m > 25$; blue) transmission phenotypes 10 days after partial denervation. **(D-F)** Same analysis as *A-C*, except for 30 day partially denervated synapses. **(G)** Mean ±SEM number of RRP vesicles at all synapses recorded from unoperated and partially denervated $NCAM^{+/+}$ (black) and $Hb9^{cre}NCAM^{flx}$ (grey) soleus muscles as determined by repetitive 1Hz stimulation. **(H)** Data from *G* segregated into either immature ($m \leq 25$; red) or mature ($m > 25$; blue) groups. **(I)** Cumulative frequency plot of RRP sizes from all $NCAM^{+/+}$ (black) and $Hb9^{cre}NCAM^{flx}$ (grey) synapses 30 days after partial denervation. **(J-L)** Same analysis as performed for *G-I* except RP values were determined using 50Hz stimulation. **$P<0.001$ effect of genotype, Mann-Whitney rank sum test; #$P<0.05$, effect of time, one way ANOVA and Dunn's multiple comparisons test.

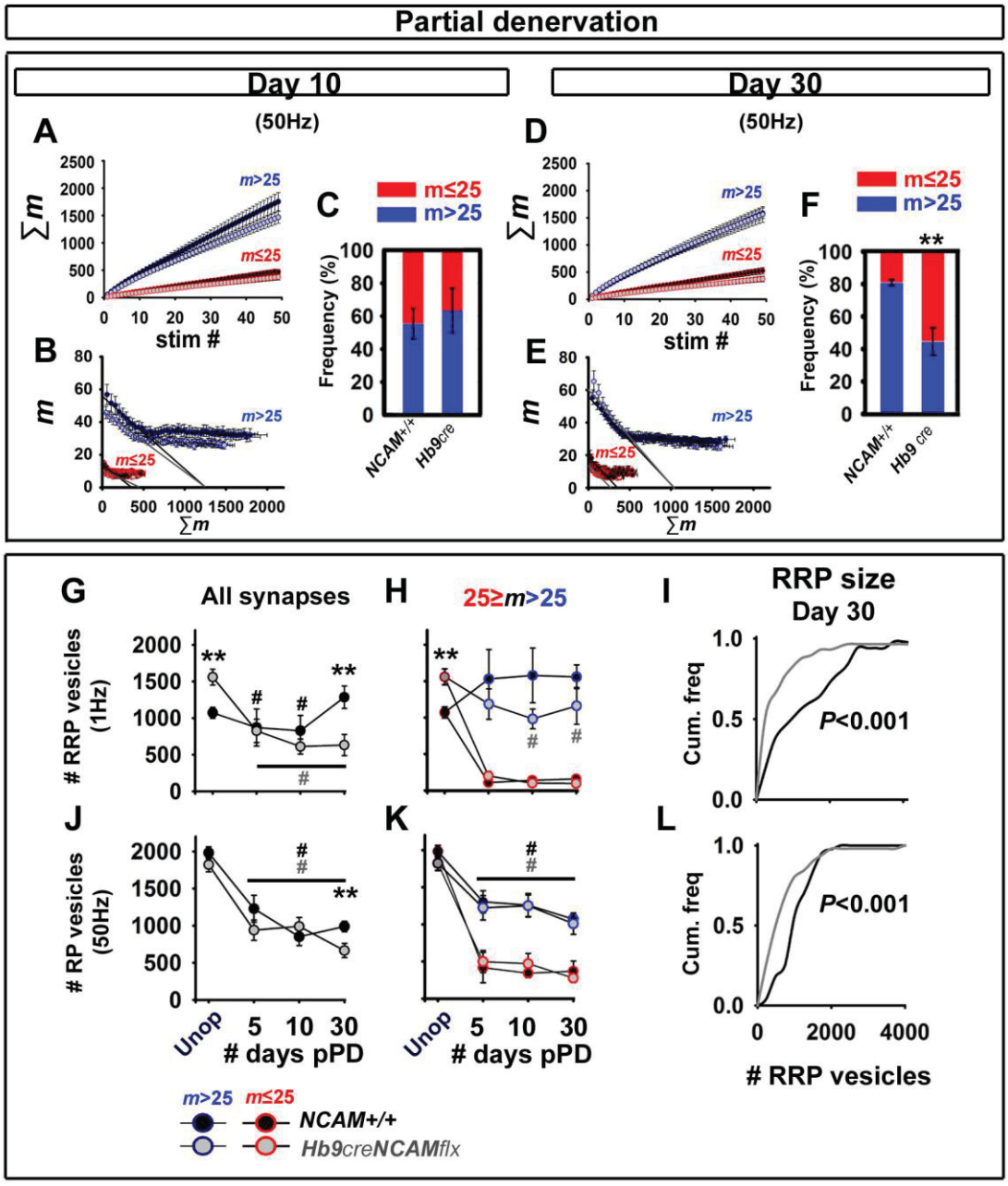
Partial denervation
Day 10
Day 30
A
(50Hz)
D
(50Hz)
∑m
stim #
m>25
m≤25
B
m
∑m
C
m≤25
m>25
Frequency (%)
NCAM+/+
Hb9cre
E
F
Hb9 cre
**
G
All synapses
RRP vesicles (1Hz)
H
25≥m>25
I
RRP size
Day 30
Cum. freq
P<0.001
RRP vesicles
J
RP vesicles (50Hz)
K
L
Unop
5
10
30
days pPD
NCAM+/+
Hb9creNCAMflx

Figure 3.10: Variable transmission during repetitive stimulation at immature motor terminals. **(A-D)** Representative traces of EPPs recorded from mature (m>25, blue) and immature (m≤25, red) $NCAM^{+/+}$ and $Hb9^{cre}NCAM^{flx}$ synapses during 50Hz stimulation for 1 sec 10 and 30 days after partial denervation. **(E)** Mean ±SEM coefficient of variation (CV) of m during the plateau phase of synapses recorded from unoperated and partially denervated $NCAM^{+/+}$ (black) and $Hb9^{cre}NCAM^{flx}$ (grey) muscles in response to 1 Hz stimulation. **(F)** Data shown in *C* segregated into populations of mature (m>25, blue) and immature (m≤25, red) terminals. **(G)** Cumulative frequency plot of CV determined by 1Hz stimulation at all sampled synapses of $NCAM^{+/+}$ (black) and $Hb9^{cre}NCAM^{flx}$ (grey) 30 days after partial denervation. **(H-J)** Same analysis as *E-F* except for CVs during trains of EPPs generated by 50Hz stimulation. *P<0.005 **P<0.001 Mann Whitney rank sum test.

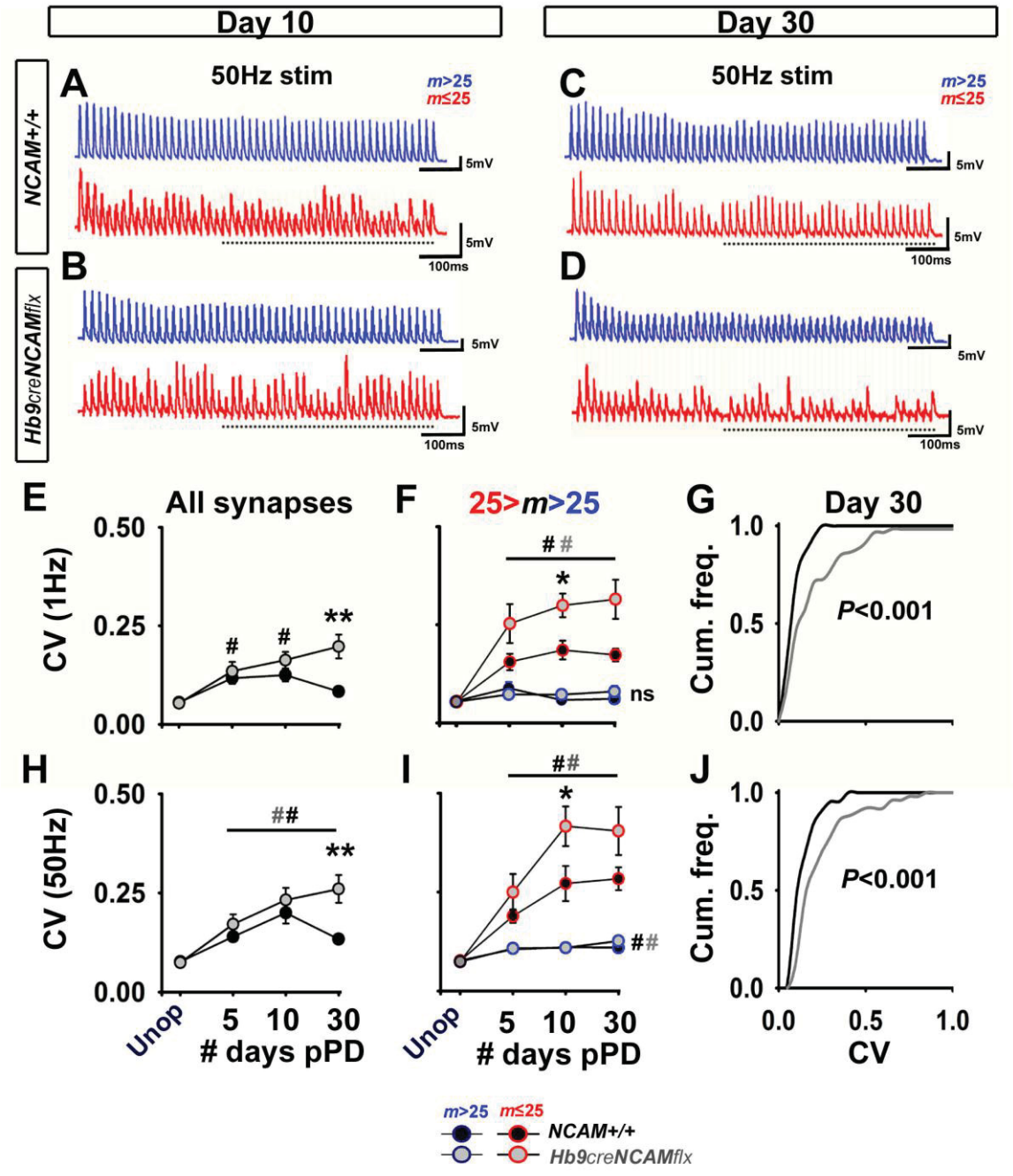
Day 10
Day 30
NCAM+/+
Hb9creNCAMflx
A
B
C
D
50Hz stim
m>25
m≤25
5mV
100ms
E
All synapses
CV (1Hz)
F
25>m>25
ns
G
Day 30
Cum. freq.
P<0.001
H
CV (50Hz)
I
J
Unop
5
10
30
days pPD
CV
NCAM+/+
Hb9creNCAMflx

Figure 3.11: L-VDCCS modulate the activity of the readily releasable pool at newly regenerated NMJs. **(A-C)** Representative intracellular recordings of EPPs and mean ±SEM of *m* recorded from unoperated (m>25; blue) and regenerated (m≤25; red) $NCAM^{+/+}$synapses before (CTRL; red) and after (dark red) application of 50μM nifedipine 7 and 14 days after partial denervation during 1 Hz stimulation. **(D)** Mean ±SEM % change in 1Hz *m* 10 minutes following application of 50μM nifedipine (nif) at unoperated and regenerated $NCAM^{+/+}$ synapses. 100nM agatoxin (ATX) was added following nifedipine to block P/Q VDCCs. **(E-H)** Same analysis as *A-D* except for $Hb9^{cre}NCAM^{flx}$ muscles. **P*<0.05 **P<0.01 one way ANOVA of normalized nifedipine treatments followed by Holm-Sidak pairwise multiple comparisons test. The number of synapses recorded per condition is shown in the bars in *D* and *H*. One regenerated NMJ was assessed for an effect of nifedipine per muscle.

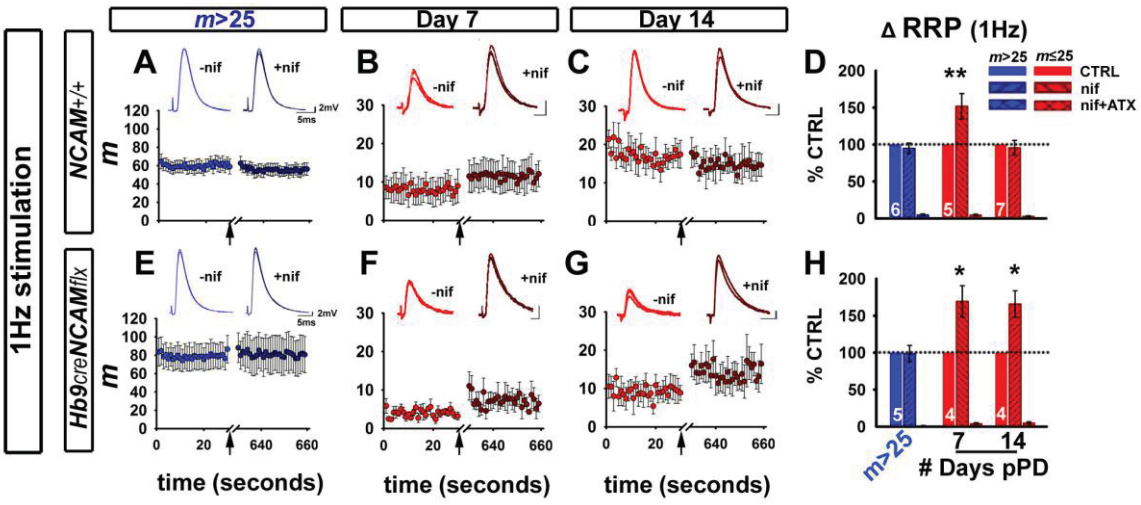
1Hz stimulation
NCAM+/+
Hb9creNCAMflx
m
m>25
Day 7
Day 14
A
B
C
D
E
F
G
H
-nif
+nif
2mV
5ms
time (seconds)
Δ RRP (1Hz)
m>25
m≤25
CTRL
nif
nif+ATX
% CTRL
**
*
Days pPD

Figure 3.12: Postsynaptic NCAM is required to stabilize sprouted synapses. **(A)** Counts of back labelled motoneurons 3 days following AlexaFluor-conjugated CTB injection into the soleus muscle of contralateral (unop) and partially denervated (L5 PD) $HSA^{cre}NCAM^{flx}$ mice. Dotted line illustrates motoneuron counts from contralateral $NCAM^{+/+}$ (WT; unop) and partially denervated (L5) spinal cords. **(B)** Mean ±SEM muscle tension generated by unoperated and partially denervated soleus muscles 7, 14 and 30 days post partial denervation (pPD) in response to a one second long train of 50Hz stimuli. Dotted line illustrates force generated by $NCAM^{+/+}$ muscles 14 days following partial denervation (*WT 14days*). **(C)** Percentage of innervated endplates as determined by co-localization of synaptophysin (syp) and TMR α-BTX immunofluorescence. Dotted line represents % of $NCAM^{+/+}$ NMJs innervated 14 days following partial denervation. **(D)** Representative image of $HSA^{cre}NCAM^{flx}$ NMJs immunolabelled for synaptophysin (syp; green; arrows), neurofilament (NF; blue) and α-BTX for postsynaptic AChRs (red) 14 days after partial denervation. A terminal sprout is shown extending away from a parent terminal (pT) to innervate and cross a reinnervated terminal (rT) to form an immature contact with a second endplate (cT). **(E)** Synaptic vesicles are localized to synaptic regions in $HSA^{cre}NCAM^{flx}$ rTs, although **(F)** reinnervated synapses are small and **(G)** exhibit significantly reduced presynaptic overlap as compared to reinnervated $NCAM^{+/+}$ NMJs. The number of spinal cords (*A*), muscles (*B*) and the number of NMJs from the number of muscles assessed (*C*) are shown in the bars. Force $*P<0.05$; one way ANOVA followed by Holm-Sidak pairwise multiple comparisons test. Innervation; $*P<0.05$ one way ANOVA followed by Dunn's pairwise multiple comparisons test. ns = not statistically significant. Pre/post synaptic overlap; $HSA^{cre}NCAM^{flx}$ parent n=53 NMJs from 3 muscles, reinnervated n=50 NMJs from 3 muscles; $NCAM^{+/+}$ parent n= 56 from 3 muscles, reinnervated n =52 from 3 muscles. Mann-Whitney rank sum test P values are shown in the figure.

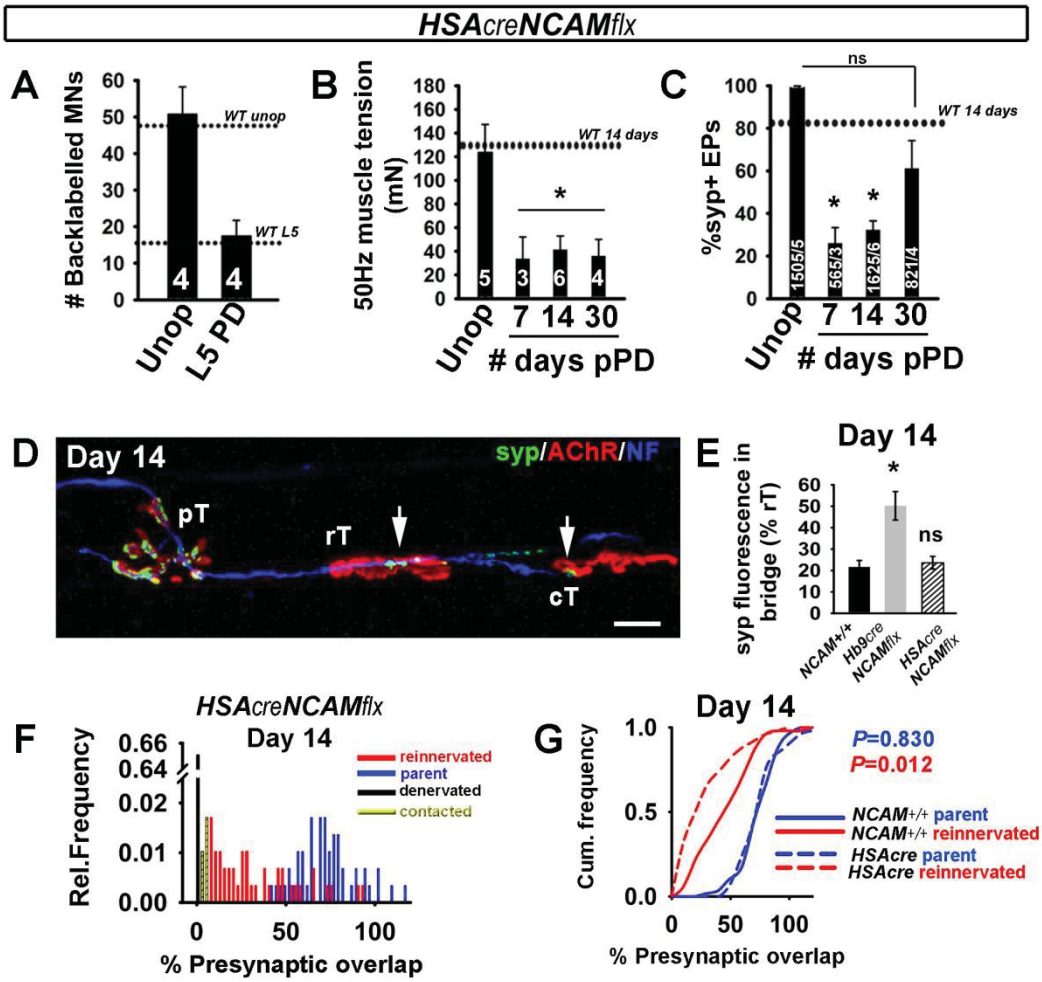
HSAcreNCAMflx
A
Backlabelled MNs
WT unop
WT L5
4
4
Unop
L5 PD
B
50Hz muscle tension (mN)
WT 14 days
*
5
3
6
4
Unop
7 14 30
days pPD
C
%syp+ EPs
ns
WT 14 days
*
*
1505/5
565/3
1625/6
821/4
Unop
7 14 30
days pPD
D
Day 14
syp/AChR/NF
pT
rT
cT
E
Day 14
syp fluorescence in bridge (% rT)
*
ns
NCAM+/+
Hb9cre NCAMflx
HSAcre NCAMflx
F
HSAcreNCAMflx
Day 14
Rel.Frequency
reinnervated
parent
denervated
contacted
% Presynaptic overlap
G
Day 14
Cum. frequency
P=0.830
P=0.012
NCAM+/+ parent
NCAM+/+ reinnervated
HSAcre parent
HSAcre reinnervated
% Presynaptic overlap

Figure 3.13: The abundance of recycling pool (RP) vesicles available for redistribution is reduced in the absence of postsynaptic NCAM following partial denervation. **(A)** Plot of *m* vs. $\sum m$ measured from 1 second trains of EPPs in response to 50Hz stimulation for the estimation of RP pool size. **(B)** Mean ±SEM of individual RP sizes measured in response to 50Hz stimulation at $NCAM^{+/+}$ (black) $HSA^{cre}NCAM^{flx}$ (white) regenerated (red) and parent (blue) synapses 14 days after partial denervation. **(C)** Mean ±SEM of individual RRP sizes measured in response to 1Hz stimulation at $NCAM^{+/+}$ (black) $HSA^{cre}NCAM^{flx}$ (white) regenerated (red) and parent (blue) synapses 14 days after partial denervation. **(D)** Mean ±SEM of coefficient of variation (CV) of EPPs generated by 1 and 50Hz stimulation at parent (m>25) NMJs. **(E)** Representative images of $NCAM^{+/+}$ and $HSA^{cre}NCAM^{flx}$ parent terminals 14 days after partial denervation co-immunolabeled with antibodies against SV2 and neurofilament (green) and with α-BTX for postsynaptic AChRs. Arrows identify the innervation by a large caliber NF/SV+ axon, while arrowheads identify thinner terminals sprouts; two defining characteristics of parent terminals. $NCAM^{+/+}$ n=59 fibers from 4 muscles; $HSA^{cre}NCAM^{flx}$ n=67 fibers from 5 muscles. *P<0.05 <0.01 Mann-Whitney rank sum test $NCAM^{+/+}$ vs. $HSA^{cre}NCAM^{flx}$; n.s. not statistically significant.

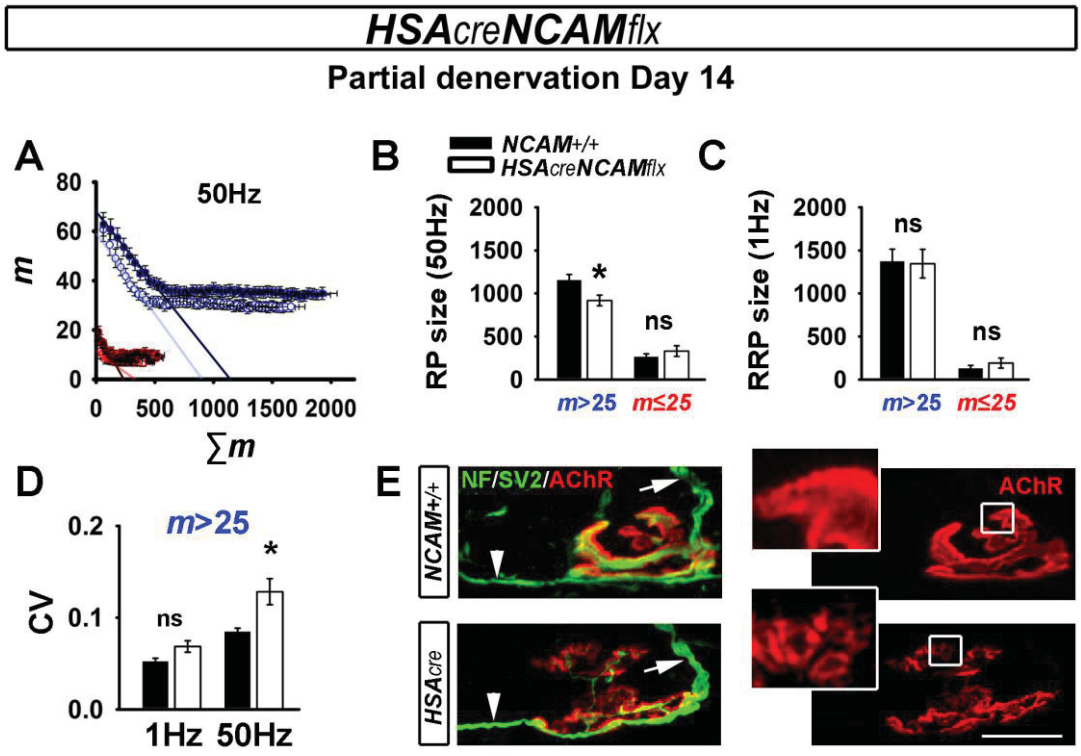
HSAcreNCAMflx
Partial denervation Day 14
A
50Hz
m
80
60
40
20
0
0 500 1000 1500 2000
∑m
B
NCAM+/+
HSAcreNCAMflx
RP size (50Hz)
2000
1500
1000
500
0
*
ns
m>25 m≤25
C
RRP size (1Hz)
2000
1500
1000
500
0
ns
ns
m>25 m≤25
D
m>25
CV
0.2
0.1
0.0
ns
*
1Hz 50Hz
E
NCAM+/+
HSAcre
NF/SV2/AChR
AChR

Figure 3.14: Pre and postsynaptic NCAM are required for functional terminal field expansion by influencing the abundance of recycling synaptic vesicles. **(A)** Cartoon summary of terminal field expansion induced by partial denervation in three gentoypes of mice examined in this study. Multicoloured diamonds illustrate spinal motoneurons extending their innervation to postsynaptic endplates (red) on the surface of myofibers in normal adult soleus muscles (left) and those responding to partial denervation (right). Sprouting $Hb9^{cre}NCAM^{flx}$ motoneurons fail to recover functional muscle innervation due to the mislocalization of synaptic vesicles and the subsequent disorganization of postsynaptic receptor clusters. $HSA^{cre}NCAM^{flx}$ spouts target synaptic vesicles appropriately to synaptic regions but do not maintain innervation because a lack of synaptic resources. **(B)** $NCAM^{+/+}$ soleus motoneurons can, on average, sprout to innervate close to 3 times their original complement of endplates while $Hb9^{cre}NCAM^{flx}$ and $HSA^{cre}NCAM^{flx}$ exhibit little to no functional sprouting capacity. **(C)** Estimation of the fold increase in the number of RP vesicles at $NCAM^{+/+}$, $Hb9^{cre}NCAM^{flx}$ soleus and $HSA^{cre}NCAM^{flx}$ under maximal sprouting conditions. These estimates were made by combining quantitative measurements of RP size with assessments of functional whole muscle innervation (see methods for detail on estimation).

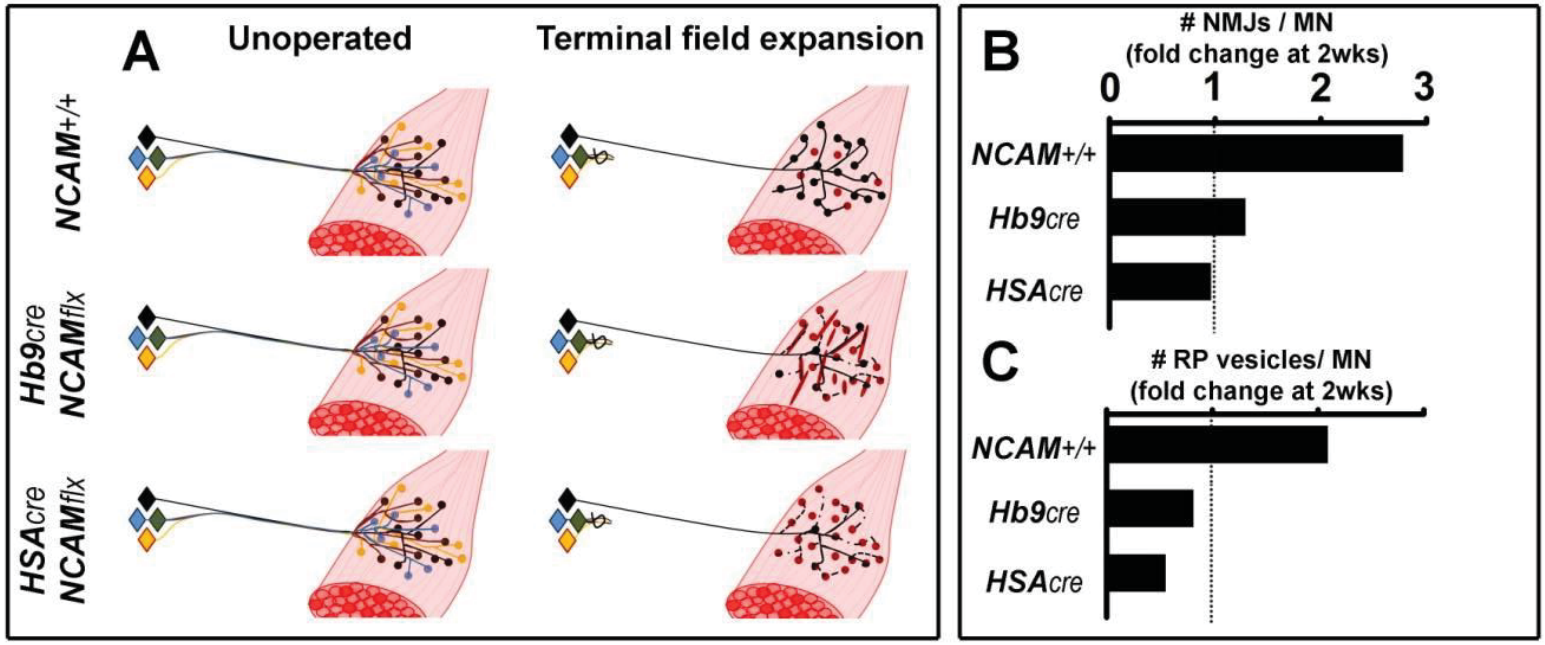
A
Unoperated
Terminal field expansion
NCAM+/+
Hb9cre NCAMflx
HSAcre NCAMflx
B
NMJs / MN
(fold change at 2wks)
0
1
2
3
NCAM+/+
Hb9cre
HSAcre
C
RP vesicles/ MN
(fold change at 2wks)
NCAM+/+
Hb9cre
HSAcre

CHAPTER 4: A long-term co-culture system for the study of diseased neuromuscular junctions

Abstract

The co-culture of motoneurons and muscle has long been used as a model system for the investigation of neuromuscular synaptogenesis and has provided fundamental insights into the organizational properties of pre and postsynaptic structures. While this system has greatly contributed to the understanding of events leading to the formation and function of immature synapses, it has yet to provide an effective platform to assess the differentiation of these synapses into mature neuromuscular junctions (NMJs). Recent derivation of motoneurons from cells isolated from patients suffering from motoneuron disease (MND) has generated renewed pressure to deliver an *in vitro* system capable of producing functionally and morphologically mature NMJs amenable to high throughput screening for novel therapeutics. Here we describe a long-term chimeric co-culture system using motoneurons derived from mouse embryonic stem cells (ESCMNs) and chick myotubes which allows a detailed analysis of synaptic function from early stages of cell-to-cell contact to mature synaptic transmission *in vitro*. Moreover, we used ESCMNs generated from *NCAM*$^{-/-}$ mice to successfully demonstrate the sensitivity of the system to detect synaptic dysfunction at NMJs formed by motoneurons harbouring known genetic mutations. This *in vitro* model of NMJ form and function is therefore a sensitive and efficient assay of mature synapses grown by differentiated pluripotent cells and can be used to reliably identify synaptic pathology such as those associated with sporadic MND.

Introduction

Embryonic spinal cord explants, co-cultured with muscle fibers have been extensively used to study cellular processes underlying the formation of neuromuscular junction (NMJs) during very early stages of synaptogenesis (James and Tresman, 1968; Crain et al 1970; Robbins and Yonezawa 1971; Fishbach, 1972; Young and Poo, 1983; Takahashi et al 1987). More recently, motoneurons derived from pluripotent cells have been co-cultured with muscle fibers to demonstrate their capacity to form functional NMJs (Miles et al 2004; Guo et al 2011; Marteyn et al 2011; Son et al 2011; Chipman et al, 2012; Umbach et al 2012). However, most studies using motoneuron/muscle fiber co-cultures have focused on early events in synaptogenesis and not those associated with mature NMJs. This is due, in part, because establishing mature synapses in culture is technically challenging.

Recent progress in neuromuscular disease modeling has introduced renewed pressure to develop *in vitro* model systems capable of generating mature NMJs in order to accurately model diseases and screen novel therapeutics (Thomson et al 2011; Chipman et al., 2012). For example, synaptic pathology appears early in the progression of motoneuron diseases (MND) such as spinal muscular atrophy (SMA) (Kariya et al 2008; Murray et al 2008; Kong et al 2009; Ruiz et al 2010) and amyotrophic lateral sclerosis (ALS) (Frey et al 2000; Schaefer et al 2005; Gould et al 2008). Whether deficits in neurotransmission and instability of the NMJ precipitate the pathophysiology of the diseases, or are simply a secondary consequence is not known. Current investigations into synaptic function during MNDs are necessarily restricted to animal models of inherited disease, which compose only a minority of cases and do not address the pathophysiology of human sporadic diseases. The directed differentiation of patient-specific somatic cells into motoneurons has provided a potential means to model sporadic cases of MND *in vitro* (Dimos et al 2008; Son et al 2011), provided an appropriate system for the analysis of synaptic function is available.

Here we describe a novel long-term co-culture system to study the morphology and function of mature NMJs *in vitro*. Using a well-described differentiation protocol (Wichterle et al 2002; Miles et al 2004; Soundararajan et al 2006, 2010; Yohn et al 2008),

Hb9:GFP mouse embryonic stem (ES) cells were differentiated into functional motoneurons (ESCMNs) and grown in co-culture with chick myofibers for up to 35 days. In addition, we co-cultured Hb9:GFP ESCMNs lacking NCAM with muscle fibers to determine whether we could reliably identity *in vitro* the same differences in NMJ morphology and function as those observed at the NMJ in transgenic mice lacking presynaptic NCAM *in vivo* (Chapter 3). In brief, we found this novel co-culture system to reliably reproduce several key *in vivo* phenotypes of *NCAM*$^{-/-}$ NMJs and further demonstrate novel insights into NCAM function at the synapse. We conclude that this co-culture system is a sensitive, effective and efficient assay of synaptic function and therefore is ideal for studying cellular mechanisms underlying MNDs.

Materials and Methods

Generation and differentiation of embryonic stem cells

Stem cells from two transgenic mouse lines were used in this study. HBG3 ES cells (a kind gift provided by Dr. T. Jessell, Columbia University, New York NY) were originally derived from the Hb9:GFP transgenic mice (Jackson Labs, Bar Harbour, Maine) and used as wild-type controls (referred throughout as Hb9:GFP *NCAM*$^{+/+}$). Hb9:GFP mice were bred with *NCAM*$^{-/-}$ mice (Cremer et al 1994) to generate Hb9:GFP *NCAM*$^{-/-}$ ES cells which were isolated from the inner cell mass of a mouse blastocysts using standard techniques. Briefly, pregnant females were sacrificed on the 3rd day of pregnancy when embryos are at the 8-16 cell stage. The uterine horn was extracted and placed in warmed M2 media (Sigma M7167). Blastocyts were flushed from the uterine horn and transferred to a 4 well plate containing a confluent monlayer of mitomycin C treated (Sigma) primary mouse embryonic fibroblasts (PMEFs). The inner cell mass (ICM) was allowed to expand for approximately 4 days then fed every two days with embryonic stem cell media (ESC media) containing DMEM (Gibco 11995-073), ESC grade fetal bovine serum (FBS; 15% by volume; Millipore ES-009-B), penicillin/streptomysin (1% by volume; Gibco 5140-122), 2-mercaptoethanol (1% by volume; Millipore ES-007-E), non-essential amino acids (1% by volume; Millipore TMS-001-C) and ESGRO LIF (leukaemia inhibitory factor; 1000u/ml; Millipore ESG1106). After another 4-6 days, the ICM was mechanically separated from the blastocyst using a tungsten needle and 2.5% trypsin. Cells were further dissociated into small clumps and transferred onto a 4 well plate containing a confluent monolayer of PMEFs and ESC media where they were allowed to expand into ES colonies and were passaged to avoid confluency.

Isolated ES cell colonies were differentiated into motoneurons as described previously (Wichterle et al 2002; Miles et al 2004; Soundararajan et al 2006). In brief, ES cells were grown as aggregated cultures in DFK-10 media to form free floating embryoid bodies. DFK10 medium consisted of DMEM (Gibco 11995-073) and Ham's F-12 media (Specialty Media) in a 1:1 ratio supplemented with knock-out serum replacement (10% by volume; Invitrogen, Burlington, Ontario, Canada), penicillin/streptomycin (1% by volume; Sigma, St. Louis, MO), N2 supplement (2.4% by volume; Invitrogen), glucose

(4500 mg/l), L-glutamine (200 mM), heparin (1 u/l; Sigma), and β-mercaptoethanol (0.1 mM; Sigma). After 2 days, the embryoid bodies were treated with a smoothened agonist and RA (1M; Sigma, St. Louis, MO) and cultured as free-floating cells for an additional 5 days. GFP expression was monitored as an assessment of differentiation and only embryoid bodies with robust and homogenous GFP expression were used for further assessment.

All procedures were conducted in accordance with the guidelines of the Canadian Council on Animal Care and the Dalhousie University Committee on Laboratory Animals.

Co-culture of embryonic stem cell derived motoneurons and embryonic chick myotubes

ESCMNs were either plated on matrigel coated coverslips for analysis of growth cones or on chick myotube cultures for analysis of NMJs. Myoblasts were harvested from the external adductor muscle of E12 White leghorn chick embryos and cultured as previously described (Rafuse and Landmesser, 1996). Briefly, external adductor muscles were dissected from stage 38 White leghorn chicks and mechanically dissociated in Ham's F-10 containing 10% horse serum (Invitrogen), 5% chicken embryo extract and 1.26 mM $CaCl_2$. 10^5 myotubes were plated on coverlips in 24-well cell culture plates and fed after 2 days in culture with Ham's F-10 media as described above. ESCMNs were plated on the chick myotubes three days after plating the myoblasts. In some cases, cells were treated after 2 days with cytosine β-D-arabinofuranoside (5μM; Sigma) to remove the fibroblasts from the culture. 1 hour prior to ESCMN plating, F-10 media was replaced with Neurobasal (Invitrogen) supplemented with 2 mM L-glutamine (Invitrogen) and penicillin/streptomycin (Invitrogen), GDNF (glial-derived neurotrophic factor) (20 ng/ml; Upstate Biotechnology, Lake Placid, NY) and CNTF (ciliary neurotrophic factor) (10ng/ml; Upstate Biotechnology). Co-cultures were fed every 2 days for up to a week with neurotrophic supplemented Neurobasal formulation. For co-cultures grown for longer periods, neurotrophic factors were omitted from the Neurobasal formulation.

Immunofluorescence and imaging

Cell cultures were fixed with 3.7% formaldehyde (Fisher Scientific, Houston, TX) for 15 minutes at room temperature after which they were washed with PBS containing 0.1M glycine (MP Biomedicals, Solon, OH) for 1 hour. ESCMNs were immunolabelled with combinations of antibodies as described in Table 1, diluted in PBS overnight at 4 degrees in the presence of 10% blocking serum and 0.3% Triton X-100 (Sigma). Secondary antibodies (Table 2) were applied for 1 hour at room termperature following extensive washing in the presence of 10% blocking serum and 0.3% Triton X-100. Tetramethylrhodamine conjugated α-bungarotoxin (α-BTX; 1:250, Invitrogen) was added in some cases along with secondary antibodies to label AChRs. Co-cultures were washed and mounted in 50% glycerol/PBS mixture containing 0.03 mg/mL ρ-phenylenediamine. For live anti-body labelling and selective permeabilization experiments, cells were incubated with a rodent specific anti-NCAM (CD56; Table 1) antibody for 2 hours in the presence of 2.5 μM TTX to block network activity. Co-cultures were then fixed with 3.7% formaldehyde and incubated with a saturating does of secondary antibody (1:100) diluated in PBS with 10% blocking serum to specfically label external NCAM. Cultures were then washed and treated with primary and secondary antibodies in the presence of Triton X-100 as described above to identify co-labeling with other proteins of interest.

For quantification of endplate morphology, co-cultures were digitally photographed using a wide-field fluorescence microscope equipped with a broad focal plane lens (Leica Microsystems, Bannockburn, IL, USA attached to a digital camera; C4742; Hamamatsu, Japan). Endplates were only used for quantification if the captured imaged accurately reflected the entire three-dimensional structure. Captured images were analyzed for pre and postsynaptic areas using IPLab software (Version 4.0; BD Biosciences) as previously described (Chipman et al 2010). All representative images are shown as collapsed z-stacks acquired using an LSM510 laser scanning confocal microscope (Zeiss Microimaging, Thornwood, NY, USA) and managed using Zen 2009 software (Zeiss Microimaging).

For live cell imaging, cells grown on coverslips were placed in a glass bottom 35mm culture dish filled with 50% Neurobasal/Hibernate low fluorescence solution

(Brain Bits, Springfield, IL) to buffer pH and placed in an incubation chamber heated to 37^{o}. Coverslips were inverterted in order to more clearly image neurite growth along the surface of myotubes. Images were acquired with Volocity software (Perkin Elmer, Waltham Mass) every 5 minutes through an inverted wide-field fluroscence microscope coupled to a digital camera. Cultures were visually monitored for cell viability and preparations would remain healthy for >3hrs under these conditions.

Western blot

Cell lysates were collected by sonication in the presence of extraction buffer as described previously (Rafuse and Landmesser, 1996). Briefly, co-cultures or ESCMN embryoid bodies were washed with HBSS and resuspended in extraction buffer containing; 50mM Hepes, 150mM NaCl, 1mM EDTA, 2mM PMSF, 100µg/ml leupeptin, 0.2 TIU/ml aprotinin and 1% NP-4 in the presence of a cocktail of protease inhibitors (Complete Mini, Roche Diagnostics, Mannheim Germany). Cells were sonicated for 10 seconds, placed on ice for 45 minutes and centrifuged for 1 hour at 100,000g. Pellets were discarded and supernatants were diluted in 5X SDS sample buffer containing 0.5M Tris (pH 6.8), 10% glycerol, 25% SDS, 10% 2-mercaptoethanol and 1% bromophenol blue diluted in distilled water. Samples were boiled for 10 minutes and separated on a 6% acrylamide gel, then transferred onto an Immobilon-P membrane and blocked for 1 hour at room temperature with 4% milk in TBS-T. Membranes were probed overnight with primary antibodies (Table 1) diluted in 1% milk TBS-T, washed the probed with secondary antibodies (table 2) for 1 hour at room temperature. Finally, membranes were developed on Kodak film (X-OMAT Blue Film XB, Kodak, Rochester, NY) using chemiluminescence (SuperSignal West Pico Chemiluminescent Substrate, Thermo Scientific, Rockford Il).

Intracellular electrophysiology of co-cultured NMJs

Sharp electrode intracellular electrophysiological techniques were used to assess synaptic function after 7 days in vitro as described previously (Miles et al 2004). Experiments were performed at room temperature in a recording chamber containing 1 ml of 50% Neurobasal/50% Hibernate low fluorescence solution (Brain Bits, Springfield, IL) to

buffer pH. Postsynaptic endplates were identified by the application of a non-blocking AChR antibody, mAb35 (Table 1) conjugated to an Alexa Fluor546 fluorchrome using a Monoclonal Antibody Labeling Kit (Invitrogen) for 1 hour prior to the recording session. NMJs were identified by the expression of GFP in apposition to mAb35 as indentified using a CCD camera coupled to an Olympus upright fluorescence microscope (Centre Valley, PA). Images were captured using a Nikon digital camera. Micropipettes which were used for recordings had tip resistances between 10 and 50MΩ were filled with 3M KCl. Reponses were recorded with a Sutter patchclamp amplifier in osciliscope mode and were acquired and processed with Clampex 10.2 software (Molecular Devices). All data were analyzed and representative traces were generated using MiniAnalysis (Synaptosoft, Decatur, GA). Events were classified as miniature endplate potentials (mEPPs) or evoked endplate potentials (EPPs) based on the Poisson distribution of event sizes when plotted as a frequency histrogram (Robbins and Yonezawa, 1971). Quantal contents were determined by the direct method (*m*= EPP/mEPP). In some cases, 5μM μ-conotoxin GIIIB (Alomone Labs, Jerusalem, Israel) was added to the recording solution to specifically block Na^+ channel-mediated myotube contraction. Cell viablilty was constantly visually monitored and preparations were found to remain healthy for recording periods lasting for at least 3-4 hours.

FM4-64FX loading and imaging

To assess synaptic vesicle cycling, co-cultures were incubated with 5 μM FM4-64FX and motor terminals were either loaded by spontaneous endocytosis in the presence of 2.5 μM tetrodotoxin (TTX) or electrically stimulated. For assessments of spontaneous endocytosis, cultures were preincubated for 30 minutes with drug or vehicle treatment in the presence of TTX, then FM4-64FX dye was added for a further 20 minutes (see Figure 4.9*A*). For stimulation induced dye-uptake, cultures were preincubated with drug or vehicle for 30 minutes after which 5 minutes of high frequency, repetitive stimulation was imposed on the cultures (see Figure 4.10*A, B*). Cultures were stimulated with 1 second trains of 50 Hz stimuli, delivered at a 0.5Hz train rate for 5 minutes. A maximum of 4 wells containing co-cultures were stimulated at a time with silver electrodes immersed into the culture media as illustrated in Figure 4.10*A*. Stimuli were generally

20V pulses with 0.5ms pulse widths and were verified to be effective by visual confirmation of myotube contraction. Flanking wells were filled with 3M KCl and used for the propagation of parallel stimulation along stimulating silver wires attached to a Grass technologies S88 stimulator. Cultures were then left to rest for 10 minutes following the stimulus train to allow for compensatory endocytosis (Gaffield and Betz, 2006), washed in 1:3 Neurobasal/HBSS solution to reduce extracellular calcium concentration (0.66mM) and with 2.5 μM TTX to inhibit further synaptic vesicle cycling then fixed with 3.7% formaldehyde. α-BTX was applied to one of the wash cycles to label postsynaptic AChRs. Z stacks of identified NMJs were captured with an LSM510 laser scanning confocal microscope (Zeiss Microimaging, Thornwood, NY, USA) and managed using Zen 2009 software (Zeiss Microimaging). GFP fluorescence was excited with a 488nm excitation laser and emission was captured with 500-530nm bandpass filter. α-BTX fluorescence was excited with a 543nm laser excitation and emission was captured with a 565-615nm bandpass filter. FM4-64FX fluorescence has a broad excitation and emission spectrum and great care was taken to ensure specific capture of FM4-64FX signal without bleedthrough from other channels. FM4-64FX was excited with a 488nm laser and emission was captured with a 685 longpass filter.

Drug treatments

For all experiments including the use of drug treatments, drug solvents (vehicles) were used as controls. Nifedipine (Sigma) was used to block L-type voltage dependent calcium channels (L-VDCCs) and was dissolved in 100% ethanol. 50μM nifedipine was used in acute experiments, while 5 μM was used for chronic experiments. ω-agatoxin IVA (Alomone Labs, Jerusalem, Israel) was used to block P/Q type VDCCs and was dissolved in distilled water and used at a final concentration of 100nM. Tetrodotoxin (TTX; Alomone Labs) was used to block Na^+ channels, was dissolved in distilled water and used at final concentrations between 2.5 and 5 μM. Tubocurarine chloride hydrate (curare; Sigma) was dissolved in distilled water and used at concentrations between 50 and 100μM to competitively block AChRs. Dynasore (Sigma) is a reversible inhibitor of dynamin 1 and 2 and blocks endocytosis at central (Newton et al 2009) and peripheral synapses (Maeno-Hikichi et al 2011). Dynasore was dissolved in DMSO and used at a

final concentration of 90μM. Brefeldin A (BFA; Sigma) was used to inhibit immature synaptic vesicle cycling (Zakharenko et al 1999; Polo-Parada et al 2001), was dissolved in 100% ethanol and used at a final concentration of 10μg/ml. SU5402 (Calbiochem, EMD Chemicals, San Diego CA) inihibits FGFR-mediated tyrosine phosphorylation of ERK 1 and 2, was dissolved in DMSO and used at a final concentration of 12.5 μM.

Statistical Analysis

One-way ANOVAs were performed to examine the differences between groups over time. Dunn's multiple comparisons post-hoc test was used to determine where the significant differences occurred if the F-value exceeded F-critical. Two tailed-Student's t-tests were then used to make comparisons between genotypes at a given time-point if normality was achieved. If normality was not achieved, Mann-Whitney tests were used to compare between two groups. Statistical significance was considered to be achieved if $P < 0.05$.

Table 4.1: Primary Antibodies

Antiserum	***Host Species***	***Dilution***	***Clonality***	***Source***
Agrin	Mouse	1:500 IF	Monoclonal	Chemicon , Temecula, CA
Bassoon	Mouse	1:400 IF	Monoclonal	Enzo Life Sciences, Plymouth Meeting, PA
Dihydropyridine Receptor (α2 subunit, L-type VDCC)	Mouse	1:500 IF	Monoclonal	Sigma, Saint Louis, Missouri
GFP	Rabbit	1:2000 IF	Polyclonal	Chemicon, Temecula, CA
mAb 35 (non-blocking AChR)	Mouse	*1:1000 IF *1:10000 WB	Monoclonal	DSHB, Iowa City, IA
NCAM (5e – chick specific)	Mouse	*1:1000 WB	Monoclonal	DSHB, Iowa City, IA
NCAM (CD56- rodent specific)	Mouse	1:2000 IF	Monoclonal	BD Biosciences, Franklin Lakes, NJ
NCAM (R050)	Rabbit	1:1000 IF	Polyclonal	Dr. U Rutishauser, Case Western University, Cleveland OH
SV2	Mouse	1:50 IF	Monoclonal	DSHB, Iowa City, IA
Synaptophysin	Rabbit	1:500 IF	Polyclonal	Zymed, San Fransisco, CA
VAChT	Goat	1:1000 IF	Polyclonal	Chemicon, Temecula, CA
VAMP7	Rabbit	1:500 IF	Polyclonal	Osenses, Keswick, Australia

* Hybridoma cell media concentrated by filtered centrifugation; IF- Immunofluorescence; WB - Western blot

Table 4.2: Secondary Antibodies

Secondary antibody	***Dilution***	***Conjugate***	***Source***
Goat anti-mouse IgG	1:500 IF	Alexa Fluor488	Invitrogen
Goat anti-mouse IgG	1:500 IF	Cy 3	Jackson Immunoresearch, Baltimore, PA
Goat anti-mouse IgG	1:500 IF	Alexa Fluor647	Invitrogen
Goat anti-rabbit IgG	1:500 IF	Alexa Fluor488	Invitrogen
Goat anti-rabbit IgG	1:500 IF	Cy 3	Jackson Immunoresearch, Baltimore, PA
Goat anti-rabbit IgG	1:500 IF	AlexaFluor647	Invitrogen
Donkey anti-goat IgG	1:500 IF	Cy 3	Jackson Immunoresearch, Baltimore, PA
Donkey anti-mouse IgG	1:500 IF	AlexaFluor647	Invitrogen
Goat anti-mouse IgG	1:5000 WB	HRP	Chemicon, Temecula, CA

IF – immunofluorescence; WB- Western blot

Results

NCAM is expressed by embryonic stem cell derived motoneurons and co-distributes with synaptic vesicles in growing neurites

Motoneurons are reliably derived from embryonic stem cells (ESCs) using a well-described differentiation protocol which includes the treatment of ESCs with the caudalizing morphogen retinoic acid (RA) and a smoothened agonist to ventralize the neuralized cells (Wichterle et al 2002). ESCs isolated from Hb9:GFP mice were used in this study to unambiguously identify motoneurons by their GFP expression (Wichterle et al 2002; Miles et al 2004; Yohn et al 2008; Soundararajan et al 2006, 2010). Previous studies have shown that Hb9:GFP ESCMNs exhibit functional, genetic and morphological characteristics comparable to motoneurons *in vivo* (Wichterle et al 2002; Miles et al 2004; Yohn et al 2008; Soundararajan et al 2006, 2010) and thus have been used to model MNDs *in vitro* (Di Giorgio et al 2007; Nagai et al 2007; Marchetto et al 2008). Because MNDs exhibit synaptic pathology that may contribute to the progression of the disease, we sought to develop a stable motoneuron/muscle fiber co-culture system to study the morphology and function of mature NMJs *in vitro*. We chose to use motoneurons derived from pluripotent cells, because ES cells can be readily isolated from transgenic models of MNDs. Furthermore, with the development of induced pluripotent stem (iPS) cell technology, motoneurons can now be derived from somatic cells harvested from patients with MNDs (reviewed by Chipman et al, 2012). This latter development will increase the versatility of an *in vitro* motoneuron/muscle fiber model system provided it accurately reflects many of the morphological and functional properties of NMJs *in vivo*.

To critically examine whether ESCMN/muscle fiber co-cultures recapitulate the properties of NMJs *in vivo* and to determine whether the model system is sensitive enough to discriminate between normal and pathological conditions, we compared NMJs formed by wild-type motoneurons with those lacking NCAM. We chose NCAM null motoneurons to test the threshold of discrimination because transgenic mice lacking presynaptic NCAM form compromised NMJs with clear deficits in morphology and synaptic transmission (Chapter 3).

Before examining NCAM null ESCMNs in a co-culture system we first needed to determine whether wild-type ESCMNs express NCAM (Soundararajan et al 2006). Protein homogenates were therefore collected from *Hb9:GFP NCAM*$^{+/+}$ and *Hb9:GFP NCAM*$^{-/-}$ ES cells 5 days following treatment with RA and a smoothened agonist (Figure 4.1*A*). Western blot analysis, using an antibody that recognizes all NCAM isoforms, showed a broad band extending from 250kD to 130kD when separated on a 6% gel (Figure 4.1*A*, EndoN - lane). Upon treatment with endoneuraminidase N (EndoN), which specifically cleaves polysialic acid (PSA) from NCAM, two distinct bands corresponding to 180 and 140kD NCAM isoforms were observed (Figure 4.1*A*, EndoN + lane). EndoN treated protein homogenates of ESCMNs that were allowed to extend neurites for 24 hours on matrigel coated coverslips continued to only express NCAM 180 and 140 kD (Figure 4.1*B*; 24 hrs). NCAM was not observed in homogenates collected from *Hb9:GFP NCAM*$^{-/-}$ ESCMNs 5 days after treatment with RA and a smoothened agonist or 24 hours after plating (Figure 4.1*B*).

NCAM is known to influence the delivery of synaptic resources from trans-Golgi network (TGN)-derived organelles to regions of putative synaptic contact (Sytnyk et al 2002; Chernyshova et al 2011), and has been identified at synaptic puncta in-over expression experiments *in vitro* (Hata et al 2007). To identify the localization of endogenous NCAM to motoneuron growth cones and neurites, *Hb9:GFP NCAM*$^{+/+}$ and *NCAM*$^{-/-}$ ESCMNs were plated for 24 hours on matrigel-coated glass coverslips, then fixed and stained for NCAM and two prominent vesicular proteins, synaptophysin (syp; Figure 4.1*C-D*) and the vesicle associated membrane protein 7 (VAMP7) (Figure 4.1*E,F*). Syp is a ubiquitous component of synaptic vesicles (Takamori et al 2006) and has been shown to influence activity-dependent synaptogenesis in dissociated hippocampal culture (Tarsa and Goda, 2002) while VAMP7 identifies a subset of functionally distinct synaptic vesicles with a low release probability (p_r) at CNS synapses (Verderio et al 1999; Hua et al 2011). VAMP7 has also been implicated in neurite outgrowth (Martinez-Arca et al 2000). Figure 4.1 shows that syp was distributed in discrete puncta, which were present midway through the GFP+ growth cone and scattered along the length of the neurite in *NCAM*$^{+/+}$ and *NCAM*$^{-/-}$ ESCMNs (Figure 4.1*C, D*). NCAM was co-distributed with syp puncta in *NCAM*$^{+/+}$ ESCMNs (see also Sytnyk et al

2002; Hata et al 2007) (Figure 4.1*C*, arrowheads). Unlike the punctate appearance of syp, VAMP7 exhibited a more uniform signal throughout the length of the neurite in both genotypes (Figure 4.1*E, F*). The expression of NCAM, while similar in general distribution, was not exclusively co-localized with VAMP7 in $NCAM^{+/+}$ neurites (Figure 4.1*E*), as regions of high VAMP7 expression often not associated with high NCAM expression (Figure 4.1*E*, arrow). Likewise, regions exhibiting strong NCAM immunoflourescence did not always correspond to regions with high VAMP7 immunolabeling (Figure 4.1*E*, black arrowhead).

A loss of NCAM results in the altered distribution of presynaptic proteins

To more closely examine the distribution of synaptic proteins and their relationship in growing neurites with or without NCAM, $NCAM^{+/+}$ and $NCAM^{-/-}$ growth cones and distal neurites were immunolabeled with a combination of synaptic vesicle associated and structural proteins, including syp, VAMP7, bassoon and agrin (see Appendix Figure A9 for representative images). Quantification of raw immunofluorescence signal intensities measured from the tip of the growth cone and along 50μm of distal neurite indicated reduced syp immunofluorescence in $NCAM^{-/-}$ distal neurites (Figure 4.1*G*; $P<0.001$ Mann Whitney rank sum test). This effect was specific for syp+ vesicles, as the distribution of VAMP7+ immunofluorescence was very similar between genotypes (Figure 4.1*H*; $P=0.799$ Mann Whitney rank sum test). In contrast, both bassoon and agrin immunofluorescence was increased in $NCAM^{-/-}$ neurites as compared to $NCAM^{+/+}$, with distribution profiles skewed towards the shaft of the neurite (Figure 4.1*I, J*; $P<0.001$ Mann Whitney rank sum test) . Such specific disruption to the distribution of a subset of presynaptic antigens suggests that NCAM may influence the sorting and distribution of synaptic vesicles and active zone transport packets (Ahmari et al 2000; Shapira et al 2003) in cultured motoneuron neurites.

NCAM is endocytosed in growing neurites and co-distributes with a subset of presynaptic proteins

Coupling between endo and exocytosis is tightly regulated during outgrowth and synaptogenesis, as growing neurites require more exocytosis than endocytosis for the net

addition of membrane, while stable synapses require a dynamic equilibrium between balanced endo and exocytosis to maintain presynaptic structural integrity (Haucke et al 2011). NCAM is known to participate in the regulation of exocytosis in growing neurites (Chernyshova et al 2011) and its role in endocytosis has also been well described (Miñana et al 2001; Polo-Parada et al 2001). Both immunoelectron microscopy and mass spectrometry have identified NCAM is a membrane component of a typical synaptic vesicle (Covault and Sanes, 1985; Takamori et al 2006) and may therefore contribute to synaptic vesicle recycling from this position. To investigate whether NCAM is involved in endocytic recycling of membrane on growing motor neurites, we sought to determine whether the molecule itself was present on recycled membrane. ESCMNs were grown on matrigel for 48 hours to allow for neurite extension then treated live for 1 hour with a mouse-specific anti-NCAM antibody. Different secondary antibodies were applied following fixation in the presence or absence of detergent to label NCAM on internal or external cell membranes respectively (Figure 4.2*A*; see methods). External NCAM (NCAM*ext*) labeling revealed a homogenous and diffuse signal along the length of the neurite and throughout the growth cone (Figure 4.2*A, a'*) which was in contrast to the internalized NCAM (NCAM*int*) signal which appeared as small puncta at both regions (Figure 4.2*A, a',* arrows). In some cases, NCAM*int* signal was found to co-localize with brighter NCAM*ext* signal at the growth cone (Figure 4.2*A*, arrowheads). In contrast, NCAM*int* puncta throughout the neurite was not associated with regions of strong NCAM*ext* signal (Figure 4.2*a'*, arrows) confirming the specificity of the selective labeling approach.

We then used this technique to identify whether other synaptic antigens were co-distributed with NCAM*int* puncta. To do so, we saturated all NCAM*ext* with an AlexaFluor 350 secondary antibody in the absence of detergent and subsequently labeled a number of other synaptic antigens with a Cy3 secondary antibody (Table 4.2) in the presence of detergent to permeabilize the cell (Figure 4.2*B-F*). For clarity, the Alexa350 (i.e. NCAM*ext*) signal is not shown. Interestingly, although many syp+ puncta were observed in the growth cone, they did not co-distribute with NCAM*int* puncta (Figure 4.2*B*, arrows). In contrast, however, some NCAM*int* puncta along the length of the neurite were positive for syp immunoreactivity (Figure 4.2*b'* arrowheads) and some were

not (Figure 4.2*b'* arrows). Likewise, some NCAM*int* puncta were immunopositive for bassoon, the vesicular ACh transporter (VAChT) and the L-VDCC in the growth cone and neurite (Figure 4.2*C, E-F* arrowheads) while others were not (Figure 4.2 *C, E-F*, arrows). In comparison, nearly all NCAM*int* puncta were negative for agrin in both the growth cone and along the axon (Figure 4.2*D*, arrows). Such a variable pattern of co-distribution with an assortment of vesicle and synapse-associated proteins may suggest that NCAM is first endocytosed in growing neurites where it can be further sorted into specific subclasses of synaptic vesicles (Voglmaier and Edwards, 2007; Uytterhoeven et al 2011).

NCAM contributes to neurite outgrowth along myotubes in co-culture

NCAM has long been implicated in the regulation of neurite outgrowth from a variety of cell types (Doherty et al 1990; Williams et al 1994a, b; Saffell et al 1997; Neithammer et al 2002; Chernyshova et al 2011), although an assessment of NCAM-dependent neurite outgrowth from motoneurons has been lacking. To assess ESCMN neurite outgrowth, motoneurons were plated on dissociated chick myoblasts which had been cultured for 3 days to allow myoblast fusion. At this time, NCAM is highly expressed on the surface of myotubes (Rafuse and Landmesser, 1996). Twenty-four hours after plating motoneurons, GFP^+ growth cones were identified and imaged over the span of one hour (Figure 4.3*A, B*). Some $NCAM^{+/+}$ growth cones were highly mobile and grew readily along the surface of the myotube (Figure 4.3*A*, white arrowhead), while others remained relatively stable and exhibited little growth over the imaging session (Figure 4.3*A*, black arrowhead). In comparison, although $NCAM^{-/-}$ growth cones were highly mobile and were found to extensively sample the extracellular environment, many lost contact with the muscle surface during the course of the imaging session and instead were found to contact and grow along the surface of the coverslip (Figure 4.3*B* white arrowheads).

To assess whether this disoriented growth influences overall neurite extension, neurite lengths were measured as they extended from the embyroid body, along the length of the neurite to the tip of the growth cone, 24 hours after motoneurons were plated on 3 day old myotube cultures (Figure 4.3*C*). $NCAM^{-/-}$ ESCMNs demonstrated reduced overall outgrowth at this time as compared to $NCAM^{+/+}$ (Figure 4.3*C*, $P<0.001$

one way ANOVA). We assessed whether postsynaptic NCAM influences presynaptic growth by saturating postsynaptic NCAM with a chick-specific functionally blocking antibody (see also Wantanabe et al 1986) for 1 hour before plating $NCAM^{+/+}$ ESCMNs. Remarkably, the extent of outgrowth exhibited by $NCAM^{+/+}$ motoneurons on myotubes treated with 5e was comparable to that exhibited by $NCAM^{-/-}$ neurites (Figure 4.3*C,* 5e $P<0.001$ one way ANOVA). These data demonstrate that chick NCAM can influence presynaptic outgrowth of cultured ESCMNs.

NCAM influences the targeting of synaptic vesicles to putative synaptic sites

Mature NMJs *in vivo* are characterized by the accumulation of synaptic vesicles and fusion machinery at defined sites of cell-to-cell contact. NCAM has been associated with the appropriate distribution of synaptic resources at the NMJ *in vivo* (Rafuse et al 2000; Chapter 3) and *in vitro* (Hata et al 2007). To verify whether the loss of presynaptic NCAM influences the distribution of synaptic vesicles, co-cultures of ESCMNs and dissociated chick myotubes were grown for 48 hours before being fixed and immunolabeled with antibodies against SV2 (Figure 4.4*A, B*), a synaptic vesicle-specific antigen widely expressed at the mouse NMJ (Bajjalieh et al 1992; Chakkalakal et al 2010). Synapses were counter-labeled with fluorescently conjugated α-bungarotoxin (α-BTX) to identify postsynaptic AChRs (Figure 4.4*a', b'*). Although both $NCAM^{+/+}$ and $NCAM^{-/-}$ motor neurites were associated with some postsynaptic receptor clustering (Figure 4.4*a', b'*), $NCAM^{-/-}$ ESCMNs maintained a high level of SV2 expression through the length of the distal axon as compared to $NCAM^{+/+}$ ESCMNs where SV2 expression was confined to regions of cell to cell contact (Figure 4.4*a'',b''*). These results are consistent with *in vivo* findings in the $NCAM^{-/-}$ mouse (Rafuse et al 2000; Polo-Parada et al 2001).

Loss of presynaptic NCAM impairs neurotransmission at developing NMJs in co-culture

To assess the functional consequences of a loss of NCAM from presynaptic motor terminals *in vitro,* $NCAM^{+/+}$ or $NCAM^{-/-}$ motoneurons were grown in co-culture with chick myotubes for seven days to allow the formation of NMJs (Miles et al 2004; Soundararajan et al 2007). At this time, NMJs were easily identifiable on the surface of

myotube by the co-localization of presynaptic GFP signal with postsynaptic AChRs-labeled using a non-blocking AlexaFluor594-conjugated antibody (mAb35) (Figure 4.5*A*). Consistent with previous reports of neurotransmission at NMJs grown *in vitro* (Robbins and Yonezawa, 1971; Miles et al 2004; Soundararajan et al 2007), $NCAM^{+/+}$ NMJs exhibited frequent activity which appeared to be both quantal and multi-quantal in nature (Figure 4.5*B*, top). Application of 2.5 μM tetrodoxin (TTX) significantly reduced the frequency and amplitude of synaptic potentials at $NCAM^{+/+}$ and $NCAM^{-/-}$ NMJs (Figure 4.5*B* middle, and *C-D*), revealing that the majority of activity in this preparation is driven by action potentials. This assessment also helped to determine the mean size of single quantal responses (miniature endplate potentials; mEPPs) which helped to guide the further analysis of neurotransmission (Figure 4.5*E, F*). Application of 50μM d-tubocurarine (dTC) completely blocked all synaptic potentials at $NCAM^{+/+}$ (Figure 4.5*B*, bottom) and $NCAM^{-/-}$ (not shown) NMJs, confirming that these events are driven by cholinergic neurotransmission. Interestingly, although $NCAM^{+/+}$ NMJs exhibited frequent multi-quantal release, $NCAM^{-/-}$ neurotransmission was significantly less frequency and appeared to be driven mostly by single quantal fusion events (Figure 4.5*C-H*). Mean quantal contents (*m,* determined by the mean mEPP/mean EPP) were significantly reduced at $NCAM^{-/-}$ NMJs (Figure 4.5*E*; $P<0.05$) and inter-event intervals were significantly longer (Figure 4.5*G, H*; $P<0.001$ Mann Whitney rank sum test), consistent observations of neurotransmission at newly formed motor terminals lacking NCAM during MU expansion *in vivo* (Chapter 3). While we did not have the capacity to directly stimulate motor terminals in this preparation, the effects of NCAM function on establishing network properties of cultured motoneurons cannot be ruled out as contributing factors to this transmission phenotype. Regardless, these data suggest that neurotransmission is reduced at NMJs formed by ESCMNs lacking NCAM in culture.

Morphological maturation of cultured NMJs

Neuromuscular junctions *in vivo* are characterized by the aggregation of postsynaptic signaling machinery, including AChRs and associated ion channels, which come to be closely opposed by presynaptic vesicles and active zones during synaptic maturation (Dahm and Landmesser, 1991; Sanes and Lichtman, 2001). The development of such

refined organization is, in part, influenced by neurotransmission early during the stabilization of NMJs (Verhage et al 2000; Heeroma et al 2003). To assess synaptic maturation in our co-culture model system, NMJ morphology was assessed at 7, 21 and 35 days after plating motoneurons on myotubes (Figure 4.6). *NCAM*$^{+/+}$ ESCMNs exhibited a time in co-culture-dependent refinement of the morphology of presynaptic arborization and innervation (Figure 4.6*A*-*C*). Although little noticeable change occurred between 7 and 21 days, the terminal arborization pattern of *NCAM*$^{+/+}$ ESCMNs became much more defined between 21 and 35 days when individual NMJs became noticeably large, cohesive and fully-innervated by presynaptic terminals (Figure 4.6*c'*). In comparison, although *NCAM*$^{-/-}$ ESCMNs exhibited similar arborization patterns at 7 and 21 days (Figure 4.6*D*-*E*) , the morphology of *NCAM*$^{-/-}$ ESCMNs arbors at 35 days exhibited less developmental maturity and individual NMJs remained small and poorly innervated (Figure 4.6*F*, *f'*). In addition, axons were found to be highly disorganized and did not seem to stop and form synapses at specific sites, consistent with observations made *in vivo* during regenerative synaptogenesis following partial denervation of presynaptic NCAM knockout mice (Chapter 3).

Further analysis of NMJs was performed in order to elucidate the nature of synaptic maturation and the role of presynaptic NCAM in the refinement of synaptic morphology (Figure 4.7). After 28 days in co-culture, synaptic vesicles were highly clustered and localized to sites specifically opposed to large AChR+ endplates at *NCAM*$^{+/+}$ NMJs (Figure 4.7*A*-*a'''*). In comparison, synaptic vesicle clustering occurred only at a minority of *NCAM*$^{-/-}$ NMJs (Figure 4.7*B*-*b'''*) and many vesicles remained localized to non-synaptic sites (Figure 4.7*b'''* arrowheads) which again is consistent with observations of *NCAM*$^{-/-}$ mice (Rafuse et al 2000; Polo-Parada et al 2001) and presynaptic conditional NCAM mutant mice during regenerative synaptogenesis *in vivo* (Chapter 3). Measurements of innervated *NCAM*$^{+/+}$ endplate areas at 28 days revealed significantly larger endplates than those measured 21 days (Figure 4.7*A,C*; $P<0.001$ Mann Whitney rank sum test). In comparison, *NCAM*$^{-/-}$ endplates did not grow over time (Figure 4.7*B, D*; $P=0.393$ Mann Whitney rank sum test). However, these endplates were larger than those formed in myotube cultures grown in the absence of motoneurons (Figure 4.7*C*-*E*), indicating a parallel, motoneuron-dependent, but NCAM-independent

mechanism of early clustering of postsynaptic AChRs. Smaller endplates are also observed at *NCAM*$^{-/-}$ (Rafuse et al 2000), further demonstrating conserved effects of NCAM deletion *in vivo* and *in vitro*. Finally, many *NCAM*$^{+/+}$ NMJs were found to transition from 'en passant' innervation at 21 days to a 'terminal' type of innervation morphology at 28 days (Figure 4.7*F*; $P<0.05$ Student's t-test), while *NCAM*$^{-/-}$ NMJs did not exhibit this transition (Figure 4.7*F*; $P=0.290$ Student's t-test). Together, these observations are consistent with those made at NCAM-deficient mice *in vivo* and strongly support the hypothesis that *NCAM*$^{-/-}$ NMJs formed in co-culture exhibit delayed synaptic maturation due to a loss of presynaptic mobilization of vesicular resources to synaptic sites.

Expression of NCAM at mature NMJs grown in co-culture

Next, we took advantage of the species-specific labeling approach of endocytosed NCAM to identify whether NCAM was internalized at these mature synapses. We found that endocytosed NCAM was localized nearly exclusively to synaptic regions on cultured motor axon arbors (Figure 4.8*A*), while NCAM*ext* was distributed homogenously along the axon (not shown). Interestingly, although the NCAM signal was exclusively presynaptic (Figure 4.8*a'* orthogonal), the localization of endocytosed NCAM seemed to align with the presence of perforations in the postsynaptic machinery (Figure 4.8*a'* arrowheads). In contrast, control *NCAM*$^{-/-}$ NMJs did not exhibit any NCAM immunolabeling and had smaller, less complex postsynaptic receptor structures (Figure 4.8*B, b'*; Figure 4.7*B, D*).

To assess whether all or only a subset of all recycling membrane at *NCAM*$^{+/+}$ NMJs contains NCAM, the total complement of recycling membrane was labeled with FM4-64FX under spontaneous loading conditions (in the presence of 2.5μM TTX) for 30 minutes. NCAM*int* was labeled alongside FM4-64FX to selectively label NCAM+ endocytosed membrane. As above, NCAM*ext* was saturated with AlexaFluor 350 and was not imaged. As expected, NCAM*int* co-localized well with the FM4-64FX signal at discrete puncta throughout the motor terminal (Figure 4.8*C*; arrowheads), although closer examination revealed that not all endocytosed membrane was positive for NCAM (Figure 4.8*c'*arrowhead). Synaptophysin and NCAM*int* (NCAM antibody was applied to

cultures for 2 hours in the presence of TTX) double immunolabeling revealed that only a subset of NCAM*int* puncta is associated with syp signal (Figure 4.8*E, e'*), while again, no labeling for NCAM was seen in *NCAM*$^{-/-}$ ESCMNs and syp immunofluorescence revealed a highly disordered synaptic vesicle distribution (Figure 4.8*F, f'*). Finally, western blots of 4 week co-cultures revealed the presence of only the 140kD isoform when probed with a rodent-specific antibody (i.e. CD56) (Figure 4.8*D*). Postsynaptic NCAM 130-155kD isoforms were identified in the same homogenates when a chick specific NCAM antibody (5e) was used to reveal muscle-specific NCAM (Figure 4.8*D*; Rafuse and Landmesser, 1996). Together, these findings demonstrate the utility of this chimeric co-culture system for the analysis of pre and postsynaptic protein expression and further demonstrate that NCAM is actively recycled at presynaptic motor terminals *in vitro*.

NCAM is required for spontaneous synaptic vesicle recycling

The observation that NCAM is present on spontaneously cycling synaptic membrane (Figure 4.8) and is required for appropriate neurotransmission (Figure 4.5) suggests that the loss of NCAM may influence spontaneous endocytosis at NMJs grown *in vitro*. To assess spontaneous endocytosis, 28 day old co-cultures were treated with FM4-64FX in the presence of TTX for 20 minutes, then washed and fixed for imaging and fluorescence analysis (Figure 4.9*A*). Postsynaptic endplates were identified with α-BTX and the mean FM4-64FX fluorescence was measured at synaptic (GFP^+, α-BTX+) and non-synaptic (GFP+, α-BTX-) sites. FM4-64FX signal was significantly higher at both synaptic and non-synaptic sites in *NCAM*$^{+/+}$ ESCMNs as compared to those measured in *NCAM*$^{-/-}$ cultures (Figure 4.9*B-E, P*<0.05 one way ANOVA). Interestingly, spontaneous cycling at synaptic *NCAM*$^{+/+}$ NMJs was reduced to *NCAM*$^{-/-}$ levels by blocking dynamin with dynasore (Newton et al 2009; Maeno-Hikichi et al 2011) (Figure 4.9*D*; 90 μM Dyn; *P*<0.001) and L-VDCC activity with nifedipine (Figure 4.9*D*; 50μM Nif; *P*<0.001). In contrast, blocking P/Q-VDCCs with ω-agatoxin IVA (100nM; Aga) had no effect on FM4-64FX fluorescence in comparison to vehicle (Figure 4.9*D*; *P*>0.05). These drugs did not have any effect on vesicle recycling at non-synaptic sites in either genotype (Figure 4.9*E* P>0.05 one way ANOVA). Overall, cycling at synaptic and non-synaptic

sites in *NCAM*$^{-/-}$ cultures was comparable (Figure 4.9*D-E*). These results indicate impaired spontaneous endocytosis in the absence of presynaptic NCAM as assessed at NMJs grown *in vitro*.

Disrupted synaptic vesicle recycling in the absence of presynaptic NCAM

NCAM$^{-/-}$ NMJs exhibit deficiencies in synaptic transmission during high frequency stimulation, which can be attributed to improper Ca^{2+}- induced activation of presynaptic kinases and immature synaptic vesicle recycling mechanisms (Polo-Parada et al 2005; Maeno-Hikichi et al 2011). To assess high frequency stimulation-driven FM4-64FX uptake at *NCAM*$^{-/-}$ NMJs grown *in vitro*, cultures were stimulated with 1 second trains of 50Hz stimuli every other second for 5 minutes and allowed for a 10 minutes rest period to fully complete activity-induced endocytosis (Gaffield and Betz, 2006; Maeno-Hikichi et al 2011) (Figure 4.10*A, B*). Cultures were stimulated 4 at a time and always involved two *NCAM*$^{+/+}$ and two *NCAM*$^{-/-}$ cultures to ensure appropriately controlled loading conditions (Figure 4.10*A*). *NCAM*$^{+/+}$ NMJs exhibited FM dye loading mostly at synaptic regions with minimal loading at non-synaptic puncta (Figure 4.10*C, E, F*). In comparison, while loading of FM dye at synaptic sites of *NCAM*$^{-/-}$ NMJs was comparable to *NCAM*$^{+/+}$ (Figure 4.10*E* Student's t-test), non-synaptic puncta exhibited significantly more FM4-64FX signal than wild-type (Figure 4.10*D, F*; $P<0.01$ Student's t-test).

Non-synaptic puncta in *NCAM*$^{-/-}$ muscles have been shown to exhibit distinct cycling characteristics *in vivo* (Polo-Parada et al 2001) and disruption to these cycling processes may limit the capability of *NCAM*$^{-/-}$ ESCMNs to form functionally and morphologically mature NMJs. A pharmacological dissection of activity-dependent synaptic vesicle cycling at co-cultured NMJs was therefore performed to investigate mechanisms permitting activity-induced vesicle cycling at synaptic and non-synaptic regions (Figure 4.11). Twenty-eight day old *NCAM*$^{+/+}$ and *NCAM*$^{-/-}$ co-cultures were incubated either in drug or vehicle for 30 minutes before FM4-64FX loading (Figure 4.11*A*). All measurements were normalized to vehicle treatment (EtOH or DMSO) which were stimulated alongside drug-treated cultures. Application of either TTX (2.5μM) or ω-agatoxin IVA (Aga; 100nM) reduced FM4-64FX loading at synaptic sites in both genotypes by~80% of vehicle values (Figure 4.11*D*, $P<0.001$), confirming that 50Hz

stimulation drives action potential-mediated activation of P/Q-VDCCs for Ca^{2+}- induced vesicle cycling at cultured *NCAM*$^{+/+}$ and *NCAM*$^{-/-}$ NMJs. Interestingly, while the application of nifedipine (Nif; 50 μM) to *NCAM*$^{+/+}$ co-cultures did not have any appreciable effect on the extent of synaptic vesicle recycling at *NCAM*$^{+/+}$ NMJs (Figure 4.11*D*,black $P>0.05$ one way ANOVA), it reduced cycling at *NCAM*$^{-/-}$ NMJs to near-spontaneous values (Figure 4.11*D*, grey; $P<0.001$ one way ANOVA). This finding was paralleled by a complementary effect of dynasore treatment (Dyn; 90μM) at *NCAM*$^{+/+}$ NMJs, which reduced cycling to approximately 35% vehicle values (Figure 4.11*D*, black $P<0.001$ Student's t-test), while it had a negligible effect on cycling at *NCAM*$^{-/-}$ NMJs (Figure 4.11*D*, grey $P>0.05$ Student's t-test). Application of brefeldin A (BFA; 10μg/μl), known to inhibit ADP-ribosylation factor (ARF)-dependant membrane trafficking from the Golgi apparatus (Donaldson et al 1992) and immature, axonally-derived synaptic transmission in *NCAM*$^{-/-}$ motoneurons (Zakharenko et al 1999; Polo-Parada et al 2001; Hata et al 2007) reduced vesicle cycling at synaptic regions of both genotypes to approximately 60% vehicle values, although these values did not differ significantly from vehicle (Figure 4.11*D*, $P>0.05$ one way ANOVA). These data strongly suggest the presence of altered calcium-dependent synaptic vesicle cycling mechanisms at *NCAM*$^{-/-}$ NMJs.

Activity-dependent recycling at non-synaptic *NCAM*$^{+/+}$ puncta reveal a similar pattern of sensitivity to blocking agents (Figure 4.11*E*). Cycling in *NCAM*$^{+/+}$ ESCMNs was inhibited by TTX, agatoxin and dynasore application (Figure 4.11*E*, $P<0.001$ one way ANOVA) but was insensitive to nifedipine and BFA (Figure 4.11*E*, $P>0.05$ one way ANOVA). In comparison, non-synaptic *NCAM*$^{-/-}$ puncta were potently inhibited by TTX, agatoxin, nifedipine and BFA (Figure 4.11*E*, $P<0.001$ one way ANOVA), but were insensitive to dynasore treatment (Figure 4.11*E*, $P>0.05$ one way ANOVA). These data are consistent with those of NCAM-deficient NMJs examined *in vivo* (Polo-Parada et al 2001; Chapter 3) and reflect the profound differences in synaptic vesicle cycling machinery that exist at *NCAM*$^{-/-}$ NMJs.

Discussion

Modeling diseased NMJs in vitro

Here we have demonstrated that ESCMNs can be grown for extended periods in co-culture with chick myotubes and used as a viable model of functional NMJ organization. NMJs grown in co-culture closely resemble their *in vivo* counterparts and exhibit neurotransmission and synaptic vesicle cycling properties consistent with those of mature vertebrate NMJs. The present study therefore offers a tool to directly investigate synapse formation from the first moments of cell-to-cell contact to full functional synaptic maturation in an easily accessible and highly manipulable system. We have validated the sensitivity of this system by identifying a variety of synaptic phenotypes associated with a presynaptic loss of NCAM (summarized in Table 4.3). We used *NCAM*$^{-/-}$ ESCMNs because NMJs are formed in *NCAM*$^{-/-}$ mice, but exhibit very specific deficits in morphology and neurotransmission which have been well characterized in the neonate, (Rafuse et al 2000), adult (Polo-Parada et al 2001, 2004, 2005) and following regeneration (Chipman et al 2010; Chapter 3). Interestingly, we observed phenotypes at cultured *NCAM*$^{-/-}$ NMJs which align more closely with those observed at presynaptic conditional NCAM knockout mice during periods of regenerative structural plasticity than those observed during development (Chapter 3). Such a difference likely suggests the presence of compensatory mechanisms derived from complex cell-to-cell interactions during development in mutant mice lacking NCAM which may mask the emergence of more severe phenotypes later in life (Gu et al, 2003). Regenerative mechanisms lack these compensatory mechanisms because only a fraction of the genes expressed during development are re-expressed during regeneration (Bosse et al, 2006). Likewise, ESCMNs grown in co-culture would be expected to largely lack such compensatory mechanisms because they are removed from the complexity of the developing organism. It can be expected therefore, that phenotypes which emerge in a co-culture environment represent a more severe phenotype than would emerge in the animal and would more closely align with conditions associated with regenerative conditions. Notably, *NCAM*$^{-/-}$ motoneurons were found to exhibit significantly disrupted Ca^{2+}-mediated synaptic vesicle recycling, impaired localization of presynaptic vesicles to synaptic sites, and highly

disorganized terminal arborizations. Interestingly, some of these phenotypes are also characteristic of NMJs in mouse models of MND (Pun et al 2006; Jablonka et al 2007; Kariya et al 2008; Kong et al 2009; Ruiz et al 2010), highlighting the similarities between diseased and NCAM-deficient motoneurons. In short, these findings suggest that the co-culture system described in this study can be used as an accurate predictor of the regenerative potential of differentiated motoneurons and their susceptibility to MND.

Presynaptic organization in vitro

A principle advantage of this co-culture system is the ability to investigate organizational processes from the moment of neurite outgrowth to full synaptic maturity. This wide range of temporal accessibility is useful to screen for deficits in ESCMNs harbouring known genetic mutations, or in motoneurons differentiated from induced pluripotent cells (iPS) isolated from patients with sporadic or inherited MNDs (Thomson et al 2011; Chipman et al 2012). We first assessed the distribution of synaptic proteins in growth cones and distal neurites of wild-type and *NCAM*$^{-/-}$ GFP+ ESCMNs before and after myotube contact. Several novel functional influences of NCAM along with evidence of several mechanisms which were disrupted by its loss emerged through this analysis. First, we identified that NCAM is internalized and recycled in growing wild-type neurites and co-distributes with a subset of puncta labeled by antibodies against a number of other synaptic-associated proteins, including synaptophysin, bassoon, VAChT and the L-VDCC. In comparison, very little co-labeling was observed with the well-described synaptogenic proteoglycan, agrin (Reist et al 1992). This variable co-distribution pattern suggests a selective packaging of NCAM into a subset of synaptic vesicles which may have a predefined functional role (Hua et al 2011). Second, we observed several deficits in the organization of presynaptic antigens in NCAM-deficient neurites, including reduced immunolabeling for the synaptic vesicle protein synaptophysin, and increased immunolabeling for agrin and bassoon. The altered distribution of some synaptic components may be due to an abnormal accumulation of TGN-derived vesicle packets in the growth cone, which is known to occur in *NCAM*$^{-/-}$ neurons in culture (Chernyshova et al 2011). In contrast, no effect was observed when VAMP7 immunofluorescence was

assessed, consistent with a specific role for NCAM in the organization of a subset of presynaptic proteins.

The above data strongly suggest that NCAM is localized to a subpopulation of recycled synaptic membrane and may regulate its sorting and distribution. Consistent with this hypothesis was the observation that NCAM was found to be present only on a subset of endocytosed membrane at mature motor terminals. Another study has identified NCAM in the participation of clathrin-mediated endocytosis in cultured astrocytes (Miñana et al 2001), and a similar mechanism may exist in motoneurons. Interestingly, clathrin-mediated endocytosis selectively replenishes the readily releasable pool (RRP) of synaptic vesicles in cerebellar neurons (Cheung et al 2010) and the absence of NCAM leads to potentiated release of RRP vesicles (Polo-Parada et al 2001; Chapter 3), and the disorganization of L-VDCC and AP3-mediated endocytic mechanisms (Polo-Parada et al 2001, 2004). These latter mechanisms replenish the reserve/reluctantly releasable pool (Cheung et al 2010; Maeno-Hikichi et al 2011) which may also be defective and/or abnormally distributed in *NCAM*$^{-/-}$ mice (Polo-Parada et al 2001, 2005). Together these findings are consistent with the hypothesis that NCAM functions via endocytosis to establish a balance between discrete populations of synaptic vesicles in presynaptic terminals.

The aggregation of presynaptic vesicles occurs *in vivo* soon after the developmental innervation of skeletal muscle through a number of postsynaptically-derived organizational cues (Nguyen et al 2000; Fox et al 2007; Hata et al 2007; Williams et al 2009; Chen J. et al 2011). The present study further confirms a role for presynaptic NCAM in synaptic vesicle mobilization to synaptic sites (Rafuse et al 2000), as *NCAM*$^{-/-}$ motoneurons demonstrated significant deficits in vesicle localization to terminal NMJs and NCAM*int* puncta were localized to synaptic sites at mature *NCAM*$^{+/+}$ NMJs grown *in vitro*. Likewise, we observed a transition from 'en passant' to a 'terminal' form of innervation observed in *NCAM*$^{+/+}$ co-cultures, but not in *NCAM*$^{-/-}$ co-cultures at later stages of synaptic maturation. Together these observations suggests the possibility that consolidation and strengthening of mature, terminal synapses occurs at the expense of immature synapses which shuttle their synaptic resources to stronger, more established synapses in response to retrograde signals from well-activated muscle fibers. Indeed,

presynaptic conditional NCAM mutants exhibit disruptions to synaptic vesicle shuttling during regenerative sprouting following partial muscle denervation (Chapter 3).

Co-cultured wild-type ESCMNs were found to exhibit frequent multi-quantal neurotransmission, consistent with other studies at NMJs grown *in vitro* suggesting the formation of functional neuromuscular connections (Robbins and Yonezawa, 1971; Miles et al 2004; Soundararajan et al 2007). Quantal content and the size of vesicle clusters at individual terminals were reduced at NMJs in the absence of NCAM, consistent with observations at presynaptic conditional NCAM mutants during structural regenerative plasticity (see Chapter 3) and suggesting NCAM is required for functional maturation of the NMJ. FM dye labeling experiments demonstrated that endocytosis at mature wild-type NMJs *in vitro* is dependent on the function of dynamin, a GTPase responsible for vesicle fission during endocytosis and activated in response to presynaptic calcium influx (Koenig and Ikeda, 1989; Smillie and Cousin, 2005). In contrast, we found that presynaptic $NCAM^{-/-}$ terminals *in vitro* recycled synaptic membrane independently of dynamin, and possessed altered Ca^{2+}-dependent vesicle cycling mechanisms which were abnormally sensitive to L-VDCC activity (Polo-Parada et al 2001). Likewise, spontaneous endocytosis was significantly impaired at $NCAM^{-/-}$ NMJs in comparison to $NCAM^{+/+}$. Interestingly, treatment of $NCAM^{+/+}$ co-cultures with dynasore and nifedipine reduced recycling to $NCAM^{-/-}$ levels, further suggesting that dynamin and L-VDCC function are disrupted at motor terminals lacking NCAM. Indeed, NCAM can bind to L-VDCCs (Bodrikov et al 2008) and may regulate its activity and/or distribution to regulate the maturation of Ca^{2+}-mediated vesicle recycling mechanisms (Hata et al 2007; Yamashita et al 2010). Overall, these findings confirm previous observations regarding the role of NCAM at NMJs and provide additional insight into the regulatory mechanisms of synaptic vesicle recycling enabled by presynaptic NCAM.

Postsynaptic complexity in vitro

A primary process indicative of synaptic stability is the clustering and elaboration of AChR rich postsynaptic endplates on the surface of muscle (Sanes and Lichtman, 2001). This process includes the appearance of perforation in the postsynaptic complex (Proszynski et al 2009) and the coordinated refinement of pre and postsynaptic apposition

(Sanes and Lichtman, 2001). Postsynaptic maturation can occur in the absence of presynaptic innervation and neurotransmission *in vivo* and *in vitro* (Verhage et al 2000; Lin et al 2001; Yang et al 2001; Kummer et al 2004; Proszynski et al 2009), although presynaptic activity is critical for the maintenance and refinement of pre and postsynaptic structures (Avila et al 1989; Missias et al 1996; Sanes and Lichtman, 2001; Heeroma et al 2003; Lin et al 2005; Misgeld et al 2005). We found that *NCAM*$^{-/-}$ endplates formed in co-culture were morphologically immature and lacked structural complexity as compared to wild-type NMJs. In addition, presynaptic terminals were disorganized and not closely localized to postsynaptic endplates. Interestingly, NCAM endocytosis was found to occur in *NCAM*$^{+/+}$ motor terminals at sites which closely overlaid postsynaptic perforations in the endplate structure. These perforations form in immature endplate plaques grown in aneural myotube cultures on laminin substrates and are influenced by structures specifically implicated in postsynaptic endocytosis (Kummer et al 2004; Proszynski et al 2009). These observations therefore suggest that regions of pre and postsynaptic endocytosis may be spatially coordinated (Gaffield et al 2009 a, b). In addition, the appearance of perforations in the absence of motoneurons (Proszynski et al 2009) suggests a potential retrograde regulation from the muscle fiber in organizing this spatial orientation.

NCAM isoforms at NMJs in vitro

We identified the presence of both NCAM140kD and 180kD in ESCMNs grown for 24 hours, and only the 140kD in mature motor terminals *in vitro*, suggesting that both isoforms may regulate early motoneuron/myotube interactions while the 140kD may be specifically implicated in synaptic stability and neurotransmission. Indeed, the phenotypes exhibited by *NCAM*$^{-/-}$ NMJs *in vitro* closely mimic several of those observed in *NCAM*$^{-/-}$NMJs, but not in 180kD-specific NCAM knockout NMJs (Polo-Parada et al 2004); implicating the loss of either NCAM 140kD or 120kD isoforms in the *in vitro* phenotypes observed here. Specifically, the loss of NCAM 140kD and the 120kD isoform results in the misdistribution of presynaptic puncta and altered synaptic vesicle recycling mechanisms (Polo-Parada et al 2001; 2004). In contrast, the loss of NCAM 180kD specifically results in periodic failures in presynaptic output (Polo-Parada et al 2005).

Slow motor terminals of conditional presynaptic NCAM mutants do not produce such failures in synaptic transmission, although they do demonstrate other phenotypes known to be generated by the loss of NCAM120kD or 140kD isoforms (Polo-Parada et al 2004) (Chapter 3). These data suggest the possibility that different NCAM isoforms may differentially participate at fast and slow NMJs. Indeed, in this study we cultured ESCMNs primarily on slow twitch myotubes (adductors) and derived motoneurons from embryonic stem cells using a procedure that preferentially generates motoneurons which project to slow twitch epaxial muscles when transplanted into the chick spinal cord *in ovo* (Soundararajan et al 2006, 2010). These ESCMNs also possess passive electrical properties consistent with those exhibited by slow motoneurons *in vivo* (Soundararajan et al 2006). It is therefore possible that we specifically generated NMJs with a 'slow' phenotype in this co-culture system (Reid et al 1999; Rowley et al 2007; Chakkalakal et al 2010). This point is not trivial, as MNDs often lead to the selective degeneration of fast twitch motor units (MUs), while slow twitch MUs are relatively resistent to disease progression and possess more robust regenerative potential (Frey et al 2000; Pun et al 2006). Therefore, screening studies which aim to accurately model disease progression *in vitro* should carefully determine the primary MU subtype which is being generated.

Patient-specific screening approaches for neurodegenerative diseases

Recent studies have demonstrated abnormal Ca^{2+} regulation at growth cones and motor terminals in a mouse model of SMA (Jablonka et al 2007; Ruiz et al 2010). These observations may, at least in part, explain the developmental immaturity of these synapses (Kariya et al 2008; Kong et al 2009). Likewise, investigations examining the pathophysiology of ALS consistently demonstrate altered Ca^{2+} signaling in motoneurons (Gonzalez et al 2011; Quinlan et al 2011; Mórotz et al 2012). Thus, disruptions to presynaptic Ca^{2+} homeostasis may be a fundamental principle of synaptic pathology associated with MND. It is clear that NCAM mutant mice demonstrate altered Ca^{2+} sensitivity (Polo-Parada et al 2001, 2005). Although NCAM can be used as a central and peripheral marker for MND progression (Warita et al 2001; Gordon et al 2009), mutation of NCAM genes has not been directly associated with the development of MND. However, NCAM dysfunction is a known hallmark of other complex neurological

diseases including schizophrenia and bipolar disorder (Barbeau et al 1995; Vawter et al 2000; Bisaz and Sandi, 2012; Varea et al 2012). Recent *in vitro* assessments of differentiated neurons from induced pluripotent stem (iPS) cells isolated from schizophrenic patients and grown in culture support a central role of NCAM in synaptic dysfunction in schizophrenia (Brennand et al 2011) and suggest that NCAM is required for maintaining normal synaptic function in the adult CNS. It is therefore possible that alterations to NCAM may be involved in the pathophysiology of MND progression without being directly implicated in its onset.

This study and others (Kiris et al 2009; Ebert and Svendson, 2010; Hempel et al 2011) have laid the groundwork for the development of more efficient high throughput screening of patient-specific synaptic function of iPS cell-derived, and induced motoneurons (iMNs) (Dimos et al 2008; Ebert et al 2009; Son et al 2011). Traditional models of cultured NMJs were originally developed to investigate early synaptic function at nerve muscle contacts which had been previously inaccessible to experimental manipulation in mammals (Crain et al 1970; Fishbach, 1970; Robbins and Yonezawa 1971). Recent developments in patient-based iPS cell and induced motoneuron (iMN) technologies now require the application of these established culture techniques for the study of diseased motoneurons in order to screen for synaptic dysfunction in sporadic and inherited cases of MND (Thomson et al 2012). The present study contributes a consistent and reproducible model system for the assessment of presynaptic function at the NMJ *in vitro* which can now be applied to the study of patient-specific motoneurons with the aim to identifying their susceptibility to MND and responsiveness to therapeutic intervention.

Table 4.3: Summary of *in vivo* and *in vitro* phenotypes of presynaptic NCAM mutant NMJs as compared to wild-type

	In vivo – $Hb9^{cre}NCAM^{flx}$		*In vitro - (NCAM-/- ESCMNs)*
	Mature	**Regenerated**	
Postsynaptic endplate size	Slightly larger	Larger	Smaller
Presynaptic terminal size	Smaller	Smaller	Smaller
Non-synaptic vesicles	Few	Many	Many
Quantal content	Larger	Smaller	Smaller
mEPP frequency	Enhanced	Reduced	Reduced
mEPP amplitude	Slightly larger	Larger (transient)	Normal
SV recycling mechanisms – synaptic	N/A	Immature - L-VDCC independent	Immature – L-VDCC dependent
SV recycling mechanisms – non-synaptic	N/A	Immature – L-VDCC dependent	Immature – L-VDCC /BFA dependent
Axon arborizations	Normal	Disorganized	Disorganized

N/A = not assessed

CHAPTER 4 FIGURES

Figure 4.1: NCAM180 and 140 is highly expressed by embryonic stem cell derived motoneurons (ESCMNs) and influences the distribution of presynaptic-associated proteins in distal neurites. **(A)** Western blot of ESCMNs 5 days after retinoic acid (RA) and smoothened agonist treatment. Endoneuraminidase-N (EndoN) treatment cleaves polysialic acid from NCAM and revealed the expression of the 180kD and 140kD isoforms indicating the expression of PSA-NCAM by ESCMNs. **(B)** ESCMNs were homogenized 5 days after RA and Shh or 24 hours after being grown on matrigel coated coverslips and treated with EndoN. The 140kD and 180kD NCAM isoforms are expressed by growing *NCAM*$^{+/+}$ ESCMNs in culture. *NCAM*$^{-/-}$ motoneurons do not express NCAM. **(C)** Co-immunolabeling for NCAM (red) and synaptophysin (syp; white or blue in merge) in *Hb9:GFP NCAM*$^{+/+}$growth cones and neurites grown in culture for 24 hours. Arrows indicate regions of NCAM and syp co-distribution. **(D)** Hb9:GFP *NCAM*$^{-/-}$ ESCMNs exhibit syp immunoreactivity in the growth cone and along the axon of growing neurites, but completely lack NCAM expression. **(E-F)** VAMP7 and NCAM co-immunolabeling of growing *NCAM*$^{+/+}$ and *NCAM*$^{-/-}$ ESCMN neurites. All scale bars 10μm. **(G)** Mean ±SEM of synaptophysin fluorescence intensity measured from the tip of the growth cone to a total length of 50 μm along the length of the neurite. *NCAM*$^{+/+}$ (black) and *NCAM*$^{-/-}$ (grey) neurites were measured and fluorescence signals are shown as cumulative frequency plots on the right. **(H)** Mean ±SEM of VAMP7, **(I)** bassoon and **(J)** agrin immunofluorescence in ESCMN neurites quantified as described for *G*. Statistical significance was assessed with Mann Whitney rank sum test. *NCAM*$^{+/+}$ syp n=8; SV2 n=7; VAMP7 n=9; bassoon n=5; agrin n=8 neurites from at least 2 separate cultures. *NCAM*$^{-/-}$ syp n=6; SV2 n=7; VAMP7 n=9; bassoon n=4; agrin n=5 neurites from at least 2 separate cultures.

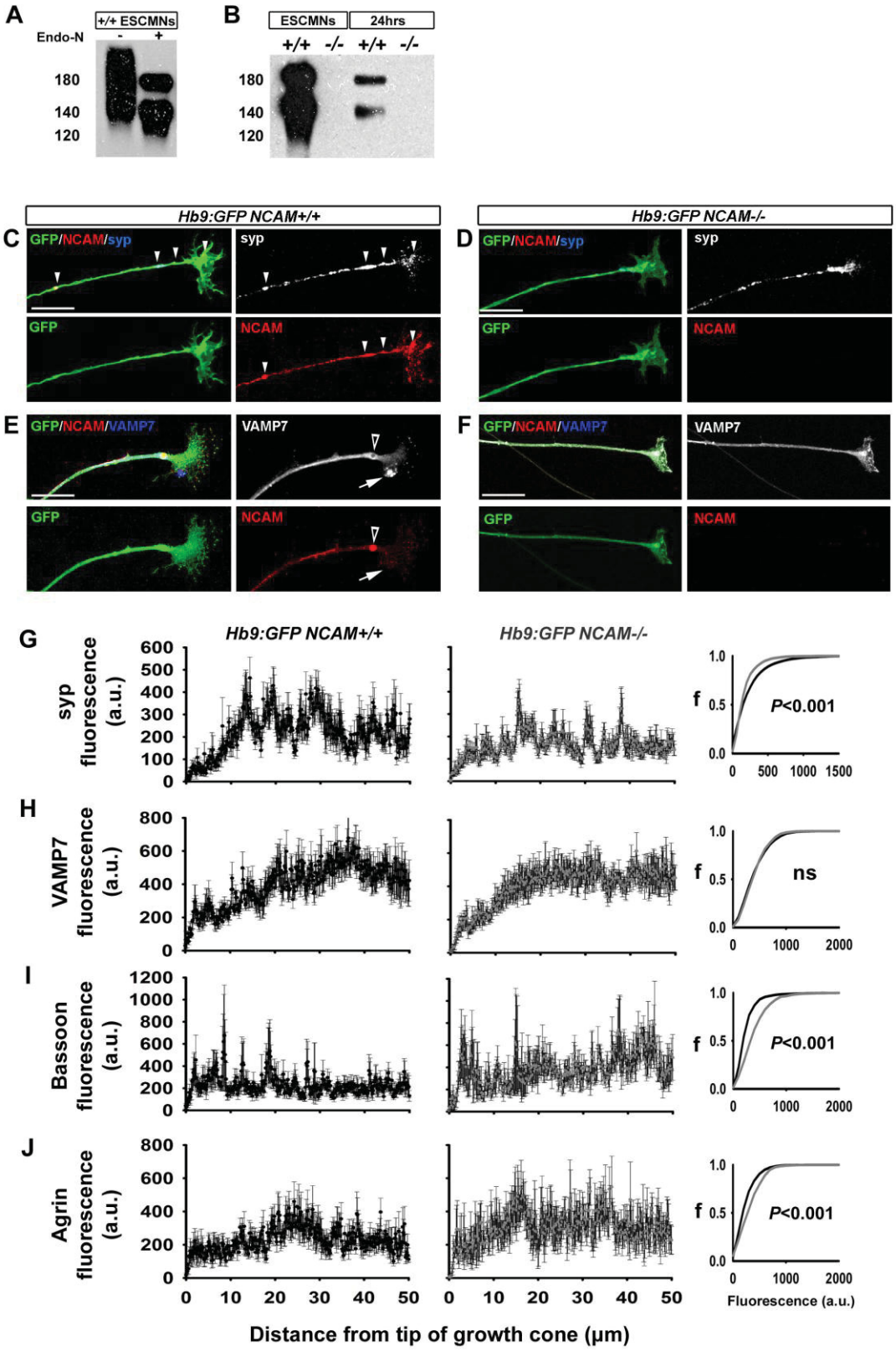
A
+/+ ESCMNs
Endo-N
-
+
180
140
120
B
ESCMNs
24hrs
+/+
-/-
+/+
-/-
180
140
120
Hb9:GFP NCAM+/+
Hb9:GFP NCAM-/-
C
D
GFP/NCAM/syp
syp
GFP
NCAM
E
F
GFP/NCAM/VAMP7
VAMP7
GFP
NCAM
G
H
I
J
Hb9:GFP NCAM+/+
Hb9:GFP NCAM-/-
syp fluorescence (a.u.)
VAMP7 fluorescence (a.u.)
Bassoon fluorescence (a.u.)
Agrin fluorescence (a.u.)
f
P<0.001
ns
P<0.001
P<0.001
Fluorescence (a.u.)
Distance from tip of growth cone (µm)

Figure 4.2: Co-distribution of endocytosed NCAM with presynaptic proteins in growing ESCMN neurites. **(A)** Growth cone and (*a'*) neurite of an *Hb9:GFP NCAM*$^{+/+}$ ESCMN, immunolabeled for NCAM*int* (white or blue in merge) and NCAM*ext* (red). Puncta corresponding to internalized NCAM (arrows) can clearly be distinguished from the extracellular signal. Some internalized puncta in the growth cone was found to correspond to strong NCAM*ext* signal (arrowheads). **(B)** Co-immunolabeling for NCAM*int* and synaptophysin (syp) in an ESCMN growth cone and (*b'*) neurite. NCAM*ext* was saturated with Alexa350 and not imaged –same for *B-F*. Some NCAM*int* puncta were positive for syp (arrowheads), and some were not (arrows). **(C)** Co-immunolabeling for NCAM*int* and bassoon (red) in an ESCMN growth cone and (*c'*) neurite. NCAM*int* puncta were observed which did (arrowheads) and did not (arrows) co-distribute with bassoon. **(D)** Co-immunolabeling for NCAMint and agrin in an ESCMN growth cone and (*d'*) neurite. The majority of NCAMint puncta did not co-distribute with agrin puncta (arrowheads). **(E)** Co-immunolabeling for NCAMint and VAChT in an ESCMN growth cone and (*e'*) neurite. NCAM*int* puncta were found which did (arrowheads) and did not (arrows) co-localize with VAChT. **(F)** Co-immunolabeling for NCAM*int* and the L-VDCC in an ESCMN growth cone and (*f'*) a neurite. The majority of NCAMint puncta were found to co-distribute with the L-VDCC (arrowheads). All scale bars 10 μm.

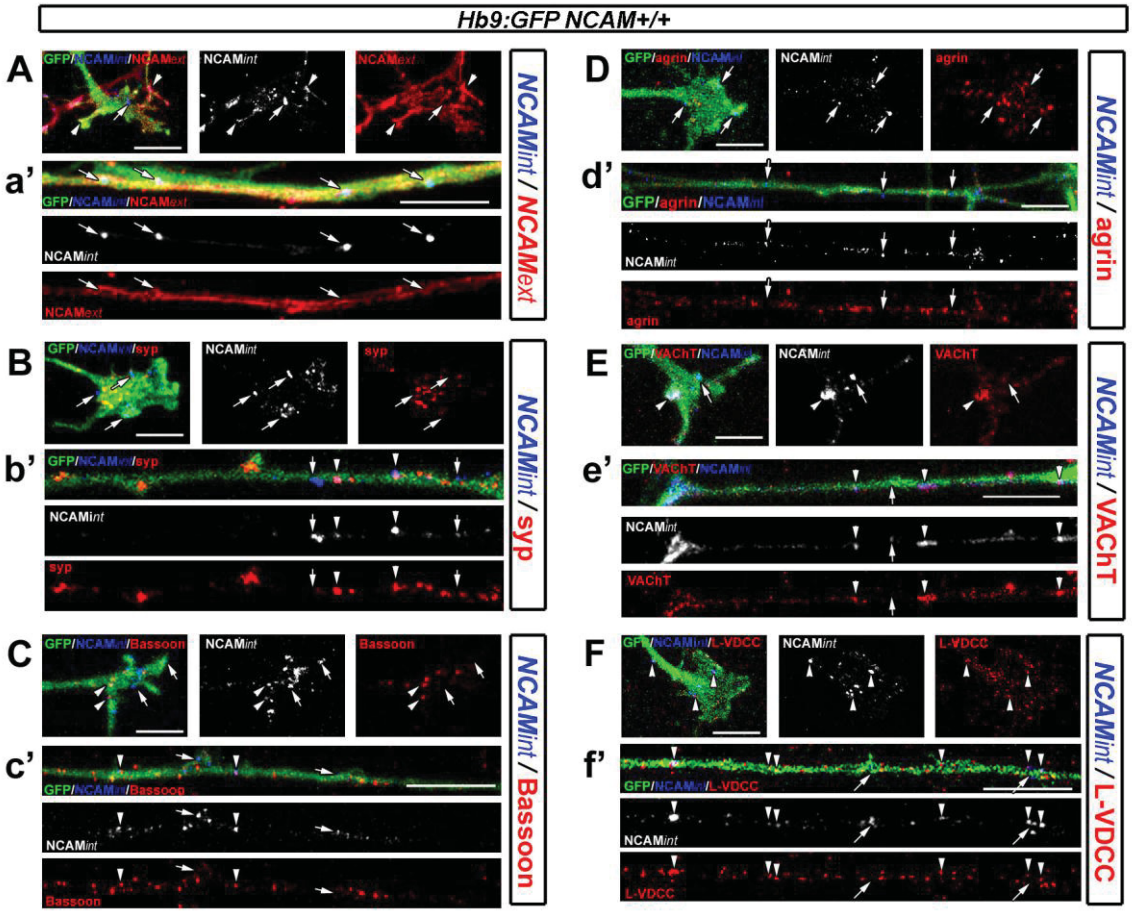
Hb9:GFP NCAM+/+
A
GFP/NCAMint/NCAMext
NCAMint
NCAMext
a'
GFP/NCAMint/NCAMext
NCAMint
NCAMext
NCAMint / NCAMext
B
GFP/NCAMint/syp
NCAMint
syp
b'
GFP/NCAMint/syp
NCAMint
syp
NCAMint / syp
C
GFP/NCAMint/Bassoon
NCAMint
Bassoon
c'
GFP/NCAMint/Bassoon
NCAMint
Bassoon
NCAMint / Bassoon
D
GFP/agrin/NCAMint
NCAMint
agrin
d'
GFP/agrin/NCAMint
NCAMint
agrin
NCAMint / agrin
E
GFP/VAChT/NCAMint
NCAMint
VAChT
e'
GFP/VAChT/NCAMint
NCAMint
VAChT
NCAMint / VAChT
F
GFP/NCAMint/L-VDCC
NCAMint
L-VDCC
f'
GFP/NCAMint/L-VDCC
NCAMint
L-VDCC
NCAMint / L-VDCC

Figure 4.3: NCAM has a functional effect on neurite outgrowth. **(A)** 1 hour time lapse images of *Hb9:GFP NCAM*$^{+/+}$ extending neurites along co-cultured myotubes. Some *NCAM*$^{+/+}$ neurites were observed to exhibit more active growth (white arrows) than others (black arrows) but all growth cones maintained contact with the muscle surface throughout the imaging session. **(B)** *NCAM*$^{-/-}$ growth cones were found to be active, but often lost contact with the myotube to grow along the surface of the coverslip (white arrowheads). Scale bars 10 μm. **(C)** Mean ±SEM neurite lengths measured as they extend away from the embryoid body 24 hours after plating on 3 day cultured chick hindlimb myotubes. Some *NCAM*$^{+/+}$ cultures were pretreated with a functionally blocking chick-specific NCAM antibody (5e; 1:100) for 1 hour prior to motoneuron plating to block postsynaptic NCAM function. The number of neurites measured is shown in the bars. **P<0.001 ANOVA on ranks and Dunn's Pairwise Multiple Comparisons test.

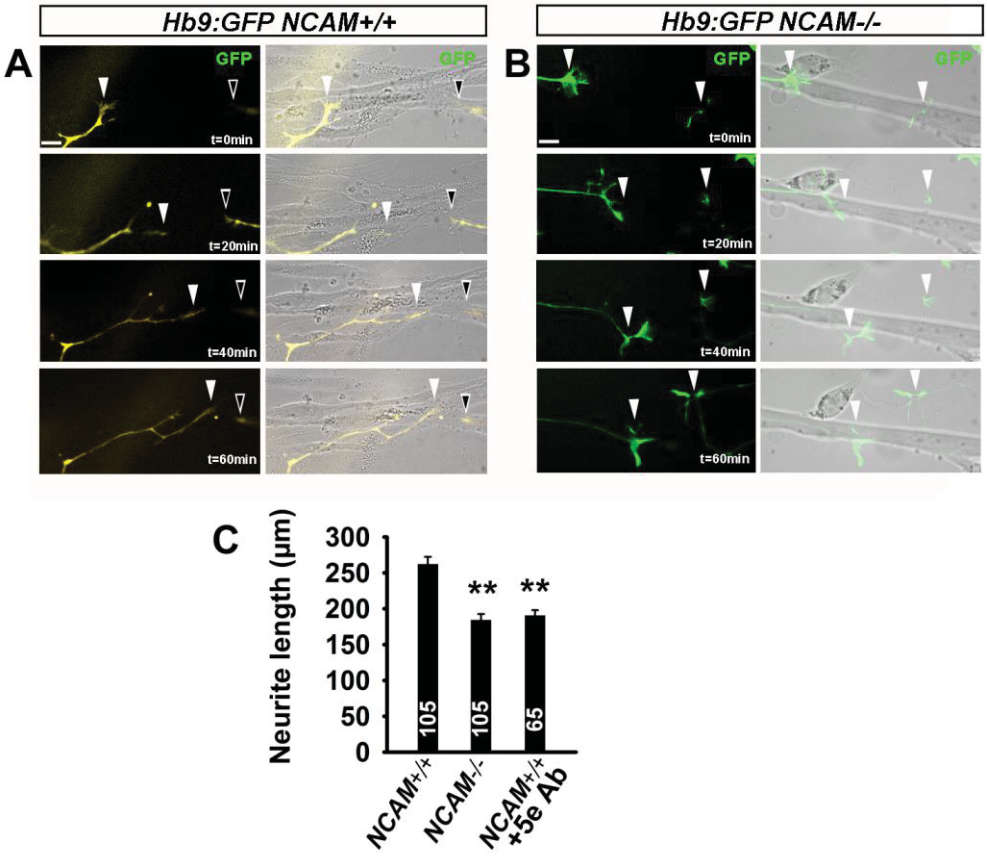
Hb9:GFP NCAM+/+
Hb9:GFP NCAM-/-
A
B
C
GFP
t=0min
t=20min
t=40min
t=60min
Neurite length (µm)
300
250
200
150
100
50
0
105
105
65
**
**
NCAM+/+
NCAM-/-
NCAM+/+ +5e Ab

Figure 4.4: The absence of NCAM influences the targeting of synaptic proteins to sites of cell to cell contact. **(A)** *Hb9:GFP NCAM*$^{+/+}$ ESCMNs form putative neuromuscular junctions after 24 hours in co-culture with chick myotubes (dashed outline) as revealed by the aggregation of postsynaptic AChRs (red) and presynaptic vesicles (SV2; white or blue in merge) to regions of myotube contact (*a'*). SV2 immunoreactivity (blue) along the axon (green) is minimal (*a''*). **(B)** *Hb9:GFP NCAM*$^{-/-}$ ESCMNs form putative NMJs after 24hrs in co-culture, with some AChR clustering (red) but exhibit reduced SV2+ fluorescence at contact sites (*b'*) and high SV2 expression in the axon (*b''*). Scale bars 20 μm.

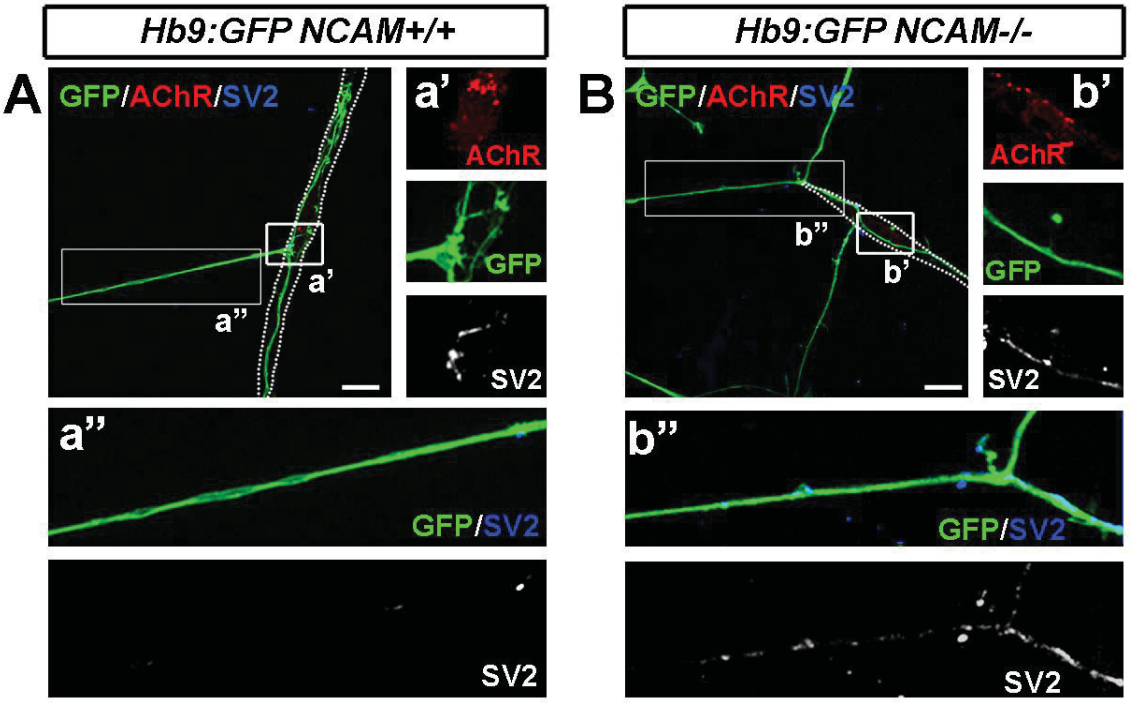
Hb9:GFP NCAM+/+
Hb9:GFP NCAM-/-
A
B
GFP/AChR/SV2
a'
AChR
GFP
SV2
a''
GFP/SV2
b'
b''

Figure 4.5: Cultured *NCAM*$^{-/-}$ NMJs exhibit reduced neurotransmission. **(A)** Representative images of a typical NMJ targeted for intracellular recording by immunolabeling with the non-blocking AChR antibody mAb35 for AChRs (red) and visualization of the GFP signal in Hb9:GFP ECSMNs. Motoneurons were grown for seven days in co-culture with myotubes and prepared for electrophysiological recording. Dashed outline indicates the postsynaptic muscle fiber; solid white lines indicate the position of the intracellular recording electrode. **(B)** Representative recording traces from an *NCAM*$^{+/+}$ NMJ in normal recording media (top), after the addition of 2.5µm tetrodotoxin (TTX; middle) and following addition of 50 µm curare (bottom). Arrowhead indicates the presence of a spontaneous miniature endplate potential (mEPP) which persist following the addition of TTX. **(C)** Representative recording traces obtained in control media and frequency histograms of synaptic events at *NCAM*$^{+/+}$ and **(D)** *NCAM*$^{-/-}$ before, and 5 minutes following the addition of TTX. **(E)** Mean ±SEM of quantal content (*m*) determined by measuring the ratio of EPP amplitude to **(F)** mEPPs amplitude at *NCAM*$^{+/+}$ black and *NCAM*$^{-/-}$ (grey) NMJs (see methods). **(G)** Cumulative frequency plot of inter-event intervals in recordings from *NCAM*$^{+/+}$ and *NCAM*$^{-/-}$ ESCMNs. *P* value was determined using Mann-Whitney rank sum test. The total numbers of endplates from the number of individual cultures is shown in the bars in *E* and are the same for *F*. * $P<0.05$, Mann-Whitney rank sum test.

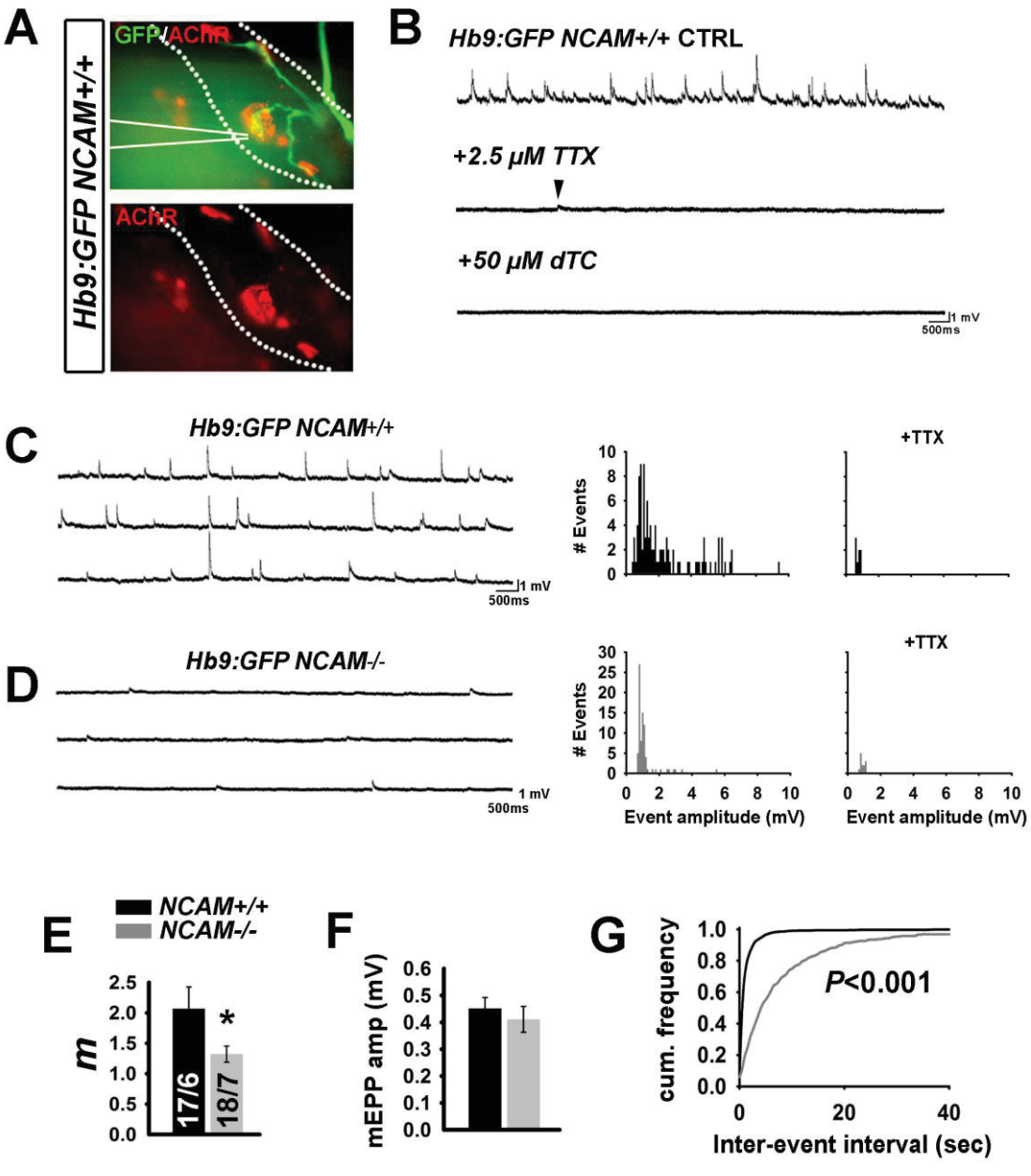
A
Hb9:GFP NCAM+/+
GFP/AChR
AChR
B
Hb9:GFP NCAM+/+ CTRL
+2.5 μM TTX
+50 μM dTC
1 mV
500ms
C
Hb9:GFP NCAM+/+
1 mV
500ms
Events
+TTX
D
Hb9:GFP NCAM-/-
1 mV
500ms
Events
+TTX
Event amplitude (mV)
Event amplitude (mV)
E
NCAM+/+
NCAM-/-
m
17/6
18/7
*
F
mEPP amp (mV)
G
cum. frequency
P<0.001
Inter-event interval (sec)

Figure 4.6: Long term co-culture of ESCMNs with chick myotubes generates morphologically mature NMJs. **(A)** *Hb9:GFP NCAM*$^{+/+}$ ESCMNs grown in co-culture with chick myotubes for 7 **(B)** 21 and **(C)** 35 days. (*c'*) By Day 35, *NCAM*$^{+/+}$ NMJs exhibit a mature morphology with synaptic vesicles (SV2, blue) clustered at endplates (AChR, red). **(D)** *Hb9:GFP NCAM*$^{-/-}$ ESCMNs grown in co-culture for 7 **(E)** 21 and **(F)** 35 days. (*f'*) By Day 35, *NCAM*$^{-/-}$ NMJs continue to exhibit an immature NMJ morphology characterized by distributed synaptic vesicles (SV2, blue) and minimally clustered AChRs (red). Scale bars A-F 200 µm. Scale bars *c'-f'* 20 µm.

Days in Co-culture
7
21
35
Hb9:GFP NCAM+/+
Hb9:GFP NCAM-/-
A
B
C
c'
D
E
F
f'
GFP/AChR
AChR
GFP/AChR/SV2

Figure 4.7: *NCAM*$^{-/-}$ NMJs fail to mature in co-culture. **(A-B)** *Hb9:GFP NCAM*$^{+/+}$ and *NCAM*$^{-/-}$ NMJs immunolabeled with antibodies against SV2 (white or blue in merge) for presynaptic vesicles and with αBTX for postsynaptic AChRs (red). Boxed regions (*a'-a''', b'-b'''*) demonstrate distribution of postsynaptic AChRs and presynaptic SV2+ vesicles in GFP+ motor axons. Arrowheads identify non-synaptic SV2+ puncta. **(C-D)** Frequency histogram and cumulative frequency plot illustrating the size of postsynaptic endplates (AChRs, red) in *NCAM*$^{+/+}$ and *NCAM*$^{-/-}$ co-cultures. Mann-Whitney rank sum test was used to compare endplate areas at 28 days to those measured at 21 days. ns = not statistically significant. **(E)** Frequency histogram of AChR cluster areas measured from aneural muscle cultures at 28 days. **(F)** Mean ±SEM of the number of terminal (black) and en passant (white) synapses in *NCAM*$^{+/+}$ and *NCAM*$^{-/-}$ co-cultures after 21 and 28 days. En passant synapses were differentiated from terminal synapses by the presence of terminals sprouts at least 10μm in length extending away from the synaptic region at en passant synapses. **P*<0.05 Student's t-test, 28 day as compared to 21 day. N=172 NMJs from 3 co-cultures, 28 days N=325 NMJs from 3 co-cultures; *Hb9:GFP NCAM*$^{-/-}$ 21 days N= 142 NMJs from 2 co-cultures, 28 days N=478 NMJs from 3 co-cultures. No MNs N=152 from 3 cultures.

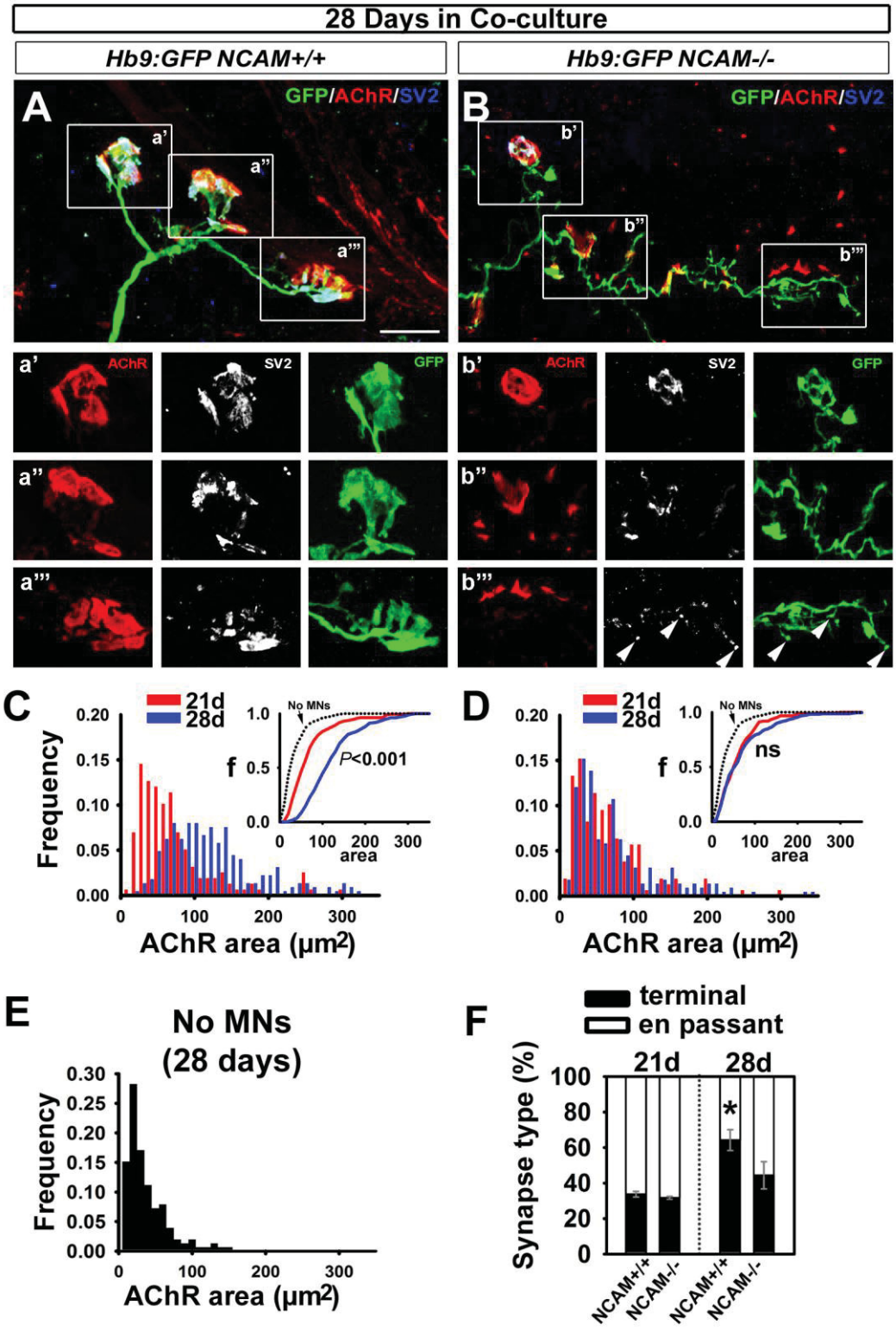
28 Days in Co-culture
Hb9:GFP NCAM+/+
Hb9:GFP NCAM-/-
A
GFP/AChR/SV2
a'
a''
a'''
B
GFP/AChR/SV2
b'
b''
b'''
AChR
SV2
GFP
C
21d
28d
Frequency
AChR area (μm2)
No MNs
f
P<0.001
area
D
ns
E
No MNs
(28 days)
F
terminal
en passant
21d
28d
Synapse type (%)
NCAM+/+
NCAM-/-

Figure 4.8: NCAM140kD is spontaneously endocytosed at mature NMJs grown in co-culture and is localized to synaptic regions. **(A)** *NCAM*$^{+/+}$ NMJs grown in co-culture for 28 days and immunolabeled with antibodies against NCAM*int* (white or blue in merge) and for postsynaptic AChRs with α-BTX (red). Endocytosed NCAM localizes to synaptic regions of terminal arbors (*a'*). **(B)** *NCAM*$^{-/-}$ NMJs do not exhibit NCAM immunoreactivity. **(C)** NCAM is present only on a subset of spontaneously endocytosed membrane as revealed by co-distribution of NCAM and FM4-64FX (*c'*; arrowhead) in the presence of 2.5 μM TTX. Scale bars 10 μm. **(D)** Western blots of 28 day myotube culture homogenates. Cultures were grown in the presence or absence (no MNs) of *NCAM*$^{+/+}$ (+/+) or *NCAM*$^{-/-}$ (-/-) ESCMNs. Blots were immunolabeled for rodent-specific (presynaptic; CD56) and chick-specific NCAM (postsynaptic; 5e). **(E)** *NCAM*$^{+/+}$ ESCMNs grown in co-culture with myotubes for 28 days immunolabeled for internalized NCAM*int (*white or blue in merge) and syp (red). Boxed region shown in *e'*. **(F)** *NCAM*$^{+/+}$ NMJs shown as a negative control for NCAM and highlight the disruption to synaptic vesicle clustering at NMJs. Boxed region shown in *f'*.

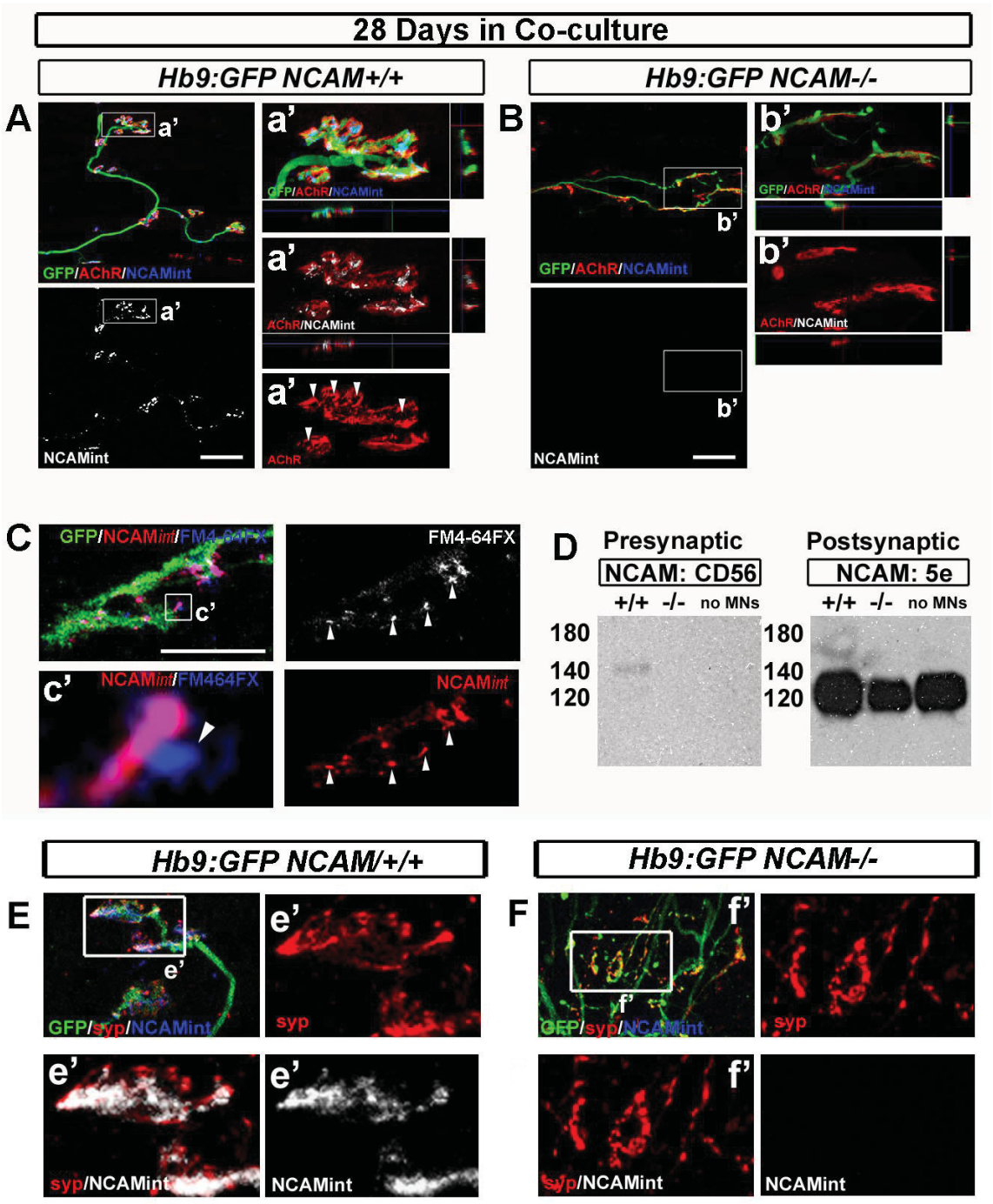
28 Days in Co-culture
Hb9:GFP NCAM+/+
Hb9:GFP NCAM-/-
A
B
a'
b'
GFP/AChR/NCAMint
AChR/NCAMint
NCAMint
AChR
C
GFP/NCAMint/FM4-64FX
FM4-64FX
c'
NCAMint/FM464FX
NCAMint
D
Presynaptic
NCAM: CD56
Postsynaptic
NCAM: 5e
+/+ -/- no MNs
180
140
120
Hb9:GFP NCAM/+/+
Hb9:GFP NCAM-/-
E
F
e'
f'
GFP/syp/NCAMint
syp
syp/NCAMint

Figure 4.9: Spontaneous endocytosis at co-cultured *NCAM*$^{+/+}$requires activation of the L-VDCC and dynamin. **(A)** Schematic of loading protocol used to assess spontaneous uptake of FM4-64FX into cultured NMJs. **(B-C)** Representative images of *NCAM*$^{+/+}$ and *NCAM*$^{-/-}$ NMJs treated with vehicle (DMSO) or dynasore (90μM). **(D)** Mean ±SEM of peak FM4-64FX fluorescence measured at synaptic sites (i.e. α-BTX+/GFP+). Fluorescence intensities were normalized to control and are shown for treatments of *NCAM*$^{+/+}$ (black) or *NCAM*$^{-/-}$ (grey) cultures with DMSO (veh), 90μM dynasore (Dyn), 50μM nifedipine (Nif) and 100nM agatoxin IVA (Aga). **(E)** Same analysis as *D* but performed at FM4-64FX+ puncta at non-synaptic sites (i.e. α-BTX-/GFP+). The total number of NMJs assessed from at least 3 co-cultures is indicated in the bars in *D* and are the same for *E*. Cycling at non-synaptic puncta was assessed by measuring the mean FM4-64FX fluorescence intensity in 50 μm of presynaptic axon. *P<0.001, one way ANOVA and Dunn's multiple comparisons test. ns - not statistically significant.

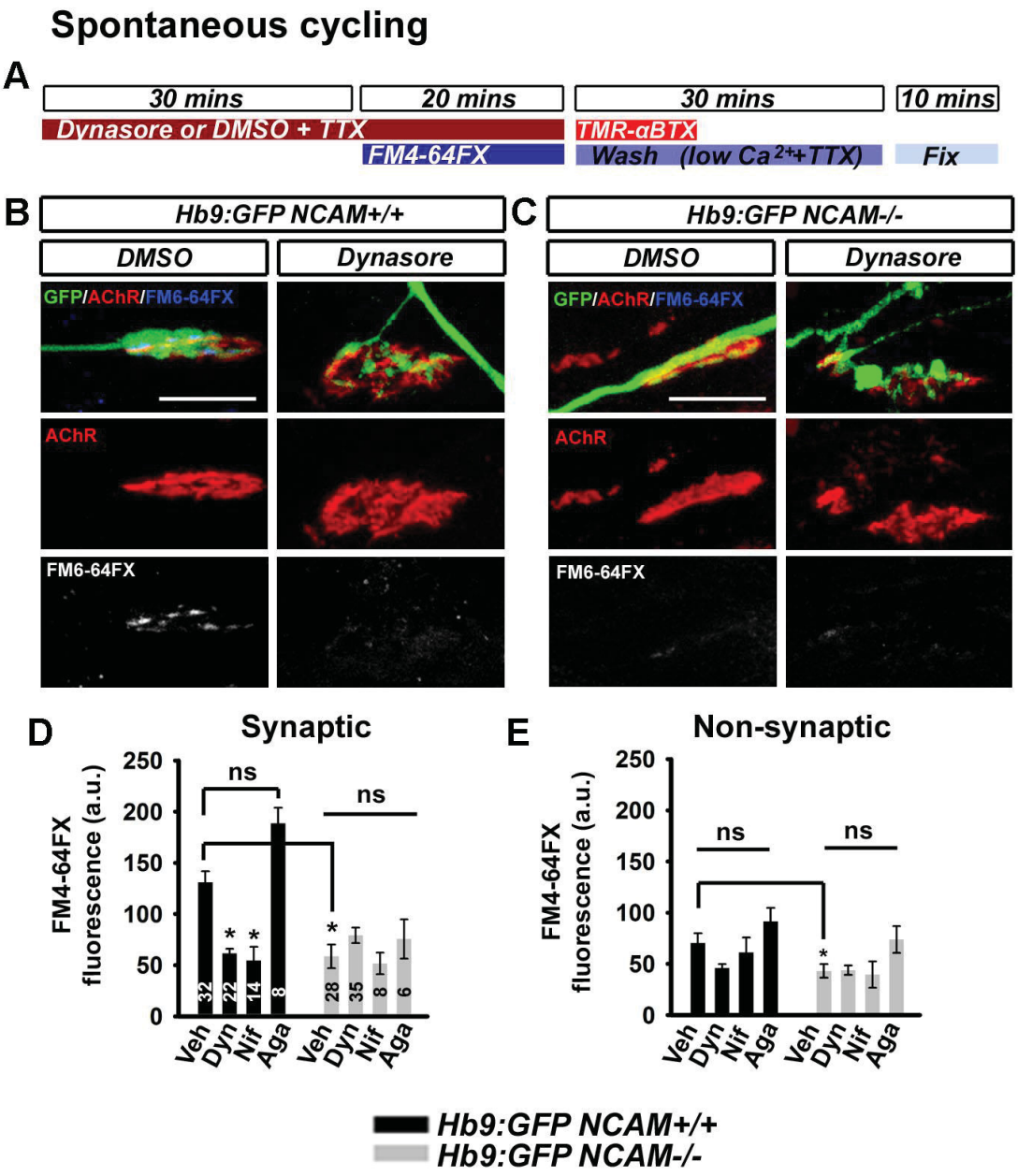
Spontaneous cycling
A
30 mins
20 mins
30 mins
10 mins
Dynasore or DMSO + TTX
TMR-αBTX
FM4-64FX
Wash (low Ca2+ +TTX)
Fix
B
Hb9:GFP NCAM+/+
C
Hb9:GFP NCAM-/-
DMSO
Dynasore
DMSO
Dynasore
GFP/AChR/FM6-64FX
AChR
FM6-64FX
GFP/AChR/FM6-64FX
AChR
FM6-64FX
D
Synaptic
E
Non-synaptic
FM4-64FX fluorescence (a.u.)
250
200
150
100
50
0
ns
ns
*
32
22
14
8
28
35
8
6
Veh
Dyn
Nif
Aga
Hb9:GFP NCAM+/+
Hb9:GFP NCAM-/-

Figure 4.10: Mature *NCAM*$^{+/+}$ NMJs grown *in vitro* cycle synaptic vesicles predominately at synaptic sites when stimulated repetitively at high frequency. **(A)** Cartoon illustration of FM4-64FX stimulation paradigm. **(B)** Loading protocol used to assess activity-dependant uptake of FM4-64FX into cultured NMJs. **(C-D)** Representative images of *NCAM*$^{+/+}$ and *NCAM*$^{-/-}$ NMJs loaded with FM4-64FX (white or blue in merge) and co-labeled with α-BTX to identify AChR-rich synaptic regions (red). Arrowheads indicate *NCAM*$^{-/-}$ non-synaptic puncta loaded with FM4-64FX. Scale bars 20 μm. **(E)** Cumulative frequency plot and mean ±SEM FM4-64FX fluorescence (*right*) of synaptic puncta following 50Hz stimulation. **(F)** Cumulative frequency plot and mean ±SEM FM4-64FX fluorescence (*right*) at non-synaptic puncta following 50Hz stimulation. The number of NMJs measured from at least 3 separate co-cultures is indicated in the bar and is the same for non-synaptic measurements. *P<0.01 Mann-Whitney rank sum test.

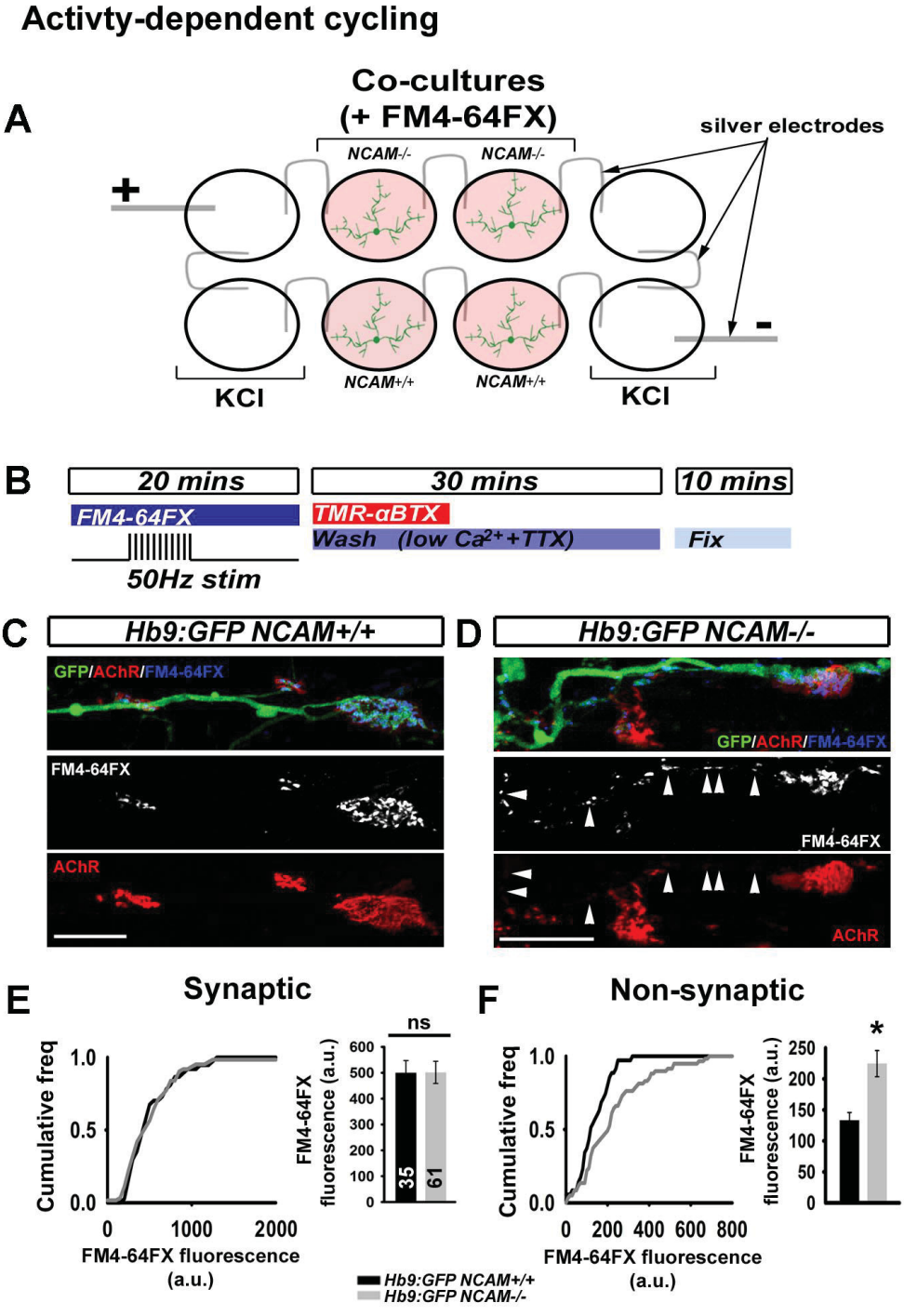
Activty-dependent cycling
A
Co-cultures
(+ FM4-64FX)
silver electrodes
NCAM-/-
NCAM-/-
+
-
NCAM+/+
NCAM+/+
KCl
KCl
B
20 mins
30 mins
10 mins
FM4-64FX
TMR-αBTX
Wash (low Ca2+ +TTX)
Fix
50Hz stim
C
Hb9:GFP NCAM+/+
D
Hb9:GFP NCAM-/-
GFP/AChR/FM4-64FX
FM4-64FX
AChR
E
Synaptic
F
Non-synaptic
Cumulative freq
FM4-64FX fluorescence (a.u.)
ns
*
35
61
Hb9:GFP NCAM+/+
Hb9:GFP NCAM-/-

Figure 4.11: Pharmacological assessment of synaptic vesicle cycling in long-term co-culture using FM4-64FX. **(A)** Schematic of loading protocol used to assess activity-dependant uptake of FM4-64FX into cultured NMJs. **(B-C)** Representative images of *NCAM*$^{+/+}$ and *NCAM*$^{-/-}$ 28 day old co-cultures treated with vehicle (DMSO), 90µM dynasore or 50µM nifedipine 30 minutes before loading with FM4-64FX. **(D)** Mean ±SEM of peak FM4-64FX fluorescence at synaptic puncta normalized to mean vehicle treated levels following treatment with DMSO or EtOH (veh), tetrodotoxin (TTX; 2.5µM), dynasore (Dyn; 90µM), nifedipine (Nif; 50µM), ω agatoxin IVA (Aga; 100nM) or brefeldin A (BFA; 10 µg/ml). **(E)** Mean ±SEM of peak FM4-64FX fluorescence at non-synaptic puncta normalized to mean vehicle treated levels following treatment with vehicle (DMSO or EtOH), tetrodotoxin (TTX; 2.5µM), dynasore (Dyn; 90µM), nifedipine (Nif; 50µM), ω agatoxin IVA (Aga; 100nM) or brefeldin A (BFA; 10 µg/ml). The number of NMJs measured from at least 3 separate co-cultures is indicated in the bar and is the same for non-synaptic measurements. *P<0.001, one way ANOVA and Dunn's multiple comparisons test. ns - not statistically significant.

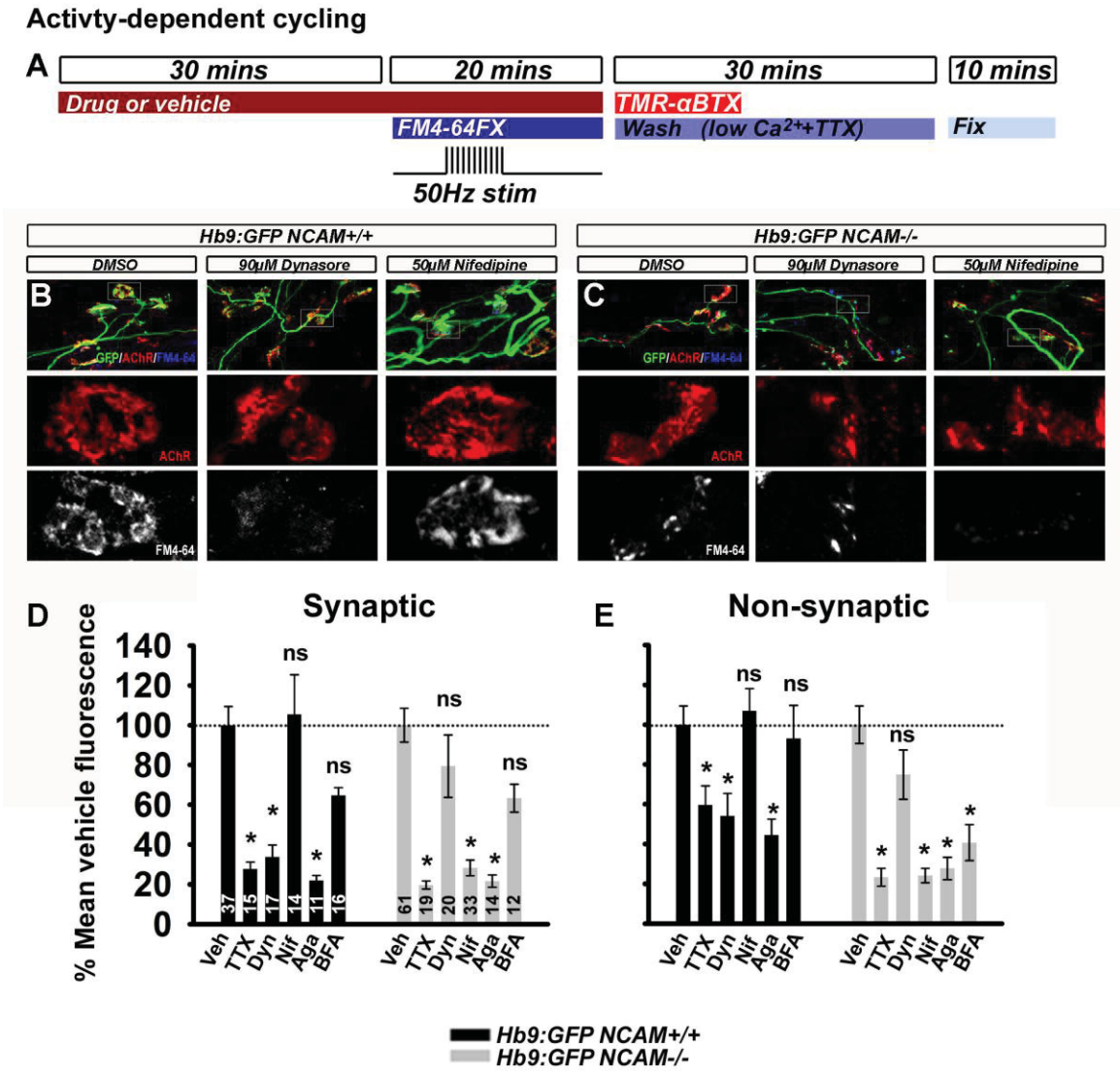
Activty-dependent cycling
A
30 mins
20 mins
30 mins
10 mins
Drug or vehicle
TMR-αBTX
FM4-64FX
Wash (low Ca2+ +TTX)
Fix
50Hz stim
Hb9:GFP NCAM+/+
Hb9:GFP NCAM-/-
DMSO
90μM Dynasore
50μM Nifedipine
B
C
GFP/AChR/FM4-64
AChR
FM4-64
D
Synaptic
E
Non-synaptic
% Mean vehicle fluorescence
140
120
100
80
60
40
20
0
ns
*
37
15
17
14
11
16
61
19
20
33
14
12
Veh
TTX
Dyn
Nif
Aga
BFA
Hb9:GFP NCAM+/+
Hb9:GFP NCAM-/-

CHAPTER 5: General Discussion

The observations outlined in this thesis describe a number of organizational processes which together function to establish and homeostatically maintain neuromuscular synaptic connections in vertebrates. Using two distinct models of regeneration *in vivo* in combination with a co-culture model of neuromuscular synaptogenesis *in vitro*, I have provided evidence that implicates NCAM signaling in the formation and stability of NMJs. Primarily, NCAM was found to influence synaptic p_r by the mobilization of synaptic vesicles from the shaft of growing axons to synaptic sites, and through its regulatory effect on the L-VDCCs and synaptic vesicle recycling. These findings suggest that the synaptic vesicle cycle is a potent locus of regenerative change and could be a key target for regenerative therapy. Here, I will review the fundamental mechanisms of regeneration that these studies have highlighted and discuss possible experimental approaches which could be used to address a key question raised in the thesis.

Mechanisms of synaptic regeneration

Regenerative responses can be initiated by a variety of cellular processes and can influence the activity of many different populations of cells. Severed axons will regrow to synapse on denervated targets, while spared axons will sprout and reallocate their synaptic resources to nearby denervated terminals. The majority of naturally occurring pathology and subsequent regeneration likely involve a combination of these mechanisms. Pluripotent stem cells are ideal cells to model regeneration *in vitro* as they can be isolated from tissues of adult animals, including humans, and differentiated into a variety of cell types which reflect the regenerative potential of their host organism. Here I have used the NMJ as a model synapse to provide evidence that the neural cell adhesion molecule (NCAM) contributes to the regenerative potential of motoneurons.

Functional motor axon regeneration occurs quickly and completely following a nerve crush injury (Sanes et al 1978) but requires a prolonged period for full stabilization (Gordon and Stein, 1982). The findings detailed in Chapter 2 suggest a critical role for NCAM in the long term stabilization of neuromuscular synapses after complete nerve injury. We observed evidence that a subset of reinnervated $NCAM^{-/-}$ endplates were in the

process of retracting, had a reduced p_r and lacked synaptic coverage by tSCs. These phenotypes emerged later in the recovery period (i.e. 3 months) but analysis of neuronal- or muscle-specific conditional mutants did not reproduce them. This data therefore suggests that either a loss of perisynaptic NCAM signaling or a loss of trans-synaptic NCAM signaling induces a degenerative phenotype in reinnervated muscles.

These findings are supplemented by observations made during the process of MU expansion induced by partial muscle denervation described in Chapter 3. Motor units are known to sprout up to 2-6 times their original size and are able to recover functional muscle activity within approximately 2 weeks in the mouse (Brown and Ironton, 1978). Neither pre nor postsynaptic conditional NCAM mutant mice demonstrated any functional expansion of sprouting motor arbors, suggesting that both pre and postsynaptic NCAM are required for the functional reorganization of terminal fields. Likewise, both genotypes demonstrated significant impairments in the formation and stabilization of reinnervated synapses which were paralleled by reductions in the number of recycling synaptic vesicles. Similar to observations in Chapter 2, poorly differentiated NCAM mutant motor terminals were found to exhibit signs of axon withdrawal (Appendix Figure A7), although on a much faster time scale than the degenerative phenotype observed in Chapter 2. These data suggest that distinct regenerative mechanisms are enabled through the functioning of NCAM during the recovery from nerve crush and from partial denervation, revealing a fundamental role of this molecule in compensatory neural repair.

The reasons for the discrepancy in the contribution of NCAM to recovery from different kinds of nerve injuries may be partially resolved by observations made in long term co-cultures of *NCAM*$^{-/-}$ ESCMNs, as described in Chapter 4. In contrast to wild-type ESCMNs, which formed structurally and functionally mature NMJs after 4 weeks in co-culture with chick myotubes, *NCAM*$^{-/-}$ ESCMNs formed small NMJs with highly disorganized presynaptic vesicles and release machinery. Furthermore, NCAM was found to be endocytosed at synaptic regions, and was required for the clustering of synaptic vesicles to synaptic sites and to establish appropriate Ca^{2+}- dependent mechanisms of synaptic vesicle recycling. Despite these disruptions, *NCAM*$^{-/-}$ ESCMNs formed many, albeit small and immature, functional synaptic contacts *in vitro* and elaborated large, albeit highly disorganized, axon arbors. Although not directly assessed, it is likely that

NCAM$^{-/-}$ arbors contained an equivalent amount of presynaptic resources as wild-type arbors, but which were distributed throughout the arbor without an effective functional organization.

Each experimental model assessed in this thesis therefore produces unique mechanisms of synaptogenesis and generates MUs of variable size. For instance, when given equal access to a completely denervated muscle, regenerating motor axons reform MUs of approximately the same size as they do during development (Gordon and Stein, 1982); sprouting MUs invariably expand following partial denervation and do so in proportion to their original size (Rafuse et al 1992); and motoneurons in culture are confronted with a very large population of muscle fibers and are likely expanded to their maximum from the moment of neurite outgrowth. The arbor-wide organizational properties of NCAM are therefore reflected in the nature of MU remodeling.

Several studies have investigated the distribution of synaptic strengths across multiple synapses of a single axon arbor and have found a high degree of variability between presynaptic release sites (Cooper et al, 1996; Branco et al 2008). Interestingly, axonal variability in p_r is largely due to the local regulation of synaptic strength by the postsynaptic cell (Branco et al 2008; Ratyanaka et al 2012), suggesting a specific retrograde regulation of presynaptic efficacy. Together these findings demonstrate that the organization of synapses on terminal arbors is, at least in part, due to a complex interaction between the abundance of presynaptic resources and the distribution of these resources in response to locally-derived retrograde cues.

Future experimental approaches

Many questions raised throughout this thesis remain unanswered. Such questions include, but are not limited to the following: 1. What mechanisms result in synapse destabilization following reinnervation in *NCAM*$^{-/-}$ mice? 2. How does pre and postsynaptic NCAM signaling regulate presynaptic efficacy and vesicle abundance on expanding MUs? 3. What is the role, if any, of endocytosed NCAM at mature NMJs grown *in vitro*? Although these are all interesting and pertinent questions, I will elaborate on only one overarching question and discuss some potential experiments which could be performed

to address its fundamental concern. The question is this – is there an optimal functional organization to axonal arborisations?

To begin to answer such a question, a detailed analysis of the distribution of synaptic strengths across a population of synapses formed by a single axon is required. The strength of individual synapses, based on estimates of *m*, *n* and *p* could be assessed and mapped according to their position along a terminal axon. Likewise, an estimate of the number of RRP and RP vesicles at each synapse could be calculated and their distributions across the arbor could be determined. A value for the total pool of functional synaptic resources could be estimated for each neuron examined and manipulations could be performed to assess the plasticity of these values.

The neuromuscular system is an excellent model system to investigate the mechanisms governing the distribution of synaptic strengths, as its functional output (i.e. muscle contraction) is directly quantifiable, each postsynaptic cell receives only one input, synapses are large and amenable to simultaneous optical and electrophysiological assessments of neurotransmission, and motoneurons only form ~10-40 synapses on some muscles (Tapia et al 2012). Furthermore, two different neuromuscular preparations can now be used to assess resource distribution in motor arbors. First, *in vivo* neuromuscular systems are ideal models to investigate resource redistribution because synapses are easily accessible to combined functional and optical investigation. Second, the *in vitro* co-culture system presented in Chapter 4 provides a highly manipulable and effective assessment of NMJ distribution which can be easily followed over time. I will consider possible experiments for each model in turn.

Naturally occurring processes such as synapse elimination or MU expansion make the *in vivo* system a very valuable tool to assess synaptic competition and resource redistribution in the neonatal or adult animal respectively. Single motor axons can be assessed in mice with a low level of fluorescent labeling of motoneurons (Buffelli et al 2003; Tapia et al 2012) or by using the brainbow mouse (Livet et al 2007). Selective excitation of individual motor axons could be achieved using a similarly low level of expression of channel-rhodopsin in subsets of motoneurons and could be used for both chronic (Kastanenka and Landmesser, 2010) or acute experiments (Llewellyn et al 2010). Selective optical excitation of motor nerves would be advantageous during synapse

elimination because it would provide a means to investigate the function of single motor terminals at polyneuronally innervated synapses, which would otherwise be largely inaccessible. During partial denervation, selective optical excitation could also be used to provide a means to generate motor output by single expanded MUs, although some luck would be required to achieve partial denervation which would spare the innervation of the one/few axon(s) expressing channel-rhodopsin.

Secondly, the co-culture system described in Chapter 4 would be well suited to complement *in vivo* investigations of axon-specific synaptic organization and could be used to assess patient-specific disease contributions to the distribution of presynaptic resources. Very low density cultures of dissociated motoneurons can provide the resolution required for an assessment of synaptic strengths across a single axon arbor and would provide access to the cell body for current clamp-driven firing of action potentials and/or concurrent Ca^{2+} imaging of activity at motor terminals and soma. Motoneurons could be transfected with exogenous genetic constructs to disrupt, rescue or image a variety of cellular processes in a temporally defined manner using single cell electroporation techniques (Haas et al 2001) or via direct injection into the cell nucleus (Tradewell et al 2011). Recently developed optical photobleaching techniques, devised to follow single dense-core vesicle distribution in *Drosophila* (Wong et al 2012) could be applied to follow the kinetics of synaptic resource distribution from the soma and throughout the entire axon arbor. Structural plasticity could be induced by selective removal of specific branches of cultured motoneurons (Turney and Lichtman, 2012), or through the local perfusion of neurotoxins (Branco et al 2008). Together, these approaches could help to identify the fine details of synaptic reorganization which are difficult to assess *in vivo*, such as the contribution of different vesicle populations to terminal remodeling and the endocytic regulation of these pools.

However, slight alterations to the co-culture design would be required to enable effective and reliable synaptic sampling. For instance, mouse muscle fibers would most likely need to be used as postsynaptic targets, as some chick muscles retain multiple innervation into adulthood which would complicate the analysis of synaptic recordings. The use of prepatterned substrates may provide more representative culture conditions to

guide axon arborisations along the midbelly of muscle fibers (Gingras et al 2009) and may contribute to the development of more consistent arborization patterns.

Together, these experiments would permit the functional and morphological analysis of large populations of synapses on single terminal arbors. To my knowledge, such experiments have yet to be performed and could yield very interesting and novel findings.

Conclusion

There is reason to believe that an optimal functional organization does indeed exist for the terminal arbors of motoneurons. Recent work has described a conserved principle of axon branch density across a variety of CNS neurons in several different species (Snider et al 2010; Teeter and Stevens, 2011). In brief, this principle describes that the density of branches in an arbor will decrease as the territory covered by the arbor increases. The authors go on to suggest that such a property may function to conserve a mean number of synapses across different arbors of different sizes, suggesting the potential for a general rule which governs the distribution of synapses along single axon arbors. Although motoneurons were not included in the analyses by Snider et al (2010) and Teeter and Stevens (2011), motoneurons do possess very large terminal arbors which undergo extensive reorganization during development to ultimately establish relatively simplistic branching schemes (Tapia et al 2012). It is therefore possible that motoneurons do indeed adhere to this general rule and it would be fascinating to find out.

Indeed, intramuscular branching patterns can differ markedly between different muscles (Dahm and Landmesser, 1991; Rafuse et al 1996; Rafuse and Landmesser, 2000; Haase et al 2002; Livet et al 2002), although, to my knowledge, neither a systematic quantification of the patterns formed by individual motor axons, nor a functional analysis of the synapses they produce has yet to be been performed. The initial state of the these branching schemes may also influence their regenerative potential in adulthood following injury or disease, as the size relationships of sprouting MUs in a muscle are highly conserved (Rafuse et al 1992) and different subtypes of developmentally defined MUs have different regenerative capacities (Frey et al 2000; Pun et al 2006). Should be abundance of presynaptic vesicles and other synaptic resources govern these stereotyped

patterns; an optimal functional organization could be attained with their proper distribution in healthy animals. Whether this optimal organization is also achieved under conditions associated with neurodegenerative is open for future investigation.

REFERENCES

A

Abercrombie M. (1946) Estimation of nuclear population from microtome sections. Anat Rec 94: 239-247

Ahmari SE, Buchanan J, Smith SJ. (2000) Assembly of presynaptic active zones from cytoplasmic transport packets. Nat Neurosci 5, 445-451

Akaaboune M, Grady RM, Turney S, Sanes JR, Lichtman JW. (2002) Neurotransmitter receptor dynamics studied in vivo by reversible photo-unbinding of fluorescent ligands. Neuron 34: 865-876

Allodi I, Udina E, Navarro X. (2012) Specificity of peripheral nerve regeneration: Interactions at the axon level. Prog Neurobiol 98: 16-73

Altiok N, Bessereau JL, Changeux JP. (1995) ErbB3 and ErbB2/neu mediate the effect of heregulin on acetylcholine receptor gene expression in muscle: differential expression at the endplate. (1995) EMBO J 14: 4258-4266

Anderson AA, Kendal CE, Garcia-Maya M, Kenny AV, Morris-Triggs SA, Wu T, Reynolds R, Hohenester E, Saffell JL. (2005) A peptide from the first fibronectin domain of NCAM acts as an inverse agonist and stimulates FGF receptor activation, neurite outgrowth and survival. J Neurochem 95: 570-583

Andersson AM, Olsen M, Zhernosekov D, Gaardsvoll H, Krog L, Linnemann D, Bock E. (1993) Age-related changes in expression of the neural cell adhesion molecule in skeletal muscle: a comparative study of newborn, adult and aged rats. Biochem J 290:641-648

Andreae LC., Fredj NB., Burrone J. (2012) Independent vesicle pools underlie different modes of release during neuronal development. J Neurosci 35: 1867-1874

Atsumi S. (1977) Development of neuromuscular junctions of fast and slow muscles in the chick embryo: a light and electron microscopic study. J Neurocytol 6: 691-709

Avila OL., Drachman DB., Pestronk A. (1989) Neurotransmission regulates stability of acetylcholine receptors at the neuromuscular junction. J Neurosci 9:2902-2906

B

Bagust J, Lewis DM, Westerman RA. (1973) Polyneuronal innervation of kitten skeletal muscle. J Physiol 229:241-255

Bajjalieh SM, Peterson K, Shinghal R, Scheller RH. (1992) SV2, a brain synaptic vesicle protein homologous to bacterial transporters. Science 257: 1271-1273

Balice-Gordon RJ, Lichtman JW. (1993) Long-term synapse loss induced by focal blockade of postsynaptic receptors. Nature 372: 519-524

Bamji SX, Rico B, Kimes N, Reichardt LF. (2006) BDNF mobilizes synaptic vesicles and enhances synapse formation by disrupting cadherin-beta-catenin interactions. J Cell Biol 174: 289-299

Bamji SX., Rico B., Kimes N., Reichardt LF. (2006) BDNF mobilizes synaptic vesicles and enhances synapse formation by disrupting cadherin/β-catenin interactions. J Cell Biol 174:289-299

Banker BQ, Kelly SS, Robbins N. (1983) Neuromuscular transmission and correlative morphology in young and old mice. J Physiol 399:355-377

Barbeau D, Liang JJ, Robitalille Y, Quirion R, Srivastava LK. (1995) Decreased expression of the embryonic form of the neural cell adhesion molecule in schizophrenic brains. Proc Natl Acad Sci USA 92, 2785-2789

Béïque JC, Na Y, Kuhl D, Worley PF, Huganir RL. (2011) Arc-dependent synapse-specific homeostatic plasticity. Proc Natl Acad Sci USA 108: 816-821

Ben Fredj N, Hammond S, Otsuna H, Chien CB, Burrone J, Meyer MP. (2010) Synaptic activity and activity-dependent competition regulates axon arbor maturation, growth arrest, and territory in the retinotectal projection. J Neurosci 30, 10939-10951

Bennett MR, Jones P, Lavidis NA. (1986) The probability of quantal secretion along visualized terminal branches at amphibian (Bufo marinus) neuromuscular synapses. J Physiol 379: 257-274

Bennett V, Baines AJ. (2001) Spectrin and ankyrin-based pathways: metazoan inventions for integrating cells into tissues. Physiol Rev 81: 1353-92.

Berg DK, Hall ZW. (1974) Fate of alpha-bungarotoxin bound to acetylcholine receptors of normal and denervated muscle. Science 184: 473- 475

Betz WJ, Bewick GS. (1993) Optical monitoring of transmitter release and synaptic vesicle recycling at the frog neuromuscular junction. J Physiol 460: 287-309

Betz WJ, Mao F, Bewick GS. (1992) Activity-dependent fluorescent staining and destaining of living vertebrate motor nerve terminals. J Neurosci 12, 363-375

Beutner D, Voets T, Neher E, Moser T. (2001) Calcium dependence of exocytosis and endocytosis at the cochlear inner hair cell afferent synapse. Neuron 29:681-690

Bezakova G, Rabben I, Sefland I, Fumagalli G, Lømo T. (2001) Neural agrin controls acetylcholine receptor stability in skeletal muscle fibers. Proc Natl Acad Sci USA 98, 9924-9929

Bhat S, Silberberg DH. (1986) Oligodendrocyte cell adhesion molecules are related to neural cell adhesion molecule (N-CAM). J Neurosci 6: 3348-3354

Bisaz R, Sandi C. (2012) Vulnerability of conditional NCAM-deficient mice to develop stress-induced behavioral alterations. Stress 15, 195-206

Bishop DL, Misgeld T, Walsh MK, Gan WB, Lichtman JW. (2004) Axon branch removal at developing synapses by axosome shedding. Neuron 44:651-661

Blake DJ, Weir A, Newey SE, Davies KE. (2002) Function and genetics of dystrophin and dystrophin-related proteins in muscle. Physiol Rev 82: 291-329

Bock E, Edvardsen K, Gibson A, Linnemann D, Lyles JM, Nybroe O. (1987) Characterization of soluble forms of NCAM. FEBS Lett 225:33-36

Bodrikov V., Sytnyk V., Leshchyns'ka I., den Hertog J., Schachner M. (2008) NCAM induces CaMKIIα-mediated RPTPα phosphorylation to enhance its catalytic activity and neurite outgrowth. J Cell Biol. 182: 1185-1200

Bolliger MF, Zurlinden A, Lüscher D, Bütikofer L, Shakhova O, Francolini M, Kozlov SV, Cinelli P, Stephan A, Kistler AD, Rülicke T, Pelczar P, Ledermann B,Fumagalli G, Gloor SM, Kunz B, Sonderegger P. (2010) Specific proteolytic cleavage of agrin regulates maturation of the neuromuscular junction. J Cell Sci 123: 3944-3955

Bonanomi D, Pfaff SL. (2010) Motor axon pathfinding. Cold Spring Harb Perspect Biol 3: a001735

Bosse F, Hasenpusch-Theil K, Küry P, Müller HW. (2006) Gene expression profiling reveals that peripheral nerve regeneration is a consequence of both novel injury-dependent and reactivated developmental processes. J Neurochem 96: 1441-57.

Branco T, Staras K, Darcy KJ, Goda Y. (2008) Local dendritic activity sets release probability at hippocampal synapses. Neuron 59: 475-485

Branco T, Staras K. (2009) The probability of neurotransmitter release: variability and feedback control at single synapses. Nat Rev Neurosci 10:373-383

Brandon EP, Lin W, D'Amour KA, Pizzo DP, Dominguez B, Sugiura Y, Thode S, Ko CP, Thal LJ, Gage FH, Lee KF. (2003) Aberrant patterning of neuromuscular synapses in choline acetyltransferase-deficient mice. J Neurosci 23: 539-549

Brennand KJ., Simone A., Jou J., Gelboin-Burkhart C., Tran N., Sangar S. Li Y., Mu Y., Chen G., Yu D., McCarthy S., Sebat J., Gage FH. (2011) Modelling schizophrenia using human induced pluripotent stem cells. Nature. 473: 221-225

Brown MC, Jansen JK, Van Essen D. (1976) Polyneuronal innervation of skeletal muscle in new-born rats and its elimination during maturation. J Physiol 261: 387-422.

Brown MC, Holland RL, Ironton R. (1980) Nodal and terminal sprouting from motor nerves in fast and slow muscles of the mouse. J Physiol 306: 493-510

Brown MC., Ironton R. (1978) Sprouting and regression of neuromuscular synapses in partially denervated mammalian muscles. J Physiol 278: 325-348

Bruneau EG, Akaaboune M. (2010) Dynamics of the rapsyn scaffolding protein at the neuromuscular junction of live mice. J Neurosci 30: 614-619

Bruneau EG, Sutter D, Hume RI, Akaaboune M. (2005) Identification of nicotinic acetylcholine receptor recycling and its role in maintaining receptor density at the neuromuscular junction in vivo. J Neurosci 25: 9949-9959

Brushart TM (1993) Motor axons preferentially reinnervate motor pathways. J Neurosci 13: 2730-2738

Buffelli M, Burgess RW, Feng G, Lobe CG, Lichtman JW, Sanes JR. (2003) Genetic evidence that relative synaptic efficacy biases the outcome of synaptic competition. Nature 424: 430-434

Bukalo O, Fentrop N, Lee AY, Salmen B, Law JW, Wotjak CT, et al. (2004) Conditional ablation of the neural cell adhesion molecule reduces precision of spatial learning, long-term potentiation, and depression in the CA1 subfield of mouse hippocampus. J Neurosci 24: 1565-77.

Buskirk DR, Thiery JP, Rutishauser U, Edelman GM. (1980) Antibodies to a neural cell adhesion molecule disrupt histogenesis in cultured chick retinae. Nature 285:488-489

C

Caccia MR, Harris JB, Johnson MA. (1979) Morphology and physiology of skeletal muscle in aging rodents. Muscle Nerve 2: 202-212

Calderó J, Casanovas A, Sorribas A, Esquerda JE. (1992) Calcitonin gene-related peptide in rat spinal cord motoneurons: subcellular distribution and changes induced by axotomy. Neuroscience 48:449-461

Cao, P., Maximov, A., Südhof, T. (2011) Activity-dependant IGF-1 exocytosis is controlled by the Ca^{2+} sensor synaptotagmin-10. Cell 145: 300-311

Caroni P, Rotzler S, Britt JC, Brenner HR. (1993) Calcium influx and protein phosphorylation mediate the metabolic stabilization of synaptic acetylcholine receptors in muscle. J Neurosci 13: 1315-1325

Carroll SL, Miller ML, Frohnert PW, Kim SS, Corbett JA. (1997) Expression of neuregulins and their putative receptors, ErbB2 and ErbB3, is induced during Wallerian degeneration. J Neurosci 17:1642-1659

Castonguay A, Robitaille R. (2001) Differential regulation of transmitter release by presynaptic and glial Ca2+ internal stores at the neuromuscular synapse. J Neurosci 21: 1911-22.

Chakkalakal JV, Kuang S, Buffelli M, Lichtman JW, Sanes JR. (2012) Mouse transgenic lines that selectively label Type I, Type IIA, and Types IIX+B skeletal muscle fibers. Genesis 50: 50-58

Chakkalakal JV., Nishimune H., Ruas JL., Spiegelman BM, Sanes JR. (2010) Retrograde influence of muscle fibers on their innervation revealed by a novel markers for slow motoneurons. Development. 137: 3489-3499

Chang TN, Keshishian H. (1996) Laser ablation of Drosophila embryonic motoneurons causes ectopic innervation of target muscle fibers. J Neurosci 16: 5717-5726

Chargé SB, Rudnicki MA. (2004) Cellular and molecular regulation of muscle regeneration. Physiol Rev 84: 209-38.

Chen F, Liu Y, Sugiura Y, Allen PD, Gregg RG, Lin W. (2011) Neuromuscular synaptic patterning requires the function of skeletal muscle dihydropyridine receptors. Nat Neurosci 14: 570-577

Chen J, Billings SE, Nishimune H. (2011) Calcium channels link the muscle-derived synapse organizer laminin β2 to Bassoon and CAST/Erc2 to organize presynaptic active zones. J Neurosci 31: 512-525

Chen C, Regehr WG. (2000) Developmental remodeling of the retinogeniculate synapse. Neuron 28: 955-966

Chernyshova Y, Leshchyns'ka I, Hsu SC, Schachner M, Sytnyk V. (2011) The neural cell adhesion molecule promotes FGFR-dependent phosphorylation and membrane targeting of the exocyst complex to induce exocytosis in growth cones. J Neurosci. 31: 3522-3535

Chernyshova Y., Leshchyns'ka I., Hsu C-S., Schachner M., Sytnyk V. (2011) The neural cell adhesion molecule promotes FGFR phosphorylation and membrane targeting of the exocyst complex in induce exocytosis in growth cones. J Neurosci 31:3522-3535

Cheung G, Cousin MA. (2012) Adaptor protein complexes 1 and 3 are essential for generation of synaptic vesicles from activity-dependent bulk endosomes. J Neurosci 32:6014-6023

Cheung G, Jupp OJ, Cousin MA. (2010) Activity-dependent bulk endocytosis and clathrin-dependent endocytosis replenish specific synaptic vesicle pools in central nerve terminals. J Neurosci 30:8151-8161

Chi P, Greengard P, Ryan TA. (2001) Synapsin dispersion and reclustering during synaptic activity. Nat Neurosci 4: 1187-1193

Chi P., Greengard P., Ryan TA. (2003) Synaptic vesicle mobilization is regulated by distinct synapsin 1 phosphorylation pathways at different frequencies. Neuron. *38*: 69-78

Chipman PH., Franz CK., Nelson A., Schachner M., Rafuse VF. (2010) Neural cell adhesion molecule is required for the stability of reinnervated neuromuscular junctions. Eur J Neurosci 32: 238-249

Chipman PH., Toma JS, Rafuse VF. (2012) Generation of motoneurons from pluripotent stem cells. Prog Neurobiol *In press*

Chung C., Barylko B., Leitz J, Liu X., Kavalali ET. (2010) Acute dynamin inhibition dissects synaptic vesicle recycling pathways that drive spontaneous and evoked neurotransmission. J Neurosci 30:1363-1376

Cifuentes-Diaz C, Frugier T, Tiziano FD, Lacène E, Roblot N, Joshi V, et al. (2001) Deletion of murine SMN exon 7 directed to skeletal muscle leads to severe muscular dystrophy. J Cell Biol 152: 1107-14.

Clegg DO, Wingerd KL, Hikita ST, Tolhurst EC. (2003) Integrins in the development, function and dysfunction of the nervous system. Front Biosci 8:d723-750

Colman H, Nabekura J, Lichtman JW. (1997) Alterations in synaptic strength preceding axon withdrawal. Science 275: 356-61.

Colomar A, Robitaille R. (2004) Glial modulation of synaptic transmission at the neuromuscular junction. Glia 47: 284-9.

Conforti L, Adalbert R, Coleman MP. (2007) Neuronal death: where does the end begin? Trends Neurosci 30: 159-66.

Cooper RL, Harrington CC, Marin L, Atwood HL. (1996) Quantal release at visualized terminals of a crayfish motor axon: intraterminal and regional differences. J Comp Neurol 375: 583-600

Cornelison DD, Olwin BB, Rudnicki MA, Wold BJ. MyoD(-/-) satellite cells in single-fiber culture are differentiation defective and MRF4 deficient. (2000) Dev Biol 224: 122-37.

Courtney J, Steinbach JH. (1981) Age changes in neuromuscular junction morphology and acetylcholine receptor distribution on rat skeletal muscle fibres. J Physiol 320: 435-447

Covault J., Sanes JR. (1986) Distribution of NCAM in synaptic and extrasynaptic portions of developing and adult skeletal muscle. J Cell Biol. 102: 716-730

Covault J, Sanes JR. (1985) Neural cell adhesion molecule (N-CAM) accumulates in denervated and paralyzed skeletal muscles. Proc Natl Acad Sci 82:4544-4548

Crain SM, Alfei L, Peterson ER. (1970) Neuromuscular transmission in cultures of adult human and rodent skeletal muscle after innervation in vitro by fetal rodent spinal cord. J Neurobiol 1: 471-489

Cremer H, Lange R, Christoph A, Plomann M, Vopper G, Roes J, Brown R, Baldwin S, Kraemer P, Scheff S, et al. (1994) Inactivation of the N-CAM gene in mice results in size reduction of the olfactory bulb and deficits in spatial learning. Nature 367: 455-459

Crossin KL, Edelman GM, Cunningham BA. (1984) Mapping of three carbohydrate attachment sites in embryonic and adult forms of the neural cell adhesion molecule. J Biol Chem 99: 1848-1855

Cunningham BA, Hemperly JJ, Murray BA, Prediger EA, Brackenbury R, Edelman GM. (1987) Neural cell adhesion molecule: structure, immunoglobulin-like domains, cell surface modulation, and alternative RNA splicing. Science 236: 799-806

D

Dahm LM, Landmesser LT. (1988) The regulation of intramuscular nerve branching during normal development and following activity blockade. Dev Biol 130:621-644

Dahm LM, Landmesser LT. (1991) The regulation of synaptogenesis during normal development and following activity blockade. J Neurosci 11: 238-255

Darcy KJ, Staras K, Collinson LM, Goda Y. (2006) Constitutive sharing of recycling synaptic vesicles between presynaptic boutons. Nat Neurosci 9: 315-321

Davis GW, Goodman CS. (1998) Synapse specific control of synaptic efficacy at the terminals of a single neuron. Nature 392: 82-86

Davis S., Aldrich TH., Ip NY., Stahl N., Scherer S., et al (1993) Released form of CNTF receptor alpha component as a soluble mediator of CNTF responses. Science. 259: 1736-1739

de Castro BM, De Jaeger X, Martins-Silva C, Lima RD, Amaral E, Menezes C, Lima P, Neves CM, Pires RG, Gould TW, Welch I, Kushmerick C, Guatimosim C,Izquierdo I, Cammarota M, Rylett RJ, Gomez MV, Caron MG, Oppenheim RW, Prado MA, Prado VF. (2009) The vesicular acetylcholine transporter is required for neuromuscular development and function. Mol Cell Biol 29: 5238-5250

Deforges S, Branchu J, Biondi O, Grondard C, Pariset C, Lécolle S, Lopes P, Vidal PP, Chanoine C, Charbonnier F. (2009) Motoneuron survival is promoted by specific exercise in a mouse model of amyotrophic lateral sclerosis. J Physiol 587: 3561-3572

Del Castillo J, Katz B. (1954a) Quantal components of the end-plate potential. J Physiol 124: 560-573

Del Castillo J, Katz B. (1954b) Statistical factors involved in neuromuscular facilitation and depression. J Physiol 124: 574-585

Del Castillo J, Katz B. (1954c) The membrane change produced by the neuromuscular transmitter. J Physiol 125: 546-565

Demireva EY, Shapiro LS, Jessell TM, Zampieri N. (2011) Motor neuron position and topographic order imposed by β- and γ-catenin activities. 147: 641-652

Denker A, Rizzoli SO. (2010) Synaptic vesicle pools: an update. Front Synaptic Neurosci 2: 135

Denzer AJ, Gesemann M, Schumacher B, Ruegg MA. (1995) An amino-terminal extension is required for the secretion of chick agrin and its binding to extracellular matrix. J Cell Biol 131: 1547-1560

DePaiva A., Meunier FA., Molgo J., Aoki KR, Dolly JO. (1999) Functional repair of motor endplates after botulinum neurotoxin type A poisoning: Biphasic switch of synaptic activity between nerve sprouts and their parent terminals. Proc Natl Acad Sci 96:3200-3205

DePaola V., Holtmaat A., Knott G., Song S., Wilbrecht L., Caroni P., Svboda K. (2006) Cell type-specific structural plasticity of axonal branches and boutons in the adult neocortex. Neuron 49: 861-875

Di Giorgio FP, Carrasco MA, Siao MC, Maniatis T, Eggan K. (2007) Non-cell autonomous effect of glia on motoneurons in an embryonic stem cell-based ALS model. Nat Neurosci 10: 608-614

Dimos JT., Rodolfa KT., Niakan KK., Weisenthal LM., Mitsumoto H., Chung W., Croft GF, Saphier G., Leibel R, Goland R., Wichterle H., Henderson CE., Eggan K. (2008) Induced pluripotent stem cells generated from patients with ALS can be differentiated into motoneurons. Science. 321: 1218-1221

Ditlevsen DK, Povlsen GK, Berezin V, Bock E. (2008) NCAM-induced intracellular signaling revisited. J Neurosci Res 86: 727-43.

Dityatev A, Dityateva G, Schachner M. (2000) Synaptic strength as a function of post- versus presynaptic expression of the neural cell adhesion molecule NCAM. Neuron 26: 207-217

Dityatev A, Dityateva G, Sytnyk V, Delling M, Toni N, Nikonenko I, Muller D, Schachner M. (2004) Polysialylated neural cell adhesion molecule promotes remodeling and formation of hippocampal synapses. J Neurosci 24:9372-9382

Doherty P, Fruns M, Seaton P, Dickson G, Barton CH, Sears TA, Walsh FS. (1990) A threshold effect of the major isoforms of NCAM on neurite outgrowth. Nature. 343: 464-466

Doherty P, Moolenaar CE, Ashton SV, Michalides RJ, Walsh FS. (1992) The VASE exon downregulates the neurite growth-promoting activity of NCAM 140. Nature 356: 791-793

Donaldson JG, Finazzi D, Klausner RD. (1992) Brefeldin A inhibits Golgi membrane-catalysed exchange of guanine nucleotide onto ARF protein. Nature 360:350-352

Douglas PM, Dillin A. (2010) Protein homeostasis and aging in neurodegeneration. J Cell Biol 190: 719-729

Douthitt HL, Luo F., McCann SD., Meriney SD. (2011) Dynasore, an inhibitor of dynamin, increases the probability of transmitter release. Neuroscience. 172: 187-195

E

Eberhardt KA, Irintchev A, Al-Majed AA, Simova O, Brushart TM, Gordon T, Schachner M. (2006) BDNF/TrkB signaling regulates HNK-1 carbohydrate expression
in regenerating motor nerves and promotes functional recovery after peripheral nerve repair. Exp Neurol 198: 500-510

Ebert AD, Svendsen CN. (2010) Stem cell model of spinal muscular atrophy. Arch Neurol 67: 665-669

Ebert AD., Yu J., Rose FF Jr., Mattis VB., Lorson CL., Thomson JA., Svendson CN. (2009) Induced pluriopotent stem cells from a spinal muscular atrophy patient. Nature. 457: 277-280

Eckhardt M, Bukalo O, Chazal G, Wang L, Goridis C, Schachner M, Gerardy-Schahn R, Cremer H, Dityatev A. (2000) Mice deficient in the polysialyltransferase ST8SiaIV/PST-1 allow discrimination of the roles of neural cell adhesion molecule protein and polysialic acid in neural development and synaptic plasticity. J Neurosci 20: 5234-5244

Edelman GM, Bencerraf B, Ovary Z, Poulik MD (1961) Structural differences among antibodies of different specificities. Proc Natl Acad Sci USA 47: 1751-1758

Edvardsen K, Chen W, Rucklidge G, Walsh FS, Obrink B, Bock E. (1993) Transmembrane neural cell-adhesion molecule (NCAM), but not glycosyl-phosphatidylinositol-anchored NCAM, down-regulates secretion of matrix metalloproteinases. 90: 11463-11467

Eguchi K, Nakanishi S, Takagi H, Taoufiq Z, Takahashi T. (2012) Maturation of a PKG-Dependent Retrograde Mechanism for Exoendocytic Coupling of Synaptic Vesicles. Neuron 74: 517-529

Elmqvist D, Quastel DM. (1965) Presynaptic action of hemicholinium at the neuromuscular junction. J Physiol 177:463-482

Elmqvist D, Feldman DS. (1965) Calcium dependence of spontaneous acetylcholine release at mammalian motor nerve terminals. J Physiol 181: 487-497

Esposito G., Ana Clara F., Verskreken P. (2012) Synaptic vesicle trafficking and Parkinson's disease. Dev Neurobiol. 72: 134-144

F

Falls DL, Rosen KM, Corfas G, Lane WS, Fischbach GD. (1993) ARIA, a protein that stimulates acetylcholine receptor synthesis, is a member of the neu ligand family. Cell 72: 801-815

Faúndez V, Horng JT, Kelly RB. (1997) ADP ribosylation factor 1 is required for synaptic vesicle budding in PC12 cells. J Cell Biol 138: 505-515

Featherstone DE, Davis WS, Dubreuil, Broadie K. (2001) Drosophila α- and β-spectrin mutations disrupt presynaptic neurotransmitter release. J Neurosci 21:4215-24

Feng Z, Ko CP. (2008) Schwann cells promote synaptogenesis at the neuromuscular junction via transforming growth factor-beta1. J Neurosci 28: 9599-609.

Fernández-Alfonso T, Kwan R, Ryan TA. (2006) Synaptic vesicles interchange their membrane proteins with a large surface reservoir during recycling. Neuron 51: 179-186

Fernández-Chacón R, Wölfel M, Nishimune H, Tabares L, Schmitz F, Castellano-Muñoz M, Rosenmund C, Montesinos ML, Sanes JR, Schneggenburger R,Südhof TC. (2004) The synaptic vesicle protein CSP alpha prevents presynaptic degeneration. Neuron 42: 237-251

Ferri A, Sanes JR, Coleman MP, Cunningham JM, Kato AC. (2003) Inhibiting axon degeneration and synapse loss attenuates apoptosis and disease progression in a mouse model of motoneuron disease. Curr Biol 13: 669-673

Fischbach GD. (1970) Synaptic potentials recorded in cell cultures of nerve and muscle. Science 169: 1331-1333

Fisher TJ, Vrbová G, Wijetunge A. (1989) Partial denervation of the rat soleus muscle at two different developmental stages. Neuroscience 28: 755-63.

Fox MA, Sanes JR, Borza DB, Eswarakumar VP, Fässler R, Hudson BG, John SW, Ninomiya Y, Pedchenko V, Pfaff SL, Rheault MN, Sado Y, Segal Y, Werle MJ, Umemori H. (2007) Distinct target-derived signals organize formation, maturation, and maintenance of motor nerve terminals. Cell 129: 179-193

Frank CA, Kennedy MJ, Goold CP, Marek KW, Davis GW. (2006) Mechanisms underlying the rapid induction and sustained expression of synaptic homeostasis. Neuron 52: 663-677

Franz CK, Rutishauser U, Rafuse VF. (2005) Polysialylated neural cell adhesion molecule is necessary for selective targeting of regenerating motor neurons. J Neurosci 25:2081-2091

Franz CK., Rutishauser U., Rafuse VF. (2008) Intrinsic neuronal properties control selective targeting of regenerating motoneurons. Brain 131: 1492-1505

Frei T, von Bohlen und Halbach F, Wille W, Schachner M. (1992) Different extracellular domains of the neural cell adhesion molecule (N-CAM) are involved in different functions. J Cell Biol 118: 177-194

Frey D., Schneider C, Xu L., Borg J., Spooren W., Caroni P. (2000) Early and selective loss of neuromuscular synapse subtypes with low sprouting competence in motoneuron diseases. J Neurosci 20: 2545-2542

Frischknecht R, Fejtova A, Viesti M, Stephan A, Sonderegger P. (2008) Activity-induced synaptic capture and exocytosis of the neuronal serine protease neurotrypsin. J Neurosci 28: 1568-1579

Fuhrer C, Hall ZW. (1996) Functional interaction of Src family kinases with the acetylcholine receptor in C2 myotubes. J Biol Chem 271: 32474-81.

Futai K., Kim MJ., Hasikawa T., Scheiffele P., Sheng M., Hayashi Y. (2007) Retrograde modulation of presynaptic release probability through signalling mediated by PSD-95- neuroligin. Nat Neurosci. 10: 186-195

G

Gaffield MA, Betz WJ. (2006) Imaging synaptic vesicle exocytosis and endocytosis with FM dyes. Nat Protoc 1: 2916-2921

Gaffield MA, Tabares L, Betz WJ. (2009a) Preferred sites of exocytosis and endocytosis colocalize during high- but not lower-frequency stimulation in mouse motor nerve terminals. J Neurosci 29: 15308-15316

Gaffield MA, Tabares L, Betz WJ. (2009b) The spatial pattern of exocytosis and post-exocytic mobility of synaptopHluorin in mouse motor nerve terminals. J Physiol 587: 1187-1200

Galimberti I, Bednarek E, Donato F, Caroni P. (2010) EphA4 signaling in juveniles establishes topographic specificity of structural plasticity in the hippocampus. Neuron 65: 627-642

García-Junco-Clemente P, Cantero G, Gómez-Sánchez L, Linares-Clemente P, Martínez-López JA, Luján R, Fernández-Chacón R. (2010) Cysteine string protein-alpha prevents activity-dependent degeneration in GABAergic synapses. J Neurosci 30: 7377-7391

Gautam M, Noakes PG, Mudd J, Nichol M, Chu GC, Sanes JR, Merlie JP. (1996) Failure of postsynaptic specialization to develop at neuromuscular junctions of rapsyn-deficient mice. Nature 377: 232-236

Gee SH, Montanaro F, Lindenbaum MH, Carbonetto S. (1994) Dystroglycan-alpha, a dystrophin-associated glycoprotein, is a functional agrin receptor. Cell 77: 675-686

Gillingwater TH, Ingham CA, Coleman MP, Ribchester RR. (2003) Ultrastructural correlates of synapse withdrawal at axotomized neuromuscular junctions in mutant and transgenic mice expressing the Wld gene. J Anat 203: 265-276

Gillingwater TH, Ribchester RR. (2003) The relationship of neuromuscular synapse elimination to synaptic degeneration and pathology: insights from WldS and other mutant mice. J Neurocytol 32: 863-881

Gingras J, Rioux RM, Cuvelier D, Geisse NA, Lichtman JW, Whitesides GM, Mahadevan L, Sanes JR. (2009) Controlling the orientation and synaptic differentiation of myotubes with micropatterned substrates. Biophys J 97: 2771-2779

Gitler D, Cheng Q, Greengard P, Augustine GJ. (2008) Synapsin IIa controls the reserve pool of glutamatergic synaptic vesicles. J Neurosci 28: 10835-10843

Gonzalez LE, Kotler ML, Vattino LG, Conti E, Reisin RC, Mulatz KJ, Snutch TP, Uchitel OD. (2011) Amyotrophic lateral sclerosis-immunoglobulins selectively interact with neuromuscular junctions expressing P/Q-type calcium channels. J Neurochem 119: 826-838

Goold R, Chan KM, Baines AJ. (1995) Coordinated regulation of synapsin I interaction with F-actin by Ca2+/calmodulin and phosphorylation: inhibition of actin binding and bundling. Biochemistry 34: 1912-1920

Gordon T, Yang JF, Ayer K, Stein RB, Tyreman N. (1993) Recovery potential of muscle after partial denervation: a comparison between rats and humans. Brain Res Bull 30: 477-82.

Gordon T, Stein RB. (1982) Time course and extent of recovery in reinnervated motor units of cat triceps surae muscles. J Physiol 323: 307-323

Gordon T., Ly V., Hegedus J., Tyreman N. (2009) Early detection of denervated muscle fibres in hindlimb muscles after sciatic nerve transection in wild type mice and in the G93A mouse model of amyotrophic lateral sclerosis. Neurol Res. 31: 28-42

Gorio A, Carmignoto G, Finesso M, Polato P, Nunzi MG. (1983) Muscle reinnervation--II. Sprouting, synapse formation and repression. Neuroscience 8: 403-16.

Gould TW, Buss RR, Vinsant S, Prevette D, Sun W, Knudson CM, Milligan CE, Oppenheim RW. (2006) Complete dissociation of motor neuron death from motor dysfunction by Bax deletion in a mouse model of ALS. J Neurosci 26: 8774-8786

Grimby L, Hannerz J, Hedman B. (1979) Contraction time and voluntary discharge properties of individual short toe extensor motor units in man. J Physiol 289: 191-201.

Groffen AJ, Martens S, Díez Arazola R, Cornelisse LN, Lozovaya N, de Jong AP, Goriounova NA, Habets RL, Takai Y, Borst JG, Brose N, McMahon HT, Verhage M. (2010) Doc2b is a high-affinity Ca2+ sensor for spontaneous neurotransmitter release. Science 327: 1614-1618

Grumbles RM, Almeida VW, Thomas CK. (2008) Embryonic neurons transplanted into the tibial nerve reinnervate muscle and reduce atrophy but NCAM expression persists. Neurol Res 30: 183-9.

Gu Z, Steinmetz LM, Gu X, Scharfe C, Davis RW, Li WH. (2003) Role of duplicate genes in genetic robustness against null mutations. Nature 421: 63-6.

Guo X, Gonzalez M, Stancescu M, Vandenburgh HH, Hickman JJ.. (2011) Neuromuscular junction formation between human stem-cell-derived motoneurons and rat skeletal muscle in a defined system. Biomaterials 32:9602-9611

H

Haas K, Sin WC, Javaherian A, Li Z, Cline HT. (2001) Single-cell electroporation for gene transfer in vivo. Neuron 29: 583-591

Haase G, Dessaud E, Garcès A, de Bovis B, Birling M, Filippi P, Schmalbruch H, Arber S, deLapeyrière O. (2002) GDNF acts through PEA3 to regulate cell body positioning and muscle innervation of specific motor neuron pools. Neuron 35: 893-905

Hamshere M, Dickson G, Eperon I. (1991) The muscle specific domain of mouse N-CAM: structure and alternative splicing patterns. Nucleic Acids Res. 19:4709-4716

Hanson MG, Landmesser LT. (2006) Increasing the frequency of spontaneous rhythmic activity disrupts pool-specific axon fasciculation and pathfinding of embryonic spinal motoneurons. J Neurosci 26: 12769-12780

Harrelson AL, Goodman CS. (1988) Growth cone guidance in insects: fasciclin II is a member of the immunoglobulin superfamily. Science 242: 700-8.

Hata K., Polo-Parada L., Landmesser LT. (2007) Selective targeting of different neural cell adhesion molecule isoforms during motoneuron-myotube synapse formation in culture and the switch between an immature to mature form of synaptic vesicle cycling. J Neurosci. 27: 14481-14493

Haucke V, Neher E, Sigrist SJ. (2011) Protein scaffolds in the coupling of exocytosis to endocytosis. Nat Rev Neurosci 12: 127-138

Hayworth CR, Moody SE, Chodosh LA, Krieg P, Rimer M, Thompson WJ. (2006) Induction of neuregulin signaling in mouse schwann cells in vivo mimics responses to denervation. J Neurosci 26: 6873-67884

He HT, Barbet J, Chaix JC, Goridis C.(1986) Phosphatidylinositol is involved in the membrane attachment of NCAM-120, the smallest component of the neural cell adhesion molecule. EMBO J 5: 2489-2494

Heeroma JH, Plomp JJ, Roubos EW, Verhage M. (2003) Development of the mouse neuromuscular junction in the absence of regulated secretion. Neuroscience 120:733-744

Hegedus J, Putman CT, Tyreman N, Gordon T. (2008) Preferential motor unit loss in the SOD1 G93A transgenic mouse model of amyotrophic lateral sclerosis. J Physiol 586:3337-51.

Hempel CM., Sivula M., Levenson JM., Rose DM., Li B., Sirianni AC., Xia E., Ryan TA., Gerber DJ., Cottrell JR. (2011) A system for performing high throughput assays of synaptic function. PLoS ONE 6: e25999

Henneman E, Olson CB. (1965) Relations between structure and function in the design of skeletal muscles. J Neurophysiol 28: 581-98.

Heuser JE, Reese TS. (1973) Evidence for recycling of synaptic vesicle membrane during transmitter release at the frogneuromuscular junction. J Cell Biol 57: 315-344

Himes BT, Tessler A. (1989) Death of some dorsal root ganglion neurons and plasticity of others following sciatic nerve section in adult and neonatal rats. J Comp Neurol 284: 215-230

Hippenmeyer S, Huber RM, Ladle DR, Murphy K, Arber S. (2007) ETS transcription factor Erm controls subsynaptic gene expression in skeletal muscles. Neuron 55:726-740

Holt, M., Reidel, D., Stein, A., Shuette, C., Jahn,. R. (2008) Synaptic vesicles are constitutively active fusion machines that function independently of Ca^{2+}. Curr Biol 18: 515-522

Hong SJ, and Chang CC. (1995) Inhibition of acetylcholine release from mouse motor nerve by a P-type calcium channel blocker, omega-agatoxin IVA. J Physiol. 482: 283-290

Hoopfer ED, McLaughlin T, Watts RJ, Schuldiner O, O'Leary DD, Luo L. (2006) Wlds protection distinguishes axon degeneration following injury from naturally occurring developmental pruning. Neuron 50: 883-895

Horstkorte R, Schachner M, Magyar JP, Vorherr T, Schmitz B. (1993) The fourth immunoglobulin-like domain of NCAM contains a carbohydrate recognition domain for oligomannosidic glycans implicated in association with L1 and neurite outgrowth. J Cell Biol 121: 1409-1421

Hua, Z., Leal-Ortiz, S., Foss, S., Waites, C., Garner, C., Voglmaier, S., Edwards, R.H. (2011) vSNARE composition distinguished synaptic vesicle pools. Neuron 71: 474-484

Husmann M, Pietsch T, Fleischer B, Weisgerber C, Bitter-Suermann D. (1989) Embryonic neural cell adhesion molecules on human natural killer cells. Eur J Immunol 19:1761-1763

I

J

Jablonka S, Beck M, Lechner BD, Mayer C, Sendtner M. (2007) Defective Ca2+ channel clustering in axon terminals disturbs excitability in motoneurons in spinal muscular atrophy. J Cell Biol 179: 139-149

James DW, Tresman RL. (1968) De novo formation of neuro-muscular junctions in tissue culture. Nature 220: 384-385

Jessell TM. (2000) Neuronal specification in the spinal cord: inductive signals and transcriptional codes. Nat Rev Genet 1: 20-29

Jevsek M, Jaworski A, Polo-Parada L, Kim N, Fan J, Landmesser LT, Burden SJ. (2006) CD24 is expressed by myofiber synaptic nuclei and regulates synaptic transmission. Proc Natl Acad Sci USA 103: 6374-6379

Jung HH, Lauterburg T, Burgunder JM. (1997) Expression of neurotransmitter genes in rat spinal motoneurons after chemodenervation with botulinum toxin. Neuroscience 78:469-479

K

Kadhiresan VA, Hassett CA, Faulkner JA. (1996) Properties of single motor units in medial gastrocnemius muscles of adult and old rats J Physiol 493: 543-552

Kania A, Johnson RL, Jessell TM. (2000) Coordinate roles for LIM homeobox genes in directing the dorsoventral trajectory of motor axons in the vertebrate limb. Cell 102: 161-173

Kariya S, Park GH, Maeno-Hikichi Y, Leykekhman O, Lutz C, Arkovitz MS, Landmesser LT, Monani UR. (2008) Reduced SMN protein impairs maturation of the neuromuscular junctions in mouse models of spinal muscular atrophy. Hum Mol Genet 17: 2552-2569

Kastanenka KV, Landmesser LT. (2010) In vivo activation of channelrhodopsin-2 reveals that normal patterns of spontaneous activity are required for motoneuron guidance and maintenance of guidance molecules. J Neurosci 30:10575- 10585

Kasthuri N, Lichtman JW. (2003) The role of neuronal identity in synaptic competition. Nature 424: 426-430

Katz E., Ferro PA., Weisz G, Uchitel OD. (1996) Calcium channels involved in synaptic transmission at the mature and regenerating mouse neuromuscular junction. J Physiol 497: 687-697

Katz B, Miledi R. (1968) The role of calcium in neuromuscular facilitation. J Physiol 195: 481-492

Kernell D. The Motoneurone and its Muscle Fibres. New York: Oxford University Press; 2006.

Kieran D, Woods I, Villunger A, Strasser A, Prehn JH. (2007) Deletion of the BH3-only protein puma protects motoneurons from ER stress-induced apoptosis and delays motoneuron loss in ALS mice. Proc Natl Acad Sci USA 104: 20606-20611

Kim N, Stiegler AL, Cameron TO, Hallock PT, Gomez AM, Huang JH, Hubbard SR, Dustin ML, Burden SJ. (2008) Lrp4 is a receptor for Agrin and forms a complex with MuSK. Cell 135: 334-342

Kiris E, Nuss JE, Burnett JC, Kota KP, Koh DC, Wanner LM, Torres-Melendez E, Gussio R, Tessarollo L, Bavari S. (2011) Embryonic stem cell-derived motoneurons provide a highly sensitive cell culture model for botulinum neurotoxin studies, with implications for high-throughput drug discovery. Stem Cell Res 6: 195-205

Kiselyov VV, Soroka V, Berezin V, Bock E. (2005) Structural biology of NCAM homophilic binding and activation of FGFR. J Neurochem 94: 1169-1179

Kleene R, Mzoughi M, Joshi G, Kalus I, Bormann U, Schulze C, Xiao MF, Dityatev A, Schachner M. (2010) NCAM-induced neurite outgrowth depends on binding of calmodulin to NCAM and on nuclear import of NCAM and fak fragments. J Neurosci 30: 10784-10798

Kobayashi H, Robbins N, Rutishauser U. (1992) Neural cell adhesion molecule in aged mouse muscle. Neuroscience 48:237-248

Kochlamazashvili G, Bukalo O, Senkov O, Salmen B, Gerardy-Schahn R, Engel AK, Schachner M, Dityatev A. (2012) Restoration of synaptic plasticity and learning in young and aged NCAM-deficient mice by enhancing neurotransmission mediated by GluN2A-containing NMDA receptors. J Neurosci 32:2263-2275

Koenig JH, Ikeda K. (1989) Disappearance and reformation of synaptic vesicle membrane upon transmitter release observed under reversible blockage of membrane retrieval. J Neurosci 9, 3844-3860

Koirala S, Reddy LV, Ko CP. (2003) Roles of glial cells in the formation, function, and maintenance of the neuromuscular junction. J Neurocytol 32: 987-1002.

Koliatsos VE, Clatterbuck RE, Winslow JW, Cayouette MH, Price DL (1993) Evidence that brain-derived neurotrophic factor is a trophic factor for motor neurons in vivo. Neuron 10: 359-367

Kong L., Wanf X., Choe DW., Polley M., Burnette BG., Bosch-Marcé M., Griffin JW., Rich MM., Sumner CJ. (2009) Impaired synaptic vesicle release and immaturity of neuromuscular junctions in spinal muscular atrophy mice. J Neurosci. 29:842-851

Kopp DM, Perkel DJ, Balice-Gordon RJ. (2000) Disparity in neurotransmitter release probability among competing inputs during neuromuscular synapse elimination. J Neurosci 20: 8771-9.

Korshunova I, Noviskaya V, Kirushko D, Pedersen N, Kolkova K, Kropotova E, et al. (2007) GAP-43 regulates NCAM-180-mediated neurite outgrowth. J Neurochem 100: 1599-1612

Kosarov D. (1974) Vectorelectromyographic control on the position of surface electrodes in relation to active motor units in the human muscles. Acta Physiol Pharmacol Bulg 1: 85-93.

Krueger SR., Kolar A., Fitzsimonds RM. (2003) The presynaptic release apparatus if functional in the absence of dendritic contact and highly mobile within isolated axons. Neuron 40:945-957

Kummer TT, Misgeld T, Lichtman JW, Sanes JR. (2004) Nerve-independent formation of a topologically complex postsynaptic apparatus. J Cell Biol 164: 1077-1087

L

Landmesser L (1978a) The development of motor projection patterns in the chick hind limb. J Physiol 284: 391-414

Landmesser L (1978b) The distribution of motoneurons supplying chick hind limb muscles. J Physiol 284: 371-389

Landmesser L, Dahm L, Schultz K, Rutishauser U. (1988) Distinct roles for adhesion molecules during innervation of embryonic chick muscle. Dev Biol 130: 645-670

Landmesser L, Dahm L, Tang JC, Rutishauser U. (1990) Polysialic acid as a regulator of intramuscular nerve branching during embryonic development. Neuron 4: 655-667

Landmesser L, Morris DG. (1975) The development of functional innervation in the hind limb of the chick embryo. J Physiol 249: 301-326

Landmesser LT (1997) Synaptic plascitiy: fastening synapses by adhesion. Curr Biol 7: R28-R30

Landmesser LT (1998) Synaptic plascitiy: keeping synapses under control. Curr Biol 8: R564-R567

Landmesser LT, Szente M. (1986) Activation patterns of embryonic chick hind-limb muscles following blockade of activity and motoneurone cell death. J Physiol 380: 157-174

Laskowski MB, Colman H, Nelson C, Lichtman JW. (1998) Synaptic competition during the reformation of a neuromuscular map. J Neurosci 18: 7328-7335

Laux T, Fukami K, Thelen M, Golub T, Frey D, Caroni P. (2000) GAP43, MARCKS, and CAP23 modulate PI(4,5)P(2) at plasmalemmal rafts, and regulate cell cortex actin dynamics through a common mechanism. J Cell Biol 149: 1455-72.

Lee, H-K., Yang, Y., Su, Z., Hyeon, C., Lee, T-S., Lee, H-W., Kweon, D-K., Shin, Y-K., Yoon, T-Y. (2010) Dynamic stimulation of vesicle fusion by membrane anchored synaptotagmin 1. Science 328: 1760-763

Leshchyns'ka I., Sytnyk V., Morrow JS., Schachner M. (2003) Neural cell adhesion molecule (NCAM) association with PKCβ_2 via β1 spectrin is implicated in NCAM-mediated outgrowth. J Cell Biol. 161: 625-639

Li XM, Dong XP, Luo SW, Zhang B, Lee DH, Ting AK, Neiswender H, Kim CH, Carpenter-Hyland E, Gao TM, Xiong WC, Mei L. (2008) Retrograde regulation of motoneuron differentiation by muscle beta-catenin. Nat Neurosci 11: 262-268

Lichtman JW, Magrassi L, Purves D. (1987) Visualization of neuromuscular junctions over periods of several months in living mice. J Neurosci 7: 1215-1222

Lichtman JW, Purves D. (1980) The elimination of redundant preganglionic innervation to hamster sympathetic ganglion cells in early post-natal life. J Physiol 301:213-228

Lin W, Burgess RW, Dominguez B, Pfaff SL, Sanes JR, Lee KF. (2001) Distinct roles of nerve and muscle in postsynaptic differentiation of the neuromuscular synapse. Nature 410: 1057-1064

Lin W, Dominguez B, Yang J, Aryal P, Brandon EP, Gage FH, Lee KF. (2005) Neurotransmitter acetylcholine negatively regulates neuromuscular synapse formation by a Cdk5-dependent mechanism. Neuron 46: 569-579

Linnoila J, Wang Y, Yao Y, Wang ZZ. (2008) A mammalian homolog of Drosophila tumorous imaginal discs, Tid1, mediates agrin signaling at the neuromuscular junction. Neuron 60:625-641

Livet J, Sigrist M, Stroebel S, De Paola V, Price SR, Henderson CE, Jessell TM, Arber S. (2002) ETS gene Pea3 controls the central position and terminal arborization of specific motor neuron pools. Neuron 35: 877-892

Livet J, Weissman TA, Kang H, Draft RW, Lu J, Bennis RA, Sanes JR, Lichtman JW. (2007) Transgenic strategies for combinatorial expression of fluorescent proteins in the nervous system. Nature 450: 56-62

Llewellyn ME, Thompson KR, Deisseroth K, Delp SL. (2010) Orderly recruitment of motor units under optical control in vivo. Nat Med 16: 1161-1165

Lorenzetto E, Caselli L, Feng G, Yuan W, Nerbonne JM, Sanes JR, Buffelli M. (2009) Genetic perturbation of postsynaptic activity regulates synapse elimination in developing cerebellum. Proc Natl Acad Sci USA 106: 16475-16480

Lou X, Fan F, Messa M, Raimondi A, Wu Y, Looger LL, Ferguson SM, De Camilli P. (2012) Reduced release probability prevents vesicle depletion and transmission failure at dynaminmutant synapses. Proc Natl Acad Sci USA 109:E515-E523

Love FM, Thompson WJ. (1998) Schwann cell proliferate at rat neuromuscular junctions during development and regeneration. J Neurosci 18: 9376-85.

Love FM, Thompson WJ. (1999) Glial cells promote muscle reinnervation by responding to activity-dependent postsynaptic signals. J Neurosci 19: 10390-6.

Love FM, Son YJ, Thompson WJ. (2003) Activity alters muscle reinnervation and terminal sprouting by reducing the number of Schwann cell pathways that grow to link synaptic sites. J Neurobiol 54:566-576

Lubischer JL, Thompson WJ. (1999) Neonatal partial denervation results in nodal but not terminal sprouting and a decrease in efficacy of remaining neuromuscular junctions in rat soleus muscle. J Neurosci 19: 8931-44.

M

Mack TG, Reiner M, Beirowski B, Mi W, Emanuelli M, Wagner D, Thomson D, Gillingwater T, Court F, Conforti L, Fernando FS, Tarlton A, Andressen C, Addicks K, Magni G, Ribchester RR, Perry VH, Coleman MP. (2001) Wallerian degeneration of injured axons and synapses is delayed by a Ube4b/Nmnat chimeric gene. Nat Neurosci 4: 1199-1206

Maeno-Hikichi Y., Polo-Parada L., Kastanenka KV., Landmesser LT. (2011) Frequency-dependent modes of synaptic vesicle endocytosis and exocytosis at adult mouse neuromuscular junctions. J Neurosci. 31: 1093-1105

Magill CK, Tong A, Kawamura D, Hayashi A, Hunter DA, Parsadanian A, et al. (2007) Reinnervation of the tibialis anterior following sciatic nerve crush injury: a confocal microscopic study in transgenic mice. Exp Neurol 207: 64-74.

Maness PF, Schachner M. (2007) Neural recognition molecules of the immunoglobulin superfamily: signaling transducers of axon guidance and neuronal migration. Nat Neurosci 10: 19-26

Marchetto MC, Muotri AR, Mu Y, Smith AM, Cezar GG, Gage FH. (2008) Non-cell-autonomous effect of human SOD1 G93R astrocytes on motoneurons derived from human embryonic stem cells. Cell Stem Cell 3: 649-657

Marques KB, Santos LM, Oliveira AL.(2006) Spinal motoneuron synaptic plasticity during the course of an animal model of multiple sclerosis. Eur J Neurosci 24: 3035-3062

Marteyn A, Maury Y, Gauthier MM, Lecuyer C, Vernet R, Denis JA, Pietu G, Peschanski M, Martinat C. (2011) Mutant human embryonic stem
cells reveal neurite and synapse formation defects in type 1myotonic dystrophy. Cell Stem Cell 8: 434-444

Martin, AR. (1955) A further study of the statistical composition of the endplate potential. J Physiol 130; 560-573

Martinez-Arca S., Alberts P., Zahraoui A., Louvard D., Galli T. (2000) Role of tetanus neurotoxin insensitive vesicle-associated membrane protein (TI-VAMP) in vesicular transport mediating neurite outgrowth. J Cell Biol 149: 889-900

Martinez-Arca S., Coco S., Mainguy G., Schenk U., Alberts P., Bouille P., Mezzina M., Prochiantz A., Matteoli M., Louvard D., Galli T. (2001) A common exocytotic mechanism mediates axonal and dendritic outgrowth. J Neurosci. 21: 3830-3838

Martini R, Schachner M. (1986) Immunoelectron microscopic localization of neural cell adhesion molecules (L1, N-CAM, and MAG) and their shared carbohydrate epitope and myelin basic protein in developing sciatic nerve. J Cell Biol 103: 2439-48.

Martinou JC, Merlie JP. (1991) Nerve-dependent modulation of acetylcholine receptor epsilon-subunit gene expression. J Neurosci 11; 1291-1299

Maselli RA, Wollman RL, Leung C, Distad B, Palombi S, Richman DP, et al. (1993) Neuromuscular transmission in amyotrophic lateral sclerosis. Muscle Nerve 16: 1193-1203.

Mattson MP, Kater SB. (1987) Calcium regulation of neurite elongation and growth cone motility. J Neurosci 7: 4034-4043

McCann CM, Nguyen QT, Santo Neto H, Lichtman JW. (2007) Rapid synapse elimination after postsynaptic protein synthesis inhibition in vivo. J Neurosci 27: 6064-6067

McLachlan EM, Martin AR. (1981) Non-linear summation of end-plate potentials in the frog and mouse. J Physiol 311:307-324

Mehta A, Reynolds ML, Woolf CJ. (1993) Partial denervation of the medial gastrocnemius muscle results in growth-associated protein-43 immunoreactivity in sprouting axons and Schwann cells. Neuroscience 57: 433-442

Meier T., Hauser DM., Chiquet M., Landmann L., Ruegg MA., Brenner HR. (1997) Neural agrin induces ectopic postsynaptic specializations in innervated muscle fibers. *J Neuro*sci. 17, 6534-6544

Meiri KF, Saffell JL, Walsh FS, Doherty P. (1998) Neurite outgrowth stimulated by neural cell adhesion molecules requires growth associated protein-43 (GAP-43) function and is associated with GAP-43 phosphorylation in growth cones. J Neurosci 18: 10429-37.

Meyer MP, Smith SJ. (2006) Evidence from in vivo imaging that synaptogenesis guides the growth and branching of axonal arbors by two distinct mechanisms. J Neurosci 26: 3604-3614

Miledi R, Slater CR. (1970) On the degeneration of rat neuromuscular junctions after nerve section. J Physiol 207: 507-528

Miles GB., Yohn DC., Wichterle H., Jessell TM., Rafuse VF., Brownstone RM. (2004) Functional properties of motoneurons derived from mouse embryonic stem cells. J Neurosci 24: 7848-7858

Milev P, Maurel P, Häring M, Margolis RK, Margolis RU. (1994) TAG-1/axonin-1 is a high-affinity ligand of neurocan, phosphacan/protein-tyrosine phosphatase-zeta/beta, and N-CAM. J Biol Chem 271: 15716-15723

Miller TM., Heuser JE. (1984) Endocytosis of synaptic vesicle membrane at the frog neuromuscular junction. J Cell Biol 98: 685-698

Milner-Brown HS, Stein RB. (1975) The relation between the surface electromyogram and muscular force. J Physiol 246: 549-69.

Miñana R, Duran JM, Tomas M, Renau-Piqueras J, Guerri C. (2001) Neural cell adhesion molecule is endocytosed via a clathrin-dependent pathway. Eur J Neurosci 13: 749-756

Miniou P, Tiziano D, Frugier T, Roblot N, Le Meur M, Melki J (1999) Gene targeting restricted to mouse striated muscle lineage. Nucleic Acids Res 27:e27

Misgeld T, Burgess RW, Lewis RM, Cunningham JM, Lichtman JW, Sanes JR. (2002) Roles of neurotransmitter in synapse formation: development of neuromuscular junctions lacking choline acetyltransferase. Neuron 36: 635-648

Misgeld T, Kummer TT, Lichtman JW, Sanes JR. (2005) Agrin promotes synaptic differentiation by counteracting an inhibitory effect of neurotransmitter. Proc Natl Acad Sci USA 102: 11088-11093

Mishina M, Takai T, Imoto K, Noda M, Takahashi T, Numa S, Methfessel C, Sakmann B. (1986) Molecular distinction between fetal and adult forms of muscle acetylcholine receptor. Nature 321: 406-411

Missias AC., Chu GC., Klocke BJ., Sanes JR., Merlie JP. (1996) Maturation of the acetylcholine receptor in skeletal muscle: Regulation of the AChR γ-to ε switch. Dev Biol 179:223-238

Mórotz GM, De Vos KJ, Vagnoni A, Ackerley S, Shaw CE, Miller CC. (2012) Amyotrophic lateral sclerosis-associated mutant VAPBP56S perturbs calcium homeostasis to disrupt axonal transport of mitochondria. Hum Mol Genet 21: 1979-1988

Moscoso LM, Cremer H., Sanes JR. (1998) Organization and reorganization of neuromuscular junctions in mice lacking neural cell adhesion molecule, tenascin C and fibroblast growth factor 5. J Neurosci. 18: 1465-1477

Muller D, Wang C, Skibo G, Toni N, Cremer H, Calaora V, Rougon G, Kiss JZ. (1996) PSA-NCAM is required for activity-induced synaptic plasticity. Neuron 17: 413-422

Murray LM, Comley LH, Thomson D, Parkinson N, Talbot K, Gillingwater TH. (2008) Selective vulnerability of motor neurons and dissociation of pre- and post-synaptic pathology at the neuromuscular junction in mouse models of spinal muscular atrophy. Hum Mol Genet 17, 949-962

Myers CP, Lewcock JW, Hanson MG, Gosgnach S, Aimone JB, Gage FH, Lee KF, Landmesser LT, Pfaff SL. (2005) Cholinergic input is required during embryonic development to mediate proper assembly of spinal locomotor circuits. Neuron 46: 37-49

N

Nagai M, Re DB, Nagata T, Chalazonitis A, Jessell TM, Wichterle H, Przedborski S. (2007) Astrocytes expressing ALS-linked mutated SOD1 release factors selectively toxic to motoneurons. Nat Neurosci 10: 615-622

Neves G., Gomis A., Lagnado L. (2001) Calcium influx selects the fast mode of endocytosis in the synaptic terminal of retinal bipolar cells. Proc Natl Acad Sci USA 98: 15282-15287

Newton AJ, Kirchhausen T, Murthy VN. (2009) Inhibition of dynamin completely blocks compensatory synaptic vesicle endocytosis. PNAS 103: 17955-17960

Nguyen QT, Sanes JR, Lichtman JW. (2002) Pre-existing pathways promote precise projection patterns. Nat Neurosci 5:861-867

Nguyen QT., Son Y-J., Sanes JR., Lichtman JW. (2000) Nerve terminals form but fail to mature when postsynaptic differentiation is blocked : In vivo analysis using mammalian nerve-muscle chimeras. J Neurosci 20:6077-6086

Nieke J, Schachner M. (1985) Expression of the neural cell adhesion molecules L1 and N-CAM and their common carbohydrate epitope L2/HNK-1 during development and after transection of the mouse sciatic nerve. Differentiation 30: 141-51.

Nielsen J, Gotfryd K, Li S, Kulahin N, Soroka V, Rasmussen KK, Bock E, Berezin V. (2009) Role of glial cell line-derived neurotrophic factor (GDNF)-neural cell adhesion molecule (NCAM) interactions in induction of neurite outgrowth and identification of a binding site for NCAM in the heel region of GDNF. J Neurosci 29: 11360-11376

Niethammer P, Delling M, Sytnyk V, Dityatev A, Fukami K, Schachner M. (2002) Cosignaling of NCAM via lipid rafts and the FGF receptor is required for neuritogenesis. J Cell Biol 157:521-532

Nishimune H, Sanes JR, Carlson SS. (2004) A synaptic laminin-calcium channel interaction organizes active zones in motor nerve terminals. Nature 432: 580-587

Nitkin RM, Smith MA, Magill C, Fallon JR, Yao YM, Wallace BG, McMahan UJ. (1987) Identification of agrin, a synaptic organizing protein from Torpedo electric organ. J Cell Biol 105: 2471-2478

Noble M, Albrechtsen M, Møller C, Lyles J, Bock E, Goridis C, Watanabe M, Rutishauser U. (1985) Glial cells express N-CAM/D2-CAM-like polypeptides in vitro. Nature 316: 725-728

O

O'Brien RA, Ostberg AJ, Vrbová G. (1978) Observations on the elimination of polyneuronal innervation in developing mammalian skeletal muscle. J Physiol 282:571-582

Okada K, Inoue A, Okada M, Murata Y, Kakuta S, Jigami T, Kubo S, Shiraishi H, Eguchi K, Motomura M, Akiyama T, Iwakura Y, Higuchi O, Yamanashi Y. (2006) The muscle protein Dok-7 is essential for neuromuscular synaptogenesis. Science 312: 1802-1805

Orenbuch A, Shalev L, Marra V, Sinai I, Lavy Y, Kahn J, Burden JJ, Staras K, Gitler D. (2012) Synapsin selectively controls the mobility of resting pool vesicles at hippocampal terminals. J Neurosci 32: 3969-3980

P

Paratcha G, Ledda F, Ibáñez CF. (2003) The neural cell adhesion molecule NCAM is an alternative signaling receptor for GDNF family ligands. Cell 113: 867-879

Patton BL, Miner JH, Chiu AY, Sanes JR. (1997) Distribution and function of laminins in the neuromuscular system of developing, adult, and mutant mice. J Cell Biol 139: 1507- 1521

Peck D, Walsh FS. (1993) Differential effects of over-expressed neural cell adhesion molecule isoforms on myoblast fusion. J Cell Biol 123: 1587-1595

Perrissinotti PP., Guigovaz Tropper B., Uchitel OD. (2008) L-type calcium channels are involved in fast endocytosis at the mouse neuromuscular junction. Eur J Neurosci 27:1333-1344

Petersen SA, Fetter RD, Noordermeer JN, Goodman CS, DiAntonio A. (1997) Genetic analysis of glutamate receptors in Drosophila reveals a retrograde signal regulating presynaptic transmitter release. Neuron 19: 1237- 1248

Pielage J., Fetter RD., Davis GW. (2005) Presynaptic spectrin is essential for synapse stabilization. Curr Biol 15: 918-928

Plomp JJ, van Kempen GT, Molenaar PC. (1992) Adaptation of quantal content to decreased postsynaptic sensitivity at single endplates in alpha-bungarotoxin-treated rats. J Physiol 458: 487-499

Pollerberg GE, Burridge K, Krebs KE, Goodman SR, Schachner M. (1987) The 180-kD component of the neural cell adhesion molecule N-CAM is involved in cell-cell contacts and cytoskeleton-membrane interactions. Cell Tissue Res 250: 227-36.

Polo-Parada L., Bose CM., Landmesser LT. (2001) Alterations in transmission machinery, vesicle dynamics, and transmitter release machinery at NCAM-deficient neuromuscular junctions. Neuron 32: 815-828

Polo-Parada L., Bose CM., Plattner F., Landmesser LT. (2004) Distinct roles of different neural cell adhesion molecule (NCAM) isoforms in synaptic maturation revealed by analysis of NCAM 180kd isoform-deficient mice. J Neurosci 24:1852-1864

Polo-Parada L., Plattner F., Bose C., Landmesser LT. (2005) NCAM180 acting via a conserved C terminal domain and MLCK is essential for effective transmission with repetitive stimulation. Neuron 46:917-931

Porter BE, Weis J, Sanes JR. (1995) A motoneuron-selective stop signal in the synaptic protein S-laminin. Neuron 14:549-559

Probstmeier R, Fahrig T, Spiess E, Schachner M. (1992) Interactions of the neural cell adhesion molecule and the myelin-associated glycoprotein with collagen type I: involvement in fibrillogenesis. J Cell Biol 116: 1063-1070

Probstmeier R, Kühn K, Schachner M. (1989) Binding properties of the neural cell adhesion molecule to different components of the extracellular matrix. J Neurochem 53: 1794-1801

Proszynski TJ, Gingras J, Valdez G, Krzewski K, Sanes JR. (2009) Podosomes are present in a postsynaptic apparatus and participate in its maturation. Proc Natl Acad Sci USA 106: 18373-1878

Pun S, Santos AF, Saxena S, Xu L, Caroni P. (2006) Selective vulnerability and pruning of phasic motoneuron axons in motoneuron disease alleviated by CNTF. Neuron 9: 408-419

Q

Quinlan KA, Schuster JE, Fu R, Siddique T, Heckman CJ. (2011) Altered postnatal maturation of electrical properties in spinal motoneurons in a mouse model of amyotrophic lateral sclerosis. J Physiol 589: 2245-2260

R

Rafuse VF, Polo-Parada L, Landmesser LT. (2000) Structural and functional alterations of neuromuscular junctions in NCAM-deficient mice. J Neurosci 20: 6529-39.

Rafuse VF, Gordon T, Orozco R. (1992) Proportional enlargement of motor units after partial denervation of cat triceps surae muscles. J Neurophysiol 68: 1261-1276

Rafuse VF, Gordon T. (1996) Self-reinnervated cat medial gastrocnemius muscles. I. comparisons of the capacity for regenerating nerves to form enlarged motor units after extensive peripheral nerve injuries. J Neurophys 75: 268-281

Rafuse VF, Landmesser LT. (2000) The pattern of avian intramuscular nerve branching is determined by the innervating motoneuron and its level of polysialic acid. J Neurosci 20: 1056-1065

Rafuse VF, Milner LD, Landmesser LT. (1996) Selective innervation of fast and slow muscle regions during early chick neuromuscular development. J Neurosci 16:6864-6877

Rafuse VF., Landmesser LT. (1996) Contractile activity regulates isoform expression and polysialyation of NCAM in cultured myotubes: Involvement of Ca2+ and protein kinase C. J Cell Biol. 132: 969-983

Ramirez DM., Khvotchev M., Trauterman B, Kavalali ET. (2012) Vti1a identifies a vesicle pool that preferentially recycles at rest and maintains spontaneous neurotransmission. Neuron 73: 121-134

Ratnayaka A, Marra V, Branco T, Staras K. (2011) Extrasynaptic vesicle recycling in mature hippocampal neurons. Nat Commun 2: 531

Ratnayaka A, Marra V, Bush D, Burden JJ, Branco T, Staras K. (2012) Recruitment of resting vesicles into recycling pools supports NMDA receptor-dependent synaptic potentiation in cultured hippocampal neurons. J Physiol 590: 1585-1597

Reddy LV, Koirala S, Sugiura Y, Herrera AA, Ko C-P. (2003) Glial cells maintain synaptic structure and function and promote development of the neuromuscular junction in vivo. Neuron 40: 563-80.

Redfern PA. (1970) Neuromuscular transmission in new-born rats. J Physiol 209: 701-709

Reid B, Slater CR, Bewick GS. (1999) Synaptic vesicle dynamics in rat fast and slow motor nerve terminals. J Neurosci 19:2511-2521

Reiff DF, Thiel PR, Schuster CM. (2002) Differential regulation of active zone density during long-term strengthening of Drosophila neuromuscular junctions. J Neurosci 22: 9399-9409

Reist NE, Werle MJ, McMahan UJ. (1992) Agrin released by motor neurons induces the aggregation of acetylcholine receptors at neuromuscular junctions. Neuron 8: 865-868

Reynolds ML, Woolf CJ. (1992) Terminal Schwann cells elaborate extensive processes following denervation of the motor endplate. J Neurocytol 21: 50-66.

Ribchester RR, Taxt T. (1983) Motor unit size and synaptic competition in rat lumbrical muscles reinnervated by active and inactive motor axons. J Physiol 344: 89-111

Rich MM, Wang X, Cope TC, Pinter MJ. (2002) Reduced neuromuscular quantal content with normal synaptic release time course and depression in canine motor neuron disease. J Neurophysiol 88: 3305-14.

Richards DA., Gautimosim C., Betz WJ. (2000) Two endocytic recycling routes fill two vesicle pools in frog motor terminals. Neuron 27:551-559

Richards DA., Gautimosim C., Rizzoli SO., Betz WJ. (2003) Synaptic vesicle pools at the frog neuromuscular junction. Neuron 39:529-541

Rieger F, Grumet M, Edelman GM. (1985) N-CAM at the vertebrate neuromuscular junction. J Cell Biol 101: 285-293

Rieger F, Nicolet M, Pinçon-Raymond M, Murawsky M, Levi G, Edelman GM. (1988) Distribution and role in regeneration of N-CAM in the basal laminae of muscle and Schwann cells. J Cell Biol 107: 707-719

Rizzoli SO, Betz WJ. (2004) The structural organization of the readily releasable pool of synaptic vesicles. Science 303: 2037-2039

Rizzoli SO, Betz WJ. (2005) Synaptic vesicle pools. Nat Rev Neurosci 6: 57-69

Robbins N, Yonezawa T. (1971) Physiological studies during formation and development of rat neuromuscular junctions in tissue culture. J Gen Physiol 58: 467-481

Robitaille R. (1998) Modulation of synaptic efficacy and synaptic depression by glial cells at the frog neuromuscular junction. Neuron 21: 847-55.

Robitaille R, Bourque MJ, Vandaele S. (1996) Localization of L-type Ca2+ channels at perisynaptic glial cell sof the frog neuromuscular junction. J Neurosci 16: 148-158

Robitaille R, Tremblay JP. (1991) Non-uniform responses to Ca2+ along the frog neuromuscular junction: effects on the probability of spontaneous and evoked transmitter release. Neuroscience 40: 571-585

Rochel S., Robbins N. (1988) Effects of partial denervation and terminal field expansion on neuromuscular transmitter release and nerve terminal structure. J Neurosci 8:332-338

Rosa JM., Conde M., Nanclares C., Orozco A., Colmena I., dePascual R., Garcia AG., Gandia L. (2011a) Paradoxical facilitation of exocytosis by inhibition of the L-type calcium channels of bovine chromaffin cells. Biochem Biophy Res Commun. 410: 307-311

Rosa JM., Torregrosa-Hetland CJ., Colmena I., Gutierrez LM., Garcia AG., Gandia L. (2011b) Calcium entry through slow inactivating calcium channels prefentially triggers endocytosis rather than exocytosis in bovine chromaffin cells. Am J Physiol Cell Physiol 301: C86-98

Rowley KL, Mantilla CB, Ermilov LG, Sieck GC. (2007) Synaptic vesicle distribution and release at rat diaphragm neuromuscular junctions. J Neurophysiol 98: 478-487

Rozas JL, Gómez-Sánchez L, Mircheski J, Linares-Clemente P, Nieto-González JL, Vázquez ME, Luján R, Fernández-Chacón R. (2012) Motorneurons Require Cysteine String Protein-α to Maintain the Readily Releasable Vesicular Pool and Synaptic Vesicle Recycling. Neuron 74: 151-165

Rubinsztein DC. (2006) The roles of intracellular protein-degradation pathways in neurodegeneration. Nature 443: 780-786

Ruiz R, Casañas JJ, Torres-Benito L, Cano R, Tabares L. (2010) Altered intracellular Ca2+ homeostasis in nerve terminals of severe spinal muscular atrophy mice. J Neurosci 30: 849-857

Ruiz R., Cano R., Casanas JJ., Gaffield MA., Betz WJ., Tabares L. (2011) Active zones and the readily releasable pool of synaptic vesicles at the neuromuscular junction of the mouse. J Neurosci 31: 2000-2008

Ruthazer ES, Akerman CJ, Cline HT. (2003) Control of axon branch dynamics by correlated activity in vivo. Science 301:66-70

Ruthazer ES, Li J, Cline HT. (2006) Stabilization of axon branch dynamics by synaptic maturation. J Neurosci 26: 3594-3603

Rutishauser U, Hoffman S, Edelman GM. (1982) Binding properties of a cell adhesion molecule from neural tissue. Proc Natl Acad Sci 79:685-689

Rutishauser U, Landmesser L. (1996) Polysialic acid in the vertebrate nervous system: a promoter of plasticity in cell-cell interactions. Trends Neurosci 19:422-427

S

Sadasivam G, Willmann R, Lin S, Erb-Vögtli S, Kong XC, Rüegg MA, et al. (2005) Src-family kinases stabilize the neuromuscular synapse in vivo via protein interactions, phosphorylation, and cytoskeletal linkage of acetylcholine receptors. J Neurosci 25: 10479-93.

Sadoul K, Meyer A, Low MG, Schachner M. (1986) Release of the 120 kDa component of the mouse neural cell adhesion molecule N-CAM from cell surfaces by phosphatidylinositol-specific phospholipase C. Neurosci Lett 72: 341-346

Saffell JL, Williams EJ, Mason IJ, Walsh FS, Doherty P. (1997) Expression of a dominant negative FGF receptor inhibits axonal growth and FGF receptor phosphorylation stimulated by CAMs. Neuron 18: 231-242

Saito M., Schwartz TL., Umbach JA., Gunderson CB., Kidokoro Y. (2001) Absence of junctional glutamate receptor clusters in Drosophila mutants lacking spontaneous transmitter release. Science 293:514-517

Sala C, O'Malley J, Xu R, Fumagalli G, Salpeter MM. (1997) Epsilon subunit-containing acetylcholine receptors in myotubes belong to the slowly degrading population. J Neurosci 17: 8937-8944

Sandrock AW Jr, Dryer SE, Rosen KM, Gozani SN, Kramer R, Theill LE, Fischbach GD.(1997) Maintenance of acetylcholine receptor number by neuregulins at the neuromuscular junction in vivo. Science 276: 599-603

Sanes JR, Engvall E, Butkowski R, Hunter DD. (1990) Molecular heterogeneity of basal laminae: isoforms of laminin and collagen IV at theneuromuscular junction and elsewhere. J Cell Biol 111:1685-1699

Sanes JR, Lichtman JW. (2001) Induction, assembly, maturation and maintenance of a postsynaptic apparatus. Nat Rev Neurosci 2: 791-805

Sanes JR, Marshall LM, McMahan UJ. (1978) Reinnervation of muscle fiber basal lamina after removal of myofibers. Differentiation of regenerating axons at original synaptic sites. J Cell Biol 78: 176-178

Sann SB, Xu L, Nishimune H, Sanes JR, Spitzer NC. (2008) Neurite outgrowth and in vivo sensory innervation mediated by a Ca(V)2.2-laminin beta 2 stop signal. J Neurosci 28: 2366-2374

Sara Y., Virmani T., Deak F., Liu X., Kavalali ET. (2005) An isolated pool of synaptic vesicles recycles at rest and drives spontaneous neurotransmission. Neuron 45:563-573

Saxena S, Cabuy E, Caroni P. (2009) A role for motoneuron subtype-selective ER stress in disease manifestations of FALS mice. Nat Neurosci 12: 627-636

Schaefer AM., Sanes JR., Lichtman JW. (2005) A compensatory subpopulation of motoneurons in a mouse model of Amyotrophic Lateral Sclerosis. J Comp Neurol 490: 209-219

Schäfer R, Wernig A. (1998) Polyclonal antibodies against NCAM reduce paralysis-induced axonal sprouting. J Neurocytol 27:615-624

Schmalbruch H, al-Amood WS, Lewis DM. (1991) Morphology of long-term denervated rat soleus muscle and the effect of chronic electrical stimulation. J Physiol 441: 233-41.

Schuster CM, Davis GW, Fetter RD, Goodman CS. (1996) Genetic dissection of structural and functional components of synaptic plasticity. I. Fasciclin II controls synaptic stabilization and growth. Neuron 17: 641-54.

Searl TJ., Silinsky EM. (2003) Phorbol esters and adenosine affect the readily releasable neurotransmitter pool by different mechanisms at amphibian motor nerve endings. J Physiol 553: 445-456

Shakiryanova D, Klose MK, Zhou Y, Gu T, Deitcher DL, Atwood HL, Hewes RS, Levitan ES. (2007) Presynaptic ryanodine receptor-activated calmodulin kinase II increases vesicle mobility and potentiates neuropeptide release. J Neurosci 27: 7799-7806

Shakiryanova D, Tully A, Levitan ES. (2006) Activity-dependent synaptic capture of transiting peptidergic vesicles. Nat Neurosci 9:896-900

Shapira M, Zhai RG, Dresbach T, Bresler T, Torres VI, Gundelfinger ED, Ziv NE, Garner CC. (2003) Unitary assembly of presynaptic active zones from Piccolo-Bassoon transport vesicles. Neuron 38:237-252

Shin JE, Cho Y, Beirowski B, Milbrandt J, Cavalli V, Diantonio A. (2012) Dual leucine zipper kinase is required for retrograde injury signaling and axonal regeneration. Neuron 74: 1015-1022

Sigrist SJ, Thiel PR, Reiff DF, Lachance PE, Lasko P, Schuster CM. (2000) Postsynaptic translation affects the efficacy and morphology of neuromuscular junctions. Nature 405:1062-1065

Silinsky EM, Mellow AM, Phillips TE. (1977) Conventional calcium channel mediates asynchronous acetylcholine release by motor nerve impulses. Nature 270: 528-530

Smillie KJ, Evans GJ, Cousin MA. (2005) Developmental change in the calcium sensor for synaptic vesicle endocytosis in central nerve terminals. J Neurochem 94: 452-458

Smillie KJ., Cousin MA. (2005) Dynamin I phosphorylation and the control of synaptic vesicle endocytosis. Biochem Soc Symp. 72: 87-97

Smith CL, Mittaud P, Prescott ED, Fuhrer C, Burden SJ.(2001) Src, Fyn, and Yes are not required for neuromuscular synapse formation but are necessary for stabilization of agrin-induced clusters of acetylcholine receptors. J Neurosci 21: 3151-60

Smith DO. (1984) Acetylcholine storage, release and leakage at the neuromuscular junction of mature adult and aged rats. J Physiol 347: 161-176

Snider J, Pillai A, Stevens CF. (2010) A universal property of axonal and dendritic arbors. Neuron 66: 45-56

Son EY, Ichida JK, Wainger BJ, Toma JS, Rafuse VF, Woolf CJ, Eggan K. (2011) Conversion of mouse and human fibroblasts into functional spinal motor neurons. Cell Stem Cell 9: 205-218

Son Y-J., Thompson WJ. (1995a) Schwann cell processes guide reinnervation of peripheral axons. Neuron. 13: 125-132

Son Y-J., Thompson WJ. (1995b) Nerve sprouting in muscle is induced and guided by processes extend by terminal Schwann cells. Neuron. 13: 133-141

Song JW, Misgeld T, Kang H, Knecht S, Lu J, Cao Y, Cotman SL, Bishop DL, Lichtman JW. (2008) Lysosomal activity associated with developmental axon pruning. J Neurosci 28:8993-9001

Soundararajan P, Fawcett JP, Rafuse VF. (2010) Guidance of postural motoneurons requires MAPK/ERK signaling downstream of fibroblast growth factor receptor 1. J Neurosci 30: 6595-6606

Soundararajan P, Lindsey BW, Leopold C, Rafuse VF. (2007) Easy and rapid differentiation of embryonic stem cells into functional motoneurons using sonic hedgehog-producing cells. Stem Cells 25:1697-1706

Soundararajan P., Miles GB., Rubin LL., Brownstone RM., Rafuse VF (2006) Motoneurons dervived from embryonic stem cells express transcription factors and develop phenotypes characteristic of medial motor column neurons. J Neurosci. 26: 3256-3268

Staras K., Branco T., Burden JJ., Pozo K., Darcy K., Marra V., Ratnayaka A., Goda Y. (2010) A vesicle superpool spans multiple presynaptic terminals in hippocampal neurons. Neuron 66:37-44

Stein, A., Radhakrishnan, A., Riedel, D., Fasshauer, D., and Jahn, R. (2007). Synaptotagmin activates membrane fusion through a Ca^{2+}-dependent trans interaction with phospholipids. Nat Struct Mol Biol 14: 904–91

Stewart BA, Schuster CM, Goodman CS, Atwood HL. (1996) Homeostasis of synaptic transmission in Drosophila with genetically altered nerve terminal morphology. J Neurosci 16:3877-3886

Storms SD, Kim AC, Tran BH, Cole GJ, Murray BA. (1996) NCAM-mediated adhesion of transfected cells to agrin. Cell Adhes Commun 3: 497-509

Storms SD, Rutishauser U. (1998) A role for polysialic acid in neural cell adhesion molecule heterophilic binding to proteoglycans. J Biol Chem 273: 27124-27129

Sugiura Y., Ko CP. (1997) Novel modulatory effect of L-type calcium channels at newly formed neuromuscular junctions. J Neurosci 17: 1101-1111

Sun Y, Bamji SX. (2011) β-Pix modulates actin-mediated recruitment of synaptic vesicles to synapses. J Neurosci 31: 17123-17133

Sutton MA., Ito HT., Cressy P., Kempf C., Woo JC., Schuman EM. (2006) Miniature neurotransmission stabilizes synaptic function via tonic suppression of local dendritic protein synthesis. Cell 125:785-799

Swash M, Schwartz MS. Biopsy Pathology of Muscle. London: Chapman and Hall; 1984.

Sypert GW, Munson JB. (1981) Basis of segmental motor control: motoneuron size or motor unit type? Neurosurgery 8:608-621

Sytnyk V, Leshchyns'ka I, Delling M, Dityateva G, Dityatev A, Schachner M. (2002) Neural cell adhesion molecule promotes accumulation of TGN organelles at sites of neuron-to-neuron contacts. J Cell Biol 159: 649-661

Sytnyk V, Leshchyns'ka I, Nikonenko AG, Schachner M. (2006) NCAM promotes assembly and activity-dependent remodeling of the postsynaptic signaling complex. J Cell Biol 174: 1071-1085

T

Takahashi T, Nakajima Y, Hirosawa K, Nakajima S, Onodera K. (1987) Structure and physiology of developing neuromuscular synapses in culture. J Neurosci 7: 473-481

Takamori S., Holt M., Stenius K., Lemke EA., Gronborg M., et al (2006) Molecular anatomy of a trafficking organelle. Cell 127: 831-846

Takeichi, M (2007) The cadherin superfamily in neuronal connections and interactions. Nat Rev Neurosci 8: 11-20

Tam SI., Archibald V., Jassar B., Tyreman N., Gordon T. (2001) Increased neuromuscular activity reduces sprouting in partially denervated muscles. J Neurosci 21:654-667

Tam SL, Gordon T. (2003) Neuromuscular activity impairs axonal sprouting in partially denervated muscles by inhibiting bridge formation of perisynaptic Schwann cells. J Neurobiol 57:221-234

Tang J, Landmesser L, Rutishauser U. (1992) Polysialic acid influences specific pathfinding by avian motoneurons. Neuron 8: 1031-1044

Tapia JC, Wylie JD, Kasthuri N, Hayworth KJ, Schalek R, Berger DR, Guatimosim C, Seung HS, Lichtman JW. (2012) Pervasive synaptic branch removal in the mammalian neuromuscular system at birth. Neuron 74: 816-829

Tarsa L., Goda Y. (2002) Synaptophysin regulates activity dependent synapse formation in cultured hippocampal neurons. PNAS 99: 1012-1016

Teeter CM, Stevens CF. (2011) A general principle of neural arbor density Curr Biol 21: 2105-2106

Thelen K, Georg T, Bertuch S, Zelina P, Pollerberg GE. (2008) Ubiquitination and endocytosis of cell adhesion molecule DM-GRASP regulate its cell surface presence and affect its role for axon navigation. J Cell Biol 283:32792-32801

Thiery JP, Brackenbury R, Rutishauser U, Edelman GM. (1977) Adhesion among neural cells of the chick embryo. II. Purification and characterization of a cell adhesion molecule from neural retina. J Biol Chem 252: 6841-6845

Thompson J, Dickson G, Moore SE, Gower HJ, Putt W, Kenimer JG, Barton CH, Walsh FS. (1989) Alternative splicing of the neural cell adhesion molecule gene generates variant extracellular domain structure in skeletal muscle and brain. Genes Dev 3: 348-357

Thompson W, Jansen JK. (1977) The extent of sprouting of remaining motor units in partly denervated immature and adult rat soleus muscle. Neuroscience 2: 523-35.

Thomson SR, Wishart TM, Patani R, Chandran S, Gillingwater TH. (2012) Using induced pluripotent stem cells (iPSC) to model human neuromuscular connectivity: promise or reality? J Anat 220: 122-130

Todd KJ, Darabid H, Robitaille R. (2010) Perisynaptic glia discriminate patterns of motor nerve activity and influence plasticity at the neuromuscular junction. J Neurosci 30: 11870-11882

Tonge DA. (1974) Physiological characteristics of re-innervation of skeletal muscle in the mouse. J Physiol 24: 141-153

Totosy de Zepetnek JE, Gordon T, Stein RB, Zung HV. (1991) Comparison of force and EMG measures in normal and reinnervated tibialis anterior muscles of the rat. Can J Physiol Pharmacol 69: 1774-83.

Tradewell ML, Cooper LA, Minotti S, Durham HD. (2011) Calcium dysregulation, mitochondrial pathology and protein aggregation in a culture model of amyotrophic lateral sclerosis: mechanistic relationship and differential sensitivity to intervention. Neurobiol Dis 42: 265-275

Tsay HJ, Schmidt J. (1989) Skeletal muscle denervation activates acetylcholine receptor genes. J Cell Biol 108: 1523-1526

Turney SG, Lichtman JW. (2012) Reversing the outcome of synapse elimination at developing neuromuscular junctions in vivo: evidence for synaptic competition and its mechanism. PLoS Biol 10: e1011352

U

Umbach JA, Adams KL, Gundersen CB, Novitch BG. (2012) Functional neuromuscular junctions formed by embryonic stem cell-derived motor neurons. PLoS One 7: e36049

Uytterhoeven V., Kuenen S., Kaprowicz J., Miskiewicz K., Verstreken P. (2011) Loss of skywalker reveals synaptic endosomes as sorting stations for synaptic vesicle proteins. Cell 145: 117-132

V

Varea E, Guirado R, Gilabert-Juan J, Martí U, Castillo-Gomez E, Blasco-Ibáñez JM, Crespo C, Nacher J. (2012) Expression of PSA-NCAM and synaptic proteins in the amygdala of psychiatric disorder patients. 46, 189-197

Vawter MP. (2000) Dysregulation of the neural cell adhesion molecule and neuropsychiatric disorders. Eur J Pharmacol 405, 385-395

Verderio C., Coco S., Bacci A., Rosetto D., DeCamilli P., Montecucco C., Matteoli M. (1999) Tetanus toxin blocks the exocytosis of synaptic vesicles clustered at synapses but not of synaptic vesicles in isolated axons. J Neurosci 19: 6723-6732

Verhage M, Maia AS, Plomp JJ, Brussaard AB, Heeroma JH, Vermeer H, Toonen RF, Hammer RE, van den Berg TK, Missler M, Geuze HJ, Südhof TC. (2000) Synaptic assembly of the brain in the absence of neurotransmitter secretion. Science 287: 864-869

Vitureira N, Letellier M, White IJ, Goda Y. (2011) Differential control of presynaptic efficacy by postsynaptic N-cadherin and β-catenin. Nat Neurosci 15: 81-89

Voglmaier SM and Edwards RH. (2007) Do different endocytic pathways make different synaptic vesicles? Curr Opin Neurobiol 17: 374-380

Voglmaier SM., Kam K., Yang H., Fortin DL., Hua Z., Nicoll RA., Edwards RH. (2006) Distinct endocytic pathways control the rate and extent of synaptic vesicle protein recycling. Neuron 51: 71-84

W

Walsh FS, Hobbs C, Wells DJ, Slater CR, Fazeli S. (2000) Ectopic expression of NCAM in skeletal muscle of transgenic mice results in terminal sprouting at the neuromuscular junction and altered structure but not function. Mol Cell Neurosci 15: 244-261

Wang J, Renger JJ, Griffith LC, Greenspan RJ, Wu CF. (1994) Concomitant alterations of physiological and developmental plasticity in Drosophila CaM kinase II-inhibited synapses. Neuron 13: 1373-1384

Warita H, Murakami T, Manabe Y, Sato K, Hayashi T, Seki T, Abe K. (2001) Induction of polysialic acid-neural cell adhesion molecule in surviving motoneurons of transgenic amyotrophic lateral sclerosis mice. Neurosci Lett 300: 75-78

Watanabe M, Frelinger AL 3rd, Rutishauser U. (1986) Topography of N-CAM structural and functional determinants. I. Classification of monoclonal antibody epitopes. J Cell Biol 103:1721-1727

Watts RJ, Hoopfer ED, Luo L. (2003) Axon pruning during Drosophila metamorphosis: evidence for local degeneration and requirement of the ubiquitin-proteasome system. Neuron 38: 871-885

Weyhersmüller A, Hallermann S, Wagner N, Eilers J. (2011) Rapid active zone remodeling during synaptic plasticity J Neurosci 31: 6041-6052

White CM, Vrbová G. (1998) Recovery of rat skeletal muscles after partial denervation is enhanced by treatment with nifedipine. Brain Res 779:125-135

Wichterle H, Lieberam I, Porter JA, Jessell TM. (2002) Directed differentiation of embryonic stem cells into motor neurons. Cell 110: 385-397

Williams AH., Valdez G., Moresi V., Qi X., McAnally J., Elliot LJ., Bassel-Duby R., Sanes JR., Olsen EN. (2009) MicroRNA-206 delays ALS progression and promotes regeneration of neuromuscular synapses in mice. Science. 326: 1549-1554

Williams EJ, Furness J, Walsh FS, Doherty P. (1994b) Activation of the FGF receptor underlies neurite outgrowth stimulated by L1, N-CAM, and N-cadherin. Neuron 13: 583-594

Williams EJ, Walsh FS, Doherty P. (1994a) The production of arachidonic acid can account for calcium channel activation in the second messenger pathway underlying neurite outgrowth stimulated by NCAM, N-cadherin, and L1. J Neurochem 62: 1231-1234

Wong MY, Zhou C, Shakiryanova D, Lloyd TE, Deitcher DL, Levitan ES. (2012) Neuropeptide delivery to synapses by long-range vesicle circulation and sporadic capture. Cell 148: 1029-1038

Woolf CJ, Reynolds ML, Chong MS, Emson P, Irwin N, Benowitz LI. (1992) Denervation of the motor endplate results in the rapid expression by terminal Schwann cells of the growth associated protein GAP-43. J Neurosci 12: 3999-4010.

X

Xu, J., Mashimo, T., Südhof, T. (2007) Synaptotagmin-1,-2 and -9: Ca^{2+} sensors for fast release that specify distinct presynaptic properties in subsets of neurons. Neuron 54: 567-581

Y

Yamashita T., Eguchi K., Saitoh N., von Gersdorff H., Takahashi T. (2010) Developmental shift to a mechanism of synaptic vesicle endocytosis requiring nanodomain Ca^{2+}. Nat Neurosci 13: 838-844

Yang X, Arber S, William C, Li L, Tanabe Y, Jessell TM, et al. (2001) Patterning of muscle acetylcholine receptor gene expression in the absence of motor innervation. Neuron 30: 399-410.

Yang YF., Stein RB., Jhamandas J., Gordon T. (1990) Motor unit numbers and contractile properties after spinal cord injury. Ann Neurol 28:496-502

Yap CC, Lasiecka ZM, Caplan S, Winckler B.(2010) Alterations of EHD1/EHD4 protein levels interfere with L1/NgCAM endocytosis in neurons and disrupt axonal targeting. J Neurosci 30:6646-6657

Yohn DC, Miles GB, Rafuse VF, Brownstone RM. (2008) Transplanted mouse embryonic stem-cell-derived motoneurons form functional motor units and reduce muscle atrophy. J Neurosci 28: 12409-12418

Young SH, Poo MM. (1983) Spontaneous release of transmitter from growth cones of embryonic neurones. Nature 305: 634-637

Z

Zakharenko S., Chang S., O`Donoghue M., Popov SV. (1999) Neurotransmitter secretion along growing nerve processes: comparison with synaptic vesicle exocytosis. J Cell Biol 144:507-518

Zhang B, Luo S, Wang Q, Suzuki T, Xiong WC, Mei L. (2008) Lrp4 serves as a coreceptor of agrin. Neuron 60: 285-297

Zhang YQ, Henderson MX, Colangelo CM, Ginsberg SD, Bruce C, Wu T, Chandra SS. (2012) Identification of CSPα clients reveals a role in dynamin 1 regulation. Neuron 74: 136-150

Zhou H, Fuks A, Alcaraz G, Bolling TJ, Stanners CP. (1993) Homophilic adhesion between Ig superfamily carcinoembryonic antigen molecules involves double reciprocal bonds. J Cell Biol 122: 951-960

APPENDIX A Supplemental material

Figure A1: Conditional knockout of NCAM from presynaptic axons and denervated muscle fibers. **(A)** NCAM immunoreactivity (green) is found associated with synaptic vesicle puncta (syp, blue) at synaptic regions of $NCAM^{+/+}$ endplates (black arrows) and in extra-synaptic growing terminal sprouts (white arrows). (*a'*) Orthogonal view highlights the presynaptic expression of NCAM in sprouts extending from endplates. **(B)** $NCAM^{+/+}$ muscles denervated by nerve crush injury highly express NCAM 3 days after the injury. **(C)** $Hb9^{cre}NCAM^{flx}$ terminal sprouts are filled with synaptic vesicles, but do not express NCAM 7 days after partial denervation. **(D)** Denervated $Hb9^{cre}NCAM^{flx}$ muscles express NCAM 3 days following tibial nerve crush. **(E)** NCAM (green) is clearly expressed at synaptic puncta (blue) in terminal spouts of partially denervated $HSA^{cre}NCAM^{flx}$ mice but **(F)** is completely absent from denervated muscle 3 days after tibial crush.

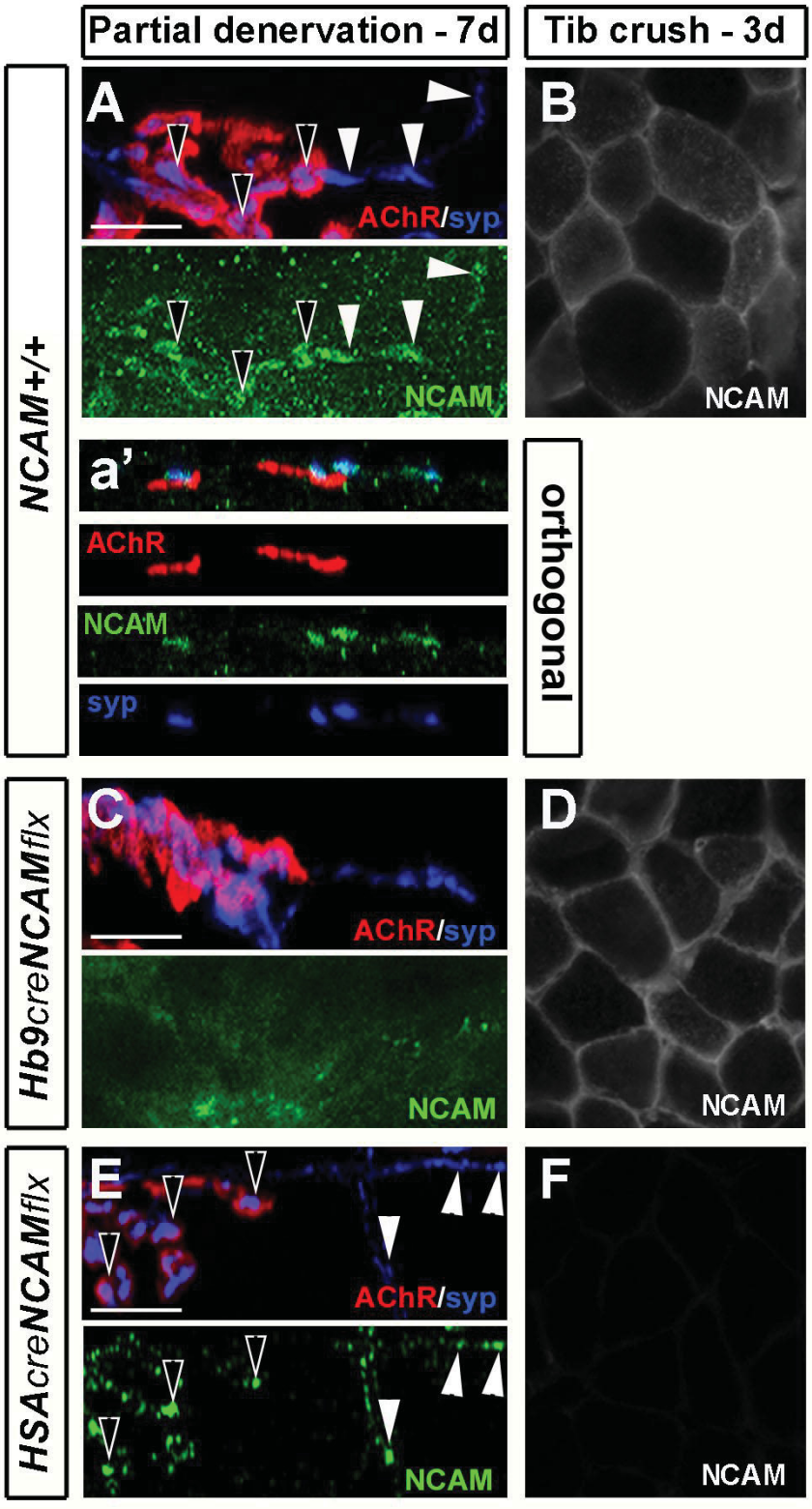
Partial denervation - 7d
Tib crush - 3d
NCAM+/+
A
AChR/syp
NCAM
B
NCAM
a'
AChR
NCAM
syp
orthogonal
Hb9creNCAMflx
C
AChR/syp
NCAM
D
NCAM
HSAcreNCAMflx
E
AChR/syp
NCAM
F
NCAM

Figure A2: Normal intramuscular branching in the absence of presynaptic NCAM. **(A)** *NCAM*$^{+/+}$ and *Hb9*^{cre}*NCAM*^{flx} phrenic motor axons (synaptophysin; syp, green) branch extensively and co-localize with postsynaptic AChRs along the central endplate band (identified with α-BTX) as they innervate diaphragm myofibres at embryonic day 15 and **(B)** 18.5. Scale bars 200μm.

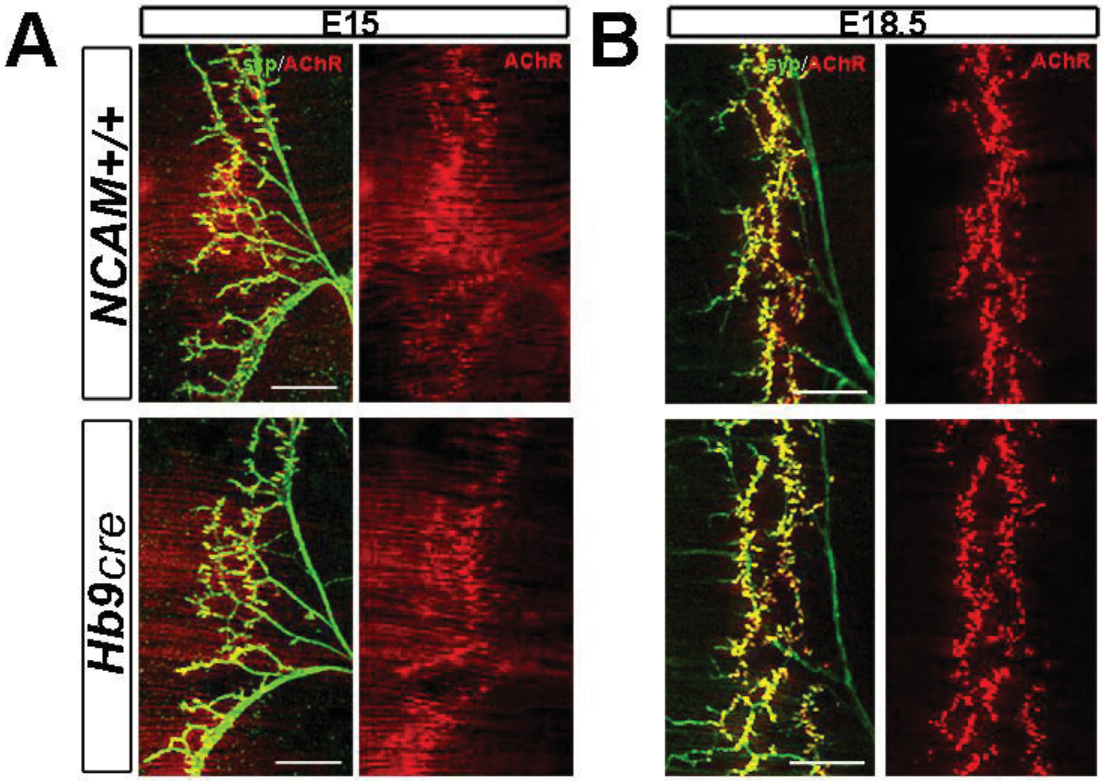
A
E15
B
E18.5
NCAM+/+
Hb9cre
Syp/AChR
AChR
Syp/AChR
AChR

Figure A3: Terminal Schwann cells (tSCs) sprout normally following partial denervation in the absence of presynaptic NCAM. **(A)** Unoperated $NCAM^{+/+}$ and **(B)** $Hb9^{cre}NCAM^{flx}$ NMJs co-immunolabeled with antibodies against S100 and p75 identify terminal (arrowhead; tSC) and myelinating (arrow) Schwann cells (green) and with α-BTX to identify postsynaptic AChRs (red). Some tSCs were found to extend short sprouts from unoperated NMJs (filled arrowhead). **(C)** Unoperated $NCAM^{+/+}$ and **(D)** $Hb9^{cre}NCAM^{flx}$ NMJs co-immunolabeled with antibodies against SV2 and NF (green), S100 (blue) and α-BTX (red). *(c', d')* A higher magnification image of boxed regions, demonstrating that tSCs completely cap presynaptic terminals and are constrained to the endplate area at the majority of NMJs. **(E-F)** Schwann cell bridges (p75/S100+; green) were readily observed bridging postsynaptic endplates (arrowheads) 10 days following partial denervation of $NCAM^{+/+}$ and $Hb9^{cre}NCAM^{flx}$ muscles. **(G-H)** Co-immunolabeling of 14 day partially denervated $NCAM^{+/+}$ and $Hb9^{cre}NCAM^{flx}$ muscles with antibodies to SV2 and NF (green), S100 (blue) and with α-BTX, reveal terminal (tSp) and nodal (nSp) axon sprout growth along tSC processes (*f', h'* arrows). Many $Hb9^{cre}NCAM^{flx}$ axon sprouts exhibit signs of stunted growth and/or retractions (black arrowhead) even in the presence of a Schwann cell bridges at 14 days (*h'*; white arrowhead). Scale bars 20μm.

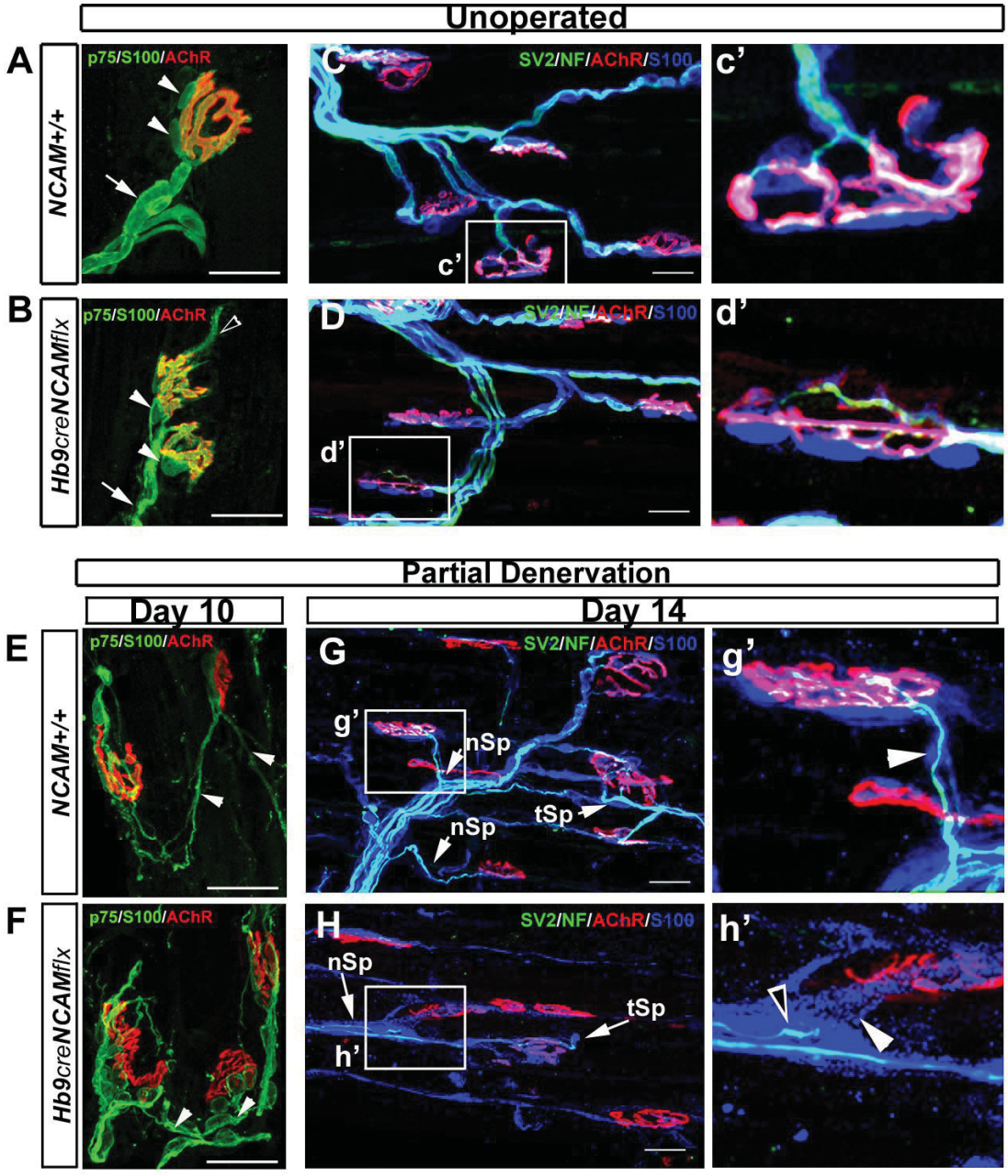
Unoperated
A
NCAM+/+
p75/S100/AChR
C
SV2/NF/AChR/S100
c'
c'
B
Hb9creNCAMflx
p75/S100/AChR
D
SV2/NF/AChR/S100
d'
d'
Partial Denervation
Day 10
Day 14
E
NCAM+/+
p75/S100/AChR
G
SV2/NF/AChR/S100
g'
nSp
nSp
tSp
g'
F
Hb9creNCAMflx
p75/S100/AChR
H
SV2/NF/AChR/S100
nSp
tSp
h'
h'

Figure A4: Immature motor terminals are less spontaneously active than mature motor terminals. **(A-B;** *top***)** Representative traces of spontaneous activity recorded from an immature ($m \leq 25$; red) and mature ($m > 25$; blue) NMJ in partially denervated $NCAM^{+/+}$ and $Hb9^{cre}NCAM^{flx}$ muscles. **(A-B;** *bottom***)** Correlation plots of the frequency of spontaneous activity in relation to presynaptic quantal strengths (*m*). Pearson correlation coefficients (r; right) and *P* values are shown. **(C)** Cumulative frequency plots of mEPP frequency at $NCAM^{+/+}$ (black) and $Hb9^{cre}NCAM^{flx}$ (grey) NMJs and **(D)** mean ±SEM of mEPP amplitude 10 days after partial denervation. **(E)** Same analysis as *A-D* except spontaneous activity was measured from muscle fibers 30 days after partial denervation. $^{**}P < 0.01$ Student's t-test. *P* values in cumulative frequency plots were determined using Mann-Whitney rank sum analysis test. The number of muscle fibers per number of muscles assessed is shown in the bars.

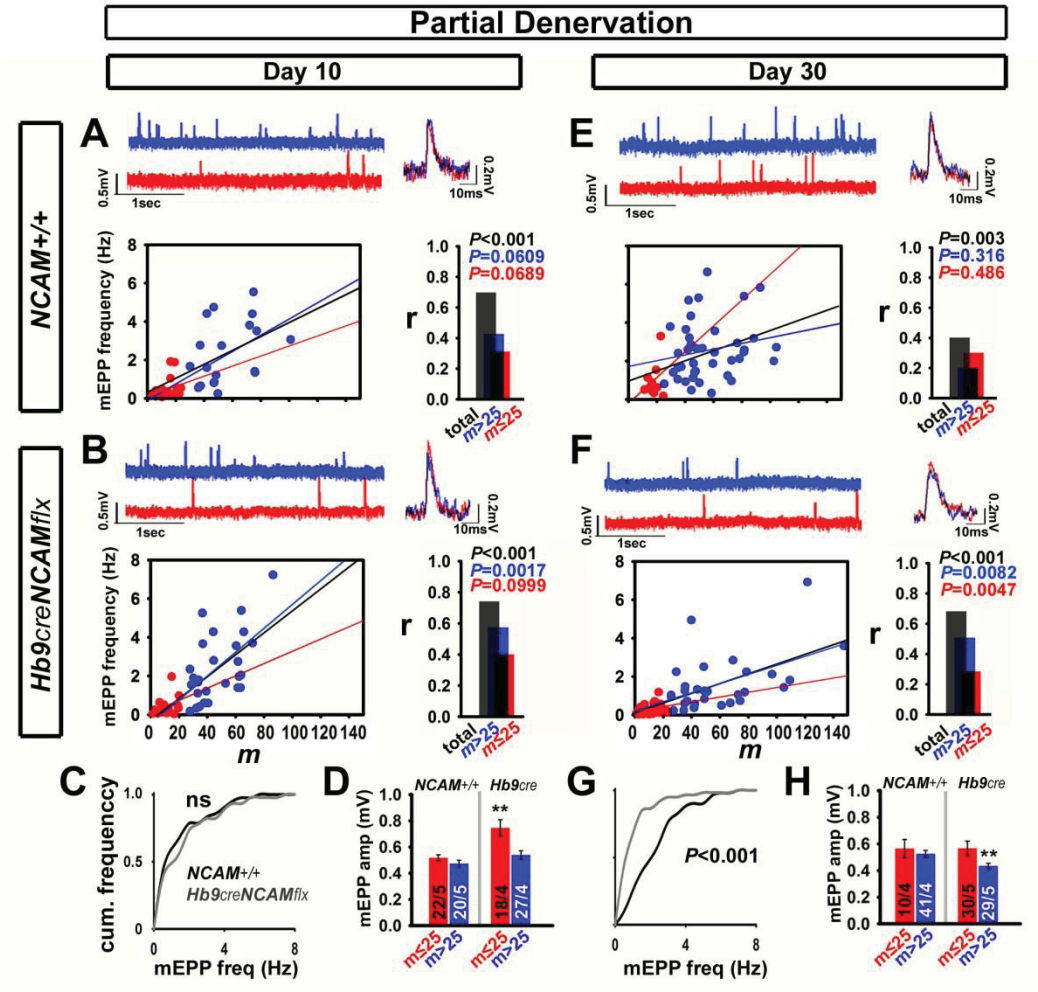
Partial Denervation
Day 10
Day 30
NCAM+/+
Hb9creNCAMflx
A
B
E
F
C
D
G
H
0.5mV
1sec
0.2mV
10ms
mEPP frequency (Hz)
m
r
total
m>25
m≤25
P<0.001
P=0.0609
P=0.0689
P=0.003
P=0.316
P=0.486
P<0.001
P=0.0017
P=0.0999
P<0.001
P=0.0082
P=0.0047
cum. frequenccy
mEPP freq (Hz)
ns
NCAM+/+
Hb9creNCAMflx
mEPP amp (mV)
NCAM+/+
Hb9cre
**
22/5
20/5
18/4
27/4
P<0.001
10/4
41/4
30/5
29/5

Figure A5: Effect of nifedipine on spontaneous transmission at synapses on reorganizing axon arbors. **(A-B)** Representative intracellular recordings of mEPPs recorded from immature ($m \leq 25$) $NCAM^{+/+}$ and $Hb9^{cre}NCAM^{flx}$ synapses before (CTRL; red) and after (dark red) application of 50μM nifedipine 7 days after partial denervation. (*a', b'*) Larger magnification of mEPPs before (red) and after (dark red) 50 μM nifedipine. **(C)** Mean mEPP amplitude, **(D)** frequency, and **(E)** 10-90 rise times assessed from mature ($m > 25$, blue) and immature ($m \leq 25$, red) $NCAM^{+/+}$ motor terminals. **(H-L)** Same analysis as performed in C-E except for $Hb9^{cre}NCAM^{flx}$ motor terminals. *$P<0.05$ Student's t-test.

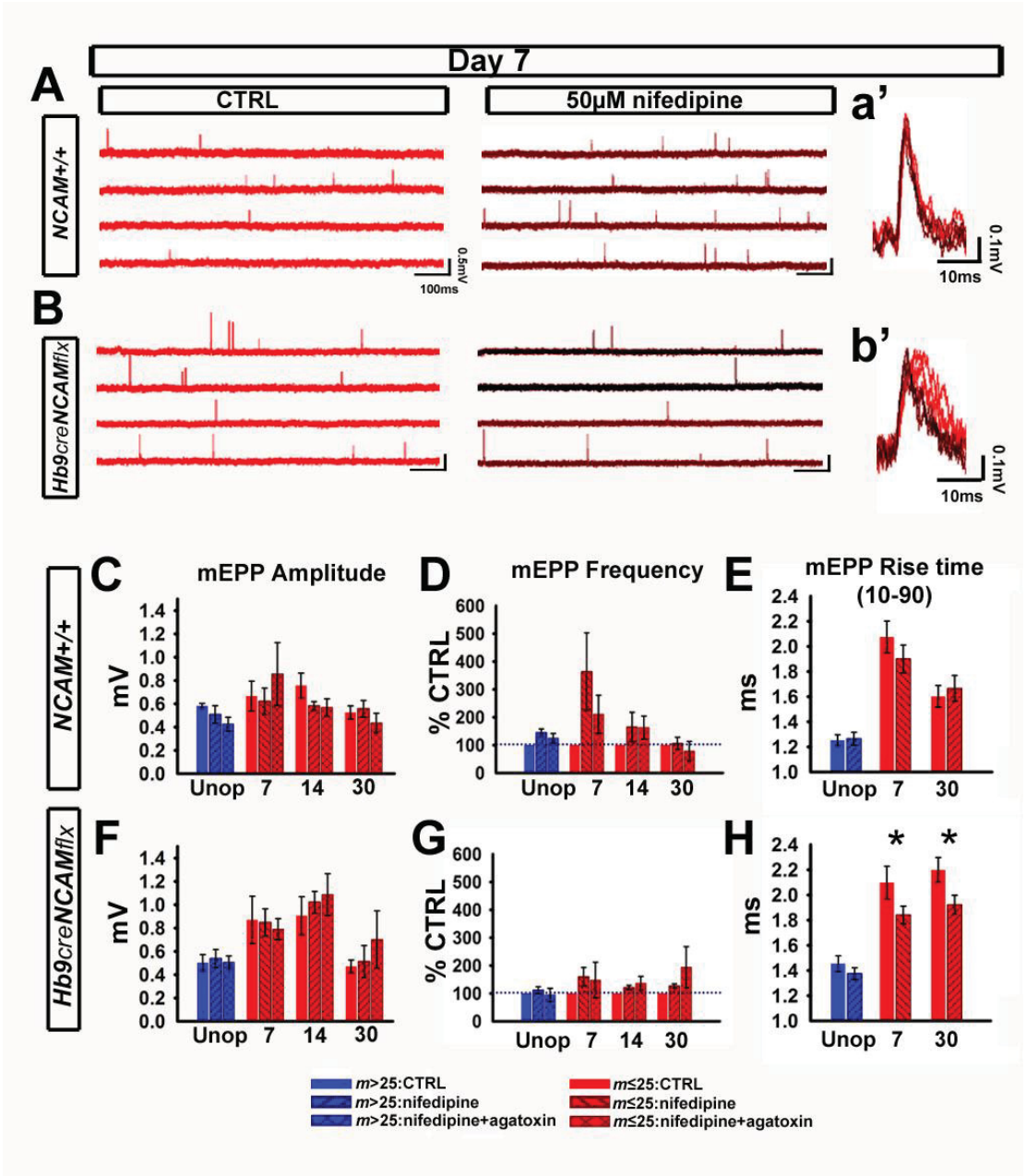
Day 7
A
CTRL
50µM nifedipine
a'
NCAM+/+
0.5mV
100ms
0.1mV
10ms
B
Hb9creNCAMflx
b'
0.1mV
10ms
NCAM+/+
C
mEPP Amplitude
mV
Unop 7 14 30
D
mEPP Frequency
% CTRL
Unop 7 14 30
E
mEPP Rise time
(10-90)
ms
Unop 7 30
Hb9creNCAMflx
F
mV
Unop 7 14 30
G
% CTRL
Unop 7 14 30
H
ms
*
*
Unop 7 30
m>25:CTRL
m>25:nifedipine
m>25:nifedipine+agatoxin
m≤25:CTRL
m≤25:nifedipine
m≤25:nifedipine+agatoxin

Figure A6: Postsynaptic conditional deletion of NCAM ($HSA^{cre}NCAM^{flx}$) does not influence developmental organization of the NMJ. **(A)** Unoperated $HSA^{cre}NCAM^{flx}$ muscles triple co-immunolabeled for presynaptic terminals (NF/SV2; green), perisynaptic Schwann cells (S100; blue) and postsynaptic AChRs (with α-BTX; red). *(a')* Terminal Schwann cells completely cap endplate regions. **(B)** Synaptic vesicle localization to soleus NMJs revealed by triple immunolabeling for synaptophysin (syp; green), neurofilament (NF; blue) and α-BTX (AChRs; red). Vesicles are localized to synaptic regions in unoperated muscles. Scale bar 20μm. **(C)** Plot of cumulative quantal content ($\sum m$) and **(D)** quantal contents (m) recorded from unoperated $HSA^{cre}NCAM^{flx}$ soleus muscle fibres in response to 50 stimuli delivered at 1Hz (triangles) or 50Hz (circles). **(E)** Plot of $\sum m$ vs. m for the estimation of RRP (1Hz) and RP (50Hz) size of unoperated $HSA^{cre}NCAM^{flx}$ NMJs. Dashed lines in *(A)* and *(B)* indicate values obtained from unoperated $NCAM^{+/+}$ NMJs. $HSA^{cre}NCAM^{flx}$ n=60 fibers from 4 muscles.

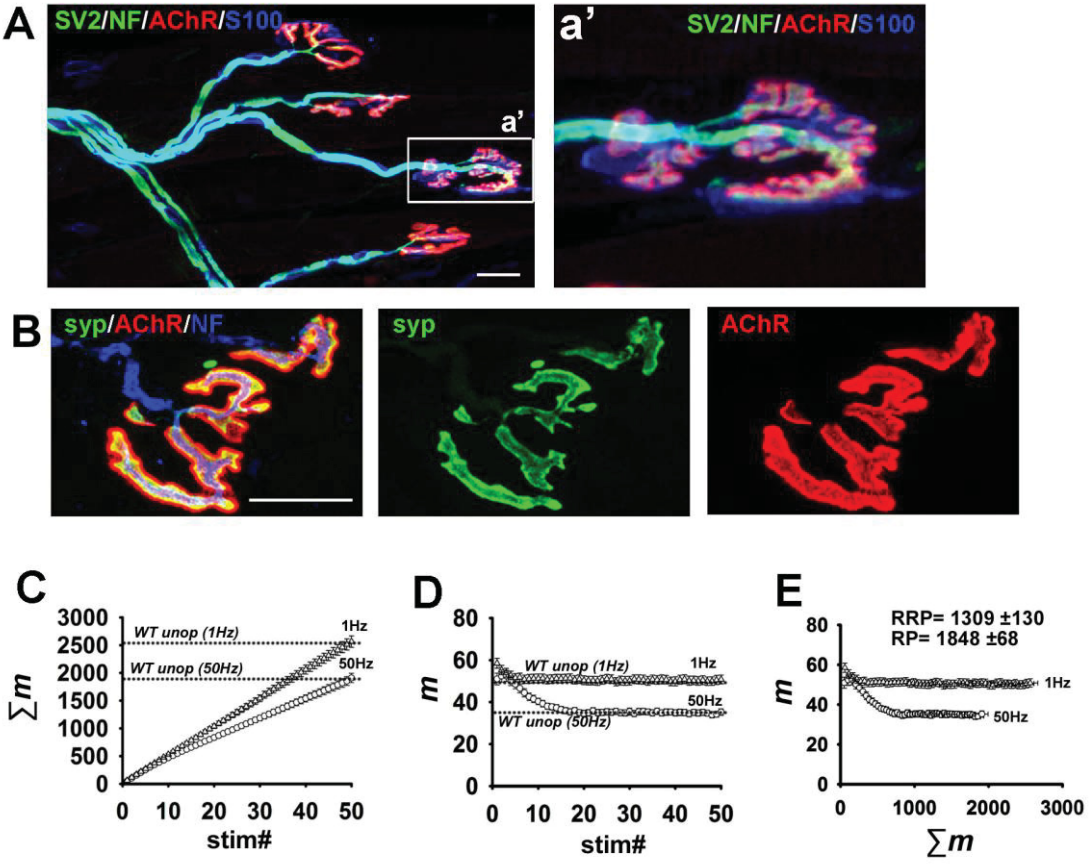
A
SV2/NF/AChR/S100
a'
a'
SV2/NF/AChR/S100
B
syp/AChR/NF
syp
AChR
C
∑m
3000
2500
2000
1500
1000
500
0
WT unop (1Hz)
WT unop (50Hz)
1Hz
50Hz
0 10 20 30 40 50
stim#
D
m
80
60
40
20
0
WT unop (1Hz)
1Hz
50Hz
WT unop (50Hz)
0 10 20 30 40 50
stim#
E
RRP= 1309 ±130
RP= 1848 ±68
m
80
60
40
20
0
1Hz
50Hz
0 1000 2000 3000
∑m

Figure A7: Reinnervated motor terminals in NCAM-deficient mice exhibit signs of retraction following partial denervation. **(A)** Stable reinnervation by terminal sprouts was readily observed at $NCAM^{+/+}$ NMJs 14 days following partial denervation. **(B-D)** In contrast, signs of axonal retraction such as the presence of bulbous axon fragments (i.e. axosomes) and retraction bulbs (arrowheads) near denervated synaptic endplates (AChR; red) were observed at many partially denervated $Hb9^{cre}NCAM^{flx}$, $HSA^{cre}NCAM^{flx}$ and $NCAM^{-/-}$ endplates 14 days after injury. Scale bars 20μm.

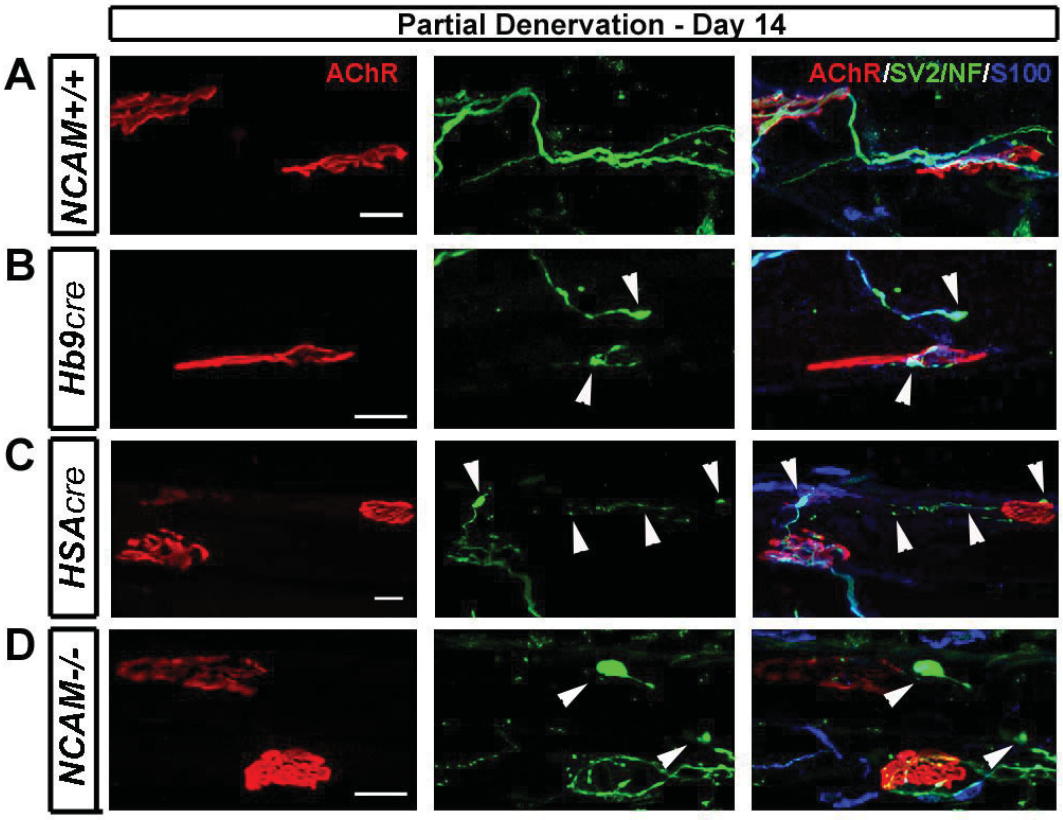
Partial Denervation - Day 14
A
NCAM+/+
AChR
AChR/SV2/NF/S100
B
Hb9cre
C
HSAcre
D
NCAM-/-

Figure A8: *NCAM*$^{-/-}$ mice exhibit progressive age-related muscle degeneration. **(A)** Mean ±SEM young (3-12 month old) twitch forces generated by *NCAM*$^{+/+}$ and *NCAM*$^{-/-}$ soleus muscles. **(B)** Forces generated by young soleus muscles in response to stimulation frequencies applied to the nerve ranging from 5 to 200Hz. **(C)** Mean ±SEM old (12-24 month old) *NCAM*$^{+/+}$ and *NCAM*$^{-/-}$ soleus muscle twitch forces and **(D)** forces generated in response to 5-200Hz stimulation. **(E)** Whole soleus muscle cross sectional area (CSA), **(F)** myofiber CSA and **(G)** total # of myofibers (calculated by muscle CSA/myofiber CSA) of 19 month old *NCAM*$^{+/+}$ and *NCAM*$^{-/-}$ mice. **(H)** Mean ±SEM weight of old mice. **P*<0.05, ***P*<0.001 effect of genotype (*NCAM*$^{+/+}$ vs *NCAM*$^{-/-}$); #*P*<0.001 effect of time (young vs old). ANOVA and Holm-Sidak pairwise multiple comparisons procedure were used to compare the effect of genotype and time on twitch strength, while two-tailed t-tests were performed to compare the effect of genotype on muscle contraction at different stimulation frequencies. The number of muscles and myofibers assessed for each condition is shown in the bars.

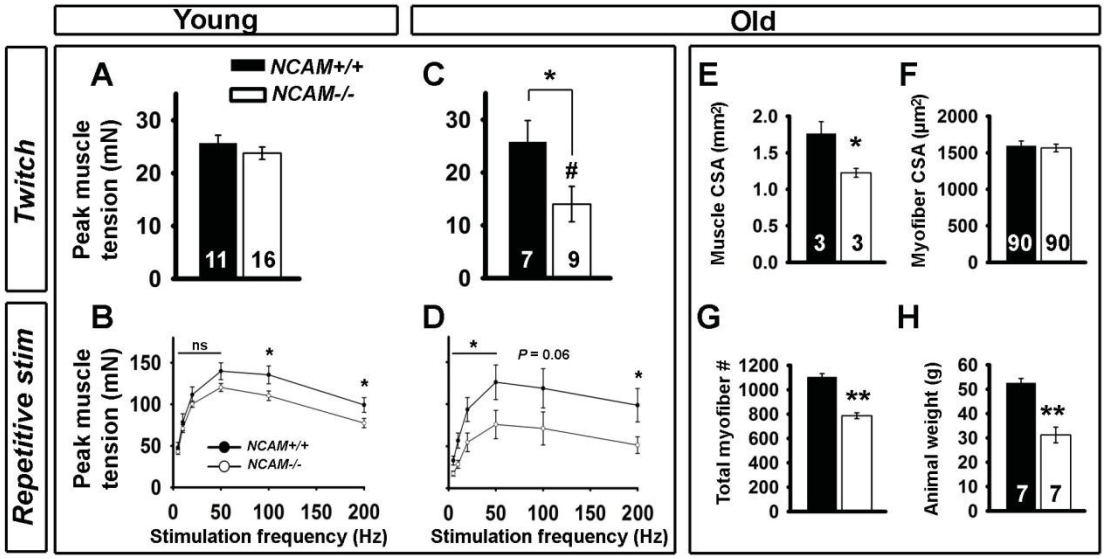
Young
Old
Twitch
Repetitive stim
A
NCAM+/+
NCAM-/-
Peak muscle tension (mN)
11
16
C
*
#
7
9
E
Muscle CSA (mm²)
3
3
F
Myofiber CSA (µm²)
90
90
B
ns
*
Peak muscle tension (mN)
NCAM+/+
NCAM-/-
Stimulation frequency (Hz)
D
*
P = 0.06
*
Stimulation frequency (Hz)
G
Total myofiber #
**
H
Animal weight (g)
**
7
7

Figure A9: Distribution of synapse-associated vesicular and structural proteins in the growth cones and axons of *NCAM*$^{+/+}$ and *NCAM*$^{-/-}$ ESCMNs. **(A)** *NCAM*$^{+/+}$ ESCMNs grown for 24hrs and co-immunolabeled for synaptophysin (syp) and SV2, **(B)** syp and bassoon, **(C)** syp and agrin, **(D)** VAMP7 and SV2, **(E)** VAMP7 and Bassoon, **(F)** and VAMP7 and agrin. **(G-L)** Same analysis as *A-F* except for *NCAM*$^{-/-}$ ESCMNs. Signal intensities were manipulated to more clearly demonstrate co-localization and distribution and do not reflect their expression levels. Scale bars 10 μm.

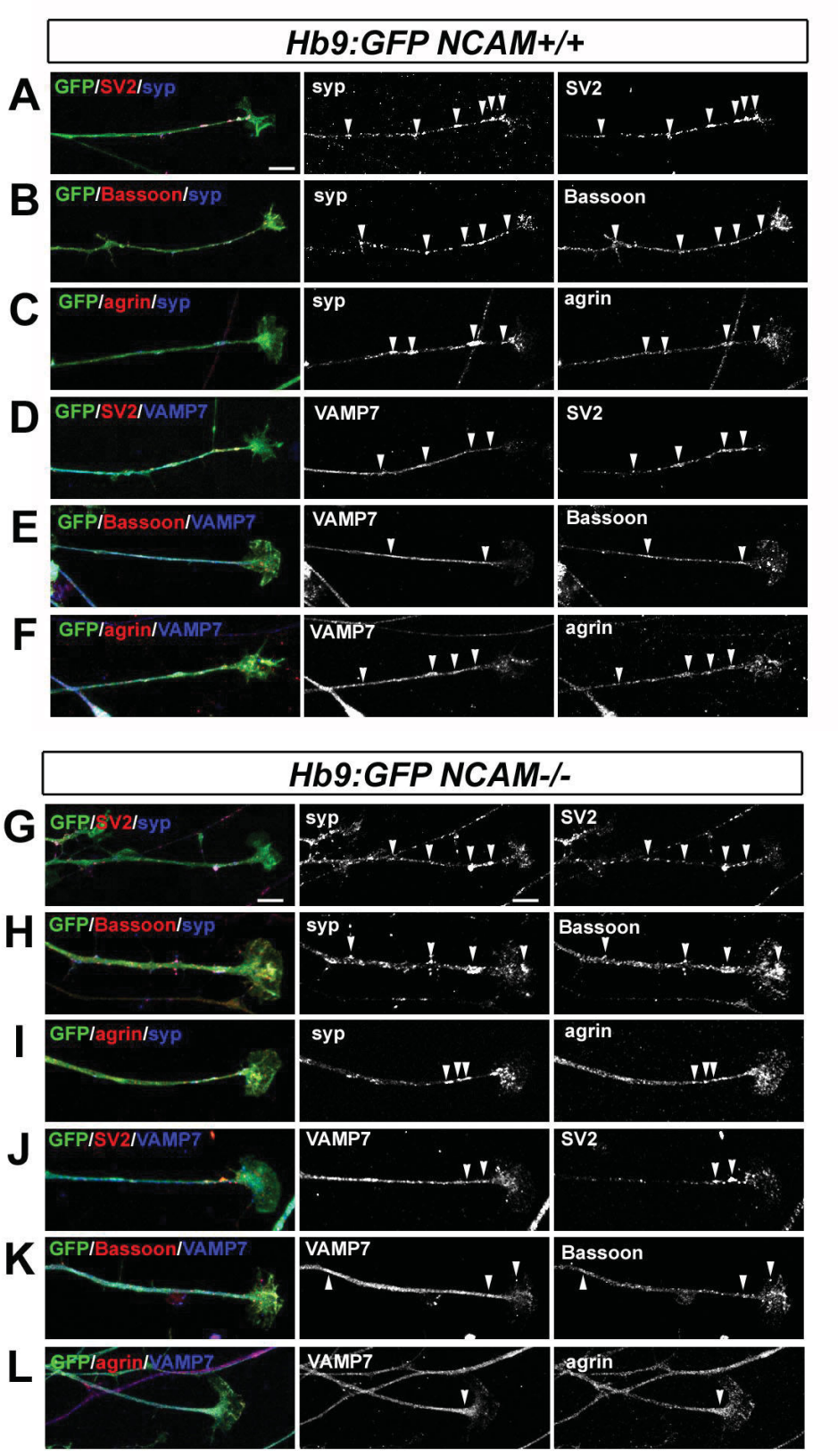
Hb9:GFP NCAM+/+
A
GFP/SV2/syp
syp
SV2
B
GFP/Bassoon/syp
syp
Bassoon
C
GFP/agrin/syp
syp
agrin
D
GFP/SV2/VAMP7
VAMP7
SV2
E
GFP/Bassoon/VAMP7
VAMP7
Bassoon
F
GFP/agrin/VAMP7
VAMP7
agrin
Hb9:GFP NCAM-/-
G
GFP/SV2/syp
syp
SV2
H
GFP/Bassoon/syp
syp
Bassoon
I
GFP/agrin/syp
syp
agrin
J
GFP/SV2/VAMP7
VAMP7
SV2
K
GFP/Bassoon/VAMP7
VAMP7
Bassoon
L
GFP/agrin/VAMP7
VAMP7
agrin

APPENDIX B Copyright Permission Letters

ELSEVIER LICENSE
TERMS AND CONDITIONS

Jun 10, 2012

This is a License Agreement between Dalhousie University ("You") and Elsevier ("Elsevier") provided by Copyright Clearance Center ("CCC"). The license consists of your order details, the terms and conditions provided by Elsevier, and the payment terms and conditions.

All payments must be made in full to CCC. For payment instructions, please see information listed at the bottom of this form.

Supplier	Elsevier Limited The Boulevard,Langford Lane Kidlington,Oxford,OX5 1GB,UK
Registered Company Number	1982084
Customer name	Dalhousie University
Customer address	6275 Yale St Halifax, NS B3H 4R2
License number	2924891333949
License date	Jun 09, 2012
Licensed content publisher	Elsevier
Licensed content publication	Neuron
Licensed content title	NCAM 180 Acting via a Conserved C-Terminal Domain and MLCK Is Essential for Effective Transmission with Repetitive Stimulation
Licensed content author	Luis Polo-Parada,Florian Plattner,Christian Bose,Lynn T. Landmesser
Licensed content date	16 June 2005
Licensed content volume number	46
Licensed content issue number	6
Number of pages	15
Start Page	917
End Page	931
Type of Use	reuse in a thesis/dissertation
Portion	figures/tables/illustrations
Number of figures/tables/illustrations	1
Format	both print and electronic
Are you the author of this Elsevier article?	No
Will you be translating?	No

Order reference number	
Title of your thesis/dissertation	The regulation of synaptic efficacy at regenerating and cultured neuromuscular junctions
Expected completion date	Aug 2012
Estimated size (number of pages)	300
Elsevier VAT number	GB 494 6272 12
Permissions price	0.00 USD
VAT/Local Sales Tax	0.0 USD / 0.0 GBP
Total	0.00 USD
Terms and Conditions	

INTRODUCTION

1. The publisher for this copyrighted material is Elsevier. By clicking "accept" in connection with completing this licensing transaction, you agree that the following terms and conditions apply to this transaction (along with the Billing and Payment terms and conditions established by Copyright Clearance Center, Inc. ("CCC"), at the time that you opened your Rightslink account and that are available at any time at http://myaccount.copyright.com).

GENERAL TERMS

2. Elsevier hereby grants you permission to reproduce the aforementioned material subject to the terms and conditions indicated.

3. Acknowledgement: If any part of the material to be used (for example, figures) has appeared in our publication with credit or acknowledgement to another source, permission must also be sought from that source. If such permission is not obtained then that material may not be included in your publication/copies. Suitable acknowledgement to the source must be made, either as a footnote or in a reference list at the end of your publication, as follows:

"Reprinted from Publication title, Vol /edition number, Author(s), Title of article / title of chapter, Pages No., Copyright (Year), with permission from Elsevier [OR APPLICABLE SOCIETY COPYRIGHT OWNER]." Also Lancet special credit - "Reprinted from The Lancet, Vol. number, Author(s), Title of article, Pages No., Copyright (Year), with permission from Elsevier."

4. Reproduction of this material is confined to the purpose and/or media for which permission is hereby given.

5. Altering/Modifying Material: Not Permitted. However figures and illustrations may be altered/adapted minimally to serve your work. Any other abbreviations, additions, deletions and/or any other alterations shall be made only with prior written authorization of Elsevier Ltd. (Please contact Elsevier at permissions@elsevier.com)

6. If the permission fee for the requested use of our material is waived in this instance, please be advised that your future requests for Elsevier materials may attract a fee.

7. Reservation of Rights: Publisher reserves all rights not specifically granted in the combination of (i) the license details provided by you and accepted in the course of this licensing transaction, (ii) these terms and conditions and (iii) CCC's Billing and Payment terms and conditions.

8. License Contingent Upon Payment: While you may exercise the rights licensed immediately upon issuance of the license at the end of the licensing process for the transaction, provided that you have disclosed complete and accurate details of your proposed use, no license is finally effective unless and until full payment is received from you (either by publisher or by CCC) as provided in CCC's Billing and Payment terms and conditions. If full payment is not received on a timely basis, then any license preliminarily granted shall be deemed automatically revoked and shall be void as if never granted. Further, in the event that you breach any of these terms and conditions or any of CCC's Billing and Payment terms and conditions, the license is automatically revoked and shall be void as if never granted. Use of materials as described in a revoked license, as well as any use of the materials beyond the scope of an unrevoked license, may constitute copyright infringement and publisher reserves the right to take any and all action to protect its copyright in the materials.

9. Warranties: Publisher makes no representations or warranties with respect to the licensed material.

10. Indemnity: You hereby indemnify and agree to hold harmless publisher and CCC, and their respective officers, directors, employees and agents, from and against any and all claims arising out of your use of the licensed material other than as specifically authorized pursuant to this license.

11. No Transfer of License: This license is personal to you and may not be sublicensed, assigned, or transferred by you to any other person without publisher's written permission.

12. No Amendment Except in Writing: This license may not be amended except in a writing signed by both parties (or, in the case of publisher, by CCC on publisher's behalf).

13. Objection to Contrary Terms: Publisher hereby objects to any terms contained in any purchase order, acknowledgment, check endorsement or other writing prepared by you, which terms are inconsistent with these terms and conditions or CCC's Billing and Payment terms and conditions. These terms and conditions, together with CCC's Billing and Payment terms and conditions (which are incorporated herein), comprise the entire agreement between you and publisher (and CCC) concerning this licensing transaction. In the event of any conflict between your obligations established by these terms and conditions and those established by CCC's Billing and Payment terms and conditions, these terms and conditions shall control.

14. Revocation: Elsevier or Copyright Clearance Center may deny the permissions described in this License at their sole discretion, for any reason or no reason, with a full refund payable to you. Notice of such denial will be made using the contact information provided by you. Failure to receive such notice will not alter or invalidate the denial. In no event will Elsevier or Copyright Clearance Center be responsible or liable for any costs, expenses or damage incurred by you as a result of a denial of your permission request, other than a refund of the amount(s) paid by you to Elsevier and/or Copyright Clearance Center for denied permissions.

LIMITED LICENSE

The following terms and conditions apply only to specific license types:

15. **Translation**: This permission is granted for non-exclusive world **English** rights only unless your license was granted for translation rights. If you licensed translation rights you may only translate this content into the languages you requested. A professional translator must perform all translations and reproduce the content word for word preserving the integrity of the article. If this license is to re-use 1 or 2 figures then permission is granted for non-exclusive world rights in all languages.

16. **Website**: The following terms and conditions apply to electronic reserve and author websites:
Electronic reserve: If licensed material is to be posted to website, the web site is to be password-protected and made available only to bona fide students registered on a relevant course if:
This license was made in connection with a course,
This permission is granted for 1 year only. You may obtain a license for future website posting,
All content posted to the web site must maintain the copyright information line on the bottom of each image,
A hyper-text must be included to the Homepage of the journal from which you are licensing at http://www.sciencedirect.com/science/journal/xxxxx or the Elsevier homepage for books at http://www.elsevier.com , and
Central Storage: This license does not include permission for a scanned version of the material to be stored in a central repository such as that provided by Heron/XanEdu.

17. **Author website** for journals with the following additional clauses:

All content posted to the web site must maintain the copyright information line on the bottom of each image, and the permission granted is limited to the personal version of your paper. You are not allowed to download and post the published electronic version of your article (whether PDF or HTML, proof or final version), nor may you scan the printed edition to create an electronic version.
A hyper-text must be included to the Homepage of the journal from which you are licensing at http://www.sciencedirect.com/science/journal/xxxxx . As part of our normal production process, you will receive an e-mail notice when your article appears on Elsevier's online service ScienceDirect (www.sciencedirect.com). That e-mail will include the article's Digital Object Identifier (DOI). This number provides the electronic link to the published article and should be included in the posting of your personal version. We ask that you wait until you receive this e-mail and have the DOI to do any posting.

Central Storage: This license does not include permission for a scanned version of the material to be stored in a central repository such as that provided by Heron/XanEdu.

18. **Author website** for books with the following additional clauses:
Authors are permitted to place a brief summary of their work online only.
A hyper-text must be included to the Elsevier homepage at http://www.elsevier.com . All content posted to the web site must maintain the copyright information line on the bottom of each image.
You are not allowed to download and post the published electronic version of your chapter, nor may you scan the printed edition to create an electronic version.

Central Storage: This license does not include permission for a scanned version of the material to be stored in a central repository such as that provided by Heron/XanEdu.

19. **Website** (regular and for author): A hyper-text must be included to the Homepage of the journal from which you are licensing at http://www.sciencedirect.com/science/journal/xxxxx. or for books to the Elsevier homepage at http://www.elsevier.com

20. **Thesis/Dissertation**: If your license is for use in a thesis/dissertation your thesis may be submitted to your institution in either print or electronic form. Should your thesis be published commercially, please reapply for permission. These requirements include permission for the Library and Archives of Canada to supply single copies, on demand, of the complete thesis and include permission for UMI to supply single copies, on demand, of the complete thesis. Should your thesis be published commercially, please reapply for permission.

21. **Other Conditions**:

v1.6

If you would like to pay for this license now, please remit this license along with your payment made payable to "COPYRIGHT CLEARANCE CENTER" otherwise you will be invoiced within 48 hours of the license date. Payment should be in the form of a check or money order referencing your account number and this invoice number RLNK500795971. Once you receive your invoice for this order, you may pay your invoice by credit card. Please follow instructions provided at that time.

Make Payment To:
Copyright Clearance Center
Dept 001
P.O. Box 843006
Boston, MA 02284-3006

For suggestions or comments regarding this order, contact RightsLink Customer Support: customercare@copyright.com or +1-877-622-5543 (toll free in the US) or +1-978-646-2777.

Gratis licenses (referencing $0 in the Total field) are free. Please retain this printable license for your reference. No payment is required.

NATURE PUBLISHING GROUP LICENSE TERMS AND CONDITIONS

Jun 06, 2012

This is a License Agreement between Dalhousie University ("You") and Nature Publishing Group ("Nature Publishing Group") provided by Copyright Clearance Center ("CCC"). The license consists of your order details, the terms and conditions provided by Nature Publishing Group, and the payment terms and conditions.

All payments must be made in full to CCC. For payment instructions, please see information listed at the bottom of this form.

License Number	2922571505401
License date	Jun 05, 2012
Licensed content publisher	Nature Publishing Group
Licensed content publication	Nature Reviews Neuroscience
Licensed content title	Stress, cognitive impairment and cell adhesion molecules
Licensed content author	Carmen Sandi
Licensed content date	Dec 1, 2004
Volume number	5
Issue number	12
Type of Use	reuse in a thesis/dissertation
Requestor type	academic/educational
Format	print and electronic
Portion	figures/tables/illustrations
Number of figures/tables/illustrations	1
High-res required	no
Figures	Box 1
Author of this NPG article	no
Your reference number	
Title of your thesis / dissertation	The regulation of synaptic efficacy at regenerating and cultured neuromuscular junctions
Expected completion date	Aug 2012
Estimated size (number of pages)	300
Total	0.00 USD
Terms and Conditions	

Terms and Conditions for Permissions

Nature Publishing Group hereby grants you a non-exclusive license to reproduce this material for

this purpose, and for no other use, subject to the conditions below:

1. NPG warrants that it has, to the best of its knowledge, the rights to license reuse of this material. However, you should ensure that the material you are requesting is original to Nature Publishing Group and does not carry the copyright of another entity (as credited in the published version). If the credit line on any part of the material you have requested indicates that it was reprinted or adapted by NPG with permission from another source, then you should also seek permission from that source to reuse the material.

2. Permission granted free of charge for material in print is also usually granted for any electronic version of that work, provided that the material is incidental to the work as a whole and that the electronic version is essentially equivalent to, or substitutes for, the print version. Where print permission has been granted for a fee, separate permission must be obtained for any additional, electronic re-use (unless, as in the case of a full paper, this has already been accounted for during your initial request in the calculation of a print run). NB: In all cases, web-based use of full-text articles must be authorized separately through the 'Use on a Web Site' option when requesting permission.

3. Permission granted for a first edition does not apply to second and subsequent editions and for editions in other languages (except for signatories to the STM Permissions Guidelines, or where the first edition permission was granted for free).

4. Nature Publishing Group's permission must be acknowledged next to the figure, table or abstract in print. In electronic form, this acknowledgement must be visible at the same time as the figure/table/abstract, and must be hyperlinked to the journal's homepage.

5. The credit line should read:
   Reprinted by permission from Macmillan Publishers Ltd: [JOURNAL NAME] (reference citation), copyright (year of publication)
   For AOP papers, the credit line should read:
   Reprinted by permission from Macmillan Publishers Ltd: [JOURNAL NAME], advance online publication, day month year (doi: 10.1038/sj.[JOURNAL ACRONYM].XXXXX)

   Note: For republication from the *British Journal of Cancer*, the following credit lines apply.
   Reprinted by permission from Macmillan Publishers Ltd on behalf of Cancer Research UK: [JOURNAL NAME] (reference citation), copyright (year of publication) For AOP papers, the credit line should read:
   Reprinted by permission from Macmillan Publishers Ltd on behalf of Cancer Research UK: [JOURNAL NAME], advance online publication, day month year (doi: 10.1038/sj. [JOURNAL ACRONYM].XXXXX)

6. Adaptations of single figures do not require NPG approval. However, the adaptation should be credited as follows:

Adapted by permission from Macmillan Publishers Ltd: [JOURNAL NAME] (reference citation), copyright (year of publication)

Note: For adaptation from the *British Journal of Cancer*, the following credit line applies.
Adapted by permission from Macmillan Publishers Ltd on behalf of Cancer Research UK: [JOURNAL NAME] (reference citation), copyright (year of publication)

7. Translations of 401 words up to a whole article require NPG approval. Please visit http://www.macmillanmedicalcommunications.com for more information. Translations of up to a 400 words do not require NPG approval. The translation should be credited as follows:

   Translated by permission from Macmillan Publishers Ltd: [JOURNAL NAME] (reference citation), copyright (year of publication).

   Note: For translation from the *British Journal of Cancer*, the following credit line applies.
   Translated by permission from Macmillan Publishers Ltd on behalf of Cancer Research UK: [JOURNAL NAME] (reference citation), copyright (year of publication)

We are certain that all parties will benefit from this agreement and wish you the best in the use of this material. Thank you.

Special Terms:

v1.1

If you would like to pay for this license now, please remit this license along with your payment made payable to "COPYRIGHT CLEARANCE CENTER" otherwise you will be invoiced within 48 hours of the license date. Payment should be in the form of a check or money order referencing your account number and this invoice number RLNK500793036. Once you receive your invoice for this order, you may pay your invoice by credit card. Please follow instructions provided at that time.

Make Payment To:
Copyright Clearance Center
Dept 001
P.O. Box 843006
Boston, MA 02284-3006

For suggestions or comments regarding this order, contact RightsLink Customer Support: customercare@copyright.com or +1-877-622-5543 (toll free in the US) or +1-978-646-2777.

Gratis licenses (referencing $0 in the Total field) are free. Please retain this printable license for your reference. No payment is required.

Copyright Clearance Center | LICENSE YOUR CONTENT | PRODUCTS AND SOLUTIONS | PARTNERS | EDUCATION | ABOUT US

1 PAYMENT 2 REVIEW 3 CONFIRMATION

Step 3: Order Confirmation

Thank you for your order! A confirmation for your order will be sent to your account email address. If you have questions about your order, you can call us at 978-646-2600, M-F between 8:00 AM and 6:00 PM (Eastern), or write to us at info@copyright.com.

Confirmation Number: 11000471
Order Date: 05/28/2012

If you pay by credit card, your order will be finalized and your card will be charged within 24 hours. If you pay by invoice, you can change or cancel your order until the invoice is generated.

Payment Information

Peter Chipman
Dalhousie University
pchipman@dal.ca
+1 (902) 405-5573
Payment Method: n/a

Order Details

The European journal of neuroscience

Order detail ID:	62488589
Order License Id:	2917890508147
Article Title:	Neural cell adhesion molecule is required for stability of reinnervated neuromuscular junctions
Author(s):	Chipman, Peter H. ; et al
DOI:	10.1111/J.1460-9568.2009.07049.X
Date:	Jan 01, 2010
ISSN:	0953-816X
Publication Type:	Journal
Volume:	31
Issue:	2
Start page:	238
Publisher:	BLACKWELL PUBLISHING LTD.
Author/Editor:	EUROPEAN NEUROSCIENCE ASSOCIATION

Permission Status: Granted
Permission type: Republish or display content
Type of use: reuse in a dissertation/thesis
View details

Note: This item will be invoiced or charged separately through CCC's **RightsLink** service. More info **$ 0.00**

Total order items: 1 **Order Total: 0.00 USD**